# Master Project 2007

## Phase B

# SwissCube structural design and flight system configuration

Student:

Guillaume Roethlisberger - Microengineering

Professor:

Maurice Borgeaud – Space Center

Advisor:

Muriel Noca – Space Center

•

EPFL
Lausanne
Switzerland

•

23/02/2007

•

Space Center

Haute Ecole Spécialisée de Suisse occidentale

ÉCOLE POLYTECHNIQUE FÉDÉRALE DE LAUSANNE

# RECORD OF REVISIONS

| ISS/REV | Date | Modifications | Created/modified by |
|---|---|---|---|
| 1/0 | 08/01/07 | Initial Issue | Guillaume Roethlisberger |
| 1/1 | 11/02/07 | Add FEA results | Guillaume Roethlisberger |
| 1/2 | 15/02/07 | M.N. comments | Guillaume Roethlisberger |
| 1/3 | 20/02/07 | Add vibration test results | Guillaume Roethlisberger |
| 1/4 | 23/02/07 | Last modifications but not the least | Guillaume Roethlisberger |

# WORK PACKAGE – STRUCTURE & CONFIGURATION

| PROJECT: SwissCube Satellite PHASE: B | WP REF: 4500 |
|---|---|
| **WP Title:** SwissCube Structures and Configuration | **Sheet 1 of 2** |
| **Responsible:** EPFL-Space Center, Muriel Noca<br>**Partner Laboratory**: EPFL-LMAF, Professor Botsis<br>**Student:** Guillaume Roethlisberger | **Issue Ref: 1**<br>**Issue Date:**<br>**08-10-06** |
| **Start date: 23-10-06**<br>**End date: 28-02-07** | |
| **WP Manager:** M. Noca | |

**Introduction and general expectations**

This Work Package summarizes the work expected from the Space Center student during phase B (master's project) of the SwissCube Project. The expected duration of the work is from 23-10-2006 till 28-02-2007. The student shall:

- Prepare a schedule for the planning of his work with milestones. Any deviation from the plan shall be reported;
- Perform the technical work with supervision from the Project Engineering Team Space Center, and the LMAF Laboratory;
- Attend appropriate engineering meetings and prepare for major reviews;
- Deliver an end-of-project report and support additional documentation when and if necessary.

This project will involve collaboration with several Swiss industries. The student shall prepare scheduled meetings with industry.

**Task Description:**

The tasks in this master's project will be both computer simulations and hardware test. The simulations will help predict the constraints ranges to be expected given the vibration environment, and provide mechanical design solutions to fit the hardware requirements. The task will also be to prepare and perform vibration tests for various satellite components, verify their applicability to the specifications.

The following tasks must be done during the project (non-exhaustive list):

- Continue structural and configuration design taking into account the update of the other subsystems.
- Document launch environment requirements.
- Document structural test requirements.
- Select adhesives and composites in compliance with environmental, test and performance requirements.
- Define PCB material and layout, define board to board connectors (collaboration with Cicorel). Test possible solutions.
- Integration and test of the kill-switch and springs plungers.
- Provide design for attachment of the reaction wheel's motor. Integration and test of a mock-up wheel motor.
- Design of the mechanical part of the "remove before flight pin".
- Provide and document integration and cabling plan (mechanical part of the cabling).
- Perform quick static and dynamic analysis of the structure with all modelled satellite components.
- Perform dynamic test of the structure with all modelled satellite components.

**Deliverables:**

- A final report including a short description of all outputs and all technical outputs (i.e. tests).
- A structural mock-up of the satellite.
- A presentation at the Preliminary Design Review that will conclude Phase B.
- A disk containing all analysis and documentation files for records.

# SwissCube structural design and flight system configuration

*Guillaume Roethlisberger, Section Microtechnique*

*Advisor:* *Muriel Noca*

*Professeur:* *Maurice Borgeaud*

---

The EPFL Space Center in partnership with the LMTS is leading the development of a small satellite, to be launched mid-2008. This satellite follows the CubeSat standard (1kg cube with a 1 liter volume) providing a fast and affordable access to space.

The primary objective of this satellite is to provide a dynamic and realistic learning environment for students. The secondary objective is to take optical measurements and characterize the Airglow phenomena, a light emitting phenomenon occurring in the low Earth atmosphere (see Figure 1)

**Figure 1 Airglow phenomena.**

The purpose of the structural subsystem for the SwissCube is to provide a simple sturdy structure that will survive launch loads and a suitable environment for the operation of all subsystems (see Figure 2).

Finite element analysis (FEA) was used to estimate the deformations and stresses that the SwissCube will experience under a variety of different loads and freedom cases (see Figure 3).

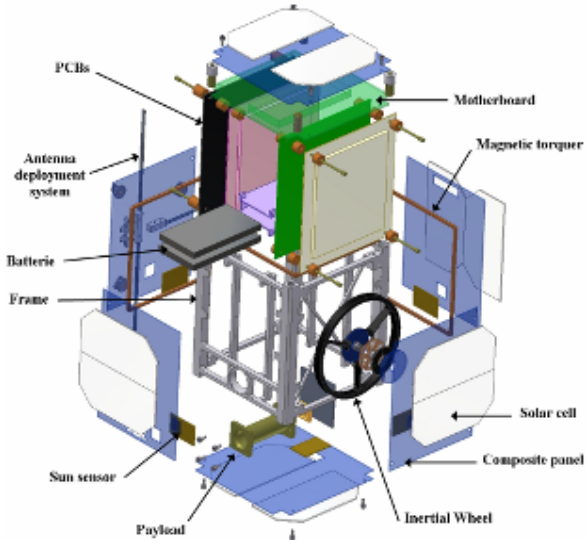


**Figure 2 3D exploded view of SwissCube.**

Vibration tests (sinusoidal and random) have been performed on a structural model of the satellite in order to confirm FEA results, as well as to validate the design of the SwissCube structure and configuration.

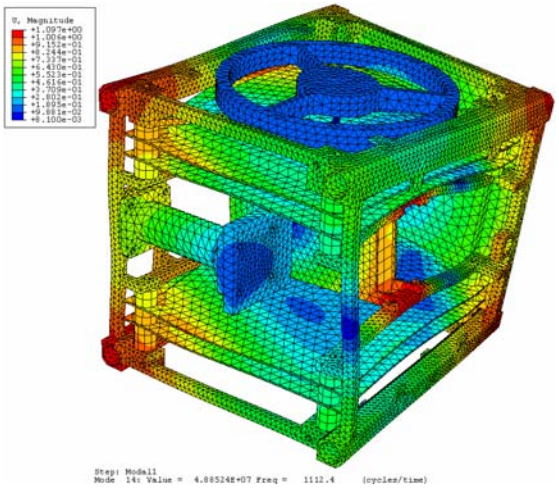

**Figure 3 14th natural frequency of the model.**

# FOREWORD

This Master project consists of a written thesis reporting the background, design processes and outcomes of a project conducted at the EPFL under the supervision of Mrs. Muriel Noca. It began October 23, 2006 and will finish March 5, 2007 with the Phase B Review.

The report documents the investigation into the design and analysis of developing the structural subsystem of a picosatellite capable of carrying a scientific payload into orbit. The design of the satellite is constrained by the specifications defined by the CubeSat Standards.

This report is divided into 9 chapters. The first chapter introduces the reader to the CubeSat program and the SwissCube objective. The design requirements are stated in Chapter 2 and design assumptions and approach are given in Chapter 3. Chapter 4 is dedicated to the technical descriptions of the various topics of this master thesis, like design of the primary and secondary structures, adhesive bonding, composite panels and choices of the diverse components. The verification methods are rapidly described in Chapter 5. Structural analyses like static or finite elements analysis are depicted in Chapter 6. The test experiences and results are written in Chapter 7. Then, Chapter 8 outlines the current progress of the project and details the areas of proposed future development. Finally Chapter 9 contains the conclusion. References and appendices are located at the end.

I hope this report will be a small, but useful, contribution to the development of space activities at the EPFL, by bringing the first Swiss-built satellite one step closer to realization.

# 1 INTRODUCTION

The purpose of this report is to present the development and advancements for the structural subsystem of the picosatellite SwissCube at the end of Phase B. The SwissCube is the first entirely Swiss picosatellite program. The SwissCube project is based on the CubeSat program started by Stanford University and California Polytechnic State University (CalPoly).

## 1.1 CubeSat

The CubeSat project is a joint venture between California Polytechnic State University San Luis Obispo and Stanford University's Space Systems Development Laboratory. Started in 1999 the purpose of the CubeSat project is to provide a conventional standard for the design and development of picosatellites such that a common deployer can be used **[1]**. The project attempts to reduce the cost and development time generally associated with satellite design, consequently increasing the accessibility to space for educational purposes. Currently there are more than 80 institutions around the world taking part or took part in the development of CubeSats.

The fundamental defining feature of that standard is its physical constraints. The standard specifies that the satellite must have the geometry of $10cm^3$ cube with a mass of no more than 1kg and that the center of gravity must be within 2cm of the geometrical center. The standard also specifies several other important guidelines that must be followed, which will be dealt with as the design progresses. The standards are outlined in the CubeSat Specification Document **[2]**. It is the purpose of the specification document to ensure that each satellite developed will integrate properly with the deployer and will not interfere with other satellites, payloads or the launch vehicle. Figure 4 is an example of a CubeSat design. It has been included to give an understanding of the basic external geometry of a typical CubeSat.

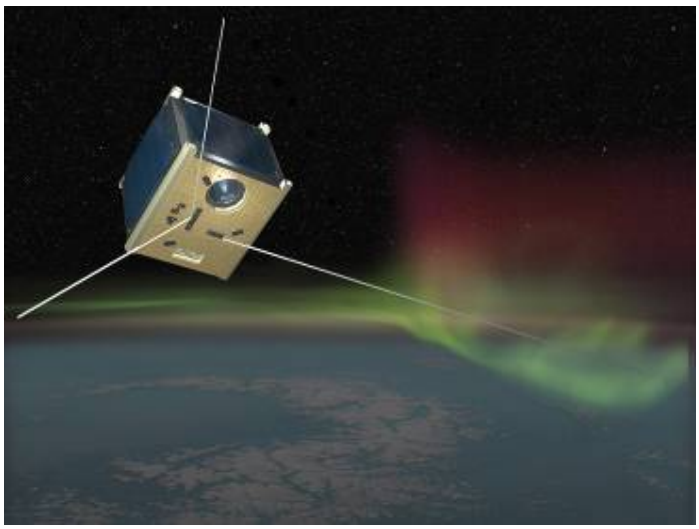

**Figure 4 View of SwissCube (artist rendition).**

## 1.2 SwissCube

SwissCube is the picosatellite being designed by students and staff at the Swiss Federal Institute of Technology Lausanne (EPFL) to be developed and launched in line with the CubeSat specifications. The primary objective of developing this satellite is to provide a dynamic and realistic learning environment for undergraduates, graduates and staff in the development of small satellite technology **[3]**. As a secondary objective it is hoped that the picosatellite will be able to house a science payload with the aim to take optical measurements and characterize the Nightglow phenomena (see Figure 5) over all latitudes and longitudes for at least a period of 3 months, with extended science mission duration up to 1 year (TBC) **[4]**.

**Figure 5 The Nightglow phenomena** [3].

In the design of the SwissCube, each of the subsystems like ADCS, EPS, etc., is being treated as an individual component and managed by a specific group of the SwissCube Team. Although each subsystem is being designed independently it is important to remember that each component is only one part of the complete satellite. Therefore to maintain a high level of integration between the various subsystems continuous communication and discussion is maintained between the designers of the individual subsystems. This report focuses on the structural design and configuration of the picosatellite, but may at times make references to other aspects of the satellite that are deemed important.

## 1.3 Structure and Configuration Objectives

The purpose of the structural subsystem for the SwissCube is to provide a simple sturdy structure that will survive launch loads and a suitable environment for the operation of all subsystems throughout all phases of the mission life, while providing an easily accessible data and power bus for debugging and assembly of components. Moreover the structural subsystem shall carry, support, and

mechanically align the spacecraft equipment. It shall also cage and protect folded components during boost.

Structural design shall aim for simple load paths, a maximization in the use of conventional materials, simplified interfaces and easy integration. Due to the size of the satellite and small expense budget, this was done with the philosophy of maximizing usable interior space, while minimizing the complexity and cost of the design. Due to the weight constraints, the structure must be the lightest possible to allow more margins for the other subsystems.

The *primary* structure is the backbone, or major load path, between the spacecraft's components and the launch vehicle. *Secondary* structures include support beams, booms, trusses and solar panels. We refer to the smallest structures, such as boxes that house electronics and brackets that support electrical cables, as *tertiary*.

# 2 DESIGN REQUIREMENTS

The following chapter gives a complete list of the preliminary requirements for the structural subsystem established during phases A and B of the SwissCube project. Requirements are grouped in six different categories: functional requirements, mission and performance requirements, design requirements, interfaces, environmental and operational.

The complete list of constraints imposed on the SwissCube by the CubeSat standard is given by the CubeSat Design Specifications document (CDS) (can be found at http://cubesat.calpoly.edu).

Besides the requirements imposed by the CDS several additional requirements for the structural subsystem were established. Data (i.e.: temperature range) are preliminarily based on values estimated by other CubeSat missions and will be updated as soon as additional information is provided by the other subsystems.

The main functions to be fulfilled by the structural subsystem of the SwissCube are given by the functional block diagram in Figure 6:

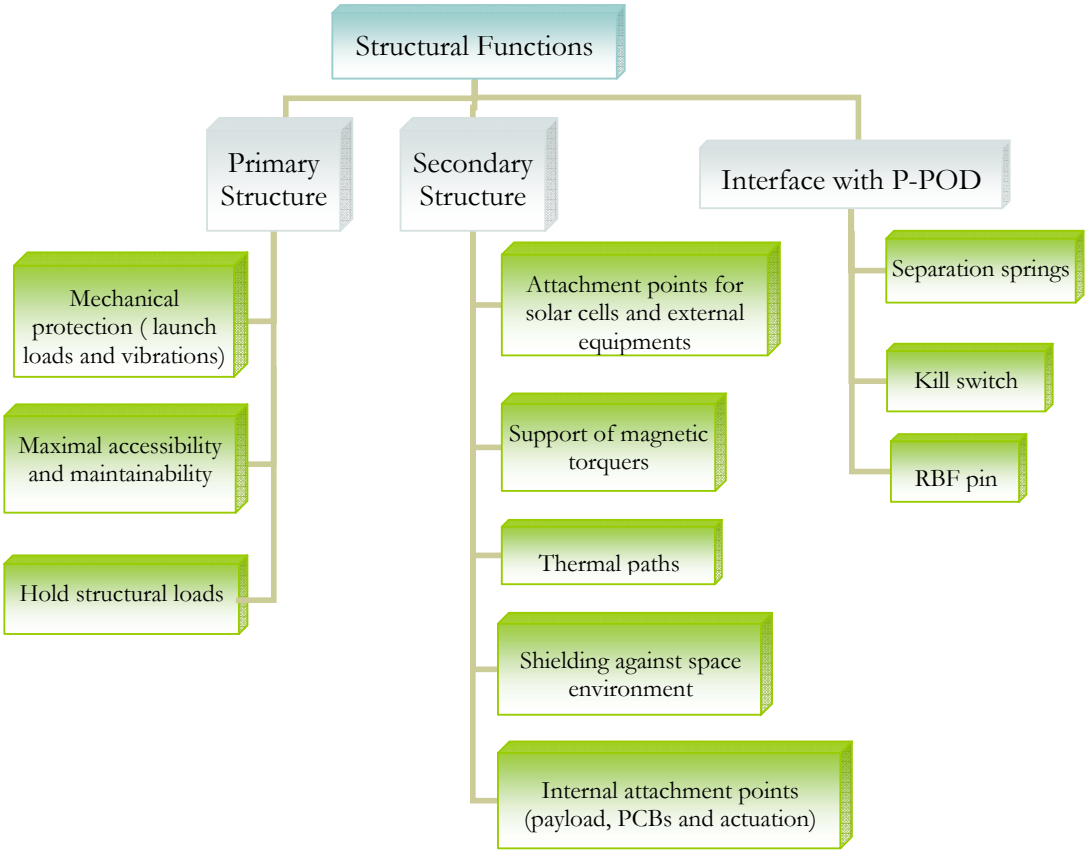


**Figure 6 Functional block diagram**

# 2.1 Functional requirements

## 2.1.1 General

4_SC_10_01 **Structure**

The structural subsystem shall carry, support, and mechanically align the spacecraft equipment.

*Primary function*

*3_SSR_10_01*

4_SC_10_02 **Attachment point**

The structure shall provide attachment points for other subsystems.

*To fulfill its primary function*

*4_SC_10_01*

4_SC_10_03 **Shielding**

The structure shall provide shielding against space environment.

*For the Space System to survive its environment*

*3_SSR_50_01*

4_SC_10_04 **Configuration**

The configuration has to accommodate all platform elements, the optics payload and the antenna mechanism.

*To fulfill its primary function*

*4_SC_10_01*

# 2.2 Mission and performance requirement

## 2.2.1 Unit state H/W performance

4_SC_23_01 **Field of view**

The space system shall have a payload with a FOV as specified in 2_PR_24_10.

*Mission Objective.*

*3_SSR_23_06*

## 2.2.2 Reliability and redundancy

4_SC_25_01 **Tests**

Reliability of the electrical and mechanics systems shall be demonstrated by tests.

*Tests requirements*

*3_SSR_25_02*

## 2.3 Design requirements

### 2.3.1 Constraints

4_SC_31_01 **Cross-contamination**

NASA approved materials should be used whenever possible to prevent contamination of other spacecraft during integration, testing and launch.

*CubeSat Design Specifications document.*

*3_SSR_31_13*

4_SC_31_02 **Deviation from Calpoly CubeSat specifications**

Any deviations from the Calpoly Cubesat specifications shall be approved by Calpoly before launch.

*To insure safety*

*3_SSR_31_14*

4_SC_31_04 **Structure material**

The structural subsystem shall be built from materials with thermal expansion properties comparable to those of Aluminum alloys 7075-T73 and 6061-T6.

*CubeSat Design Specifications document.*

4_SC_31_05 **Unobstructed field of view**

The structural subsystem shall insure that the science instrument's field of view is not obstructed during science observations as specified in 2_PR_24_01.

*Mission Requirement.*

*3_SSR_31_03*

4_SC_31_06 **Outgassing**

The structural subsystem materials shall have a Total Mass Loss (TML) ≤ 1 % and a Collected Volatile Condensable Material (CVCM) ≤ 0.1 %.

*Worst case between Vega, Soyuz, Dnepr and Ariane 5 LVs*

*3_SSR_31_13*

4_SC_31_07 **Unobstructed FOV for sun sensor**

The structural Space System shall ensure that sun sensors FOV in unobstructed and of [100°].

*To ensure determination of attitude*

*4_ADCS_10_02*

4_SC_31_08 **Factors of safety (FOS)**

The following minimum factors of safety shall be used for standard metallic materials:

- yield stress factor of safety 1.25
- ultimate stress factor of safety 1.5
- minimum fatigue factor (cycle) 4

*ECSS standards-E-30-Part 3A*

4_SC_31_09 **Margins of safety (MOS)**

MOS shall be positive.

*ECSS standards-E-30 Part 3A*
*MOS = (allowable stress limit/ (actual stress x FOS))-1*

### 2.3.2 Thermal

4_SC_32_01 **Qualification temperature range**

The structural subsystem shall be designed to survive its qualification temperature range as described in the thermal management report.

*Thermal analysis*

*3_SSR_32_02*

4_SC_32_02 **Thermal isolation**

The structural subsystem shall ensure that the science instruments are thermally isolated.

*Thermal analysis*

*3_SSR_32_01*

## 2.4 Interfaces

### 2.4.1 Structural

4_SC_41_01 **Remove before flight pin**

The structural subsystem shall have a remove before flight pin access area located on a side face with dimension limits shown in Appendix A.

*CubeSat Design Specifications document*

*3_SSR_43_02*

4_SC_41_02 **External components**

No externally mounted components shall exceed 6.5 mm in height from exterior surface of the structural subsystem.

*CubeSat Design Specifications document*

*3_SSR_41_01*

4_SC_41_03 **Contact with the P-POD**

75% (85.125 mm) of flat rail surface area shall be available for rail contact within P-Pod. Rails must be smooth and edges must be rounded to a minimum radius of 1 mm.

*CubeSat Design Specifications document.*

*3_SSR_41_03*

4_SC_41_04 **Anodization**

All rails must be hard anodized.

*CubeSat Design Specifications document*
*to prevent cold-welding, reduce wear, and provide electrical isolation between the CubeSats and the P-POD.*

*3_SSR_43_04*

4_SC_41_05 **Deployables**

Deployables must be constrained by the CubeSat. The P-POD rails and walls should not to be used to constrain deployables.

*CubeSat Design Specifications document*

*3_SSR_41_02*

4_SC_41_06 **Separation springs**

Separation springs must be included at designated contact points in Appendix A. Spring plungers are recommended (McMaster-Carr P/N: 84985A76). A custom separation system may be used, but must be approved by CalPoly launch personnel.

*CubeSat Design Specifications document*

*3_SSR_31_14*

4_SC_41_07 **Access port**

The structural subsystem shall have an access port area located on a side face with the dimension limits shown in Appendix A.

*CubeSat design sepc. Document*

*3_SSR_41_04*

### 2.4.2 Electrical

4_SC_43_01 **Access port**

The structural subsystem shall have an access port area for electrical alimentation located as described in 4_SC_41_07.

*CubeSat Design Specifications document*

*3_SSR_41_04*

4_SC_43_02 **Electrical isolation**

The structural subsystem shall ensure electrical isolation with the P-POD.

*CubeSat Design Specifications document*

*3_SSR_43_04*

### 2.4.3 Data interfaces

4_SC_44_01 **Access port**

The structural subsystem shall have an access port for data exchange area located as described on 4_SC_41_07

*CubeSat Design Specifications document*

*3_SSR_41_01*

### 2.4.4 Physical properties

4_SC_45_01 **External geometry**

External geometry of the structural subsystem shall meet with the specifications detailed in Appendix A.

*CubeSat Design Specifications document*

*3_SSR_41_01*

4_SC_45_02 **Center of Mass**

Center of mass of the whole satellite must be within 2 cm of its geometric center.

*CubeSat Design Specifications document*

*3_SSR_45_02*

4_SC_45_03 **Mass**

The structural subsystem shall weight less than [275]g.

*SSR mass budget*

*3_SSR_45_01*

## 2.5 Environmental requirements

### 2.5.1 Thermal

4_SC_51_01 **Aerothermal flux**

The structural subsystem shall be able to support a thermal flux density of [1000] W/m2 before fairing jettisoning and [1135] W/m2 after fairing jettisoning.
Remark: Solar-radiation flux, albedo and terrestrial infrared radiation and conductive exchange with LV must be added to this aerothermal flux.

*Worst case between Vega, Soyuz, Dnepr and Ariane 5 LVs*

*3_SSR_51_02*

### 2.5.2 Static and dynamic loads

4_SC_52_01 **Quasi-static loads**

The structural subsystem shall be able to support a maximal acceleration of [10,4]g and [2,6] g, including margins, in longitudinal and in lateral axes respectively.

*Worst case between Vega, Soyuz, Dnepr and Ariane 5 LVs*

*3_SSR_52_02*

4_SC_52_02 **Sinusoidal vibration**

The structural subsystem shall be able to sustain the sine vibration qualification test along each axis and for the frequency range specified in Figure 7.
Sinusoidal excitations shall be applied at the base of the mounting adapter, and shall be swept through at a sweep rate of 2 octaves/min and 4 octaves/min in qualification and acceptance respectively.

*Worst case between Vega, Soyuz, Dnepr and Ariane 5 LVs*

*3_SSR_52_03*

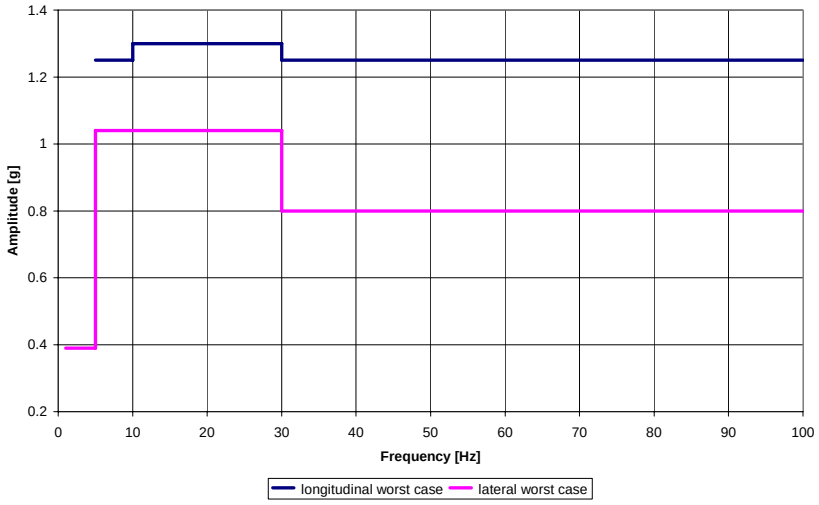


**Figure 7 Amplitude of the sinusoidal vibtation qualification test.**

4_SC_52_03 **Random vibration**

The structural subsystem shall be able to sustain the random vibration qualification and acceptance tests for the frequency range specified in Figure 8.
The durations are 120 and 831 seconds in qualification and acceptance respectively.

*Worst case between Vega, Soyuz, Dnepr and Ariane 5 LVs*

*3_SSR_52_04*

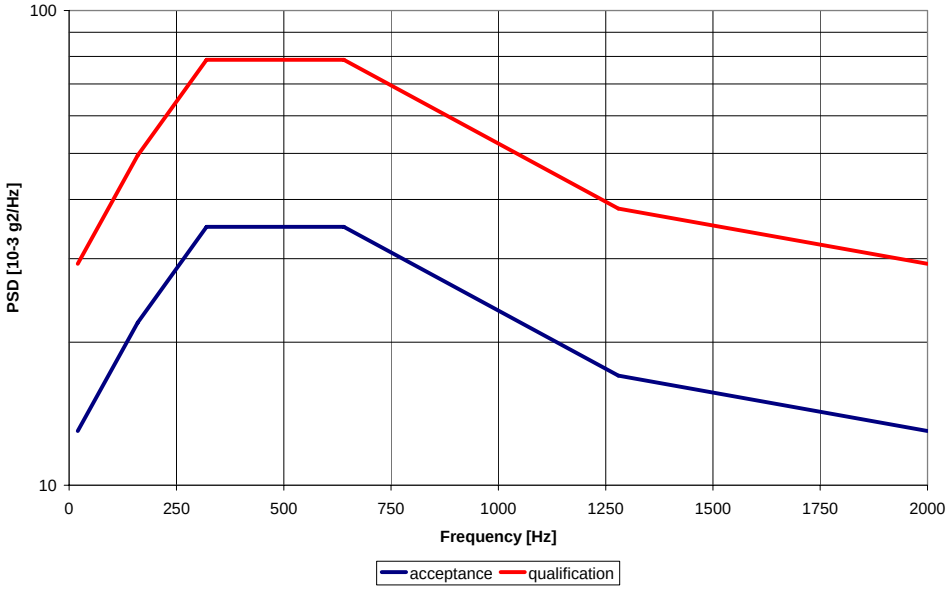


**Figure 8 PSD for qualification and acceptance.**

4_SC_52_04 **Acoustic vibration**

The structural subsystem shall be able to sustain acoustic vibration for the frequency range specified in Figure 9.

The durations are 120 and 60 seconds in qualification and acceptance respectively.

*Worst case between Vega, Soyuz, Dnepr and Ariane 5 LVs*

*3_SSR_52_05*

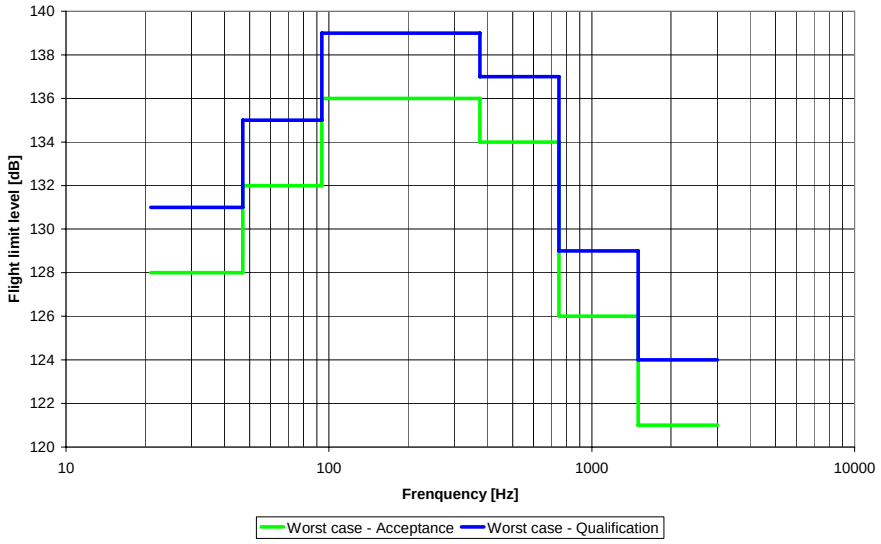


**Figure 9 Acoustic noise spectrum.**

4_SC_52_05 **Shock**

The structural subsystem shall be able to sustain the shock qualification test for the frequency range specified in Figure 10.

*Worst case between Vega, Soyuz, Dnepr and Ariane 5 LVs*

*3_SSR_52_06*

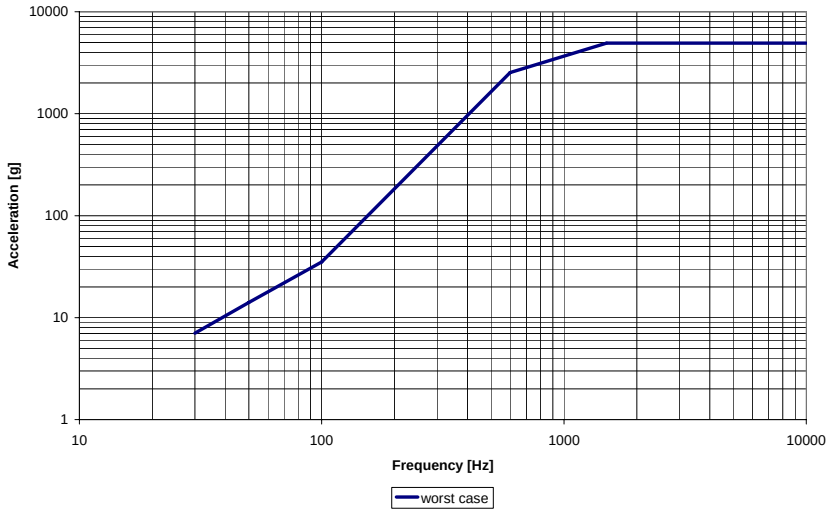


**Figure 10 Envelope acceleration shock response spectrum for the shock qualification test.**

4_SC_52_06 **Fundamental frequency**

The structural subsystem shall be designed with a structural stiffness, which ensures that the values of fundamental frequency of the spacecraft, hard mounted at the separation plane, are equal or superior of [35] Hz and [15] Hz in longitudinal and in lateral cases respectively.

*Worst case between Vega, Soyuz, Dnepr and Ariane 5 LVs*

*3_SSR_52_01*

4_SC_52_07 **Depressurization**

The structural subsystem shall be able to support a depressurization rate of [5] kPa/s.

*Worst case between Vega, Soyuz, Dnepr and Ariane 5 LVs*

*3_SSR_52_07*

### 2.5.3 Vacuum

4_SC_53_01 **Vacuum**

The structural subsystem shall survive high vacuum environment.

*Space Environnent survival*

*3_SSR_53_01*

### 2.5.4 Radiation

4_SC_54_01 **Total dose**

The strutcural subsystem shall survive to a TID of maximum [37.4]kRad.

*Analysis using ESA Spenvis Tool.*
*This is the value for 1 year in orbit*

*3_SSR_54_02*

# 3 DESIGN ASSUMPTIONS AND APPROACH

The following chapter outlines the approach applied during the design of the SwissCube's structural subsystem, as well as the assumptions made about the previous work during Phase A and the launch environment.

## 3.1 Design approach

The "Aerospace Design Engineers Guide" of the AIAA **[5]** provides a comprehensive discussion of the stages involved in the structural design of a spacecraft. These stages are described schematically in Figure 11. In this section the preliminary structural design is considered, including the development of a preliminary mass budget and an initial structural configuration while considering all engineering constraints.

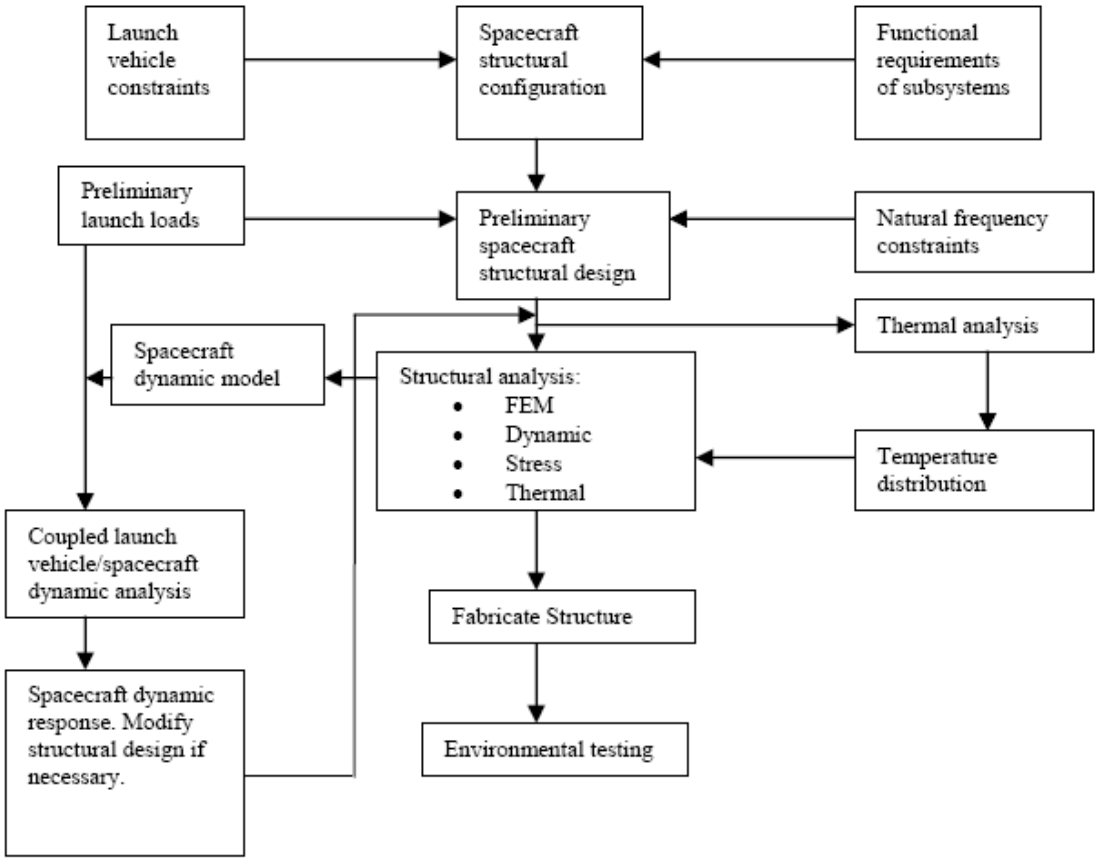


**Figure 11 Spacecraft structural design procedure.**

To summarize, structural design consists of three phases: conceptual design, preliminary design, and detail design. During conceptual design, feasibilities and estimations of costs and risks are established for one or more spacecraft configuration. We derive requirements; identify candidate type of structures, material and attachments; develop designs enough to estimate and compare weight, cost and risk; and select from our options. This work has been done during the last semester, for more info, please refer to report "S3-A-STRU-1-5-Structure_Configuration.pdf".

During the preliminary design, we take a closer look at the winning candidates and identify the best arrangement, shapes, and sizes of structural members. During this phase, we also select types and forms of materials, develop design of attachments, start to plan manufacturing, and begin development testing. This master thesis corresponds to this phase of design.

Detail design is the time for specifying final dimensions and manufacturing tolerances, identifying fasteners sizes and installation torques, designing tertiary structures such as cable-support brackets, and doing all analyses necessary to justify our decisions. At the same time, the product team develops manufacturing processes and plans verification tests. This phase will start next semester (summer semester 2007).

## 3.2 Design assumptions

The design assumptions consist of the approach taken for this project. The baseline of the Phase A is explained and assumptions about launch environment and mechanical loads are stated in this chapter.

### 3.2.1 Baseline of the Phase A

This project is the continuation of the Phase A Structure and Configuration study (see report S3-A-STRU-1-5-Structure_Configuration.pdf). During this precedent project a baseline design of the structural elements as well as a definition of a baseline internal configuration were established. This baseline design was based on the optimization of the advantages resulting from the design principles of using the fewest possible parts for the structure as well as keeping maximal flexibility for the configuration. The material choice and fastening methods were also studied.

For the structural baseline the decision to keep a "full" monobloc was made, in order to assure that the frame will be sufficiently rigid, notably from a vibration point of view. After having defined the general shape of the main frame, its weight is investigated, and in order to satisfy our limited mass budget, weight has been minimized everywhere possible. For that, through holes of 6.5 mm diameter are bored in each rail, and the exterior and interior edges of each rail are chamfered to 2 mm In order to further reduce the mass, the crossbars are also optimized. Their sections are very small in order to save the maximum of weight while remaining sufficiently rigid.

Figure 12 represents the structural baseline at the end of Phase A. The body structure consists of only one part, the main frame, whereas the structural subsystem consists of no more than three major structural components. These components are:

- the main frame (in grey)

- spacers (in orange)
- faceplates (side, top and "payload" panels) (in pale yellow and aqua respectively)

The advantages of the monobloc option are a reduction in the tolerance stack-up, the optimal thermal and electrical conductivity, and the saved mass because no joints are required between the various parts of the frame. But there are also disadvantages, for example the manufacturing problem, the accessibility of the subsystems, or the low flexibility, making design changes difficult.

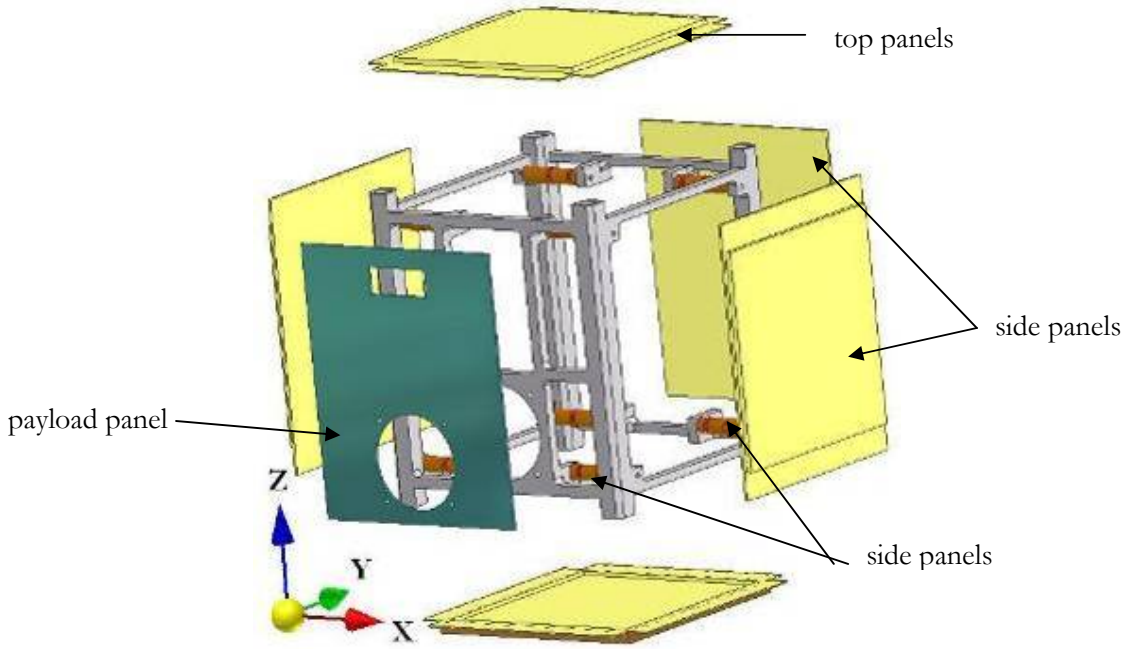


**Figure 12 SwissCube body structure and Reference Coordinate System (Phase A).**

For the configuration baseline, the kind of internal layout is directed by two principal restrictions: the payload and the arrangement of PCBs. The ideal baseline is that which optimizes these both constraints at the same time.

Concerning the payload, the best choice for the orientation is along the direction perpendicular to the rails. In this case the camera points out of the side face which already features the access ports. This has the advantage that payload, antennas and the access port are all on the same face and hence, there are five faces free for the solar panels. The payload points in the Y- direction.

For the placement of the camera, the "full" center solution is not the best way for a key reason: when the camera is in the center of a face, it is difficult to fix it in a solid way. The strategy to fix the payload at a corner can seem like a good idea, especially in a fastening point of view, but in this case the inertial properties of the whole satellite are unpleasant. This is why we chose to displaced the payload from the center only along one direction of the reference frame (see Figure 47).

Relating to the PCBs, the following option is selected: a motherboard is used in order to connect the various electronic subsystems and to reduce the number of wires. Moreover the PCBs are stacked two by two giving a rigid structure. Finally, the both stacks are fixed on the faces of the satellite,

allowing a large amount of free space for the payload subsystem and keeping an increased accessibility to the PCBs placed in the middle of satellite.

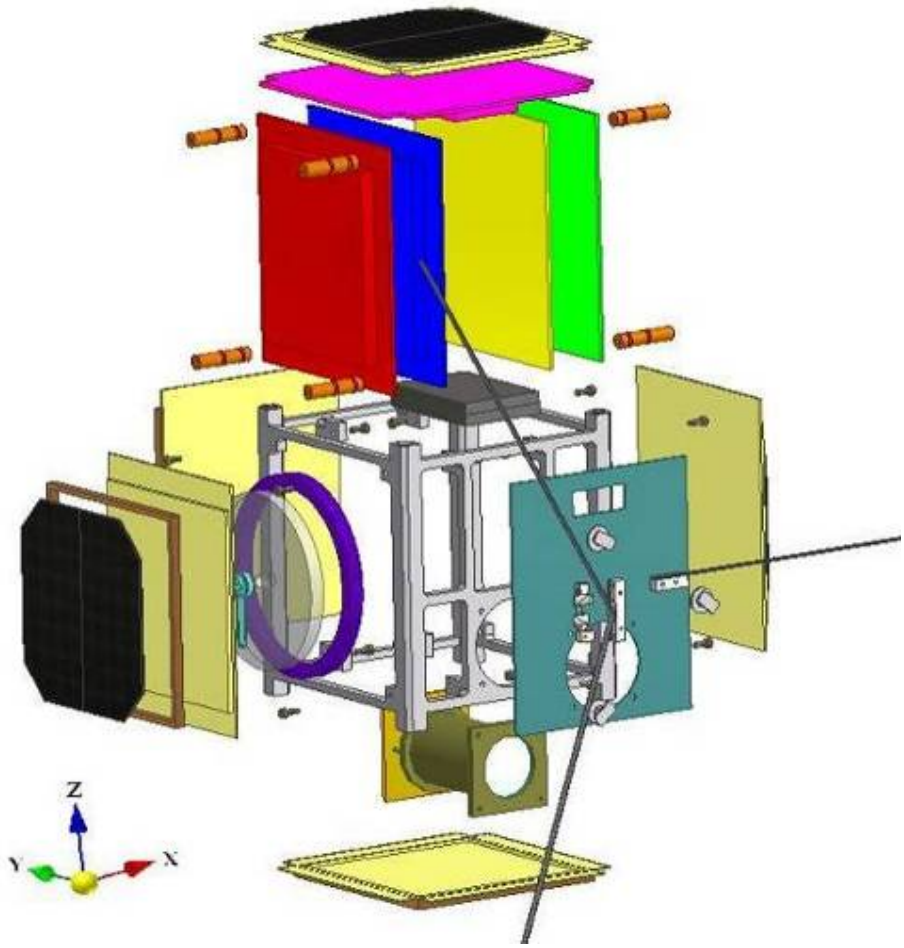


**Figure 13 3D exploded view of the SwissCube (Phase A).**

Concerning the material baseline, an aluminum alloy is used for the main frame because the CubeSat standard specifies that the satellite must be constructed of a material with a similar coefficient of thermal expansion (CTE) to the materials used for the construction of the P-POD. We use the Aluminum alloy called Certal® (Al-7022-T651) with properties similar to Al–7075–T73 (P-POD aluminum alloy).

Even if not adequate for the main structure of the satellite, the titanium will be used to make the structure of the payload because it has a CTE similar to the glass which is used for the optics.

For the external panels of the CubeSat, a reinforced composite of carbon fibers in epoxy resin matrix or sandwich structure panels are proposed. These choices are motivated by the following advantages: a density lower than aluminum (approximately 40-60%, depending on the product), as well as a CTE that lies between that of the solar cells and the main aluminum frame. The drawbacks of composite materials are the low thermal conductivity as well as a lower capacity to absorb of radiations compared to aluminum.

At the end of Phase A the proposed fastening methods were: screws for the various pieces of the structure like the main frame and the spacers. The main reason for this choice is that parts can be disassembled and reassembled numerous times. For the final assembly, screws have to be glued in order to prevent the risk of disassembly during launch due to vibrations.

Concerning the exterior panels, adhesives are proposed, because they provide a weak stress concentration on the interface and can be used to join different kinds of materials, like carbon reinforced composites and aluminum in our case.

### 3.2.2 Launch vehicle environment

In order to establish the launch environment, four launchers have been compared. These launch vehicles are: Vega, Ariane 5, Soyuz and DNEPR. During the preparation for launch and then during the flight, the spacecraft is exposed to a variety of mechanical, thermal, and electromagnetic environments. Appendix B provides a description of the environment that the spacecraft is intended to withstand.

### 3.2.3 Assumptions about mechanical loads

Structures shall be designed to meet the mechanical performance requirements and to withstand the specified environment during launch without damage or degradation. Structures shall conform to the specified stiffness, strength and safety requirements derived from the launcher and the spacecraft structural requirements. The factors of safety (FOS) is a coefficient by which the design loads are multiplied in order to account for uncertainties in the statistical distribution of loads, uncertainties in structural analysis, manufacturing process, material properties and failure criteria

In the computation of safety margins the following minimum FOS shall be used for standard metallic materials [6]:

- yield stress factor of safety 1,25
- ultimate stress factor of safety 1,5
- minimum fatigue factor (cycles) 4

In order to develop the design of the structure, worst case assumptions of the launch load as well as possible vibration frequency ranges were established based on the information given for the types of potential launch vehicles that are Vega, Ariane 5, Soyuz and DNEPR.

To summarize the data given in Appendix B, the highest longitudinal and lateral quasi-static loads for various launch vehicles are given in Table 1. The quasi-static loads are the more severe combinations of dynamic and steady-state accelerations that can be encountered at any instant of the mission (ground and flight operations).

**Table 1 Quasi-static loads.**

| Launch vehicle | Longitudinal acceleration (g) | Lateral acceleration (g) |
|---|---|---|
| Vega | 5.5 | 0.9 |
| Dnepr | 8.3 | 1.0 |
| Soyuz | 5.0 | 1.8 |
| Ariane 5 | 6.0 | 2.0 |

The maximal estimated launch acceleration is 8.3g (DNEPR case) axially with largely inferior lateral launch accelerations. The worst case positioning of the satellite is in the lowest position of a vertically posed P-POD, since the SwissCube then has to support the entire load of the CubeSats above (see remarks in §**6.2.1**). In order to account for uncertainties in the statistical distribution of loads a factor of safety must be used. The yield stress factor of safety recommended by ECSS **[6]** is 1.25, so the resultant acceleration is 10.4 g and is rounded to 10 g. for convenient reason.

Concerning of the sinusoidal (or sine-equivalent) vibration, the envelope levels does not exceed the values given in Figure 81 for the longitudinal case, and Figure 82 for the lateral case.

# 4 TECHNICAL DESCRIPTION

This section describes the technical choices and design for the primary and secondary structures as well as the flight system configuration. Figure 14 shows the layout of all the components forming the satellite.

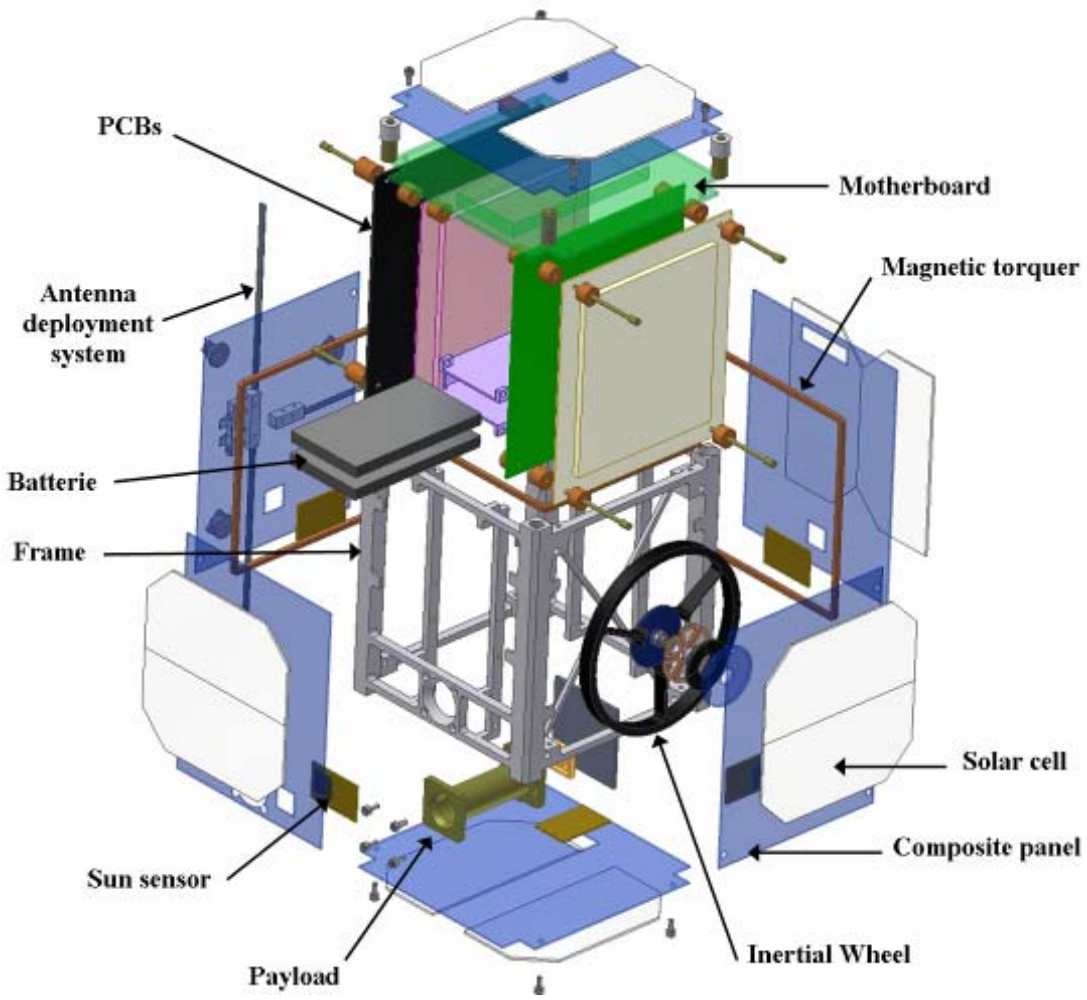


**Figure 14 3D exploded view of SwissCube.**

## 4.1 Structural members

Figure 15 represents the structural members. The body structure consists of only one part, the monobloc frame, whereas the structural subsystem consists of no more than three major structural components. These components are:

- the monobloc frame (in grey)

- spacers (in orange)
- faceplates (side, top and "payload" panels) (in pale blue)

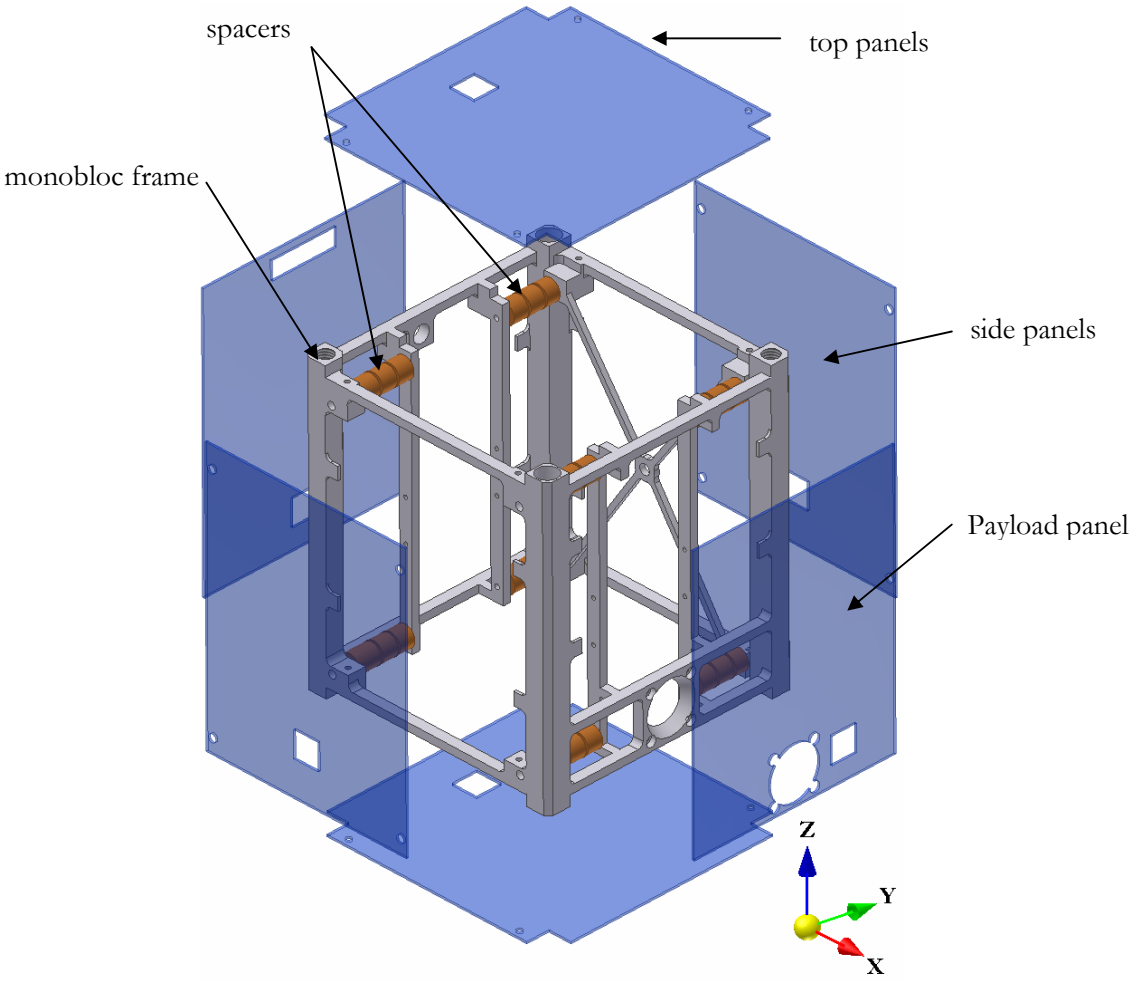


**Figure 15 SwissCube body structure and Reference Coordinate System.**

### 4.1.1 Monobloc frame

The design of the frame has been meticulously investigated in order to minimize mass. As one can see in Figure 16 holes and chamfers are machined at each rail to save mass. The diameter of the holes is 7.5 mm and the chamfers are 2 mm at 45°. The external crossbars have a rectangular shape with a section of 3 x 4 mm. Between the rails and the external crossbars in the X direction, material is kept in order to have a counter fixation for the spacers at a mechanically rigid point of the main structure.

The internal crossbars (in the Z direction) have a rectangular shape of 3 x 5 mm. These internal crossbars serve for the attachment of the PCBs stacks and for this reason have M2 holes. Moreover, the battery box is also fixed to these crossbars thanks to the use of M2 (see §4.8).

The Z+ extremity of each rail is special. A pair of diagonal rails has a threaded M6 hole in order to integrate the separation springs (see §4.9), the other pair of diagonal rails has a bigger hole of 8mm for the integration of the kill-switches (see §4.6).

The sides of the main frame are the same, except the X+ side which contains additional structural elements in order to fix the payload. This face must be enough rigid to support the weight of the payload and since the payload subsystem is fixed like a cantilever beam some additionally crossbars are needed to guarantee that the payload's axis doesn't undergoes any misalignment. This face also includes the payload baffle i.e. a conical aperture (see details in §4.2.1).

Moreover the monobloc frame contains interfaces for the attachment of the wheel subassembly (crossbars in X), attachment points for the external composite panels and for the RBF pin. More information about dimensions of the monobloc frame can be found in Figure 17.

The machining of the frame uses traditional CNC milling machine for the 6 sides of the cube, and electro-erosion technology for the interior of the part. The final mass of the monobloc frame is 106.5 g.

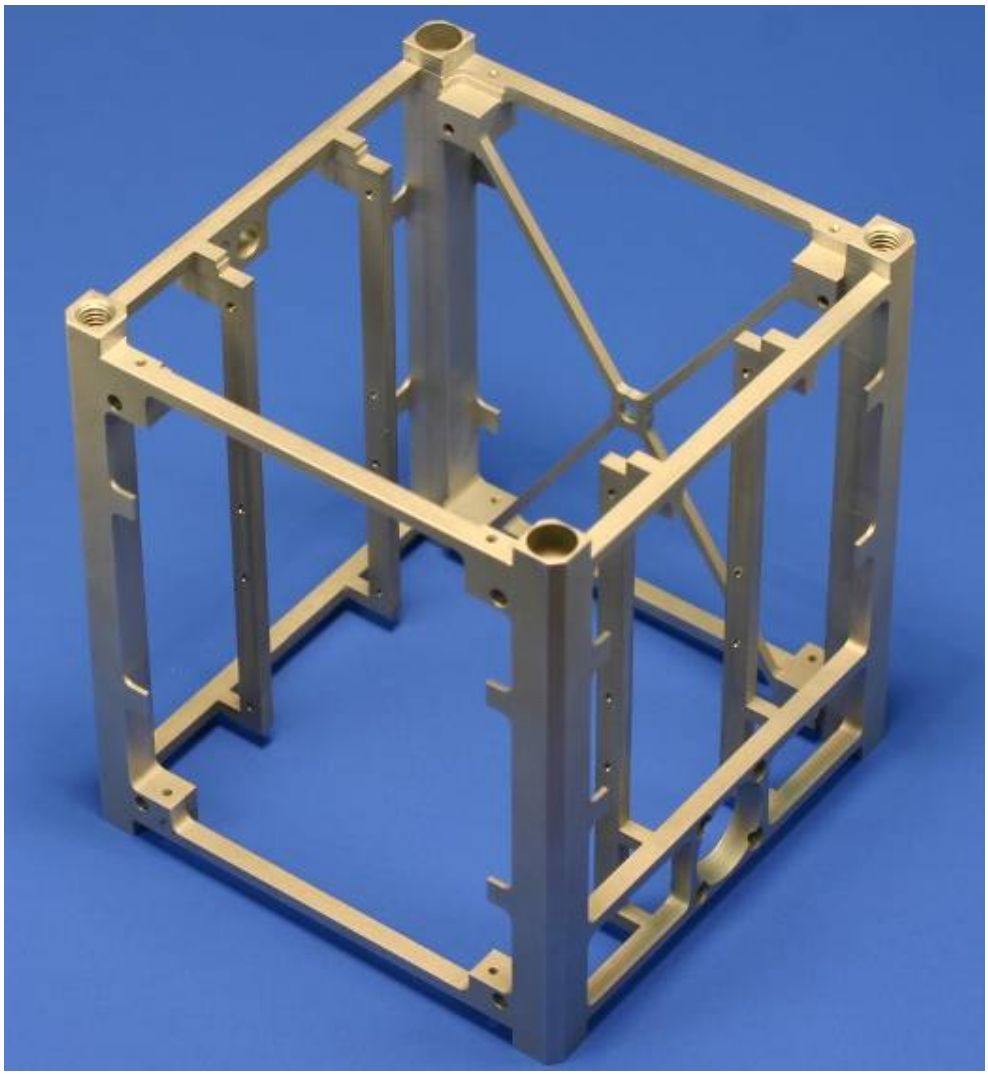

**Figure 16 View of the SwissCube monobloc frame.**

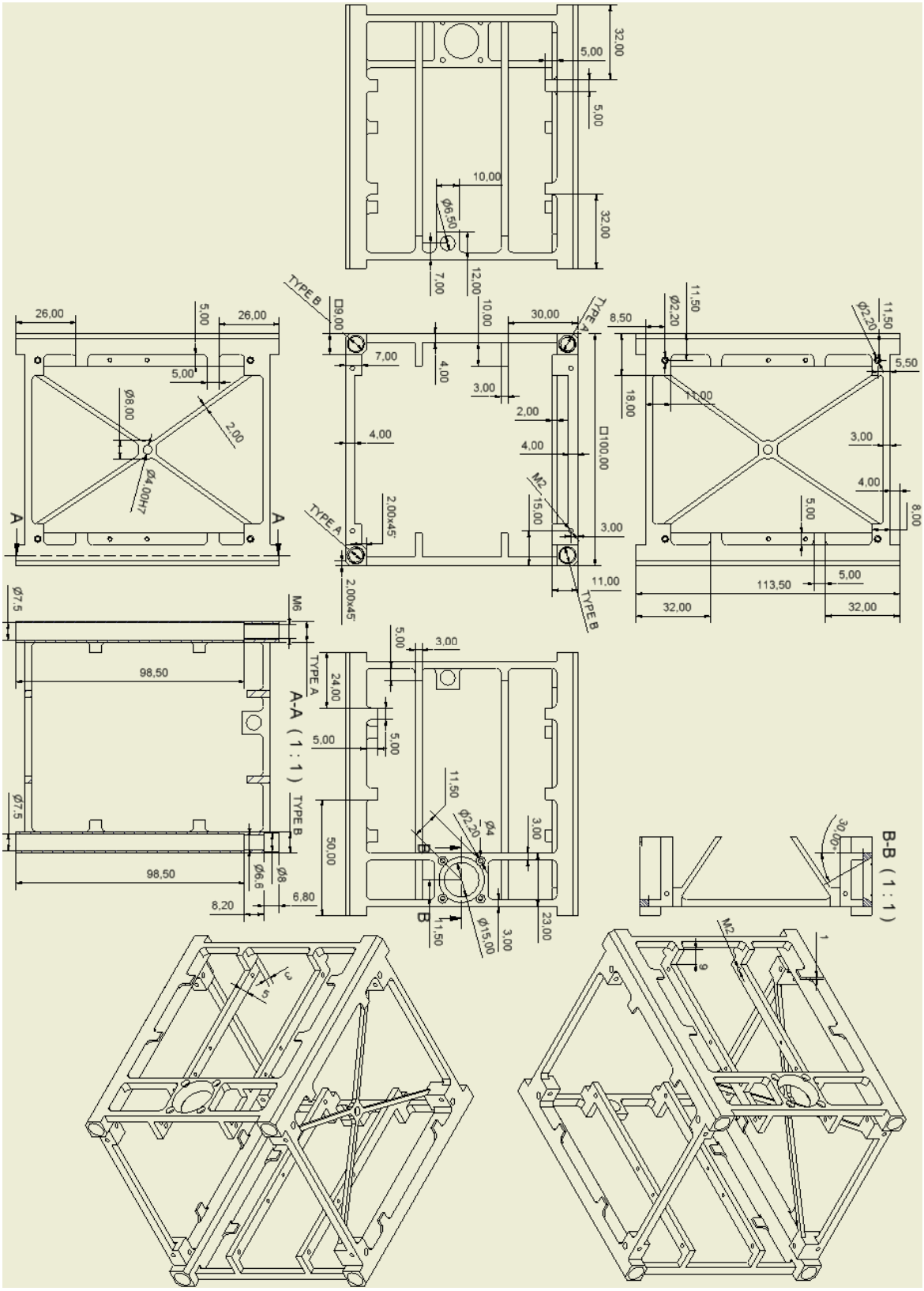


**Figure 17 SwissCube monobloc frame engineering drawing.**

### 4.1.2 Spacers

The role of the spacers is to connect the different PCBs between each other and at the same time to fix the PCB's stack to the main frame. Additionally, the spacers serve as a thermal path between the PCBs and the aluminum frame. Therefore, the spacers will also be fabricated from the Certal aluminum alloy (Appendix C). A whole spacer like in Figure 18 is composed of three basic spacers.

The external diameter is 8 mm whereas the internal diameter is 2.2 mm. The exact length of each individual spacer is actually not known because the distance between different PCBs depends on the dimensions of the electronic components which can fluctuate. Nevertheless, the lengths of a whole spacer unit are 19 and 23mm, depending of the PCB stack. The total mass for all the spacers is 24 grams.

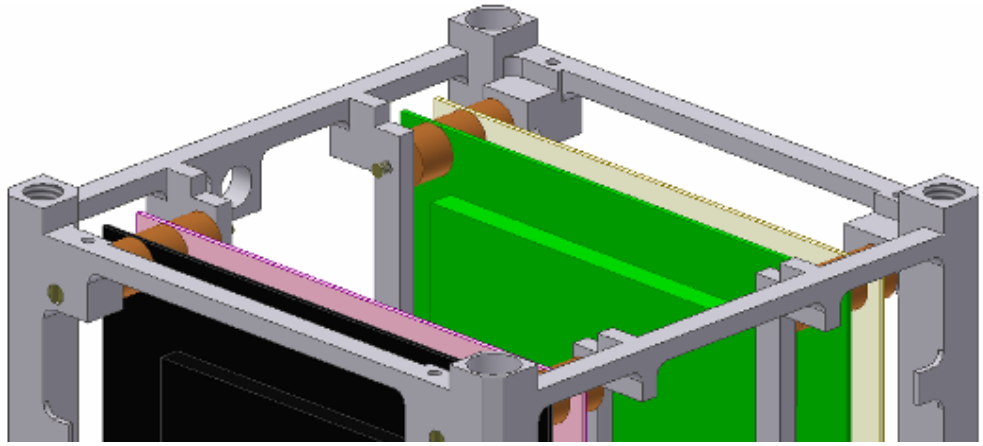

**Figure 18 View of the spacers stacked with PCBs.**

### 4.1.3 Sides and top panels

The face plate provides the surface for the mounting of external components (solar cells, magnetic torquers, sun sensor).

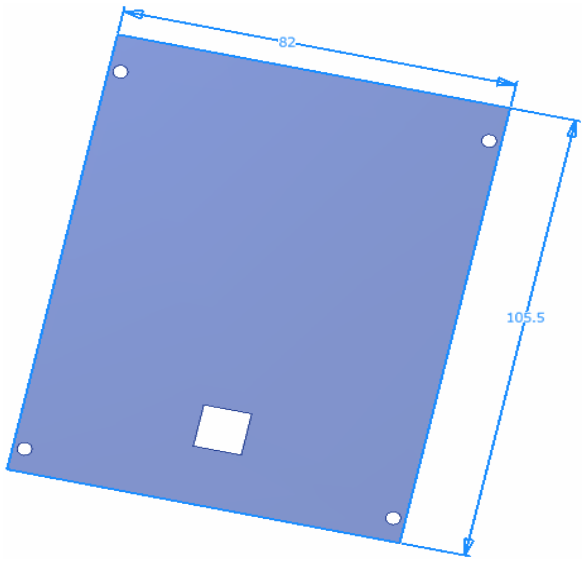


**Figure 19 View of the side panel.**

As shown in Figure 19 the side panel is a rectangular composite plate with a size of 82mm wide by 105.5mm long and a thickness of 0.8 mm. This part includes a hole for the sun sensor. Two or three side panels are used in the structural subsystem, with a mass of 13g for each one. The number depends if a composite or aluminum side panel is used for the mounting of the antenna deployment subsystem.

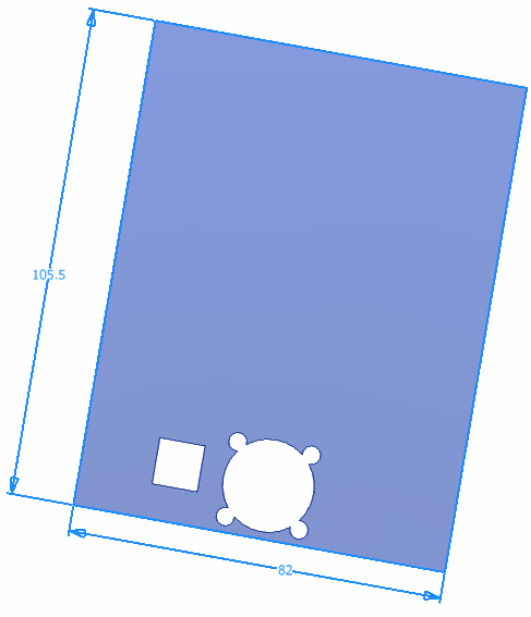


**Figure 20 View of the payload panel.**

The payload panel has the same external dimensions as the side panel, and includes an extra hole for the optic aperture of the payload. One payload panels is used in the structural subsystem, with a mass of 13g.

The top and bottom plates have a slightly different geometry; 100mm wide by 100mm long with cut-outs at the corners (see Figure 21). These parts include a hole for the sun sensor. They are fabricated from the same 0.8 mm thick composite plate as the side plates. The mass is 13g. Two top panels are used in the structural subsystem.

It must be noted that there is a possibility to have more holes in some of the panels for depressurizing.

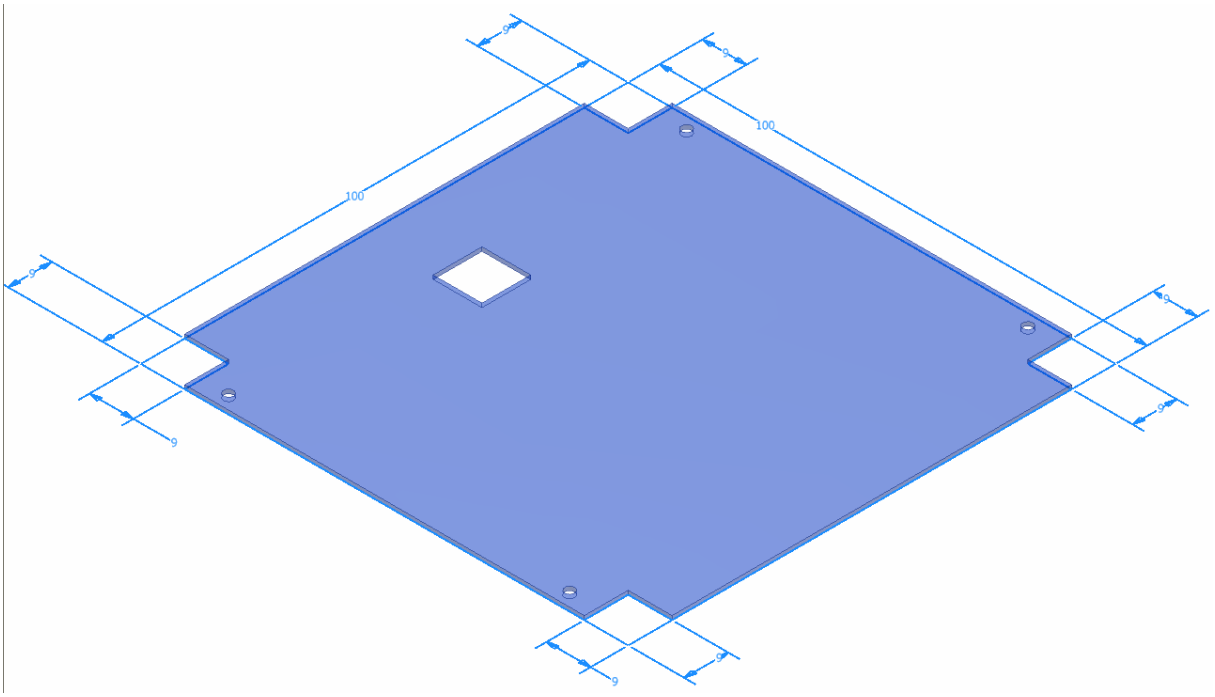


**Figure 21 View of the top panel.**

## 4.2 Configuration

The kind of internal layout is directed by two principal restrictions: the payload and the arrangement of PCBs. The ideal configuration is that which optimizes these both constraints at the same time.

### 4.2.1 Payload subassembly

The payload subassembly is composed by (see Figure 22):

- The payload frame. From Titanium (see Appendix C.2) in order to have a CTE near the lens CTE. One extremity of the frame integrates the payload baffle i.e. a conical aperture that permits to have a field of view of 120° (see Figure 23).
- The detector; its dimensions are 12x12x2.5 $mm^3$.
- The headboard; it contains some electronics; the rest of the payload electronic is on another PCB (TBD).

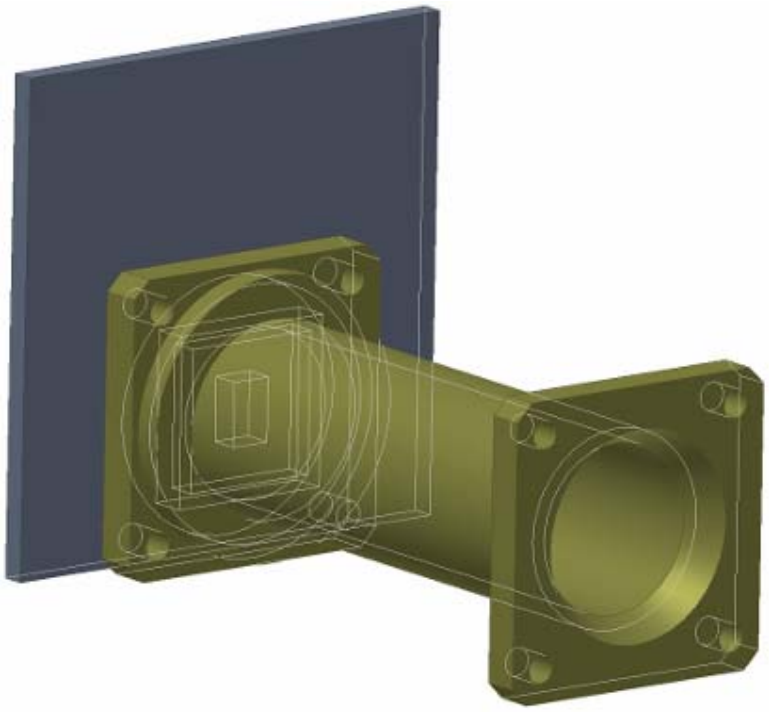

**Figure 22 Payload subassembly.**

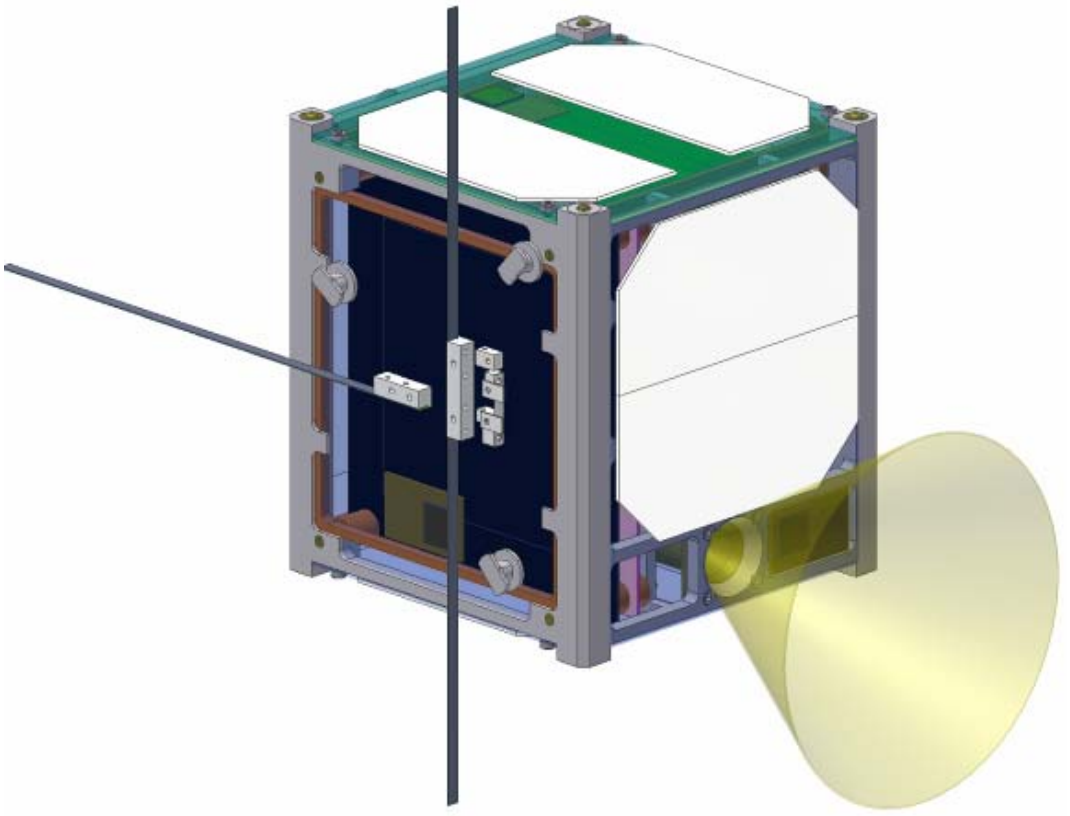

**Figure 23 Payload with its FOV.**

### 4.2.2 Electronic boards

The various electronics boards are:

- basic PCB
- motherboard

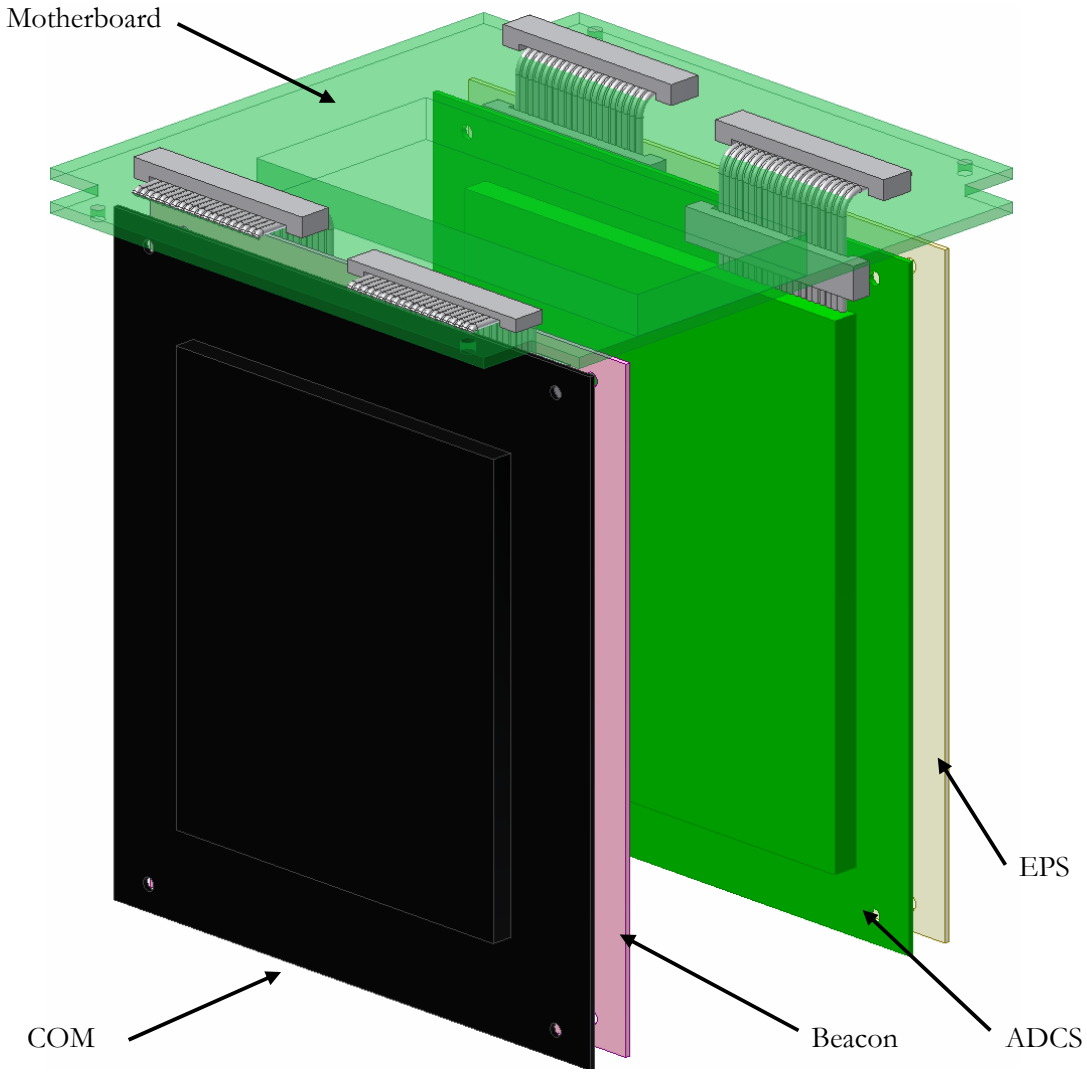


**Figure 24 SwissCube PCBs.**

The basic PCB is a rectangular shape with dimensions of 90x99mm (see Figure 25). Additionally, there will be holes passing through the PCBs for the screws. The spacers hold the PCB in the four corners and establish a thermal contact to the main frame. The PCBs will be fabricated from FR-4

material (TBC), which is a composite material (glass fiber reinforced epoxy). The standard thickness of a 6 layers PCB being 0.8mm, the weight of a PCB of this surface will be 13g. The estimated free place for electronic components corresponds to the external dimensions without the corners, for the both faces.

The following subsystem will have their proper PCB: EPS, ADCS, BEACON and COM (see Figure 24). For connectical reasons the COM and BEACON as well as ADCS and EPS PCBs have to be next to each other.

Additionally, the payload subsystem requires a small proper PCB which will be fixed on the battery boy or attached onto the internal crossbars. This PCB will only feature few components and thus the estimated dimensions where taken as 30mm x 40mm (TBC).

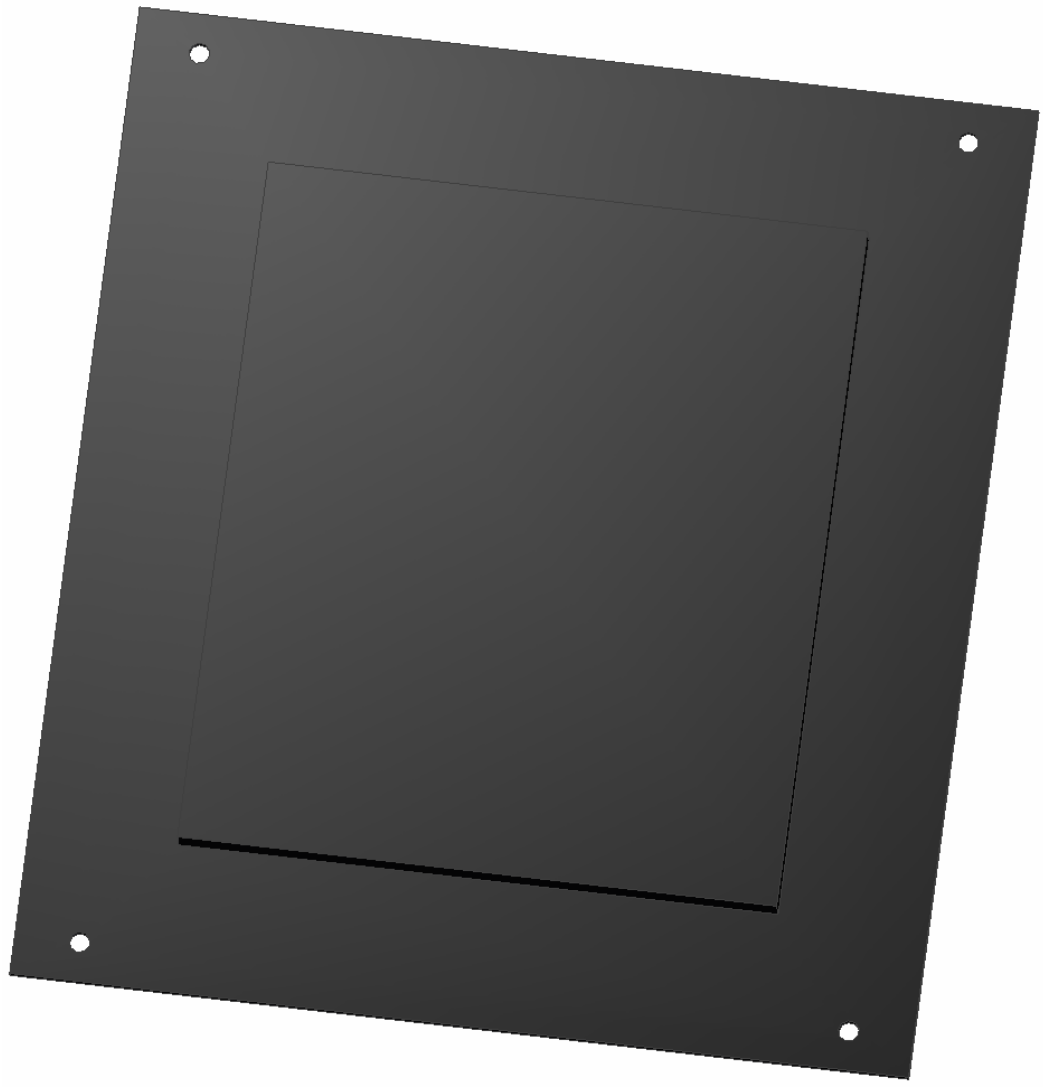

**Figure 25 View of the basic PCB.**

The motherboard PCB does not only serve as a connectic board, but has also the function of a proper electronic board for the CDMS subsystem. This has the advantage of having an essential subsystem for the data flow between the various subsystems in a central position of the data

transfer. Its dimensions are 100x100mm$^2$ with cut-outs at the corners and with a thickness of 0.8mm. The placement of an electronic subsystem on the motherboard is due to additional free place in center because of the placement of the PCBs at the sides (see Figure 26). The estimated free place for electronic components is 40mm x 85mm (TBC) for the internal face.

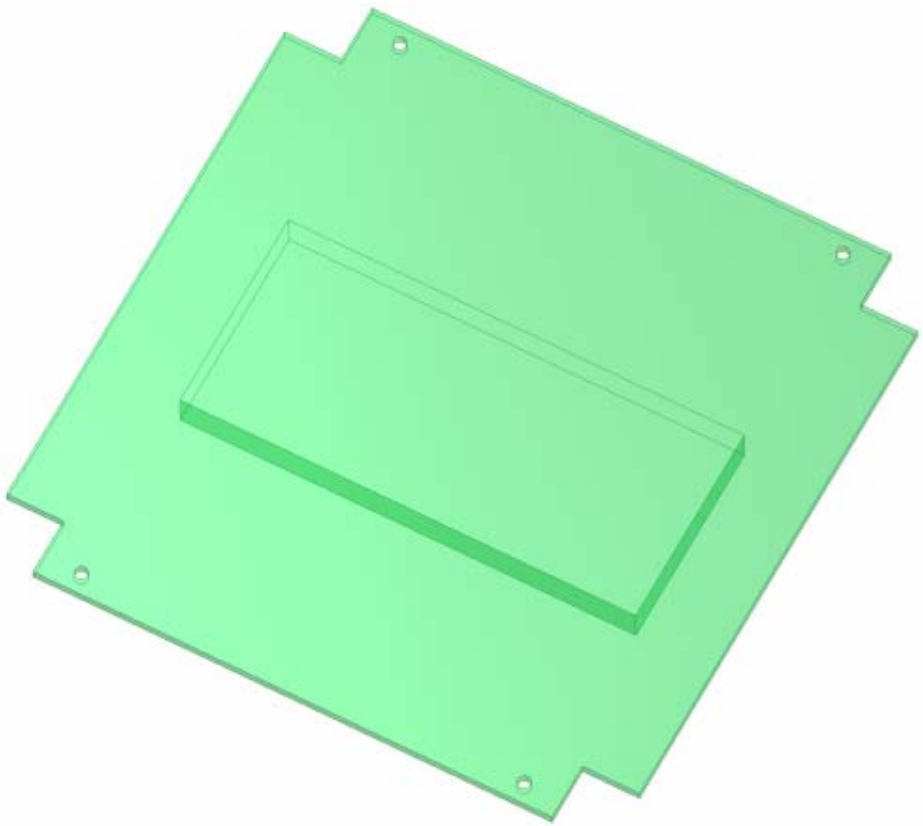

**Figure 26 View of the motherboard.**

### 4.2.3 ADCS subsystem

The ADCS subsystem is formed by (see Figure 27):

- 6 sun sensors, one per face, attached to the internal face of composite panel
- 3 magneto-torquers, one per axis. Currently they are inserted and attach on the frame (between the rails), but one of them is very complicated to insert. A solution can be to reduce a little bit the dimensions of them and attach them to the internal face of composite panel
- 1 wheel subassembly, attached by its axis to the frame. With a thickness of 7mm.

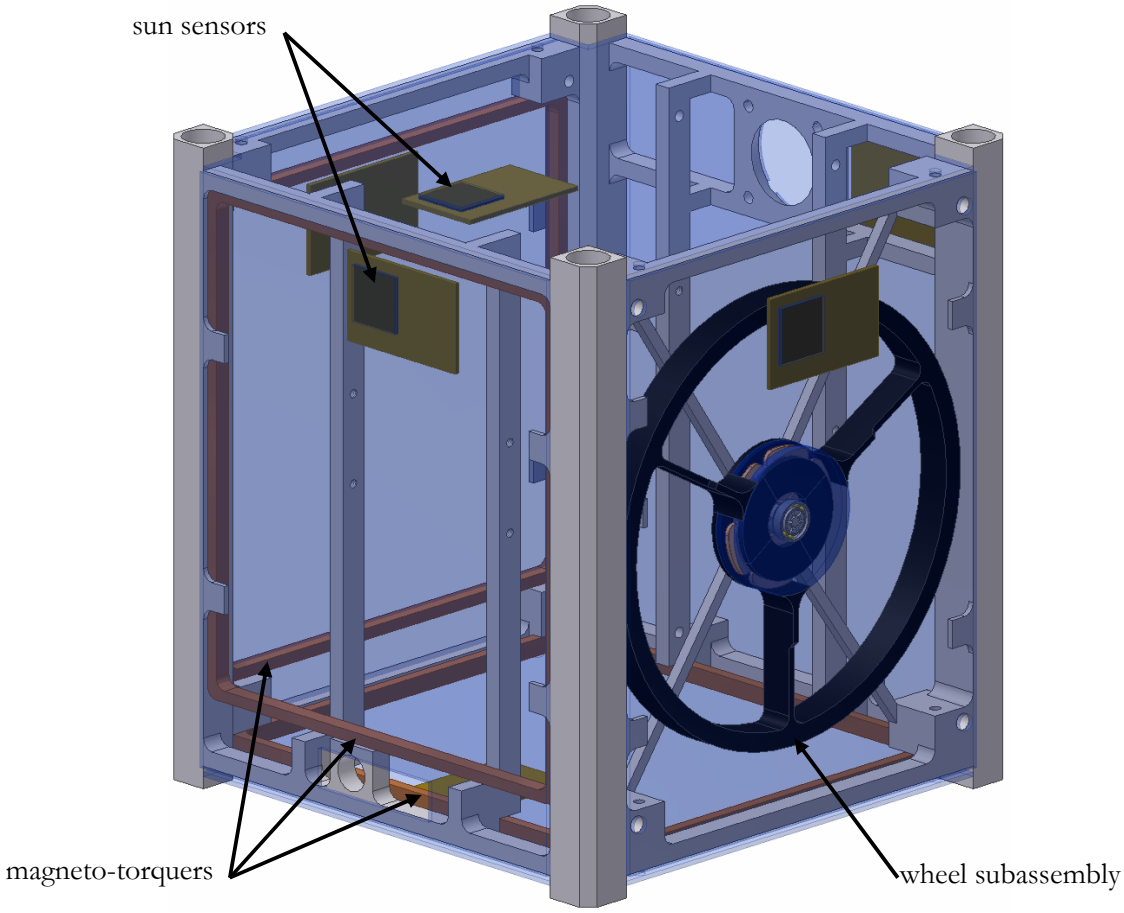


**Figure 27 Components of ADCS subassembly.**

## 4.3 Composite panels

Composite panels have been selected mostly because of the lightweight; a density lower than aluminum, approximately 40-60%, depending on the product. But the use of composite will engender drawback: lower thermal conductivity as well as a lower capacity to absorb of radiations compared to aluminum. One solution of the last disadvantage could be to use a thin layer of aluminum on one face of the composite panels.

There are six panels that will be glued and screwed to the aluminum frame. The four sided panels (82x105mm) would be glued before the qualification test to the frame. The upper and lower panels (100x100mm, +Z and -Z, see referential in Figure 15) would be screwed for the qualification and acceptance tests, and in the flight configuration.

The function of these composites panels are the following:

- structural support for the solar cells

- structural support for the deployment mechanism
- structural support for the magnetic torquers and sun sensors
- thermal path between the solar cells and the frame
- electrical isolator between the solar cells (positive pole) and the frame (ground)
- micrometeoroids protection and radiation protection

### 4.3.1 Elastic behavior of multidirectional laminates

To understand the particular properties of composite materials, a short overview coming from *Engineering mechanics of composite materials* [7] are stated in the following paragraphs.

Composite materials can be viewed and analyzed at different levels and on different scales, depending on the particular characteristics and behavior under consideration. A schematic diagram of the various levels of consideration and the corresponding types of analysis is shown in Figure 28

At the constituent level the scale of observation is on the order of the fiber diameter, particle size, or matrix interstices between reinforcement. *Micromechanics* is the study of the interactions of the constituents on this microscopic level. *Micromechanics* allows for the prediction of average behavior at the lamina level as a function of constituent properties and local conditions.

At the lamina level it is usually more expeditious to consider the material homogeneous, anisotropic, and use average properties in the analysis. This type of analysis is called *macromechanics* and considers the unidirectional lamina as a quasi-homogeneous anisotropic material with its own average stiffness and strength properties.

At the laminate level the macromechanical analysis is applied in the form of lamination theory dealing with overall behavior as a function of lamina properties and stacking sequence.

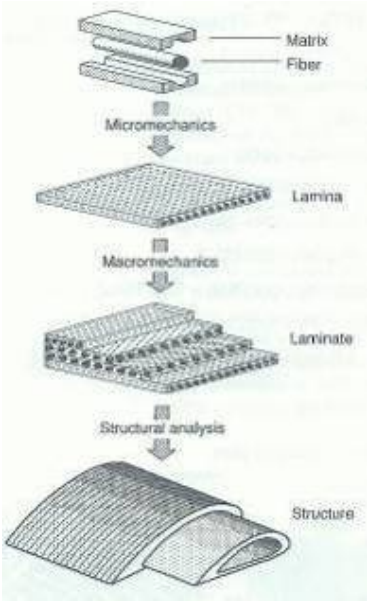


**Figure 28 Levels of observation and types of analysis for composite materials.**

### 4.3.2 Type of Fiber

The reinforcement phase of a composite may be in the form of continuous or short fibers, or particles of various shapes. It contributes to or determines the composites stiffness and strength.

A large variety of fibers are available as reinforcement for composites. The desirable characteristics of most reinforcing fibers are high strength, and stiffness, and relatively low density. Each type of fiber has its own advantages and disadvantages.

The selected fibers are unidirectional fibers M55J from TORAY (see datasheet in D.1). Its main characteristics are a tensile strength of 4.02 GPa, a tensile modulus of 540 GPa and a density of 1.91 g/cm$^3$. It should be noted that this fiber is one of the best high modulus fiber, in term of tensile modulus.

### 4.3.3 Type of Matrix

The main role of the matrix, especially in the case of high-performance composites, is to provide protection and support for the sensitive fibers and local stress transfer from one fiber to another.

The selected matrix is HexPly M18 from Hexcel (see D.2), an epoxy matrix. Its main characteristics are a tensile strength of 81.1 MPa, a tensile modulus of 3.5 GPa and a density of 1.16 g/cm$^3$. The matrix volume ratio is 44%, the mass ratio is 32%.

### 4.3.4 Type of Lamina

A lamina, or ply, is a plane (or curved) layer of unidirectional fibers or woven fabric in a matrix. The lamina is a orthotropic material with principal material axes in the direction of the fibers (longitudinal), normal to the fiber in the plane of the lamina (in-plane transverse), and normal to the plane of the lamina, see Figure 29

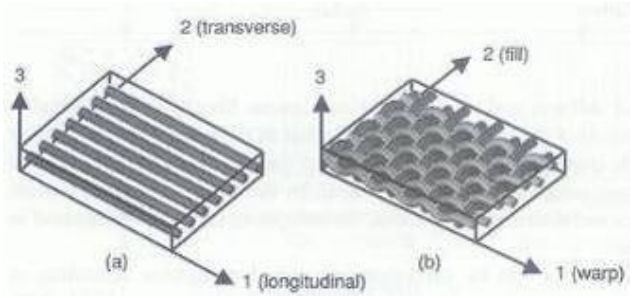


**Figure 29 Lamina and principal coordinate axes: (a) unidirectional reinforcement (b) woven fabric reinforcement.**

For our project, unidirectional fibers are used since the desired composite parts have a simple shape (plate) and in order to have a high stiffness.

The physical properties of each ply are computed from the properties of the fibers and the matrix using the so-called rule of mixtures. For example, longitudinal properties of a lamina are:

$$E_1 = V_f E_{1f} + V_m E_m$$

where $E_{1f}$ and $E_m$ are longitudinal fiber and matrix moduli, respectively, and $V_f$ and $V_m$ are the fiber and matrix volume ratio, respectively. In the relation above it is assumed that the fiber can be anisotropic and that the matrix is isotropic. The same assumptions lead to a similar relation for the major (longitudinal) Poisson's ratio:

$$\nu_{12} = V_f \nu_{12f} + V_m \nu_m$$

This method gives the following values for the physical properties of a ply:

$E_1$ = 297GPa $E_2$ = 6.5GPa $G_{12}$ = 3GPa

$\eta_{12}$ = 0.35 $\alpha_1 = -1 \cdot 10^{-6}\ K^{-1}$ $\alpha_2 = 4{,}1 \cdot 10^{-5}\ K^{-1}$

### 4.3.5 Type of Laminate

A laminate is made up of two or more unidirectional laminae or plies stacked together at various orientations. The laminae (or plies, or layers) can be of various thicknesses and consist of different materials. Since the orientation of the principal material axes varies from ply to ply, it more convenient to analyze laminates using a common fixed system or coordinates (x, y, z). The orientation of a given ply is given by the angle between the reference x-axis and the major principal material axis of the ply, measured in counterclockwise direction on the x-y plane (see Figure 30).

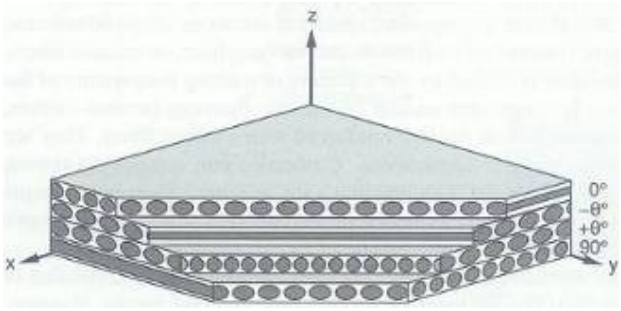


**Figure 30 Multidirectional laminate and referred coordinate system.**

It is apparent that the overall behavior of a multidirectional laminate is a function of the properties and stacking sequence of the individual layers.

An eight plies composite panel of 320mm x 470mm has been manufactured. The desired orientation was $[0,90,45,-45]_s$ but due to a human mistake the achieved orientation is [0,90,45,-45,45,-45,90,0]. The consequence of this error is a warpage of the panel due to asymmetry of the stacking sequence.

### 4.3.6 Determination of properties for multidirectional laminates

The *Engineering mechanics of composite materials* [7] gives the following flowchart for the determination of engineering properties of multidirectional laminates:

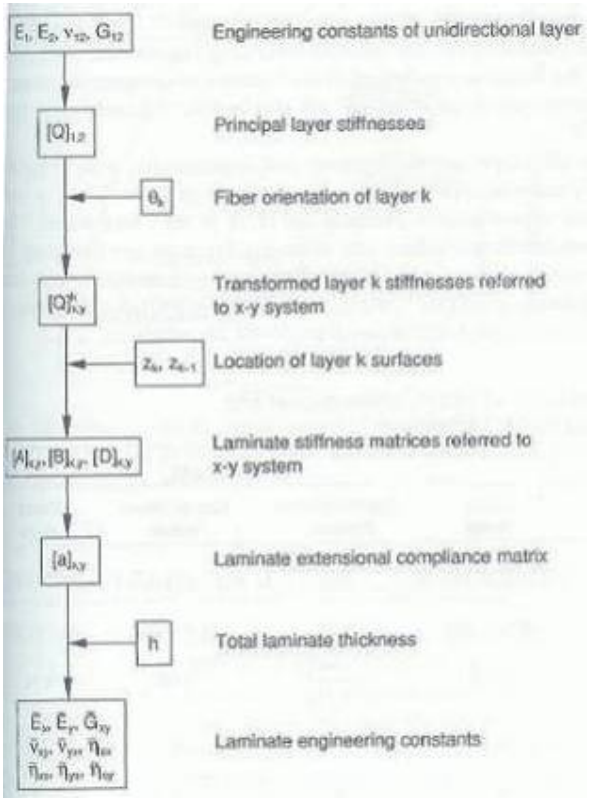


**Figure 31 Flowchart for computation of engineering elastic properties of multidirectional laminates.**

After having defined the physical properties of a ply, the orientation and thickness of each ply are considered in order to obtain the properties of the whole laminate. A mathematical script developed in a Material Science lab of the EPFL has been used to obtain the Young's modulus, shear modulus and CTE. The results are:

$E_x = 103.6GPa$ $E_y = 103.6GPa$ $G_{xy} = 38.9GPa$

$CTE_x = 3.26 \cdot 10^{-7}\ K^{-1}$ $CTE_y = 3.26 \cdot 10^{-7}\ K^{-1}$

Remarks: the CTE is very low. The reason is the negative CTE of a ply in the 0° direction combined with a very high tensile modulus is the same direction. The low CTE for the multidirectional laminate is maybe a problem, because the adhesive joint is between the aluminum with a CTE of 23.6 μm/m ·K and composite panel with a CTE of 0.326 μm/m ·K. Another kind of fiber with a lower tensile modulus or positive CTE in 0° direction could be envisaged in order to have a global CTE closer of the aluminum CTE.

### 4.3.7 Manufacturing of composite panels

In January 2007 an eight plies composite panel of 320mm x 470mm has been manufactured at RUAG-Aerospace.

The plies have been stacked one onto another between two aluminium plates (see Figure 32).

**Figure 32 Preparation of the aluminum plate and cutting of plies.**

The selected manufacturing method was hot pressing. The temperature has been progressively increased from ambient temperature to 180°C and maintained at that level during 2 hours. The initial force of the press was 85 kN. Due to the warming and dilatation of the machine, the final force after 2 hours at 180°C was around 180 kN.

The data concerning the manufacturing process are in Appendix D.3. To finish, the big composite panel has been cutted using waterjet cutting technology.

**Figure 33 Hot press used for the manufacturing.**

## 4.4 Structural adhesive

Structural adhesives present different major advantages over more traditional fastening methods. Firstly, adhesives are the most lightweight method for joining different mechanical parts. Additionally, they only create a weak stress concentration at the interface. Adhesives can be used to join different kinds of materials which in some cases are beneficial since they provide stress relief through deformation for materials with different thermal expansion coefficients.

The major disadvantage of adhesive bonding is that disassembly is generally impossible once parts are attached. In addition to this, adhesives that are subject to thermal cycling may degrade and thus become brittle. Different types of adhesives (silicones…) are prohibited for space use since contamination is risked in vacuum conditions. Adhesives also provide a weak thermal and electrical conductivity, which might certainly lead to problems for joining parts where heat dissipation is required [9].

The selection of the optimal adhesive will be based on different parameters. First of all, thermal properties have to be suitable for an optimal heat transfer between the different structural parts and the solar cells and the adhesive has to be applicable in a large temperature range. Additionally, the cure temperature of the epoxy resin should be as low as possible, in order to allow fixing of the side plates without endangering any of the electronic components. A reasonable cure temperature is 80°C since the electronic components will have to be designed for these temperatures in order to pass thermal vacuum testing. In addition to this, the adhesives' physical properties such as the shear strength need to be as high as possible, in order to resist stresses induced by the CTE mismatch between the aluminum frame and the composite plates.

During Phase A, the preferred choice for the structural adhesive was ScotchWeld 2216 from 3M. For the Phase B, more researches was made in order to find a more suitable adhesive (see in Appendix E the table with various options), especially to have a very good thermal conductivity and at the same time to be an electrical insulator. The backside of the solar cells is the positive pole, so no electrical connection between the cell and the composite panels shall take place.

To satisfy the selection criteria like low outgassing, good thermal conductivity, high resistivity, low cure temperature as well as a high shear stress, the epoxy H74 from EPO-TEK manufacturer is selected for the Phase B. The typical properties of its glue are stated in Appendix E.2.

### 4.4.1 Process of adhesive bonding [8]

Process conditions and environments shall be specified and strictly controlled during all stages of adhesive bonding, i.e. during preparation, application, curing or drying, inspection or testing and storage.

- Surfaces to be bonded shall be cleaned and prepared by a surface treatment process (e.g. abrasion and chemical etching) under strict control. Prepared surfaces shall be protected from contaminants. During the bonding process, the adhesive cure cycle shall be controlled. For guidelines on structural adhesive bonding see ECSS--E--30--05.
- Good toughness and peel strength are applicable characteristics for structural adhesives. Bonded primary structural joints shall demonstrate cohesive failure modes in shear.

- An insert system consists of a removable threaded fastener and a fixture that is embedded into the honeycomb structure using a potting compound. The general processing steps for installing inserts include: machining the honeycomb panel, normally using specific tools; potting the insert; curing the potting material. For guidelines on the use of inserts see ECSS--E--30--06.

It is very easy to misuse adhesives, particularly in critical applications. They normally have a limited shelf life (marked on the packaging and suppliers' data sheets) which shall be respected, and the conditions under which they are stored shall be adequately controlled (see ECSS--Q--70--22). They frequently have a short "pot-life" or "working life" after their component parts are mixed or brought to activation temperature.

The adhesive shall be physically and chemically compatible with the component parts to be bonded:

- Physically, the adhesive shall attach itself to the two surfaces to be bonded and in general this needs special pre-treatment (cleaning, etching, priming). The adhesive shall also be capable of accommodating dimensional changes in the bonded surfaces (expansion-coefficient matching).
- Chemically, the adhesive shall not be corrosive to the adherents used (corrosion action is frequently due to hardeners).

## 4.5 Mechanical fastener

Screws are used to attach various components like payload frame, PCBs stacks, top and bottom composite panels. The currently size is M2. In order to save weight, the long M2 screws will be machined from Titanium, because the density is 40% smaller as stainless steel.

It should be noted that the screws will probably be glued after all the functional test, just before launch, in order to avoid unscrew due to launch vibrations. The type of adhesive for this case should be investigated more into details.

## 4.6 Kill-switch

When loaded into the deployer, all CubeSat power must be completely off, and the CubeSats may only be powered on once clear of the tube. This is a requirement of the P-POD deployment mechanism. To accomplish this, one or two kill switches (microswitches) must be mounted to the exterior of each CubeSat (in designated areas stipulated on the requirements drawings) to turn off all power when compressed, so when stacked in the P-POD, no error should cause a malicious early

deployment of antennas, and in the same time this conserves power for the early stages of the space mission. Also, the microswitches must be flush with the CubeSat surface when compressed. Two switches are used. As the satellite is released from the deployment device, the buttons are allowed to spring out, deactivating the kill-switches and allowing electricity to get to the timer, which will then start a countdown for the deployment of the antennas. For more details about the electrical role of these two switches, see the report of the EPS team.

The deployment switches should be located at designated points from CubeSat design specifications document of Calpoly (see Figure 34).

To satisfy the designated location, many options were studied. The most elegant solution is to have a pushbutton switch directly in the feet of the structure. In this case, the switch shall have very small external dimensions such as an external diameter no more than 8 mm.

The selected pushbutton switch is the 39-2 from Grayhill. These main dimensions and characteristics are given in Figure 35. From more details, see Appendix F.

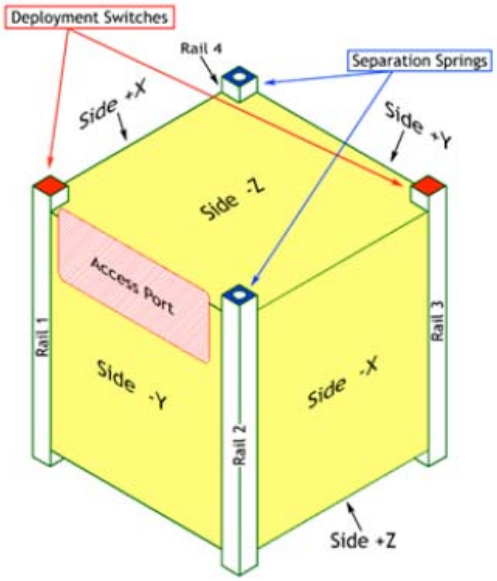


**Figure 34 Location of the kill switches.**

These switch electrical properties can seem to be very poor, but the number of commutation will be very low in our case. So the switch can accept a higher current than specified in datasheet. This component has been tested to ensure that it will satisfy our specifications concerning electrical properties and environment. The tests are explained in the EPS report of F. Jordan.

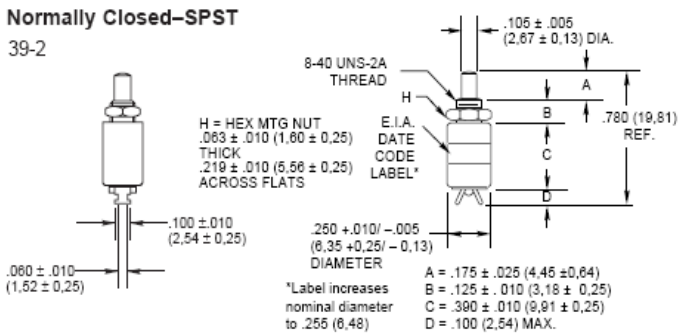


| Rating at 115 Vac Resistive | Rating at 220 Vac Resistive | Operations at Rated Load | Part Number | Cap Color |
|---|---|---|---|---|
| 1/4 Amp | 1/8 Amp | 250,000 | 39-2 | Black |

| Action | Total Travel | Actuating Force (oz.) | Mtg. Hole |
|---|---|---|---|
| Momentary | .042 ± .010 (1,07 ± 0,25) | + 4 4 – 2 | .172 (4,37) DIA. |

**Figure 35 39-2 Pushbutton Switch from Grayhill.**

Some investigations should still be done to ensure that this component has suitable properties regarding the outgassing because no information was found for the plastic constituting the push-button.

For the interface of the kill-switches with the monobloc frame, a cylindrical adapter is used (see Figure 36). This adapter is screwed onto the threaded head of the switch, and then this subassembly is inserted into the foot and glued with epoxy. Holes in the both feet shall be included in order to connect the switch to the EPS board.

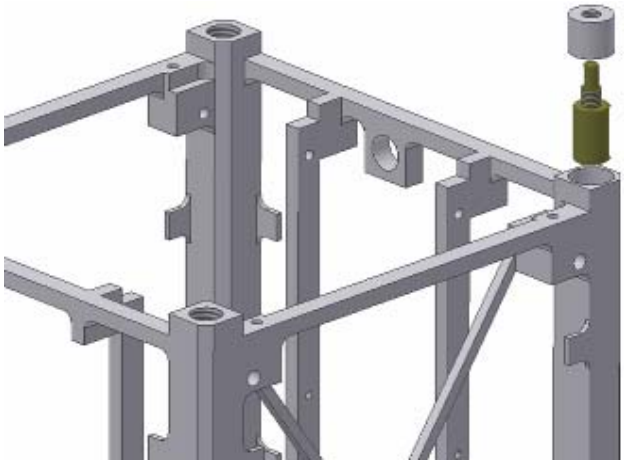

**Figure 36 Interface of the kill-switch.**

## 4.7 Remove before flight pin

Along with the kill switches there is also a requirement for a "remove before flight" (RBF) pin, to disable the satellite before and during integration with the deployer. Once the satellites are loaded into the P-POD, the RBF pin is removed. The RBF pins must fit within the designated data ports, see Appendix A. The RBF pins should not protrude more than 6.5 mm from the rails when fully inserted.

The main criteria for the selection of this component are: mass, volume electrical reliability. To satisfy these conditions, the selected component for the RBF pin is the same as the kill-switch, the pushbutton switch 39-2 from Grayhill.

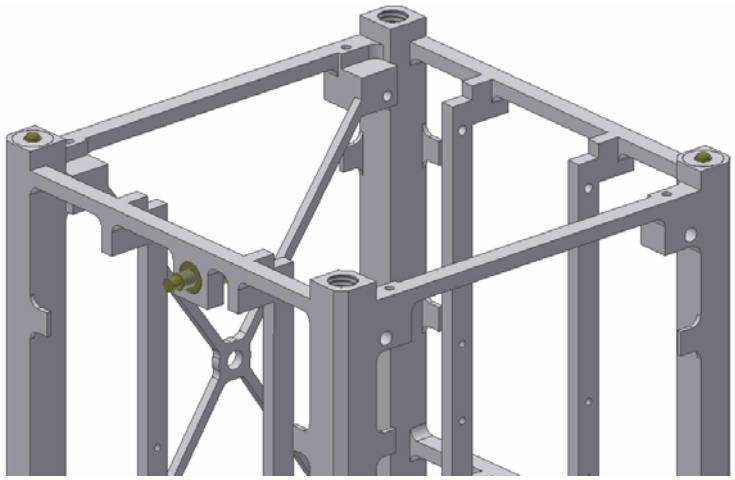

**Figure 37 Interface of the RBF pin.**

For the interface of RBF pin with the monobloc frame, a cylindrical hole is included in the frame (see Figure 37). The switch is simply inserted and glued in this hole.

## 4.8 Battery box

A common problem with LiPo battery cell is that they may rapidly loose performance and eventually entirely cease function when subjected to a high vacuum. Typically this effect is related to a physical expansion of the battery block. To counteract this effect on SwissCube, it is enclosed in a milled aluminum box. The gap between this box and the both LiPo cell is filled with epoxy resin. Beside the need to protect the cell from the harsh environment, this is also a solution to provide mechanical interface between the cell and the satellite structure. Depending of the results of thermal simulations and tests, the batteries can be insulated with something like Kapton film or at the opposite, glued with a thermally conductive glued.

This part uses electro-erosion technology for its machining. In this way, thin walls (around 0.8mm) and inner right angles are possible.

Figure 38 shows the interface of the battery box with the monobloc frame. This box will be slided into the frame and then attached thanks to the use of M2 screws.

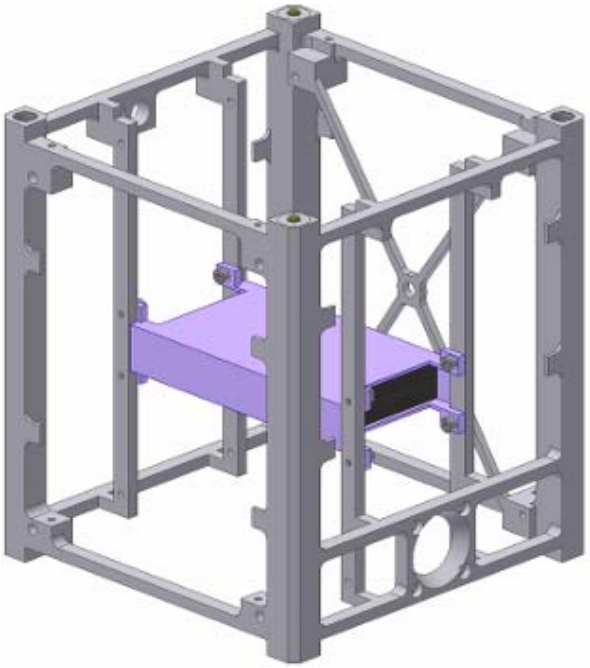

**Figure 38 Interface of the battery box.**

## 4.9 Separation Springs

SwissCube will have a total of two separation springs, each of which will be in diagonally opposite rail feet on the top side of the CubeSat. These springs will give a relative velocity after deployment from the P-POD to separate from the other two CubeSats. The separation springs should be located at designated points in Figure 34. To accommodate the plungers, a threaded hole must be included in the top ends of the rails.

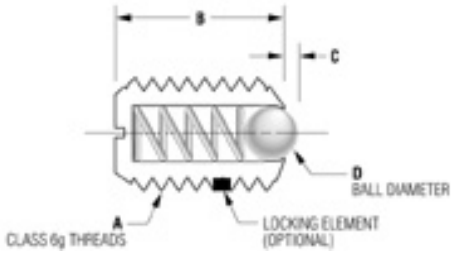


**Figure 39 Ball plunger SBML6 from Vlier.**

The springs suggested in the CubeSat Specification Document are McMaster Carr (P/N: 84985A76). For practical reason, ball plunger SBML6 from Vlier has been selected. The dimensions and initial and final end forces are the same as component from McMaster Carr, the only difference is the metric thread, more useful in our case. This spring is represented in Figure 39, with the following values: A = M6 x 1.0; B = 14 mm; C = 1 mm; D = 3.5 mm. This component is threaded in the main frame (see Figure 40). To ensure no unscrew, epoxy is used.

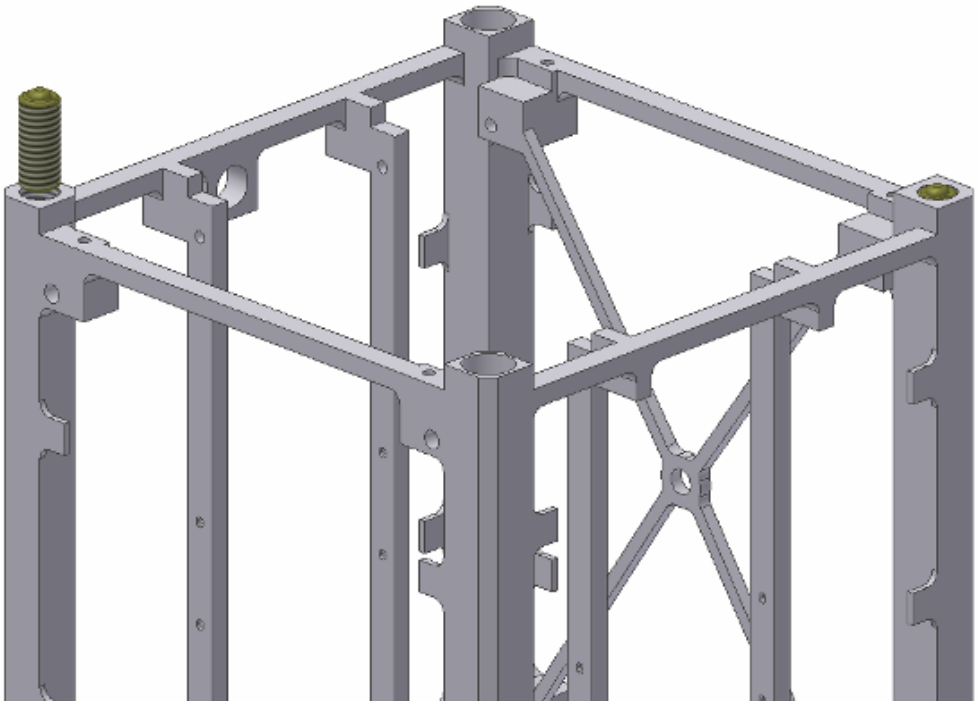

**Figure 40 Interface of the separation springs.**

## 4.10 Ribbon cables

In order to connect the various electronic boards, a solution with flat ribbon cable was examined. The selected type of cable was UHV Ribbon cables from Caburn, see Appendix H.

This ribbon cable is directly welded onto the PCBs and a stress relief protects the welding from mechanical stress. This option has the following advantages: lightweight in comparison with traditional connectors, possibility to mount/unmount in comparison with full flex-rigid PCB solution.

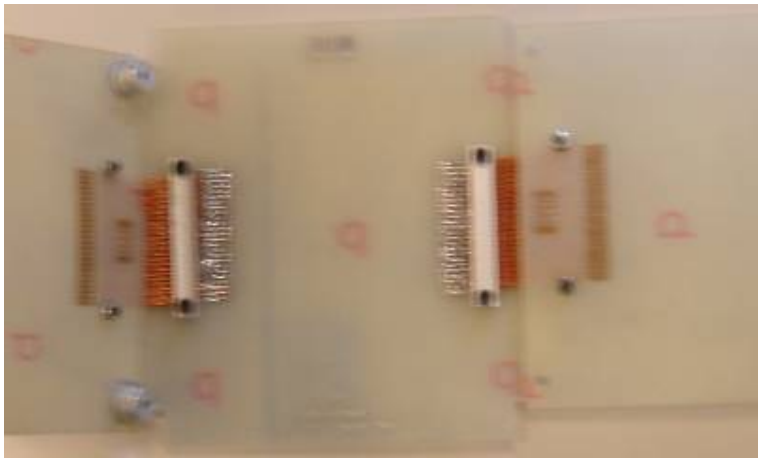

**Figure 41 Ribbon cable connections and stress relief.**

Unfortunately, during integration of the structural model, the high stiffness of this type of cable has been noticed. This problem makes the integration of the PCB in the structure more difficult than envisaged. The reason of this high stiffness is probably the Kapton material used as insulator.

Other options shall be foreseen during next semester. A possibility is maybe the use of ribbon cables with PTFE as insulator (see Appendix H about HV PTFE Ribbon cable).

## 4.11 Access port

The access port allows communicating with the satellite when inserted inside the P-POD. It should be located at designated area in Appendix A. The main criteria for this component are: weight, volume, space grade component and reliability.

The selected type of access port is a D-Sub miniature from Omnetic, the model Bi-lobe Nano, see Figure 42 and datasheet in Appendix I. The interface with the frame shall still to be defined, maybe screwed or glued.


**Figure 42 Omnetics Bi-Lobe connectors.**

## 4.12 Spring Washers

To damp the vibration at the PCB level, spring washers can be used between the frame and a spacer. The datasheet is stated in Appendix J. For the structural model the spring washers was not used. The reason is the relative flexibility of the internal crossbars; the small clearance necessary to insert the PCBs and spacer can be compensating when screwing all these things together.

## 4.13 Hard-anodizing

To achieve anti-friction properties, it is required that parts, which are in direct contact with the deployer, will be hard-anodized. Hard-anodizing is a term used to describe the production of anodic coatings with film hardness or abrasion resistance as their primary characteristic. The coatings give also very good electrical insulation. The thicknesses are usually between 25 and 250 μm, and the anodizing time can be up to 240 minutes. Most hard anodizing processes are based on sulphuric acid.

Another advantage of the hard-anodizing of aluminum is the surface treatment. The condition for good adhesion properties are clean and stable surface. The surface of metals is generally covered with several impurities. The role of the anodization is to remove doubtful oxide layers and to create a new solid and protective layer of oxide in order to promote adhesion.

Due to limited time in the integration of the satellite, the hard anodizing has not been achieved. A specialized firm has been contacted, and the next version of the frame will be fully hard-anodized, except one spot for the electrical ground.

For the structural model, the following surface treatment has been used: areas of the aluminum frame have been etched with sulphuric acid in order to remove the thin oxide layer, then these areas have been cleaned with acetone and at once glued with composite panels.

## 4.14 Assembly procedure

It is assumed that major assemblies of the panels are done in advance, meaning that solar cells, sun sensors and magnetic torquers are mounted on the panels. The electrical boards are also assembled together before the integration into the satellite. The assembly procedure is based on the allowed design space of each PCB, which gives a relatively complicated assembly procedure, since the design space only allows small clearance during assembly.

Here is a summary of the spacecraft assembly steps. During assembly two side panels the battery subassembly and inertial wheel are first attached to the spacecraft (stages 1 to 3). Secondly the internal PCB's including the motherboard and the payload are inserted and connected with the external components (4-7). The remaining side-panels are attached and connected (8).

The assembly procedure starts with the monobloc frame (see Figure 43 - I). The both springs plungers are screwed and glued in the feet of the frame. At the same time the both kill-switches are integrated and glued in the two remaining feet, using an adapter (see description in §4.6), their cables are routed in direction of the EPS position.

After that the battery subsystem is inserted and screwed on the internal crossbars, the cables are also routed in direction of the EPS position. The following stage consists of the integration of the access port and RBF pin (see Figure 43 - II). Afterwards two side panels (X+, X-) are glued (or screwed TBD) to the frame. The corresponding cables of these panels are arranged into the frame along the crossbars in order to optimize the future connections with the PCBs (see description in §4.15.1).

The next step consists of the integration and gluing of the wheel subassembly onto the frame (see Figure 43 - III).

The PCBs are mechanically connected together two by two thanks to the spacers. These components are glued onto the PCBs (see Figure 43 - IV). The both pairs of PCBs are fixed inside the satellite frame on the Y+ and Y- sides by M2 screws.

The motherboard is screwed (or glued TBD) onto the Z+ side of the frame and the connections between the PCBs and motherboard are done (see Figure 43 - V).

The inertial wheel is connected to the ADCS board and simultaneously the connections from the solar cells, sun sensors and magnetic torquers can be done to the corresponding PCBs. In addition the connections between batteries and EPS board can be established.

Then two remaining side panels (Y+, Y-) are glued (or screwed TBD) to the frame (see Figure 43 - VI). The corresponding cables of these panels are arranged into the frame along the crossbars in order to optimize the future connections with the PCBs (see description in §4.15.1).

Afterwards the payload subsystem is introduced between the PCB's stacks and fixed on the X+ side of the frame by M2 screws (see Figure 43 - VII). The electrical connections between the payload subsystem and the corresponding PCB are established.

To finish the top and bottom panels are fixed onto the frame by M2 screws and remaining wires from the solar cells sun sensors and magnetic torquers can be connected to the corresponding PCBs (see Figure 43 - VIII).

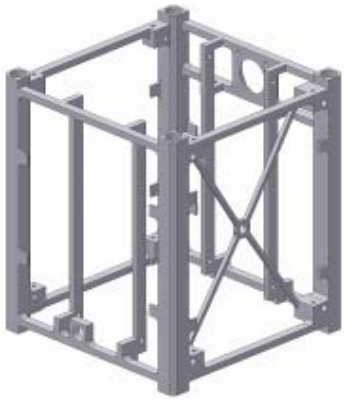

I

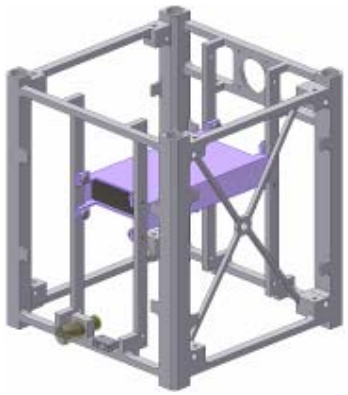

II

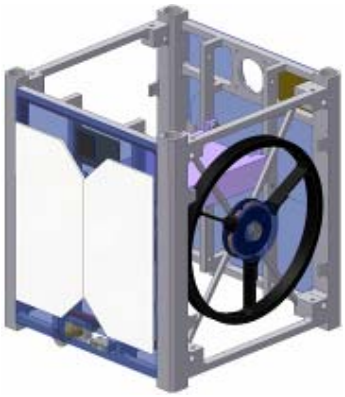

III

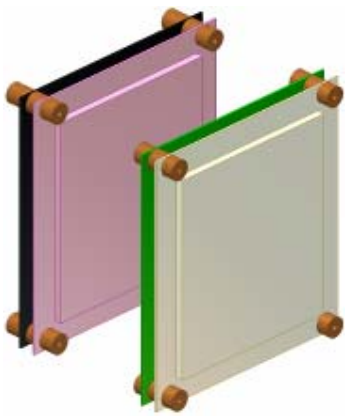

IV

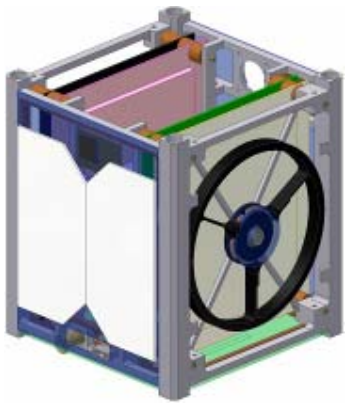

V

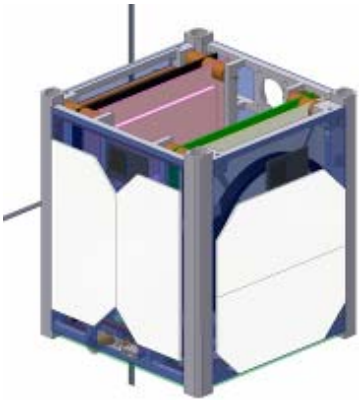

VI


**Figure 43 SwissCube assembly procedure.**

## 4.15 Cabling plan

Thanks to the use of a motherboard, the number of necessary wires will be reduced to a minimum. There will however, remain some separate wires, in particular to connect the solar panels as well as the magneto-torquers, sun sensors, batteries or wheel subassembly.

### 4.15.1 Between PCBs and external components

The various cables for the connections of external components are listed in Table 2.

**Table 2 I/O of external components.**

| From | To | Number of wire |
|---|---|---|
| Sun sensor X+ | ADCS | 6 |
| Sun sensor X- | ADCS | 6 |
| Sun sensor Y+ | ADCS | 6 |
| Sun sensor Y- | ADCS | 6 |
| Sun sensor Z+ | ADCS | 6 |
| Sun sensor Z- | ADCS | 6 |
| Solar cells X+ | EPS | 2 |
| Solar cells X+ | Ground | 2 |
| Solar cells X- | EPS | 2 |
| Solar cells X- | Ground | 2 |
| Solar cells Y+ | EPS | 2 |
| Solar cells Y+ | Ground | 2 |
| Solar cells Y- | EPS | 2 |

| | | |
|---|---|---|
| Solar cells Y- | Ground | 2 |
| Solar cells Z+ | EPS | 2 |
| Solar cells Z+ | Ground | 2 |
| Solar cells Z- | EPS | 2 |
| Solar cells Z- | Ground | 2 |
| Kill-switch 1 | EPS | 2 |
| Kill-switch 2 | EPS | 2 |
| RBF pin | EPS | 2 |
| Wheel subassembly | ADCS | 12 |
| Payload headboard | Payload | TBD |
| Antennas | COM | TBD |
| Access port | CDMS | TBD |

Like explained before, cables of these components are arranged into the frame along the various crossbars in order to optimize the future connections with the corresponding PCBs. The possibilities of directly weld these cables or the use of small connectors should be examined. During next semester, a real cabling plan will be done. The type of cables and possible very small connectors shall be evaluated.

### 4.15.2 Between PCBs

The connections between the various PCBs of the satellite are done with a ribbon cable. Like described previously the spacers will probably be glued on the PCBs in order to form 2 pairs of PCBs. After that these both PCBs stacks are inserted into the main frame and the cables of external components are connected to the corresponding boards (see Figure 44 - I). Afterwards, the motherboard is fixed (glued or screwed TBD) on the Z+ face of the frame. Then the connections between PCBs and motherboard are welded (see Figure 44 - II).

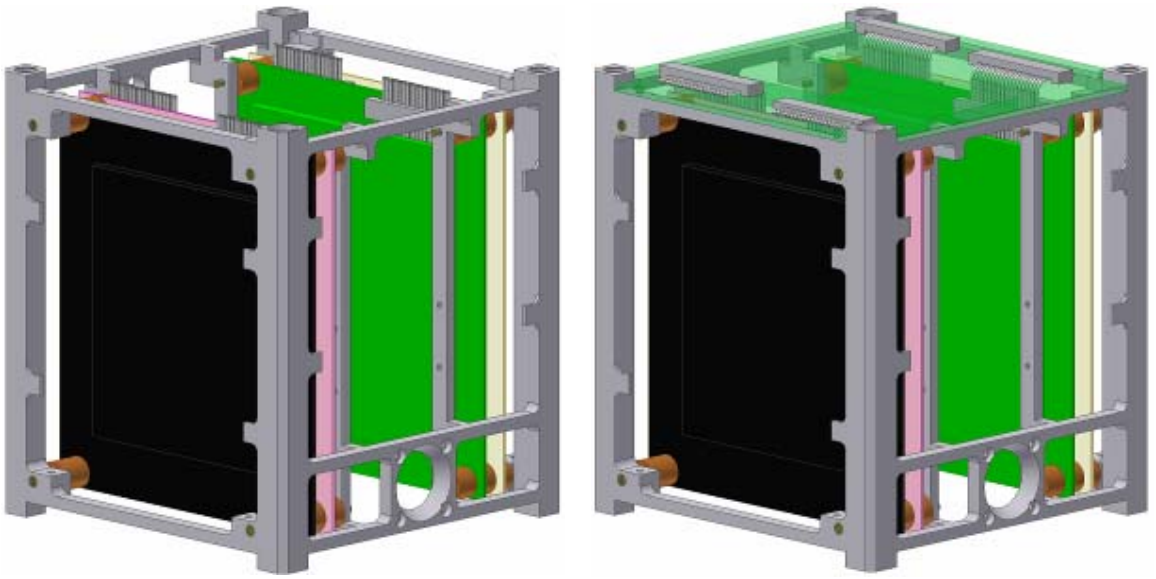

I II

**Figure 44 Connections between PCBs and Motherboard.**

# 5 VERIFICATION

The verification goals are primarily the design qualification ensuring moreover that the final product will be free from workmanship defects and acceptable for use. Furthermore the verification process must allow to assess that the satellites will be able to fulfil mission requirements and to confirm product integrity and performance after particular steps of the project life cycle (e.g. integration, test, pre-launch).

Coming from the Assembly Verification and Integration (AVI) plan, the verification process flow are subdivided in the following steps:

1. identifying a consistent set of verifiable project requirements which can be subjected to the verification process,
2. selecting methods of verification,
3. selecting levels of verification and the associated model philosophy,
4. selecting facilities,
5. identifying resources required, and
6. identifying the stages and the events in which the verification is implemented.

## 5.1 Verification methods

Verification shall be accomplished by one or more of the following verification methods:

a) test (including demonstration);
b) analysis (including similarity);
c) review-of-design;
d) inspection.

In the frame of this Master thesis, the verification methods were test, analysis and inspection.

#### 5.1.1.1 Test

The tests consist in vibration (random and sinusoidal) of the structural model of the satellite and three point flexural test of the solar cell. The details for these tests are stated in Chapter 7.

#### 5.1.1.2 Analysis

The analyses include inertial, static analysis as well as finite elements analysis of a simplified model of the satellite (see §6.5.1).

#### 5.1.1.3 Inspection

The verification method includes also inspection, especially after each vibration or shock test. The role of the inspection is to verify that the physical characteristics of the structural subsystem and other subsystem remain the same after every test.

## 5.2 Verification levels

The requirement verification is performed incrementally at different verification levels. The usual verification levels for a space project (in line with the definition of ECSS-E-00) are:

- equipment (e.g. valves, batteries and individual electronic boxes);
- subsystem (e.g. electrical power, attitude control, structure, thermal control and software);
- element (e.g. launcher, satellite and ground station);
- system (e.g. manned infrastructure system).

In the case of the vibration tests, the verification level is the whole satellite, so the element level. Concerning the FEA and static analyses, the verification levels are the whole satellite and in some case subsystems (main frame, structural components).

## 5.3 Verification stages

The verification process is implemented in subsequent verification stages all along the program life cycle. The verification stages are:

- qualification,
- acceptance,
- pre-launch,
- in-orbit.

The SwissCube project is in Phase B, so the verification stage is the qualification. The next stages will happen during the following Phase.

In the qualification stage the verification shall demonstrate that the design, including margins, meets all applicable requirements. The qualification levels shall be defined in order to cover the worst case environmental conditions, so they shall exceed the maximum predicted levels by a factor of safety which assures that, even with the worst combination of test tolerances, the flight levels will not exceed the qualification test levels.

# 6 STRUCTURAL ANALYSIS

After having described the structure and configuration design, its inertial or physical properties as its static and dynamic analysis were studied.

## 6.1 Physical and inertial Properties of the satellite

A mass analysis is performed on the complete structural model using Autodesk Inventor and the information received from this (center of mass location, total mass, moments of inertia etc.) is given below. Using this preliminary configuration, with the estimated masses and dimensions supplied by the other team members it is shown that the SwissCube will meet with the CubeSat specification with regard to the location of its center of mass.

### 6.1.1 Total mass

The mass budget is based on subsystem mass estimates. The maximum mass of the SwissCube cannot exceed one kilogram. Thus it is critical that the approximate mass of the satellite is known and updated throughout its development to ensure it stays within the weight restriction. The current mass budget, as of February 2007, is given in Table 3. The detailed mass budget can be found in the System Engineering Report of Bastien Despont.(S3-B-ADCS-1-4-AHWRepport.doc)

**Table 3 Mass budget per subsystems of boards/faces.**

| Subsystem | Mass [g] |
|---|---|
| Structure & Configuration | 273 |
| EPS | 188 |
| ADCS | 114 |
| CDMS | 33 |
| Payload | 47 |
| COM | 30 |
| Mechanism & antenna | 20 |
| Thermal | 4 |
| | |
| **Total** | **709** |
| | |
| **Boards / Faces** | **Mass [g]** |
| EPS board | 162 |
| ADCS board | 28 |
| CDMS board | 33 |
| Payload module | 48 |
| COM board | 30 |
| General structure | 234 |

| | |
|---|---|
| face +x | 20 |
| face -x | 36 |
| face +y | 49 |
| face -y | 15 |
| face +z | 36 |
| face -z | 20 |
| | |
| **Total** | **709** |

Currently, the SwissCube is within the 1 kg limit with a margin of 291 g. Though the CubeSat will most likely be heavier when finished, these 291 g provides a margin to work within.

### 6.1.2 Center of Mass and moments of Inertia

The center of mass and inertial properties are calculated from the center of reference frame, which is in the geometrical center of the cube (see Figure 45).

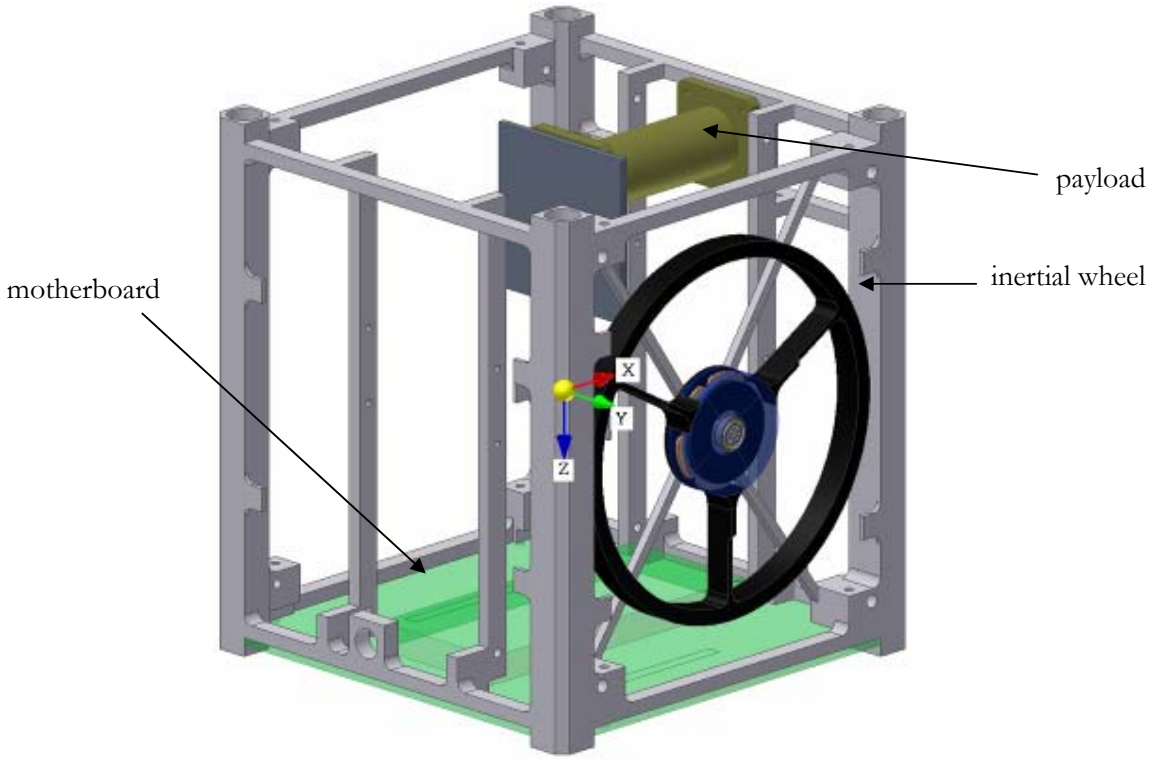


**Figure 45 Reference frame**

Table 4 and Table 5 give the various physical and inertial properties of the SwissCube. These values come from the CAD software, AutoDesk Inventor 11.

**Table 4 General properties.**

| Mass | 0.709 kg |
|---|---|
| Center of mass | (mm) |
| $X_c$ | -1.01 |
| $Y_c$ | -1.54 |
| $Z_c$ | 1.64 |

**Table 5 Inertial properties.**

| Physical moments of inertia | ($kg \cdot mm^2$) |
|---|---|
| $I_{xx}$ | 1580 |
| $I_{yy}$ | 1510 |
| $I_{zz}$ | 1410 |
| Principal moments of inertia | ($kg \cdot mm^2$) |
| $I_1$ | 1580 |
| $I_2$ | 1500 |
| $I_3$ | 1400 |
| Rotation XYZ/principal | (deg) |
| $R_x$ | -0.09 |
| $R_y$ | 7.6 |
| $R_z$ | 10 |

These numbers will change slightly when the final masses are known. They should be recalculated to ensure that the satellite remains compatible with the CubeSat requirements. As we can see, the center of mass (C.o.M.) is largely within the specifications (The C.o.M. must be in 20 mm, in our case: 2.09 mm).

Concerning the inertial values, the ADCS is not so satisfied because the principal axis of inertia shall be the Y-axis, in order to have a certain stability for the pointing of the payload. Moreover, a rotation of 17 to 20 degree around the Y-axis is desired because the payload must have such an inclination to be able to take picture of the Nightglow (see Figure 46). If this rotation can be done thanks to the inertial characteristic of the satellite, this makes things easier for the ADCS team, especially for the control division.

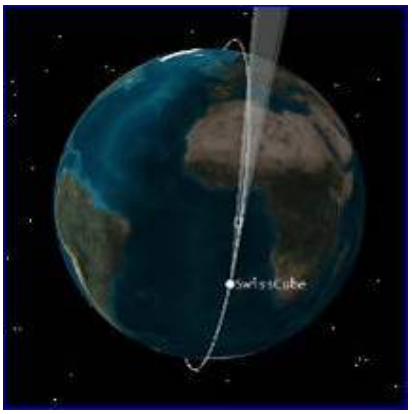


**Figure 46 Scanning mode of the SwissCube.**

For the next moths, we can imagine to add some "punctual" mass if possible according to the mass budget, in order to optimize the inertial properties of the satellite.

## 6.2 Static analysis

The structure must be sufficiently rigid to withstand all static loads encountered during the manufacturing, transportation and operational life of the satellite. As a consequence the satellite should be designed to withstand the highest potential loads encountered during its lifespan. This is known as designing for the worst case. By ensuring that the satellite will not fail under worst case static loading conditions, it can be shown that the satellite will not fail under any static loads during its lifecycle.

### 6.2.1 Worst Case Load

It is perceived that the worst-case static loading will be experienced by the satellite during the launch sequence. For the worst case loading consider the arrangement of CubeSats with in the P-POD shown below.

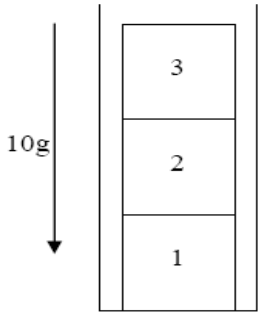


**Figure 47 Layout of CubeSats in P-POD during launch.**

For the worst case we shall consider the P-POD in a direction parallel to the direction of maximum acceleration during launch. It means that the acceleration will be parallel to the Z axis of the satellite (see Figure 45). As the deployment system holds three CubeSats the worst case will be experienced by the CubeSat in location 1 of Figure 47. During the launch sequence this CubeSat must maintain structural integrity while supporting not only its own weight but the weight of the two overlying picosatellites. Using the CubeSat design specifications the following assumptions can be made regarding the worst case static load of the SwissCube:

- The maximum acceleration will be equivalent to 7.5 g (Dnepr maximum acceleration)
- The mass of each of the three satellites is equal to 1kg

With a factor of safety of 1.25, the acceleration is 9.375 g, so it can be rounded to 10 g.

Therefore the worst-case loads on our satellite are simplified to those shown in Figure 48. The SwissCube will need to be able to tolerate a loading equivalent to an axial force of 196.2N with an acceleration of 10 g. This will be known as the worst case axial loading condition.

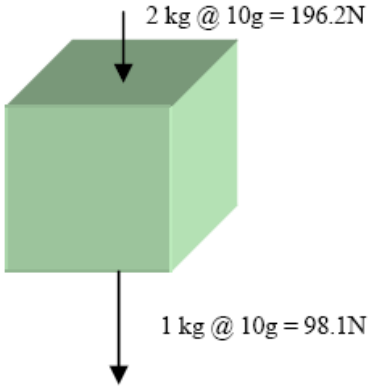


**Figure 48 Worst case axial loading.**

Now consider a case when the P-POD is aligned in a direction perpendicular to the direction of maximum acceleration. This is represented in Figure 49. In this case all three satellites will experience the same loading condition irrelevant of their location within the P-POD. Assume that the P-POD does not transfer any forces into the CubeSats. Then the CubeSats will only be required to support their self weight in a 10 g. gravity field. This will be known as the worst case lateral loading condition. There are two lateral cases, one with the acceleration in the X direction, the other in the Y direction (see Figure 45).

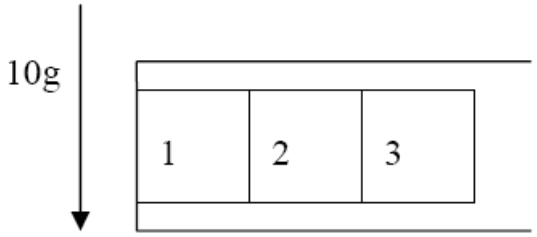


**Figure 49 Layout of CubeSats in P-POD during launch.**

## 6.3 Simplified model for Static Analysis

For simplicity the structure of SwissCube will be simplified for the static analysis. The structure includes both internal and external components. The internal structure adds extra complexity (and extra strength) to the static analysis and shall be ignored in this analysis. As a result the estimate for the strength of SwissCube is an underestimated conservative approximation.

The basic external structure, shown in Figure 50, will consist of four square (8.5x8.5 mm) solid extruded aluminum bars 113.5mm long connected by thin crossbars.

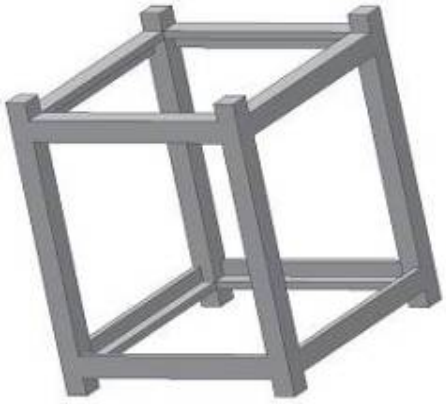

**Figure 50 Basic External Structure.**

As the rails extend beyond the surface of the internal box structure all the weight of the overlying satellites will be carried through these bars. The rails are the only part of the satellite in contact with a reaction surface (base of the P-POD, or underlying satellite), therefore the entire axial load will be reacted through these rails.

Therefore it shall be assumed that only the rails are effective in supporting a compressive load and that the aluminum faceplates do not offer any structural support.

Assuming the satellite is evenly loaded by the overlying satellites then the loading condition becomes of the form shown in Figure 51.

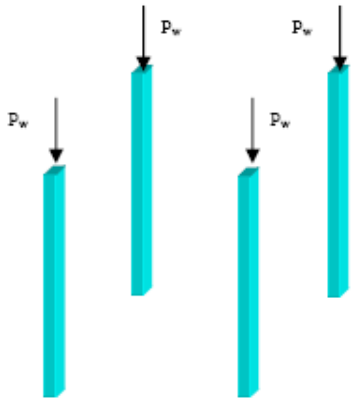


**Figure 51 Simplified static analysis.**

Where, for the worst case axial loading condition, $P_{wa}$ = (3kg@10g)/4 = 73.6N. Similarly the worst case lateral loading condition finds the maximum load in the cross bars to be $P_{wl}$ = (1kg@10g)/4 = 24.5 N.

### 6.3.1 Maximum Compressive Stresses in Structure

The maximum stresses that are expected to occur in the various components of the structure caused by the worst case loading condition have been determined. Calculations used to estimate these values are shown in Appendix K.1. A summary of these values and MOS (using a FOS of 1.25) with regard to compressive yield strength are shown below in Table 6.

**Table 6 Maximum compressive stresses in structural components.**

| Component | $\sigma_{max}$ (MPa) | MOS |
|---|---|---|
| Rail | 0.91 | 350 |
| Cross-bar | 2.04 | 155 |

These are very large margin of safety, i.e. the components will not fail in compressive yield for any of the worst case loading conditions. These values are verified by FEA in the following pages.

## 6.4 Static Failure Modes

As the maximum stresses in the structural components are sufficiently less than the yield strength of aluminum the critical failure modes are expected to be buckling.

In mechanical structures, in addition to the stable elastic deformations, for high stresses there is a risk that the deformation of the structure becomes mechanically unstable. This phenomenon is called buckling. The differential equation for the buckling of a column is given in Appendix K.2.

### 6.4.1 Results

The calculations used to estimate the critical buckling loads are presented in Appendix K. With a FOS of 1.25 and the maximum compressive stresses listed in Table 6, MOS are calculated and given in the two following tables. The results of the buckling analyses are summarized below in Table 7.

**Table 7 Critical buckling loads and margins of safety.**

| Component | Critical buckling stress (MPa) | MOS |
|---|---|---|
| Rail | 718.5 | 629 |
| Cross-bar | 140.9 | 54 |

This table shows that the proposed design of the structural subsystem will be safe in buckling. These values are verified by FEA in the following pages.

## 6.5 Finite Element Analysis

The finite element method is a powerful mathematical tool used for the numerical solution of a wide range of engineering problems. In this case finite element analysis was used to estimate the deformations and stresses that the SwissCube will experience under a variety of different loads and freedom cases.

Finite Element Analysis (FEA) uses a complex system of points called nodes which make a grid called a mesh. This mesh represents the geometry of the structure and can be programmed to contain the material and structural properties which define how the structure will react to certain loading conditions.

### 6.5.1 The model

Due to the complexity of the design and the abundance of components inside the CubeSat, it would be difficult and unnecessary to model everything inside of SwissCube. Instead, the design is simplified to represent only the basic structural components of the satellite that will be load bearing. Figure 52 shows the simplified version used in our analysis. The satellite is reduced to just a few parts: the monobloc main frame, the spacers, the four rectangular PCBs, the motherboard, the inertial wheel, the battery box including two batteries, and the payload frame with a dummy mass (headboard PCB) at the end.

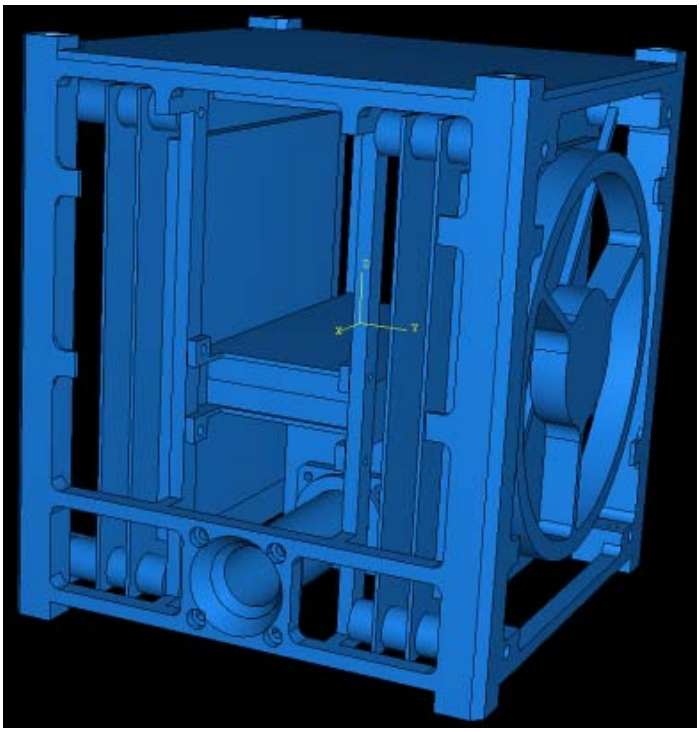

**Figure 52 Simplified version used for FEA.**

For simplicity, the joints between all the pieces are assumed to be tied so that there is no relative motion between them. In reality, the pieces will be bolted or glued together resulting in extremely rigid unions validating this assumption. The properties of the three different materials, aluminum Certal for the main frame, FR4 for the PCBs, titanium for the payload's frame, can be found in Appendix C.

### 6.5.2 Loading and boundaries conditions

It is still unknown whether the satellite will be launched horizontally, as illustrated in Figure 49, or vertically, as shown by Figure 47. This fact necessitated three separate finite element analyses; two horizontal cases, acceleration in X or Y direction, and one vertical case, in the Z direction. The force applied to each structure was a constant gravitational load of ten times the acceleration on the surface of the Earth and in the case of a vertical launch, an additional axial load of 196.2 N resulting from the two overlying picosatellites is present, so the load on each top of feet is one quarter, 49 N.

In the vertical case, the standard boundary conditions are that the four bottom feet are fixed in the z-direction and pressure loads from the two overlying CubeSats evenly distributed on the four top feet (see Figure 53-II). In the two horizontal cases, the standard boundary condition is only that two rails are fixed in one direction (see Figure 53-I).

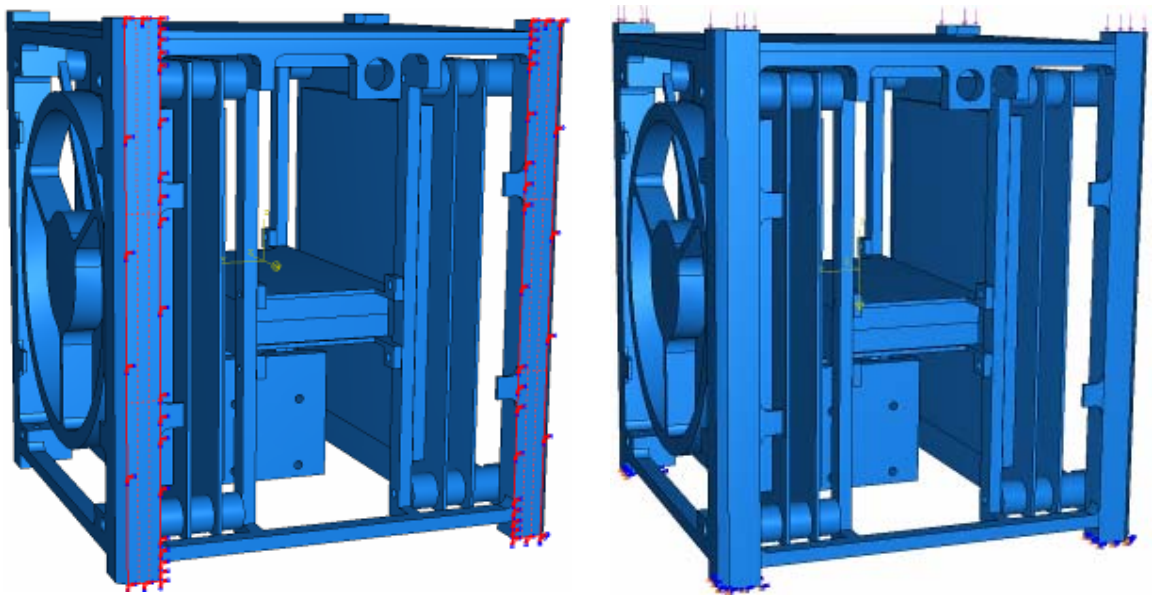

I II

**Figure 53 Boundary conditions for X-horizontal and vertical cases.**

## 6.6 Static FEA results

These scenarios probably overestimate the loads the spacecraft will experience during launch, because of the factor of safety. Nonetheless, the structure resisted without difficulties. We found that the maximum stresses in the structure in the both cases are well below the yield strength of the aluminum. For the X and Y horizontal case, the stresses computed by the Von Mises criteria are 0.74 and 2.5 MPa respectively; for the vertical case, we have a stress of 5.73 MPa (see Appendix L). With a yield stress of 400 MPa for the aluminum, a factor of safety (FOS) of 1.25 and the formula for the margin of safety (MOS) [6]:

$$MOS = \frac{(allowable\ load)}{(applied\ load) \times FOS} - 1$$

**Equation 1**

The MOS in the X and Y horizontal case are 431 and 127; for the vertical case we obtain a MOS of 54. This means that the satellite can support a load 431, 127 and 54 times higher before entering the plastic region.

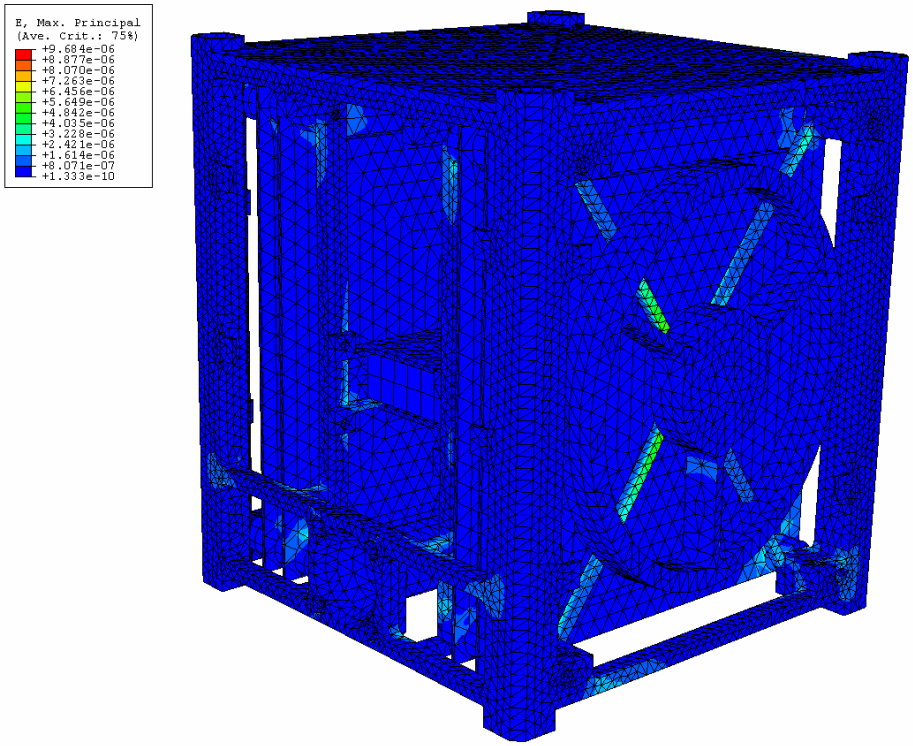


**Figure 54 Strain in the X-horizontal worst case.**

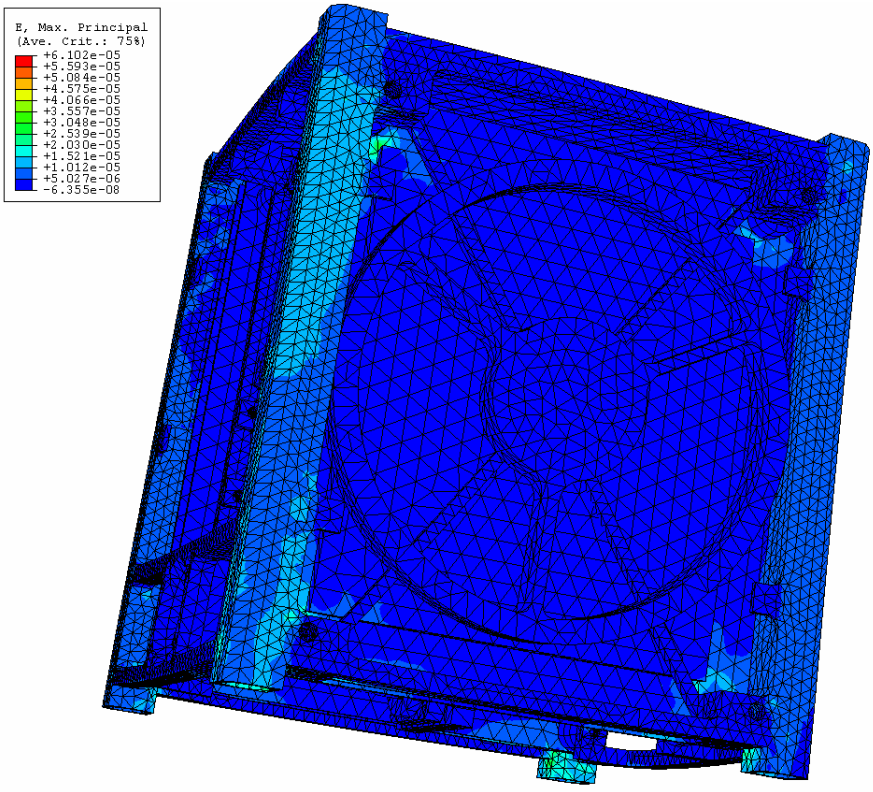


**Figure 55 Strain in the vertical worst case.**

The maximum strains are $9.7 \cdot 10^{-4}$ % and $2.9 \cdot 10^{-3}$ % in the X and Y horizontal cases respectively; for the vertical case, the maximum strains are $6.1 \cdot 10^{-3}$ % (see Figure 54 and Figure 55). These very small deformations will have no impact on the structural integrity of the satellite.

Since this structure is basically constructed of thin beams, one final check is made to ensure that the reduced-section cross-bars and rails will not fail in buckling. Critical stresses of buckling for the rails and crossbars have been calculated as follows: $\sigma_{cr}$ are equal to 718.5MPa, 140.9MPa and 78.3MPa for the rail, main crossbar and wheel attachment crossbar respectively. For the detailed calculations see Appendix K.2. With the most important maximum stress of 2.05 MPa for the crossbars of the wheel attachment in the Y horizontal case (see Appendix L) and the formula for the MOS with a FOS of 1.25, the margin is 29 for these crossbars. For the vertical case, the most significant maximum stresses are 5.7 MPa and 1.3 MPa for the rails and wheel attachment crossbars respectively, so the MOS are 99 and 47 for the rails and wheel attachment crossbars in the vertical case.

Figure 54 and Figure 55 represent the deformation with various colors, but Abaqus allows a variety of other parameters to be displayed in a comparable format. For example, both stress and total displacement can be similarly displayed. For these analyses, see Appendix L.

## 6.7 Dynamic FEA

It is important to verify that the structure will maintain structural integrity, and provide a suitable environment for the various subsystems under the dynamic loading conditions that are expected to be experienced during launch. These loading conditions can be found in Appendix B.

The types of dynamic analysis that have been performed include:

- Modal analysis
- Sinusoidal vibration analysis
- Random vibration analysis
- Acoustic vibration analysis

Due to limited time, only the research of the first modes of the model was performed using finite element analysis (FEA) Abaqus software. The other types of dynamic analysis will be performed during the next semester.

### 6.7.1 Modal analysis

The first stage in performing a dynamic analysis of the structure is to determine the first several modes of vibration (natural frequencies).

Modal analysis is the process of characterizing the dynamic properties of an elastic structure by identifying its modes of vibration. That is, each mode has a specific natural frequency and damping factor which can be identified from practically any point on the structure. In addition, it has a characteristic "mode shape" which defines the mode spatially over the entire structure.

It is useful to know the modal frequencies of a structure as it allows you to ensure that the frequency of any applied periodic loading will not coincide with a modal frequency and hence cause resonance, which leads to large oscillations. The method of a modal analysis is:

1. Find the natural modes and natural frequencies
2. Calculate the response of each mode
3. Optionally superpose the response of each mode to find the full modal response to a given loading

**Table 8 Natural frequencies of the satellite.**

| Mode | Frequency [Hz] | Zone of interest |
|---|---|---|
| 1 | 153 | Wheel attachment crossbars |
| 2 | 158 | Wheel attachment crossbars |
| 3 | 175 | Wheel attachment crossbars |
| 4 | 189 | Wheel attachment crossbars |
| 5 | 537 | Monobloc frame (payload attachment) |
| 6 | 634 | Monobloc frame (battery box attachment) |
| 7 | 685 | PCBs stack & Payload attachment |
| 8 | 698 | PCBs stack & Payload attachment |
| 9 | 713 | PCBs stack & Payload attachment |
| 10 | 778 | PCBs stack |
| 11 | 808 | PCBs stack & monobloc frame |
| 12 | 953 | Monobloc frame |
| 13 | 997 | Monobloc frame |
| 14 | 1112 | Monobloc frame |

The shapes of the first 14 vibration modes are stated in Appendix L.4. The deformations have been arbitrarily enhanced to allow the reader to more easily identify the difference in the shapes of the modes.

As example, the 14$^{th}$ mode of vibration is shown in Figure 56. In this case, the mode of vibration concerns the whole structure.

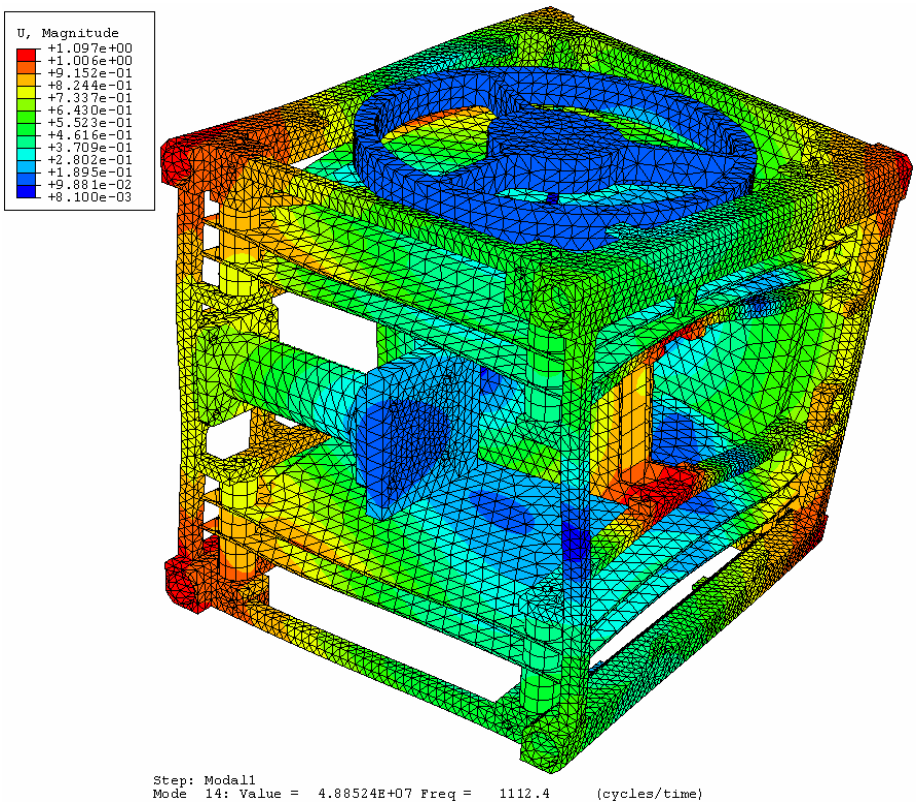


**Figure 56 14th mode of vibration of the model, 1112 Hz.**

The four first natural frequencies concern the crossbars of the wheel attachment. The frequencies are passably low (between 153 and 189 Hz) and that can be a problem. When the wheel will rotate, vibration with a frequency proportional with the rotation speed will be produced. As the max rotation speed of the wheel is 11'000 rpm, the corresponding frequency is 183 Hz. With the actual design, the wheel can excite the crossbars during the acceleration. So the crossbars of the wheel attachment shall be redesigned in order to obtain natural frequencies above 200 Hz.

The 5$^{th}$ and 6$^{th}$ natural frequencies concern the monobloc frame. These modes of vibration appear at 537 and 634 HZ. These values are rather high, in comparison with the requirement concerning the fundamental frequency of the satellite. This requirement specifies that the satellite shall have a structural stiffness, which ensures that the values of fundamental frequency of the satellite, hard mounted at the separation plane, are equal or superior of 35 Hz.

The five following natural frequencies (685 to 808 Hz) concern the PCBs. These results are probably not so representative, because real multilayer PCBs are constituted of stacked FR4 and copper layers. So the physical properties are not the same as FR4.

Additional mass of components on the subsystem boards were not considered at this stage. The true frequency considering the mass of the components will be slightly lower than the from the simulation result. This is assumed according to the theory of dynamics that the natural frequency of a system decreases if the mass increases for constant stiffness:

$$f_{nat} = \frac{1}{2\pi}\sqrt{\frac{k}{m}}$$

# 7 TEST

Test programmes are an essential part of the overall verification to ensure that the product achieves all the design, performance and quality requirements. Test planning, test requirements, and test criteria are derived from the design requirements.

The objective of development testing is to support the design feasibility and to assist in the evolution of the design. Development tests are used to validate new design concepts and the application of proven concepts and techniques to a new configuration.

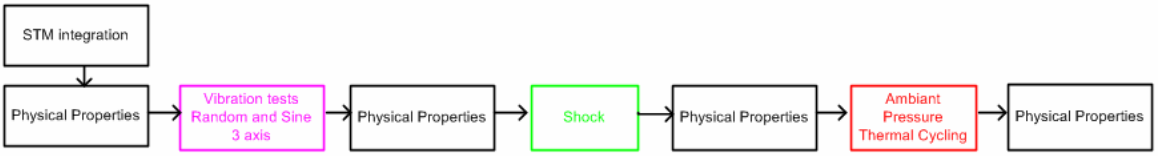


**Figure 57 Structural Model test flow.**

The various tests to be achieved on the Structural model are shown in Figure 57. Some tests have been already performed during this Master thesis, the other should be done the next semester.

## 7.1 Physical properties test

The results of the physical properties test described in Appendix M.1 are:

**Table 9 Physical properties of the monobloc frame.**

| **Width** | **[mm]** |
|---|---|
| Side 1 | 99.94 |
| Side 2 | 99.92 |
| Side 3 | 100.02 |
| Side 4 | 99.93 |
| **Height** | **[mm]** |
| Rail 1 | 113.46 |
| Rail 2 | 113.52 |
| Rail 3 | 113.48 |
| Rail 4 | 113.49 |
| **Diagonal** | **[mm]** |
| Top 1&3 | 138.47 |

| | |
|---|---|
| Top 2&4 | 138.49 |
| Bottom 1&3 | 138.28 |
| Bottom 2&4 | 138.62 |

The values concerning the diagonal are not the same as the value of the checklist in Appendix M.1.4 because the frame has chamfers of 2mm instead of 1mm. The theoretical value of the diagonal is 138.59 mm.

The results are passably excellent. The requirement specifies margins of ± 0.1mm for the widths and heights of the rails. The manufactured frame is in these margins.

Concerning the diagonals, the results are not so good, but this should not be a problem. As we have a bigger chamfer as specified in the requirements, there is no risk of interference between the main frame and the P-POD.

## 7.2 Sinusoidal vibrations qualification test

The sinusoidal vibration test procedure is described in Appendix M.2. As explained in the test procedure, the structural model has been tested in the X, Y, Z-axis chronologically.

For the X-axis, four accelerometers are used. Their locations are:

- accelerometer n°1: centered, on the backside (X-) of the payload dummy PCB
- accelerometer n°2: centered, on the Z- face of the battery box
- accelerometer n°3: centered, on the external face of the X+ composite panel
- accelerometer n°4: centered, on the external face of the X- composite panel

The results are the following (see Figure 58):

- Reference; it's passably difficult to see the various steps of amplitudes, their differences is very small. At the beginning the amplitudes are bigger than the command (for the desired shape of amplitudes, see §2.5.2) because the control has some oscillations when starting.
- Accelerometer 1; from 108 seconds (around 78Hz), the amplitude increases and are more or less 2g.
- Accelerometer 2: this component was not mounted in a right direction (on a face perpendicular of the displacements). So the results are not exploitable.
- Accelerometer 3: from 108 seconds (around 78Hz), the amplitude increases up to 5g.

- Accelerometer 4: from 108 seconds (around 78Hz), the amplitude increases suddenly. Unfortunately due to wrong calibration of the accelerometer charge amplifiers, the data concerning are saturated.

To summarize, for the X-axis the four accelerators have shown that from 78Hz the amplitudes increase. The reason could be the clearance of the Test-POD. The gap where the satellite is inserted is 100.8mm, while the widths between the rails are around 100.00mm (±0.1mm). This gap doesn't play any role at low frequency, because the Test-POD is constraint by springs in the Z direction of the satellite. But at higher frequency, the satellite begins to shock inside the Test-POD.

Remarks: more information about the Test-POD and P-POD should be obtained. In particular, if the P-POD has this clearance too.

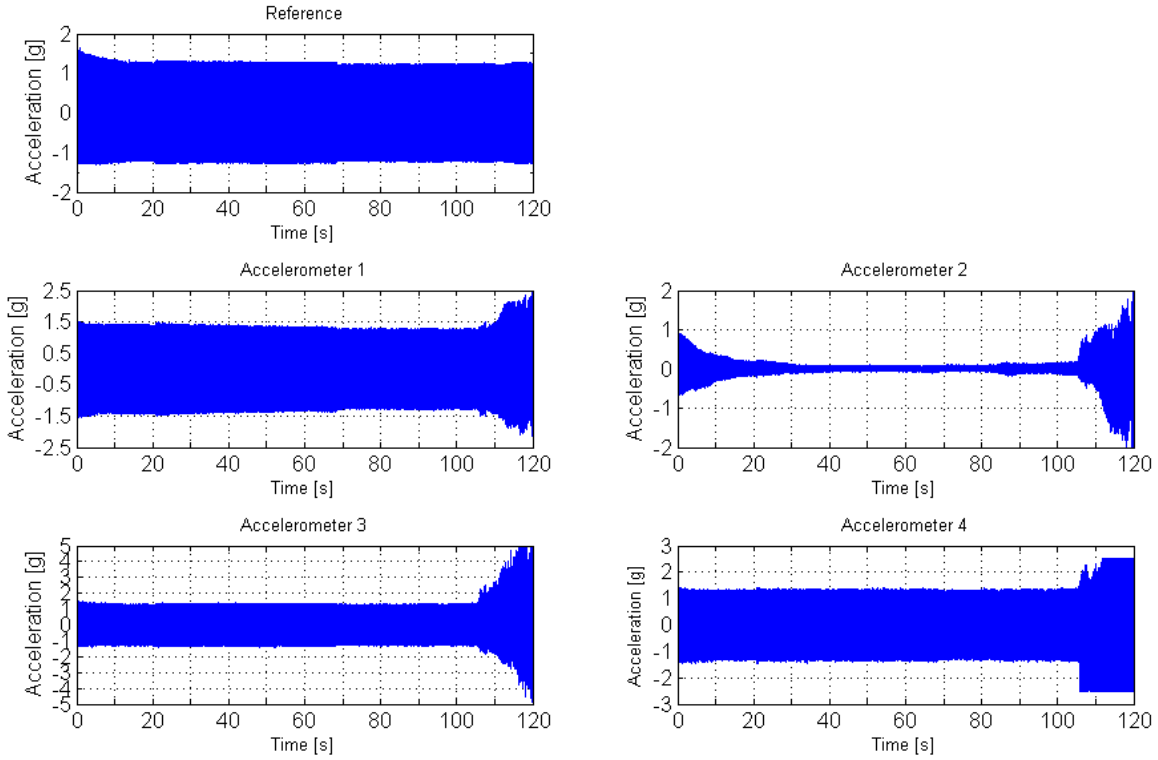


**Figure 58 Sinusoidal vibration in X-axis.**

For the Y-axis, four accelerometers are used. Their locations are:

- accelerometer n°1: centered, on the Y+ edge of the payload dummy PCB
- accelerometer n°2: centered in X, decentered of 20mm in Y+, on internal side of EPS PCB
- accelerometer n°3: centered, on the external face of the Y+ composite panel
- accelerometer n°4: centered, on the external face of the Y- composite panel

The results are (see Figure 59):

- Reference; the data are not so regular like before, probably due to control problems.
- Accelerometer 1; the amplitudes follow the command, at the end there are some small oscillations.
- Accelerometer 2: the amplitudes follow the command very well.
- Accelerometer 3: some oscillations at the beginning, then the amplitudes follow the command.
- Accelerometer 4: some oscillations at the beginning, then the amplitudes follow the command.

To summarize, for the Y-axis the four accelerators have shown a passably good answer of the sinusoidal vibrations. There aren't increases of amplitude.

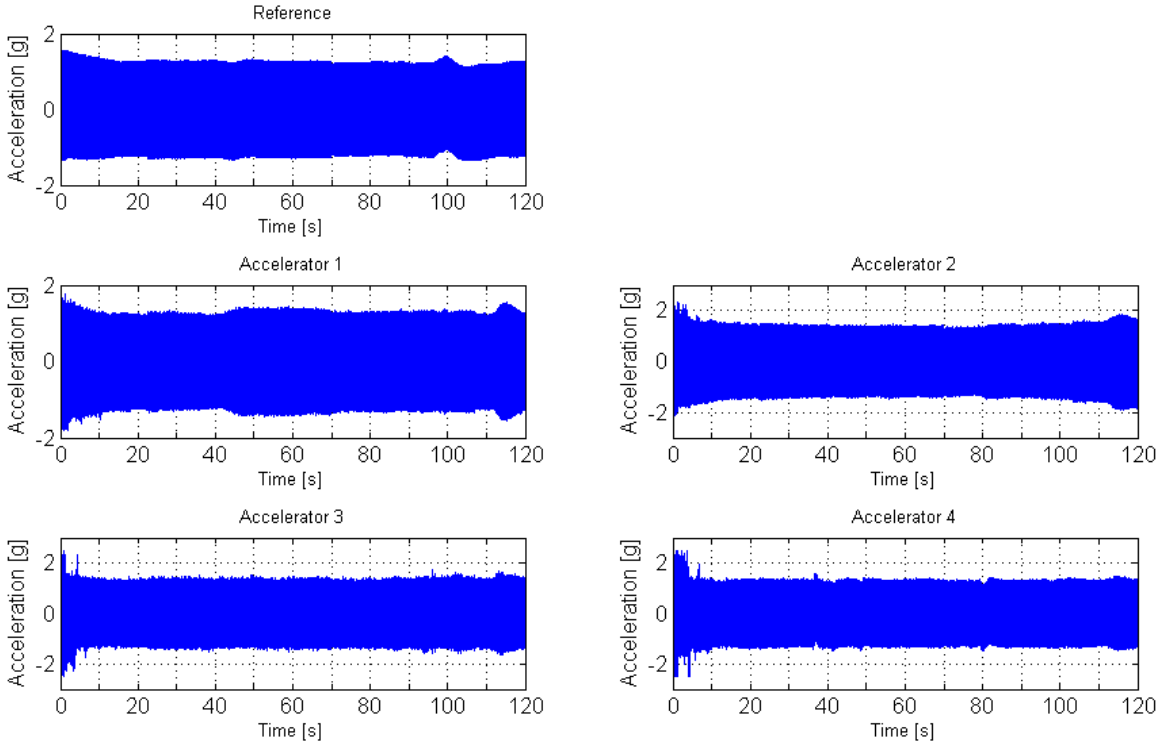


**Figure 59 Sinusoidal vibration in Y-axis.**

For the Z-axis, four accelerometers are used. Their locations are:

- accelerometer n°1: on the slide of the wheel, in Z+ direction
- accelerometer n°2: centered, on the Z- face of the battery box
- accelerometer n°3: centered in Y, at the X- end of the cylindrical shape of payload frame
- accelerometer n°4: centered, on the internal face of the Z- composite panel

The results are the following (see Figure 60):

- Reference; the data are regular. At the beginning the amplitudes are bigger than the command because the control takes time to be stabilized when starting.
- Accelerometer 1; the data aren't useful; the accelerometer was sticked on the slice of the moving wheel. It was to try if something measurable was potential.
- Accelerometer 2: the amplitudes follow the command passably well, except for the first third of the test, the amplitude is a little bit bigger.
- Accelerometer 3: the amplitudes follow the command very well
- Accelerometer 4: the amplitudes follow the command very well

To summarize, for the Z-axis the accelerators 3 and 4 have shown a passably good answer of the sinusoidal vibrations. There aren't increases of amplitude. Concerning the accelerator 2, the small increase of amplitude can have many reasons; maybe there is a mode around these frequencies (25Hz), or another part excites attachments of the battery box.

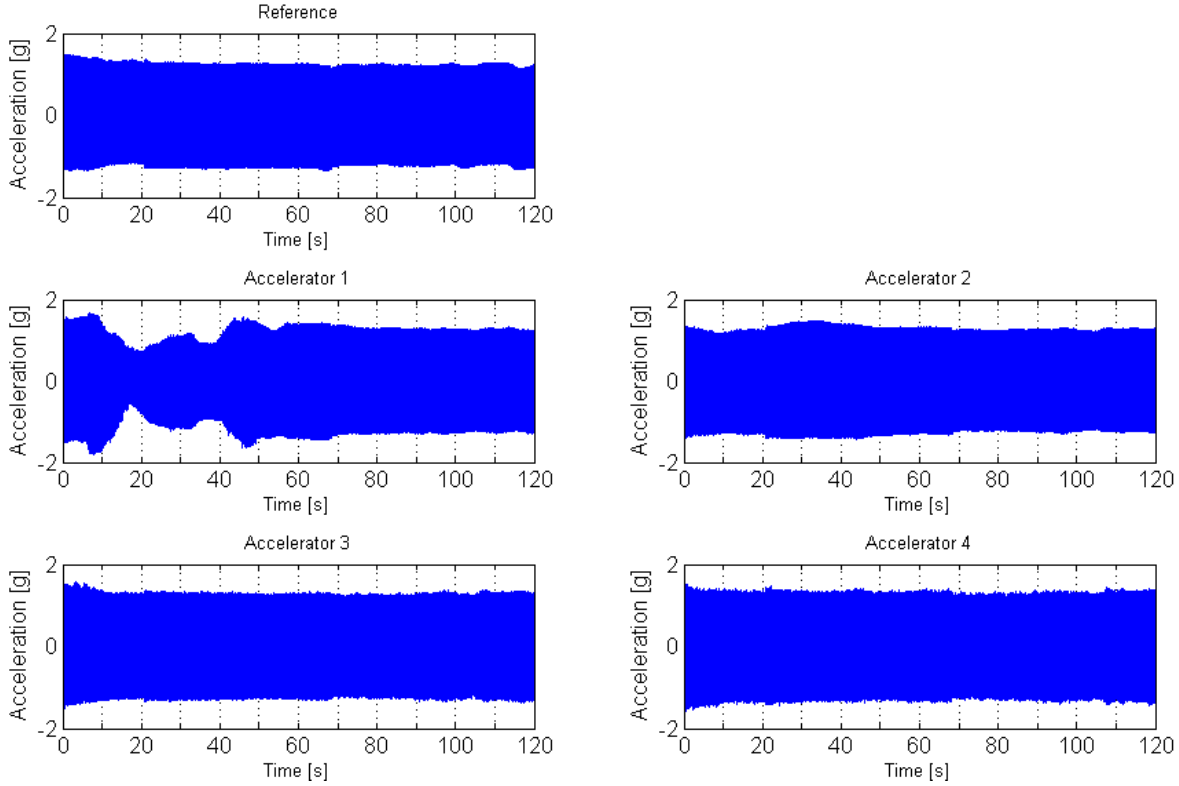


**Figure 60 Sinusoidal vibration in Z-axis.**

To recapitulate the results of sinusoidal test, the satellite has passed it without damages. The physical properties didn't change.

## 7.3 Random vibration qualification test

The random vibration test procedure is described in Appendix M.3. As explained in the test procedure, the structural model has been tested in the X, Y, Z-axis chronologically.

### 7.3.1 Transfer function and Power spectral density

**Transfer function** is a mathematical representation of the relation between the input and output of a system. The transfer function is the linear mapping of the Laplace transform of the input *X(s)*, to the output *Y(s)*:

$H(s) = \frac{Y(s)}{X(s)}$ , where H(s) id the transfer function of the linear, time-invariant system.

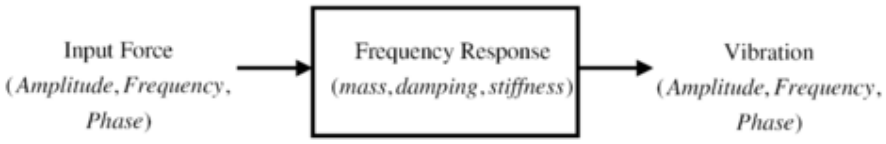


**Figure 61 Transfer function model.**

With the excitation signal and a response signal, a comparison of these two signals in the frequency domain (by calculating the transfer function) gives one the idea how the object moves or vibrates at modal frequencies (see Figure 61). If adequate measurement points are available, mode shapes of the object can be evaluated from the transfer functions.

The **power spectral density** (PSD) function is a statistical tool used widely in the analysis of nondeterministic behavior. The power spectral density function is a function of the square of the magnitude of the amplitude and can be expressed as:

$$y(\Omega) = \frac{|Y(\Omega)|^2}{T}$$ **Equation 2 Power Spectral Density function.**

For example, when testing a launch vehicle the acceleration at a certain attachment points would be recorded for a certain period of time. The frequency and amplitude information would then be extracted and organized into a probability density curve. The random vibration acceleration power spectral density function is then obtained by integrating the vibration over its frequency bandwidth and then dividing by the same bandwidth. The result will have units of acceleration squared per unit frequency, i.e. $g^2$/Hz.

The area underneath the power spectral density function is the mean square value, and can be expressed:

$$\overline{y^2(t)} = \frac{1}{2\pi}\int_0^\infty y(\Omega)\partial\Omega$$ **Equation 3 Mean square.**

The square root of this is equal to the root mean square and also equals one standard deviation of the quantity of interest. Using a 3 standard deviation limit load as the worst case design load will provide a probability of 0.13% that the condition will not be exceeded during launch.

### 7.3.2 Results of tests

For the X-axis, four accelerometers are used. Their locations are:

- accelerometer n°1: centered, on the backside (X-) of the payload dummy PCB
- accelerometer n°2: centered, on the Z- face of the battery box
- accelerometer n°3: centered, on the external face of the X+ composite panel
- accelerometer n°4: centered, on the external face of the X- composite panel

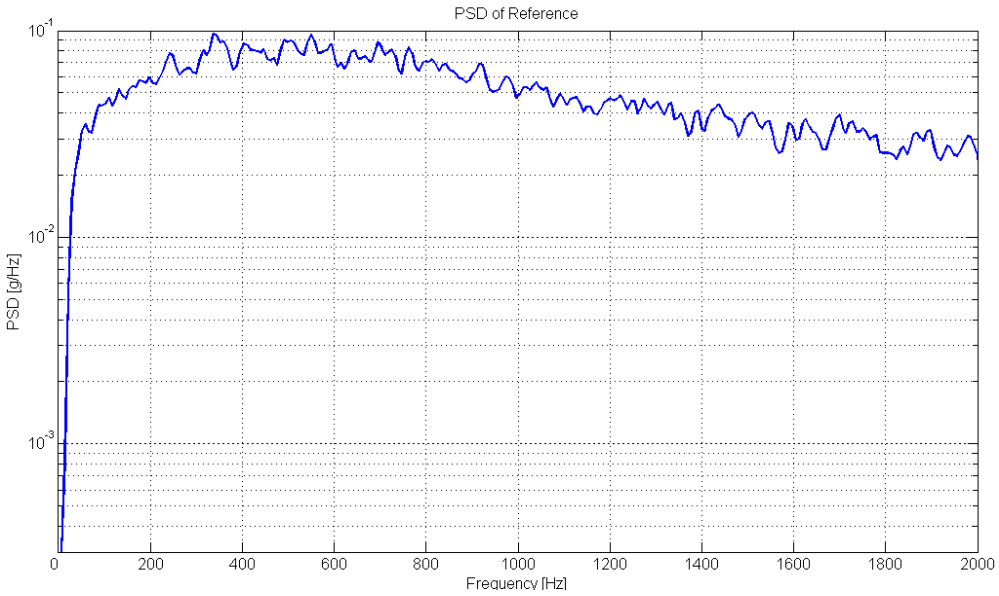


**Figure 62 Random vibration in X-axis, PSD of Reference.**

Figure 62 shows the PSD of the accelerometer used like reference (feedback loop). As expected, the curve has the same shape as the qualification curve (see Figure 8). The maximal and minimal peak accelerations of the Reference are **49.3g and -50.8g**, respectively.

The interesting thing in the following plots of Transfer Function is the research of natural frequencies. The presence of modes is symbolized by peaks in the transfer function plot with dynamic factor of amplification bigger than one, and at the same time with a phase sift of -π.

A common way to verify values of natural frequencies found by FEA is to perform random vibration tests in order to extract mode from transfer functions. But to validate the FEA model, the boundary conditions shall be clearly defined and constant.

In our case, the results of the random vibration tests aren't so representative because the Test-POD has some clearance, like explained before. This gap doesn't play any role at low frequency, because the Test-POD is constraint by springs in the Z direction of the satellite. But at higher frequency, the satellite begins to shock inside the Test-POD and the boundary conditions aren't constant (the system is no more linear). That's why any final conclusions can be made, only suppositions.

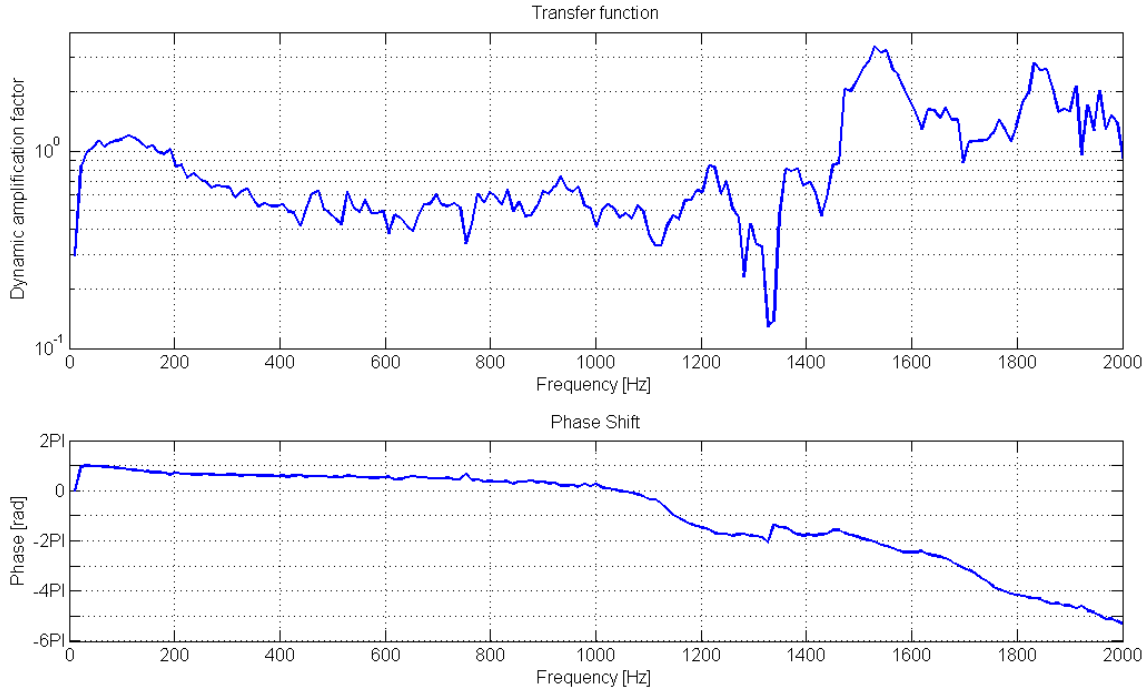


**Figure 63 Random vibration in X-axis, Transfer function and Phase shift for Accelerometer 1.**

The possible areas for natural frequencies are around 1500 and 1850Hz.

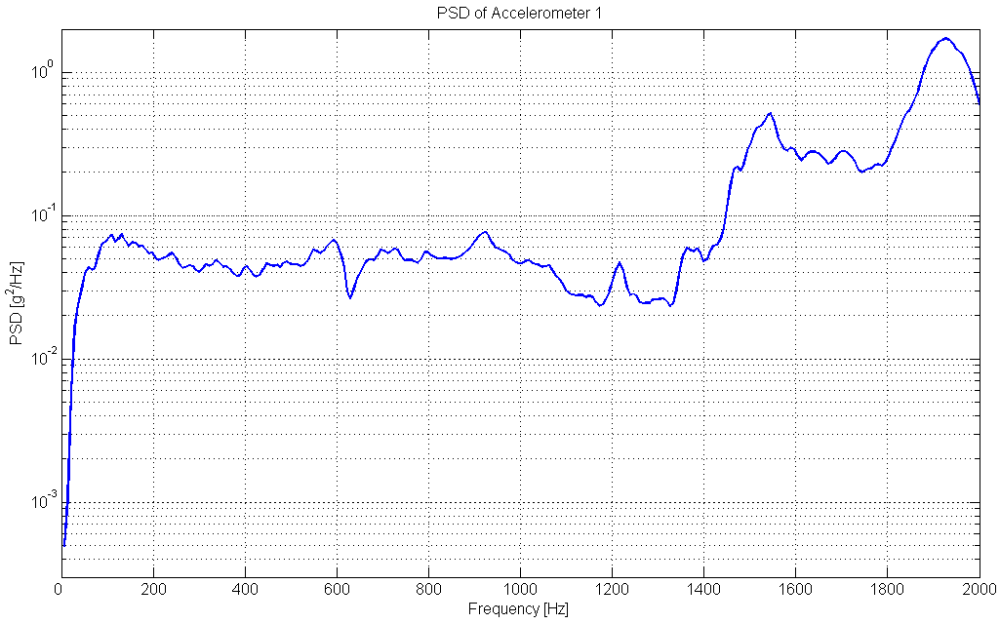


**Figure 64 Random vibration in X-axis, PSD of Accelerometer 1.**

The maximal and minimal peak accelerations of Accelerometer 1 are **178.4g** and **-160g** respectively. These values are in line with the Figure 63. The amplification factor is around 3, it means that the maximal peak acceleration of this accelerometer is 3 times the one of the Reference.

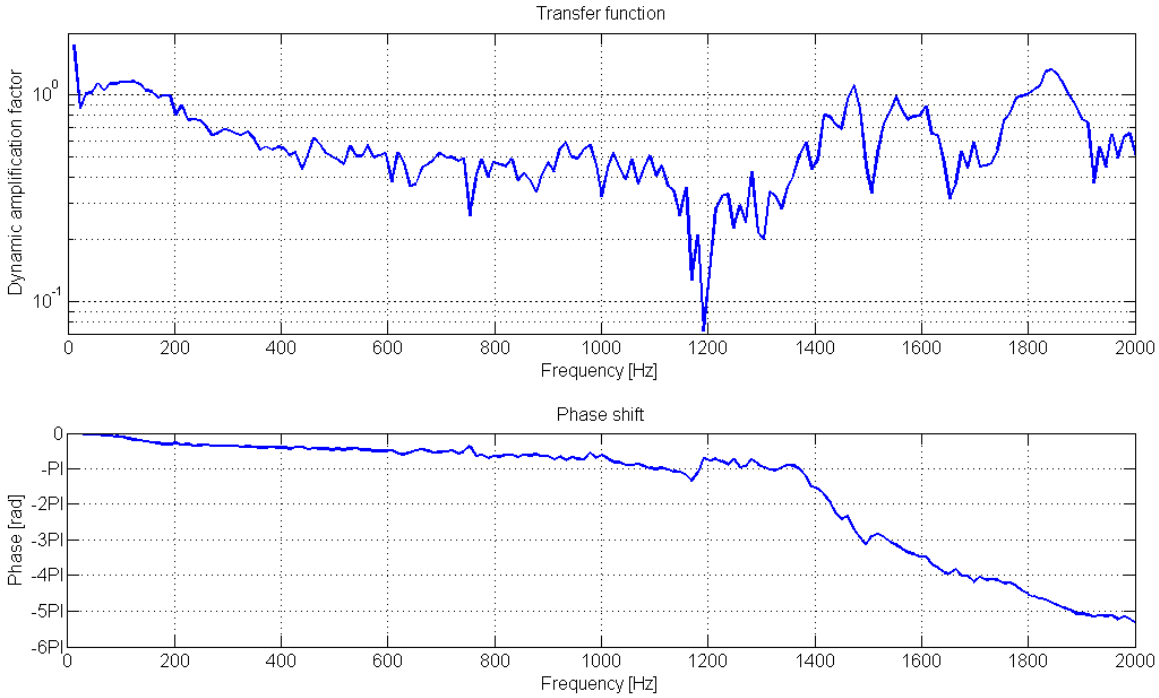


**Figure 65 Random vibration in X-axis, Transfer function and Phase shift for Accelerometer 2.**

The possible areas for natural frequencies are around 1450 and 1850Hz.

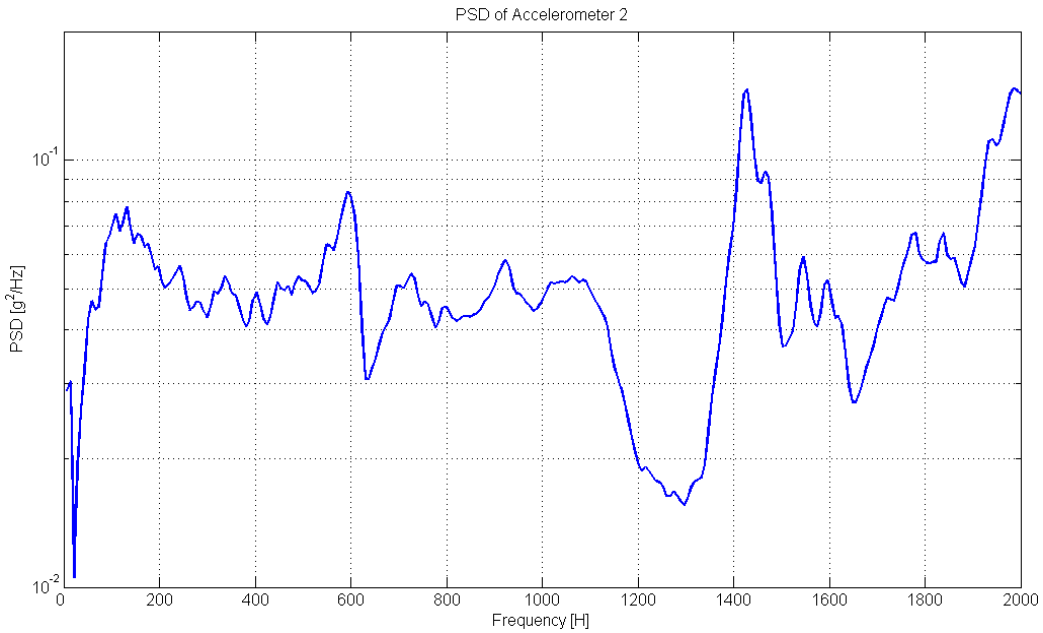


**Figure 66 Random vibration in X-axis, PSD of Accelerometer 2.**

The maximal and minimal peak accelerations of Accelerometer 2 are **208.5g** and **-233.4g** respectively.

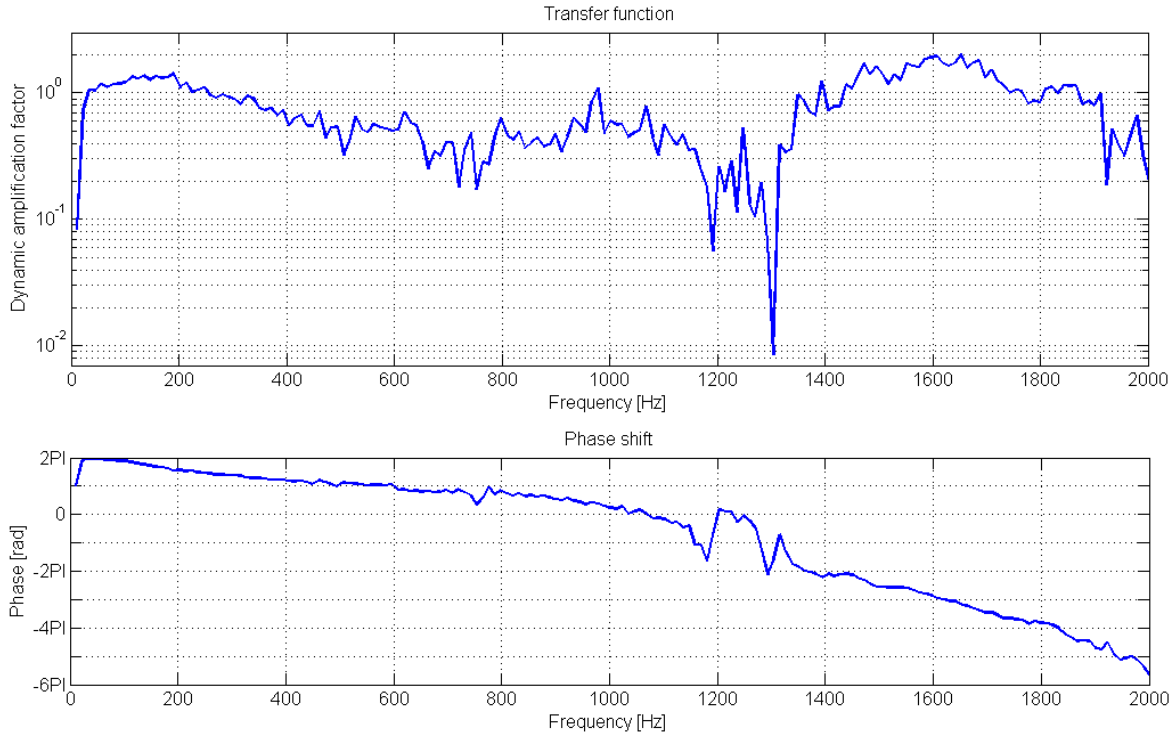


**Figure 67 Random vibration in X-axis, Transfer function and Phase shift for Accelerometer 3.**

The possible areas for natural frequencies are around 100, 1350 and 1600Hz.

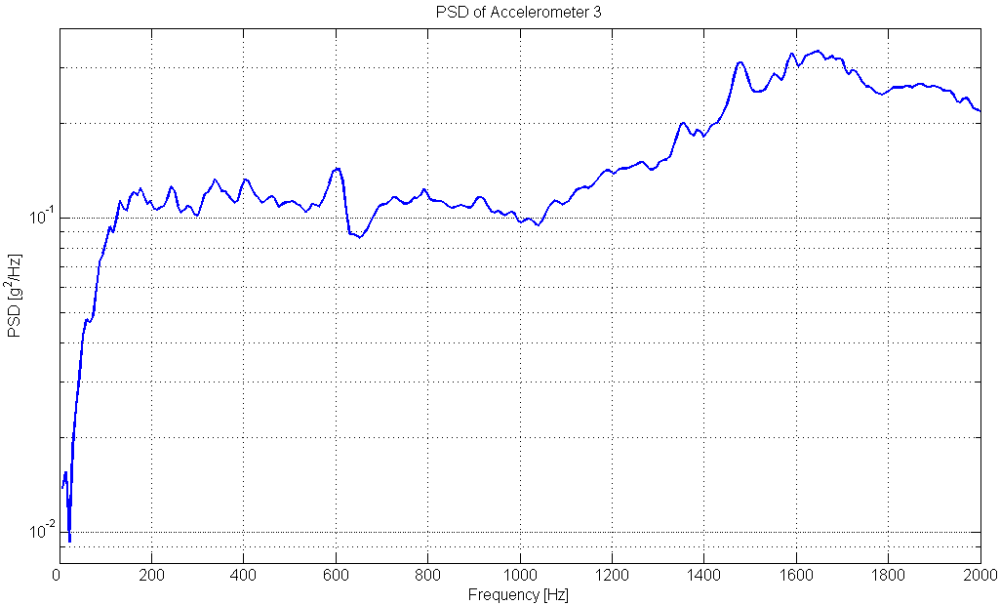


**Figure 68 Random vibration in X-axis, PSD of Accelerometer 3.**

The maximal and minimal peak accelerations of Accelerometer 3 are **139.3g** and **-380.2g** respectively. The dissymmetry of these results can be explained by the floating reference of the signal for this kind of accelerometer. This has no influence in the computation of PSD and transfer function.

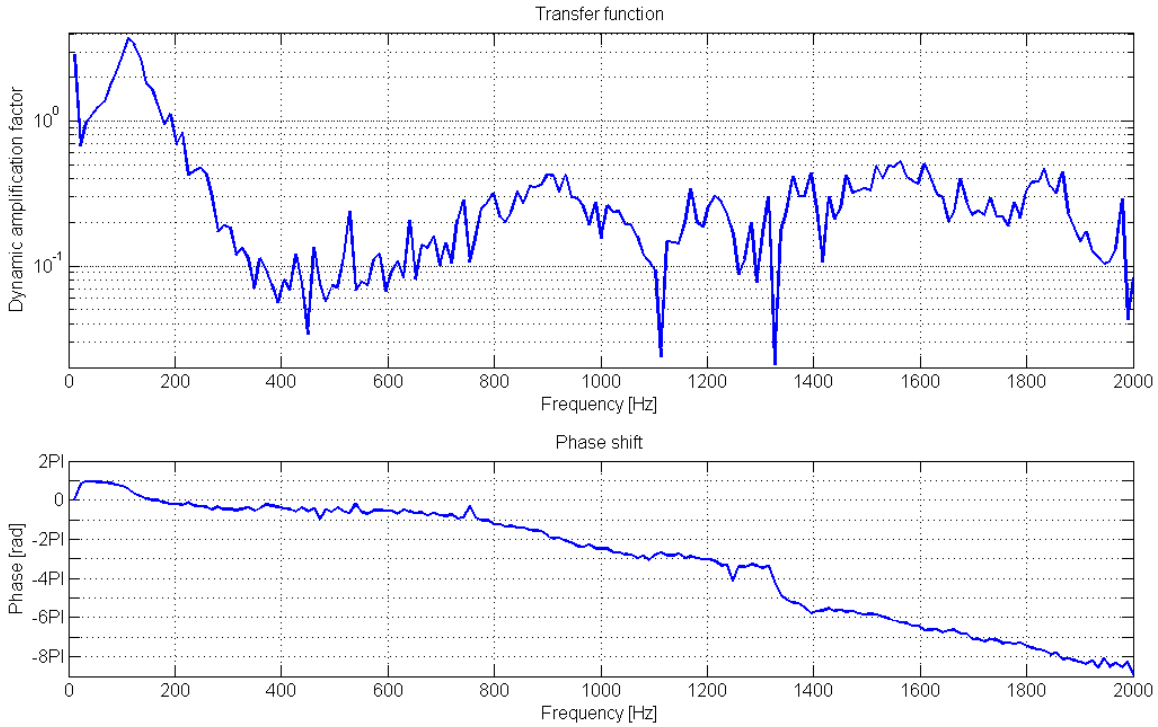


**Figure 69 Random vibration in X-axis, Transfer function and Phase shift for Accelerometer 4.**

A possible area for natural frequencies is around 100Hz.

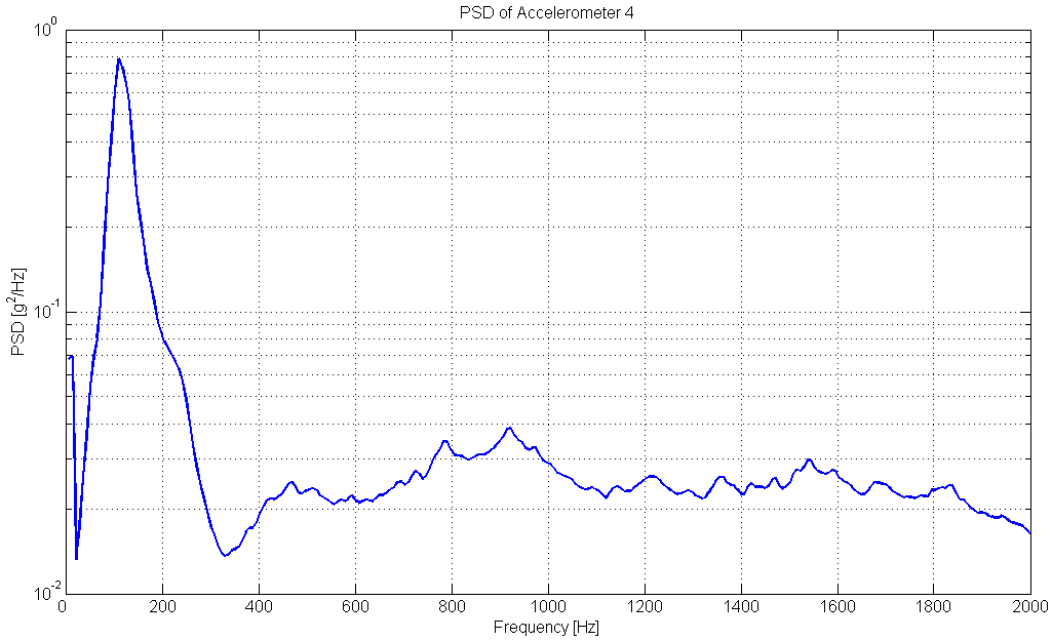


**Figure 70 Random vibration in X-axis, PSD of Accelerometer 4.**

The maximal and minimal peak accelerations of Accelerometer 4 are **69.5g** and **-272g** respectively. Like before there is a dissymmetry of the signal.

For the Y-axis, four accelerometers are used. Their locations are:

- accelerometer n°1: centered, on the Y+ edge of the payload dummy PCB
- accelerometer n°2: centered in X, decentered of 20mm in Y+, on internal side of EPS PCB
- accelerometer n°3: centered, on the external face of the Y+ composite panel
- accelerometer n°4: centered, on the external face of the Y- composite panel

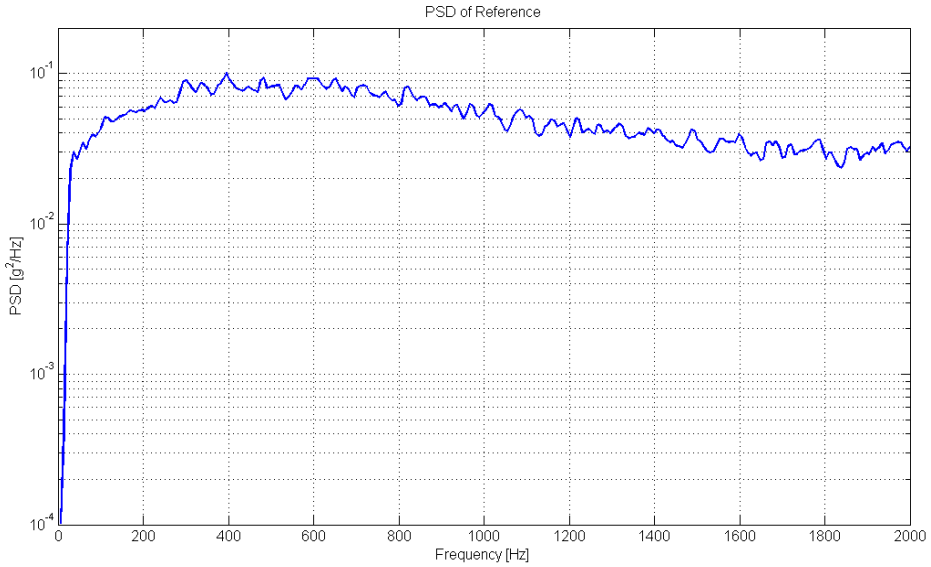


**Figure 71 Random vibration in Y-axis, PSD of Reference.**

Figure 71 shows the PSD of the accelerometer used like reference for the Y-axis test As expected, the curve has the same shape as the qualification curve (see Figure 8). The maximal and minimal peak accelerations of Reference are **57.3g** and **-51g** respectively.

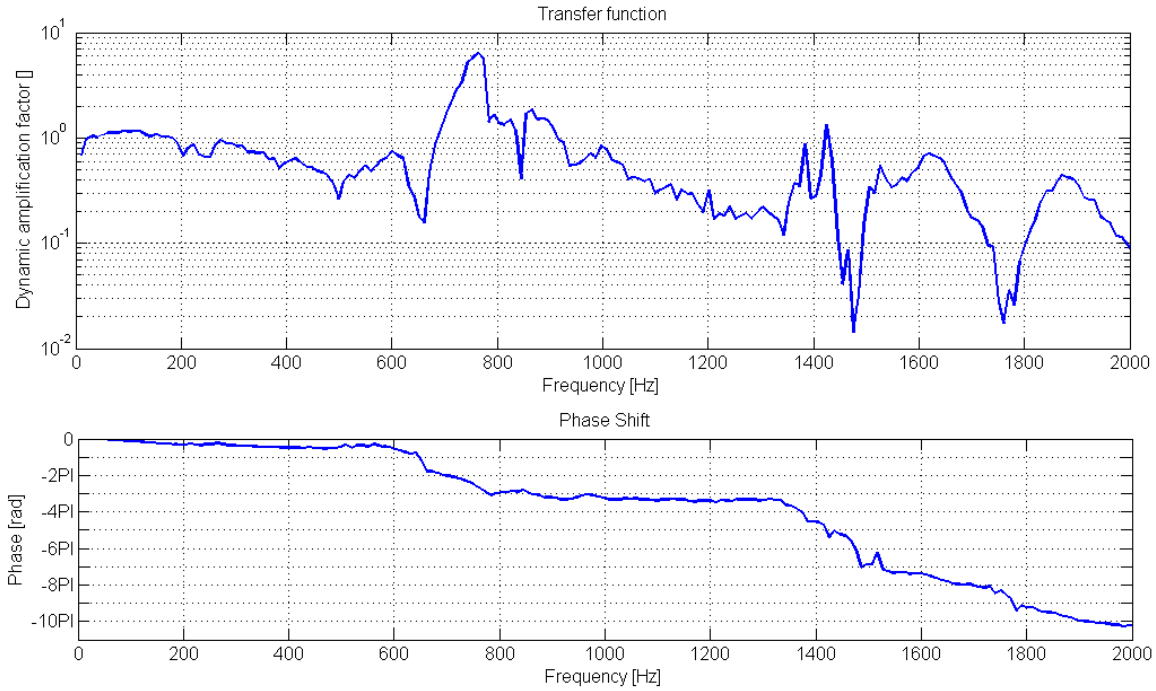


**Figure 72 Random vibration in Y-axis, Transfer function and Phase shift for Accelerometer 1.**

Figure 72 shows that possible areas for natural frequencies are around 700 and 1400Hz.

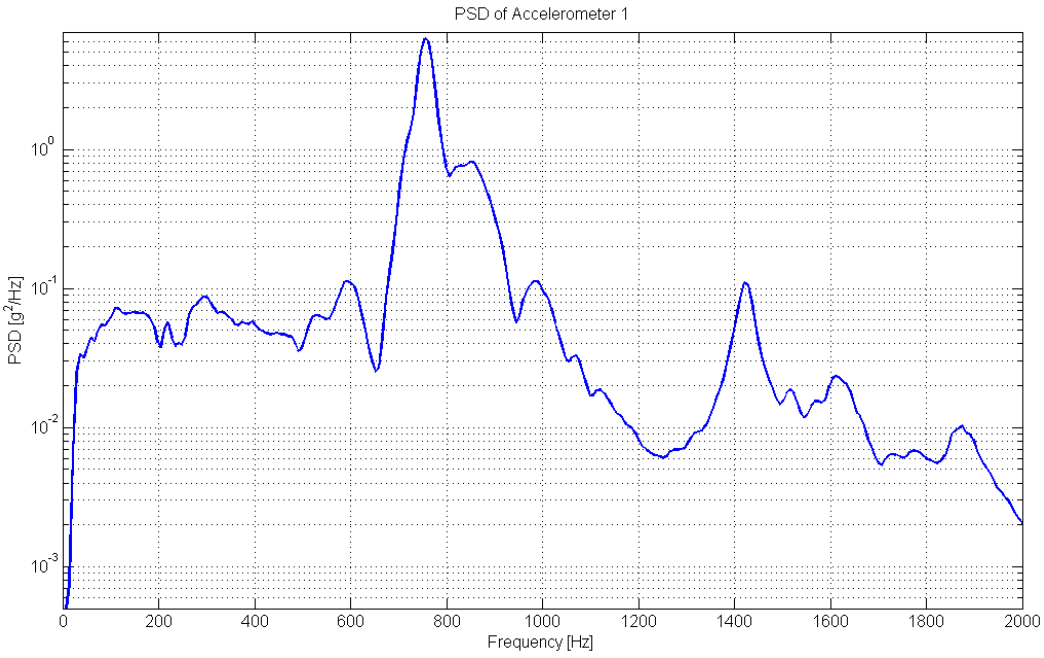


**Figure 73 Random vibration in Y-axis, PSD of Accelerometer 1.**

The maximal and minimal peak accelerations of Accelerometer 1 are **99.7g** and **-125g**, respectively.

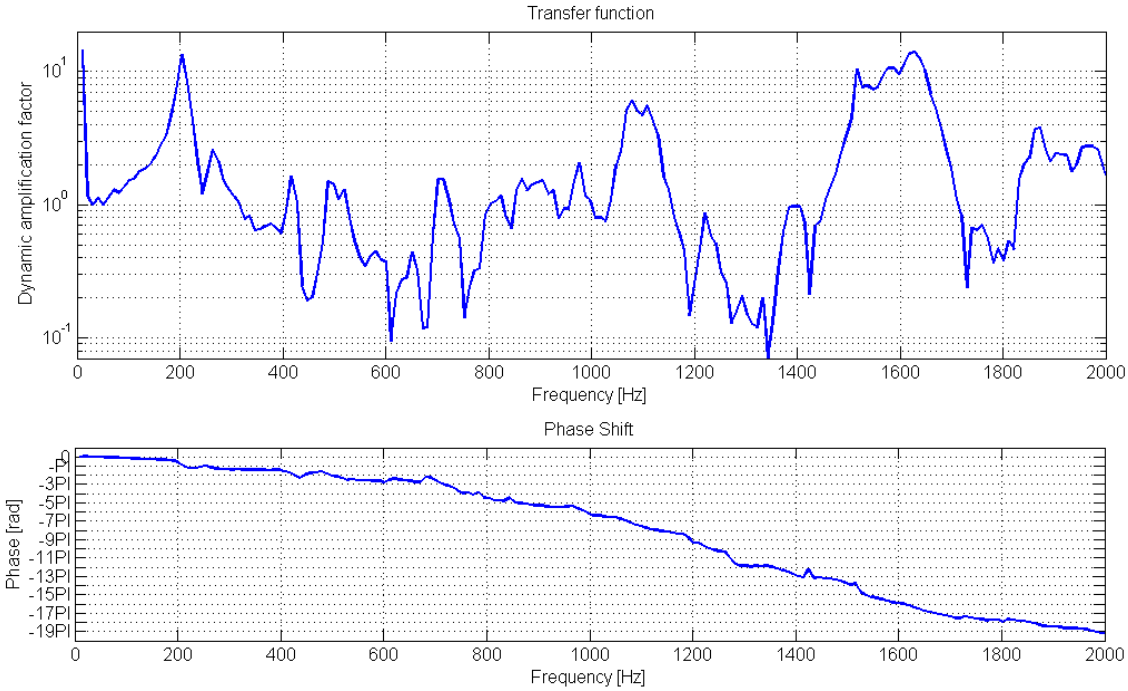


**Figure 74 Random vibration in Y-axis, Transfer function and Phase shift for Accelerometer 2.**

Figure 74 shows that there are a lot of modes (numerous picks, and a huge total phase shift). Possible areas for natural frequencies are around 200, 400, 500, 700, 1100 and 1600Hz.

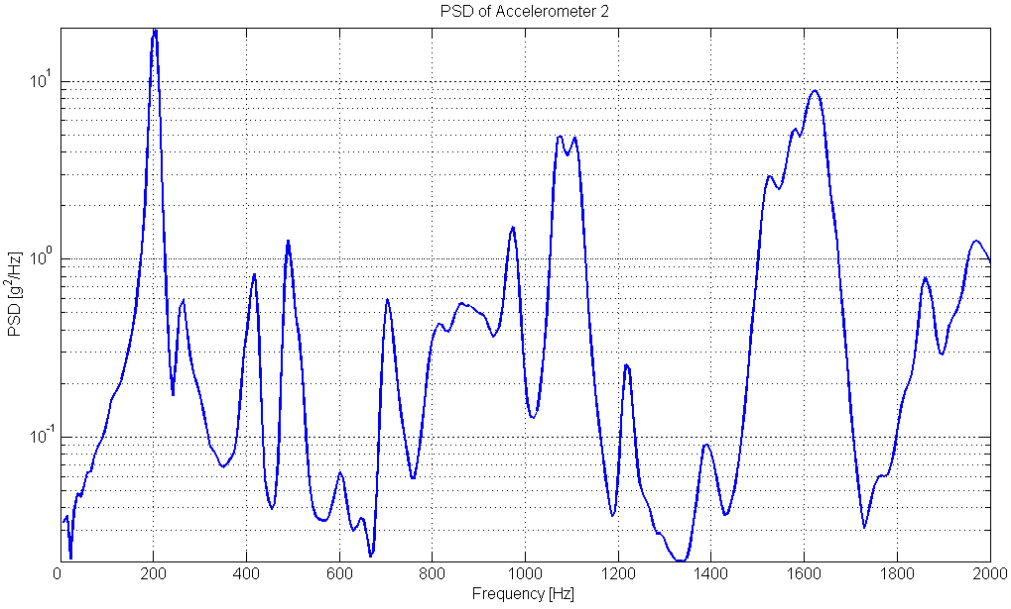


**Figure 75 Random vibration in Y-axis, PSD of Accelerometer 2.**

The maximal and minimal peak accelerations of Accelerometer 2 are **342g** and **-259.5g**, respectively.

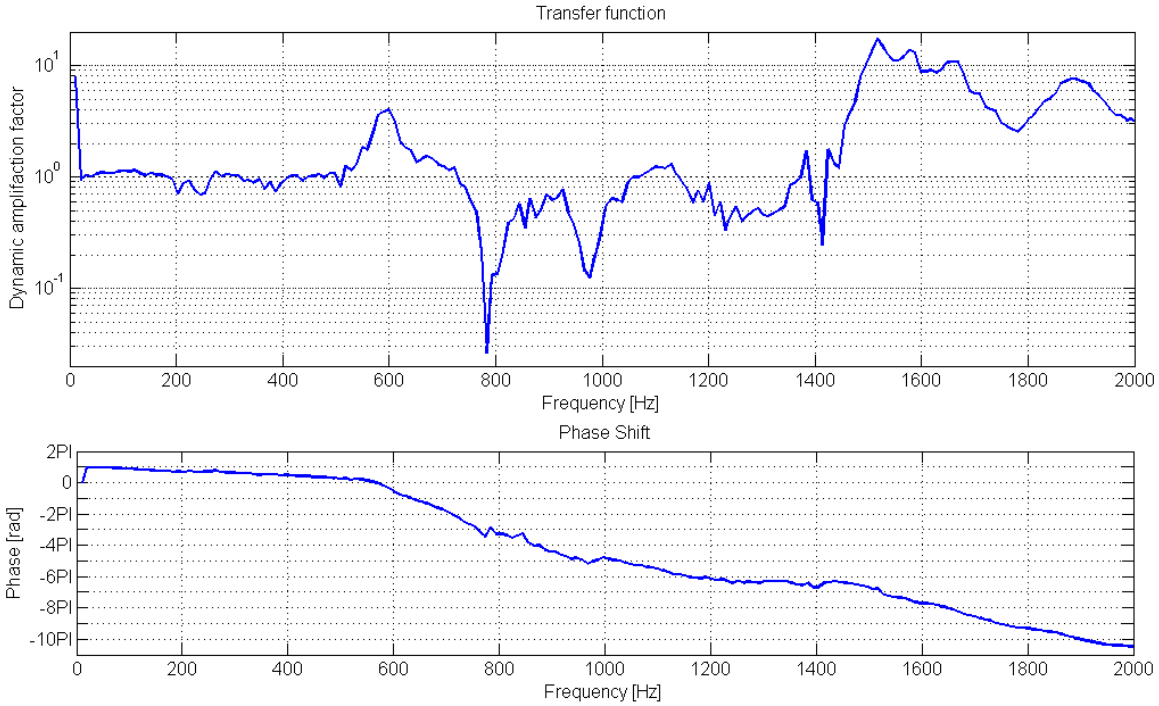


**Figure 76 Random vibration in Y-axis, Transfer function and Phase shift for Accelerometer 3.**

Possible areas for natural frequencies are around 600, 1100, 1550 and 1900Hz.

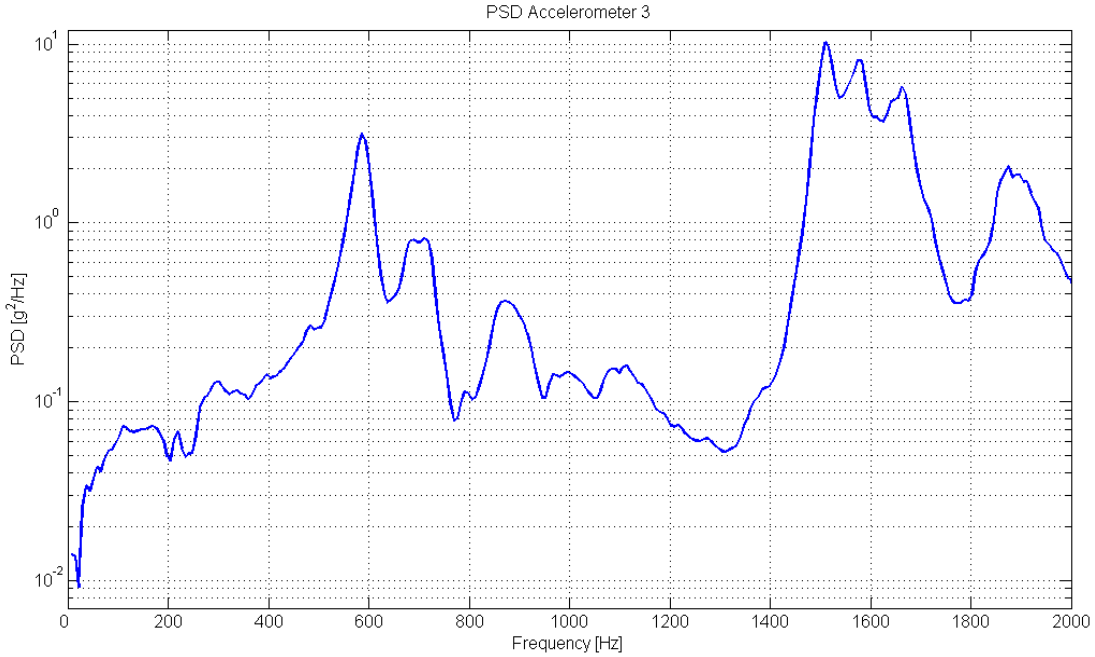


**Figure 77 Random vibration in Y-axis, PSD of Accelerometer 3.**

The maximal and minimal peak accelerations of Accelerometer 3 are **281.7g** and **-219.4g**, respectively.

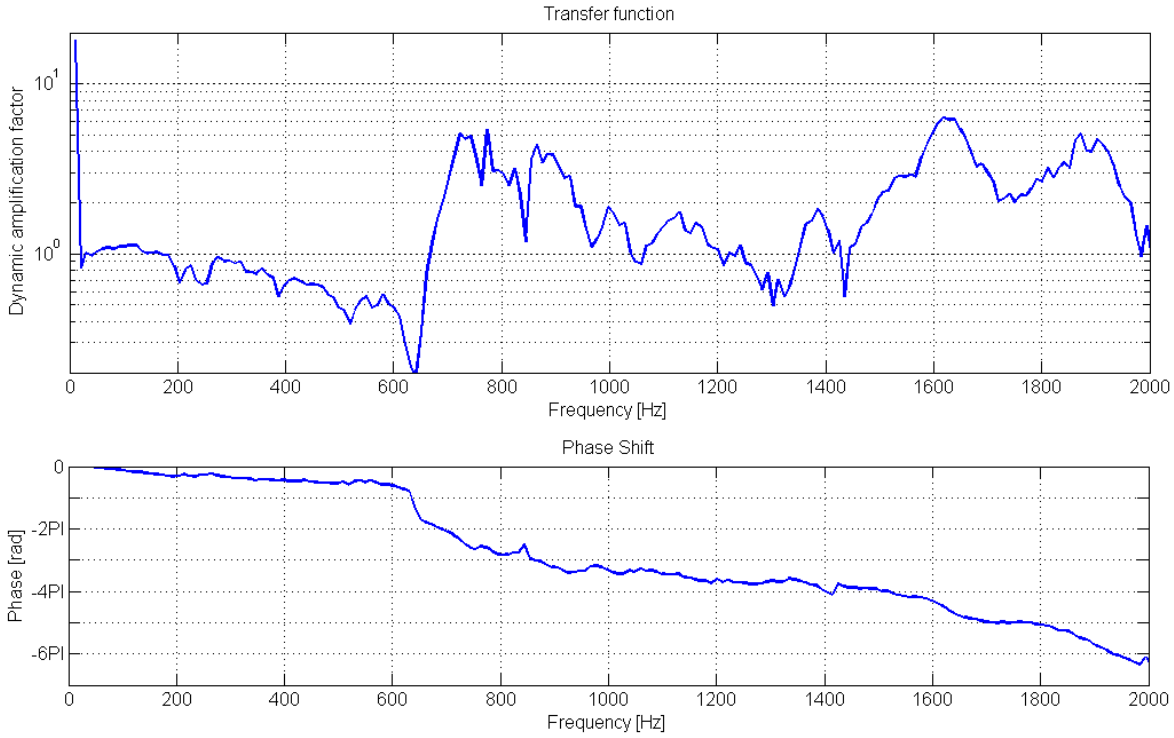


**Figure 78 Random vibration in Y-axis, Transfer function and Phase shift for Accelerometer 4.**

Possible areas for natural frequencies are around 650, 900, 1400, 1600 and 1900Hz.

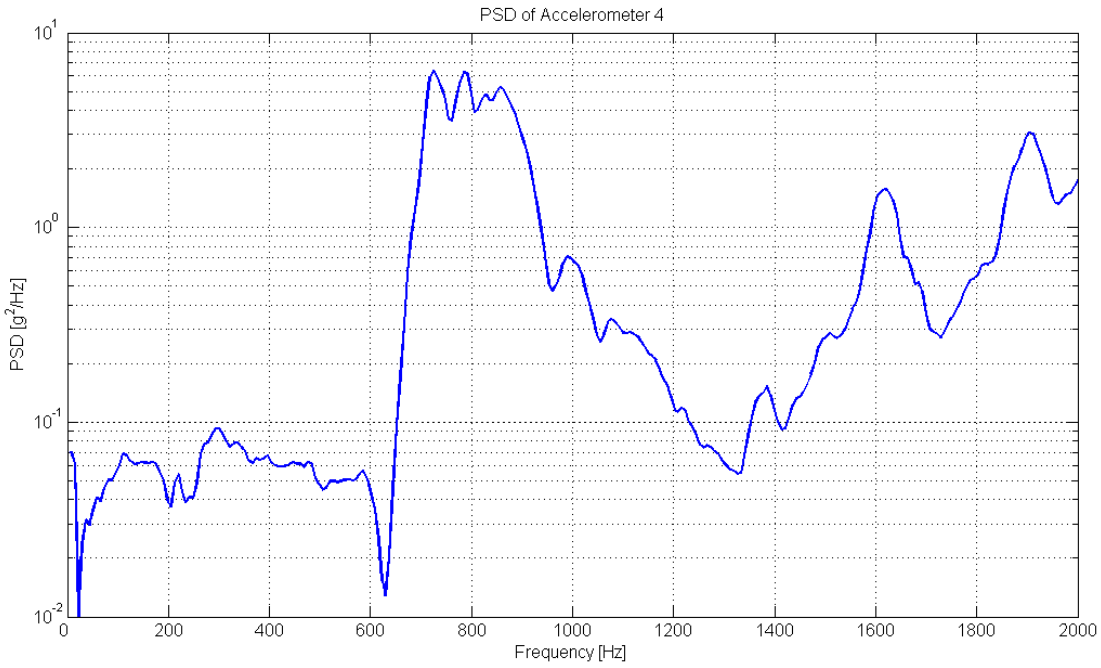


**Figure 79 Random vibration in Y-axis, PSD of Accelerometer 4.**

The maximal and minimal peak accelerations of Accelerometer 4 are **312g** and **-355.7g**, respectively.

For the Z-axis, four accelerometers are used. Their locations are:

- accelerometer n°1: on the slide of the wheel, in Z+ direction
- accelerometer n°2: centered, on the Z- face of the battery box
- accelerometer n°3: centered in Y, at the X- end of the payload frame D14 section,
- accelerometer n°4: centered, on the internal face of the Z- composite panel

Due to wrong calibration of the accelerometer charge amplifiers, the data concerning the four accelerometers are saturated and cannot be used.

To summarize the random vibration tests, the results show that the clearance of the Test-POD provokes bigger peak accelerations and makes the analyses more difficult. In particular it's hard to find the natural frequencies.

The dimensions of the satellite remained the same. The structural members have passed this without damages, but the wheel subassembly undergoes some damages, probably because some components have been glued with cyan-acrylic adhesive (to save time).

## 7.4 Shock qualification test

Due to limited time and lack of test facility, the shock test has not been achieved this semester. It should be performed during Phase C. Despite everything, a preliminary shock test procedure is described in Appendix M.4.

## 7.5 Three points flexural test of solar cell

Test of the mechanical resistance of the solar cells are performed in order to determine their bending resistance. This will permit to determine maximal allowable bending/vibration amplitude of the composite panels during launch that will not endanger the solar cells.

The value about Young's modulus is given by the manufacturer and with the maximal deformation of the cell, the maximal bending stress can be calculated (see equations in Appendix M.5.5). The three points flexural test procedure is described in Appendix M.5.

The results are the following:

- maximal deformation of **7.4 mm** with the active face on the top (see Figure 80)
- maximal deformation of **3.85 mm** with the backside on the top

- **Figure 80 Three points flexural test of a solar cell.**

This test has been performed only one time per side, because of the small quantity of cells in our possession. The explanation of the difference for the results between the both sides can be that the gold layer on the backside is in traction in one case and in compression in the other.

With these maximal deformations, the maximal bending stresses are:

- **85.2 MPa** in the first case
- **44.3 MPa** in the second case

The comparison of these maximal bending stresses with the bending stress of the composite panels due to a 10g gravity field (see Appendix K.3) confirms that the solar cells should not break and also that the composite panels are enough stiff.

To summarize, the three points flexural tests have shown that the solar cells are more flexible that we can imagine, but only if the constraints are uniform. When the solar cells are handled, the risk of damage is really present.

# 8 RECOMMENDATIONS

During the design process it has become evident that there are certain areas that justify further consideration. Some aspects of the project that are worthy of further investigation are listed below.

- With more time it would have been valuable to conduct a more detailed structural analysis. In particular the detailed response of the system to various dynamic loading conditions is extremely important.
- Compare FEA and vibration tests results.
- Find a method and facilities to perform the shock qualification test
- Perform again vibration tests without clearance between satellite and Test-POD. This will allow to obtain natural frequencies of the satellite in another way as FEA.
- Mechanical interfaces have to be clearly defined for each part and a schematic of the electrical connections through the motherboard needs to be established.
- Interface testing has to be achieved in order to determine the performance of the selected epoxy adhesive. This will include thermal cycling to temperatures below as well as above the expected temperature range to check resistance of the bond due to the CTE difference. Additionally, thermal cycling has to be performed to check fatigue performance of the bond.
- Another kind of adhesive could be considered, maybe more compliant in order to be able to connect materials with very different CTE
- Concerning the connections between electronic boards, a backup solution should be found, in order to avoid the problem of to stiff ribbon cable.
- Improve the adhesive process of the solar cells, to avoid contamination of the active surface of the cell, also to guarantee a constant and continuous adhesive layer between composite panels and solar cells.
- Furthermore, an assembly protocol including the electrical connections for the existing configuration needs to be established in more details, accessibility and maintainability of the different components have to be verified.

# 9 CONCLUSION

Phase B in the design of the SwissCube structure and configuration consisted of the selection of technical solutions for the system concept chosen in Phase A.

It was discussed the secondary layout of the SwissCube structure. Several elements that make up the spacecraft were examined and solutions for their design were presented.

A structural model composed of the aluminum monobloc frame, the spacers, composite panels, dummy PCBs connected together with ribbon cables, dummy wheel subassembly, battery box including two batteries, and the payload frame with a dummy mass (headboard PCB) at the end, has been assembled.

In the analysis section, a computational analysis of a structural model has been conducted to determine stresses and deflections of structural members under various static and dynamic load conditions.

Sinusoidal and random vibration tests have been performed on structural model of the satellite in order to validate the design of the SwissCube structure and configuration. The satellite endured these tests without damages.

# TERMS, DEFINITIONS AND ABBREVIATED TERMS

| | |
|---|---|
| ADCS | Attitude Determination and Control System |
| CalPoly | California Polytechnic Institute |
| CDMS | Command and Data Monitoring System |
| CDR | Critical Design Review |
| CDS | CubeSat Design Specifications document |
| C.o.M. | Center of Mass |
| COTS | Commercial off The Shelf |
| CSDS | CubeSat Design Specification Document |
| CTE | Coefficient of thermal Expansion |
| CVCM | Collected Volatile Condensable Material |
| ECSS | European Cooperation for Space Standardization |
| EPS | Electrical Power System |
| FEA | Finite Element Analysis |
| FOS | Factor of Safety |
| GaAs | Gallium Arsenide |
| IC | Integrated Circuit |
| ICD | Interface Control Document |
| LV | Launch Vehicle |
| MDD | Mission Description Document |
| MOS | Margin of Safety |
| MTP | Mission Test Plan |
| P-POD | Poly Picosatellite Orbital Deployer |
| PCB | Printed Circuit Board |
| PDR | Preliminary Design Review |
| RBFP | Remove Before Flight Pin |
| RF | Radio Frequency |
| TBC | To be confirmed |
| TBD | To be defined |
| TML | Total Mass Loss |

# REFERENCES

[1] Armen Toorian, *CubeSat as responsive Satellites*, California Polytechnic State University, 3rd Responsive Space Conference, 2005.

[2] CubeSat Design Specification, Revision 9, CalPoly, May 2005.

[3] R. Krpoun, *CubeSat Project – Mission Description Document*, EPFL, May 2005.

[4] M. Noca, *SwissCube Project Specifications*, EPFL, January 2006.

[5] AIAA Aerospace Design Engineers Guide, Fifth Edition, Published by AIAA, 2003.

[6] ECSS-E-30 Part 3A Mechanical - Part 3 Mechanisms (25 April 2000)

[7] I. M. Daniel, O. Ishai, *Engineering mechanics of composite materials*, Second Edition, 2006, Oxford University Press.

[8] ECSS-Q-70-71A rev. 1(18 June 2004) QA selection of space materials

[9] S3-A-STRU-1-5-Structure_Configuration.doc

[10] ECSS-Q-70-71A rev. 1(18 June 2004) QA selection of space materials

[11] M. Del Pedro, T. Gmür, J. Botsis, *Introduction à la mécanique des solides et des structures*, PPUR, 2004.

[12] Warren C. Young, *Roark's Formulas for Stress & Strain*, Sixth Edition, 1989, McGraw-Hill Book Company.

[13] CubeSat Test Pod User's Guide, Revision 4, CalPoly, June 2005.

**Other non-referenced documents:**

Caillibot, Grant, Kekez, *Formation Flying Demonstration Missions Enabled by CanX Nanosatellite Technology*, University of Toronto, 19th Annual AIAA/USU Conference on Small Satellites.

Canada's Smallest Satellite: The Canadian Advanced Nanospace eXperiment (CanX-1), University of Toronto.

Charles D. Brown, *Elements of spacecraft design*, AIAA education series, American Institute of Aeronautics and Astronautics, Inc., Reston, 2002.

Chen-Joe Fong, *Lessons Learned of NSPO's Picosatellite Mission: YamSat - 1A, 1B & 1C*, National Space Program Office Taiwan, 16th Annual AIAA/USU Conference on Small Satellites, 2002.

CNES, Centre National d'Etudes Spatiales, France: *Techniques et technologies des véhicules spatiaux, vol.3 Plates-formes*, Cours de technologie spatiale, Cépaduès-Editions, Toulouse, 1998.

CubeSat Project Critical Design Review, University of Tokyo, April 2001.

Hank Heidt, CubeSat, *A new Generation of Picosatellite for Education and Industry Low-Cost Space Experimentation*, 14th Annual/USU Conference on Small Satellites, 2000.

Illinois Observing Nanosatelite (ION) final report, University of Illinois, May 2003.

Jacob H. Oehrig, *TU Sat 1 An Innovative Low-Cost Communications Satellite*, Taylor University, 15th Annual/USU Conference on Small Satellites.

Jake A. Schaffner, *The Electronic System Design, Analysis, Integration, and Construction of the CalPoly State University CP1 CubeSat*, California Polytechnic State University, 16th AIAA/USU Conference on Small Satellites, 2002.

KUTESat Critical Design Review, Kansas University.

Matzen, Jespersen, *Design specifications for the mechanical part of the DTUsat,* Technical university of Denmark, January 2004.

QuakeSat Lessons Learned: Notes from the Development of a Triple CubeSat, 2004.

R. Krpoun, *CubeSat Project – Management Plan*, EPFL, May 2005.

R. Krpoun, *Preliminary Interface Control Document (ICD)*, EPFL, September 2005.

The AAU-CubeSat student satellite project: Architectural overview and lessons learned, 2004.

The Design and Operation of The Canadian Advanced Nanospace eXperiment (CanX-1), University of Toronto.

UH CubeSat Critical Design Review, System Integration and Testing, University of Hawaii, May 2002

Zheng You, *MEMSSat: a TestBed of MEMS Technologies for Space,* Tsinghua University, 19th Annual AIAA/USU Conference on Small Satellites, 2005.

**Internet links:**

Aalborg University AAU CubeSat : www.cubesat.auc.dk

AMSAT - Launch Information : www.amsat.org/amsat-new/satellites/cubesats.php

ArianEspace : http://www.arianespace.com

California Polytechnic State University PolySat : www.polysat.org

Cornell University CubeSat : www.mae.cornell.edu/cubesat

CubeSat Community : http://cubesat.calpoly.edu

CubeSat Kit : www.cubesatkit.com

Dartmouth College DartSat : http://engineering.dartmouth.edu/~dartsat/

Iowa Sate University CySat : http://cosmos.ssol.iastate.edu/cysat/resources.html

Material Property Data : www.matweb.com

Montanna State University MEROPE : http://www.ssel.montana.edu/merope/

Norwegian Student Satellite Project NCUBE : http://www.ncube.no

SatnfordStanford University CubeSat : http://ssdl-delta.stanford.edu/narcissat

Stanford University QuakeSat : http://www.quakefinder.com/quakesat.htm

Taylor University TU SAT 1 : http://www.css.tayloru.edu/~physics/picosat/

Technical University of Denmark DTUsat : www.dtusat.dtu.dk

The Stensat Group : http://www.stensat.org

University of Hawaii CubeSat Project : http://www-ee.eng.hawaii.edu/~cubesat/

University of Illinois CubeSat UIUC : http://courses.ece.uiuc.edu/cubesat/

University of Nevada NevadaSat : http://www.unr.edu/NevadaSat/

University of New South Wales BlueSat : http://www.bluesat.unsw.edu.au/

University of Tokyo CubeSat : www.space.t.u-tokyo.ac.jp/cubesat/index-e.html

University of Toronto CanX , http://www.utias-sfl.net

# DATE AND SIGNATURE

Lausanne, February the 23rd

Guillaume Roethlisberger

# Appendix A CubeSat Specification Drawing

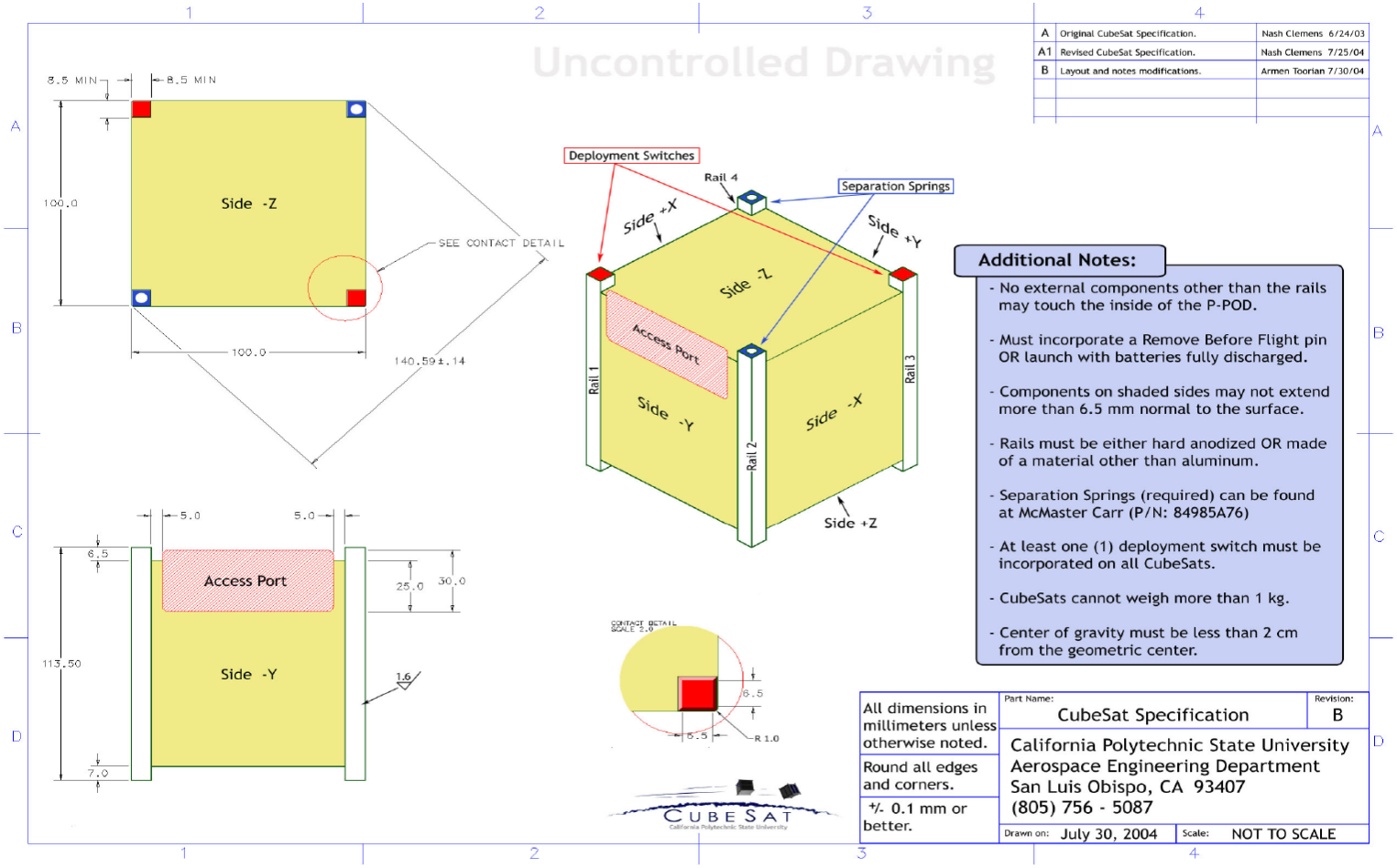


Ref.: **S3-B-STRU-1-4-StructureConfiguration.doc**

# Appendix B Launch Environment

During the preparation for launch and then during the flight, the spacecraft is exposed to a variety of mechanical, thermal, and electromagnetic environments. This chapter provides a description of the environment that the spacecraft is intended to withstand.

All environmental data given in the following paragraphs should be considered as limit loads, applying to the spacecraft. The related probability of these figures not being exceeded is 99 %.

Without special notice all environmental data are defined at the spacecraft base, i.e. at the adapter/spacecraft interface.

## B.1 Frequency requirements

To prevent dynamic coupling with fundamental modes of the LV, the spacecraft should be designed with a structural stiffness which ensures that the following requirements are fulfilled, see Table 10. In that case the design limit load factors given in next paragraph are applicable.

The cantilevered fundamental mode frequencies of a spacecraft hard-mounted at the interface with an off-the shelf adapter must be:

**Table 10 Stiffness criteria for the various LVs.**

| | In lateral axis | In longitudinal axis |
|---|---|---|
| Vega[1] | ≥ 15 Hz | 20 Hz ≤ F ≤ 45 Hz |
| Soyuz[2] | ≥ 15 Hz | ≥ 35 Hz |
| Dnepr | ≥ 10 Hz | ≥ 20 Hz |
| Ariane 5 | ≥ 10 Hz | ≥ 31 Hz |

[1] for spacecraft mass ≤ 2500 kg

[2] for spacecraft mass ≤ 5000 kg

## B.2 Steady state acceleration

During flight, the spacecraft is subjected to static and dynamic loads. Such excitations may be of aerodynamic origin (e.g., wind, gusts, or buffeting at transonic velocity) or due to the propulsion systems (e.g., longitudinal acceleration, thrust build-up or tail-off transients, or structure-propulsion coupling, etc.). The highest longitudinal and lateral static accelerations for various launch vehicles are given in Table 11.

**Table 11 Static accelerations induced on structure during launch.**

| Launch vehicle | Longitudinal acceleration (g) | Lateral acceleration (g) |
|---|---|---|
| Vega | 5,5 | 0,9 |
| Dnepr | 7,8 | 0,8 |
| Soyuz | 4,3 | 0,4 |
| Ariane 5 | 4,25 | 0,25 |

## B.3 The design load factors

The design load factors are represented by the quasi-static g-loads that are the more severe combinations of dynamic and steady-state accelerations that can be encountered at any instant of the mission (ground and flight operations).

The QSL reflects the line load (sometimes named mechanical fluxes, Φ) at the interface between the spacecraft and the adapter.

The flight limit of the QSL for a spacecraft launched on various LVs and complying with the previously described frequency requirements are given in the Table 12, Table 13, Table 14 and Table 15.

**Table 12 Vega: Quasi-Static Loads.**

| Load Event | | QSL (g) (+ = tension; − = compression) | | | | | |
|---|---|---|---|---|---|---|---|
| | | Longitudinal | | | Lateral | | |
| | | Static | Dynamic | Total | Static | Dynamic | Total |
| 1 | Lift-off phase | − 1.5 | ± 2.0 | min − 3.5<br>max+ 0.5 | - | - | ± 0.9 |
| 2 | Flight with maximum dynamic pressure (Qmax) | − 2.5 | ± 0.5 | min − 3.0<br>max − 2.0 | - | - | ± 0.9 |
| 3 | First-stage flight with maximal acceleration | − 4.5 | ± 0.5 | min − 5.0<br>max − 4.0 | - | - | ± 0.5 |
| 4 | Third stage maximal acceleration | - 4.5<br>See note 1 | ± 0.2 | min − 4.7<br>max − 4.3 | - | - | ± 0.2 |
| 6 | Stages ignition | - | - 5.0<br>+ 3.0 | min − 5.0<br>max+ 3.0 | - | - | ± 0.2 |

**Table 13 Soyuz: Quasi-Static Loads.**

| Load Event | | QSL (g) (+ = tension; – = compression) | | | | | |
|---|---|---|---|---|---|---|---|
| | | Lateral | | | Longitudinal | | |
| | | Static | Dynamic | Total | Static | Dynamic | Total |
| 1 | Liftoff | ±0.2 | ±1.6 | ±1.8 | –1.0 | ±0.6 | min –1.6<br>max –0.4 |
| 2 | Flight with maximum dynamic pressure (Qmax) | ±0.4 | ±0.6 | ±1.0 | –2.2 | ±0.4 | min –2.6<br>max –1.8 |
| 3 | First-stage flight with maximal acceleration | ±0.1 | ±0.4 | ±0.5 | –4.3 | ±0.7 | min –5.0<br>max –3.6 |
| 4 | Separation between first and second stages | ±0.2 | ±0.8 | ±1.0 | –4.1<br>–1.0 | 0.0<br>±0.3 | min –4.1<br>max –0.7 |
| 5 | Second-stage flight | ±0.1 | ±0.7 | ±0.8 | –2.6<br>–1.0 | ±1.2<br>±0.3 | min –3.8<br>max –0.7 |
| 6 | Separation between second and third stages | ± 0.2 | ± 0.6 | ± 0.8 | –2.6<br>–0.2 | 0.0<br>±1.5 | min –2.6<br>max +1.3 |
| 7 | Beginning of third-stage flight | ± 0.2 | ± 0.5 | ± 0.7 | –1.2 | ±1.5 | min –2.7<br>max +0.3 |
| 8 | Third-stage engine cutoff | ± 0.1 | ± 0.2 | ± 0.3 | –3.7<br>0.0 | 0.0<br>±1.5 | min –3.7<br>max +1.5 |

**Table 14 Ariane 5: Quasi-Static Loads.**

| Acceleration (g) / Critical flight events | Longitudinal | | Lateral | Additional line load (N/mm) |
|---|---|---|---|---|
| | Static | Dynamic | Static + Dynamic | |
| Lift-off | - 1.7 | ± 1.5 | ± 2 | 10 (15*) |
| Maximum dynamic pressure | - 2.7 | ± 0.5 | ± 2 | 14 (21*) |
| SRB end of flight | - 4.55 | ± 1.45 | ± 1 | 20 (30*) |
| Main core thrust tail-off | - 0.2 | ± 1.4 | ± 0.25 | 0 |
| Max. tension case: SRB jettisoning | + 2.5** | | ± 0.9 | 0 |

**Table 15 Dnepr: Quasi-Static Loads.**

| Load Source | Acceleration | |
|---|---|---|
| | Longitudinal (X) | Lateral (y, z) |
| LV movement inside TLC | 2.5±0.7 | ±0.3 |
| After LV exit from TLC | ±1.0 | ±0.8 |
| 1st stage burn: | | |
| Maximum dynamic head | 3.0±0.5 | 0.5±0.5 |
| Maximum longitudinal acceleration | 7.5±0.5 | 0.1±0.5 |
| 2nd stage burn – maximum longitudinal acceleration | 7.8±0.5 | 0.2 |
| 3rd stage burn | -0.3...-0.5 | 0.25 |

## B.4 Safety factors

Spacecraft qualification and acceptance test levels are determined by increasing the design load factors (the flight limit levels) — which have been previously presented — by the safety factors given in Table 16, Table 17 and Table 18 for the various LVs. The spacecraft must have positive

margins of safety for yield and ultimate loads. The factors of safety (FOS) is a coefficient by which the design loads are multiplied in order to account for uncertainties in the statistical distribution of loads, uncertainties in structural analysis, manufacturing process, material properties and failure criteria.

**Table 16 Vega: Test Factors, rate and duration.**

| SC tests | Qualification | | Protoflight | | Acceptance | |
|---|---|---|---|---|---|---|
| | Factors | Duration/ Rate | Factors | Duration/ Rate | Factors | Duration/ Rate |
| Static (QSL) | 1.25 ultimate<br>1.1 yield | N/A | 1.25 ultimate<br>1.1 yield | N/A | N/A | N/A |
| Sine vibrations | 1.25 | 2 oct/min | 1.25 | 4 oct/min | 1.0 | 4 oct/min |
| Acoustics | 1.41 (or +3 dB) | 120 s | 1.41 (or +3 dB) | 60 s | 1.0 | 60 s |
| Shock | N/A | 2 releases | N/A | 2 releases | N/A | 1 release |

**Table 17 Soyuz: Test Factors, rate and duration.**

| SC tests | Qualification | | Protoflight | | Acceptance | |
|---|---|---|---|---|---|---|
| | Factors | Duration/ Rate | Factors | Duration | Factors | Duration |
| Static (QSL) | 1.3 ultimate<br>1.1 yield | N/A | 1.3 ultimate<br>1.1 yield | N/A | N/A | N/A |
| Sine vibrations | 1.3 | 0.5 oct/min | 1.3 | 1.0 oct/min | 1.0 | 1.0 oct/min |
| Random vibrations | 2.25(*) | TBD | 2.25(*) | TBD | 1.0 (*) | TBD |
| Acoustics | 1.41 (or +3 dB) | 120 s | 1.41 (or +3 dB) | 60 s | 1.0 | 60 s |
| Shock | 1.41 (or +3 dB) | N/A | 1.41 (or +3 dB) | N/A | N/A | N/A |

Note:

(*) - Factor by which to multiply the Power Spectral Density.

**Table 18 Ariane 5: Test Factors, rate and duration.**

| S/C tests | Qualification | | Protoflight | | Acceptance | |
|---|---|---|---|---|---|---|
| | Factors | Duration/Rate | Factors | Duration/Rate | Factors | Duration/Rate |
| Static (QSL) | 1,25 ultimate<br>1,1 yield | N/A | 1,25 ultimate<br>1,1 yield | N/A | N/A | N/A |
| Sine vibrations | 1,25 | 2 oct/min | 1,25 | 4 oct/min | 1.0 | 4 oct/min |
| Acoustics | 1.41 (or +3 dB) | 120 s | 1.41 (or +3 dB) | 60 s | 1.0 | 60 s |
| Shock | 1.41 (or +3 dB) | N/A | 1.41 (or +3 dB) | N/A | N/A | N/A |

For Dnepr, spacecraft dimensioning and testing must take into account safety factors, which are defined by the spacecraft authority, but should be no less than the values given below:

- 2.0 for ground handling;
- 1,5 during launch while LV is moving inside the TLC;

- 1,3 during launch after the LV exits from the TLC;
- 1,3 during the LV flight.

## B.5 Sine-equivalent dynamics

Sinusoidal excitations derived from motors pressure oscillations and controlled POGO effect [1]may affect the LV during its flight (mainly the atmospheric flight), as well as during some of the transient phases of the flight.

The envelope of the sinusoidal (or sine-equivalent) vibration levels does not exceed the values given in Figure 81 for the longitudinal case, and Figure 82 for the lateral case.

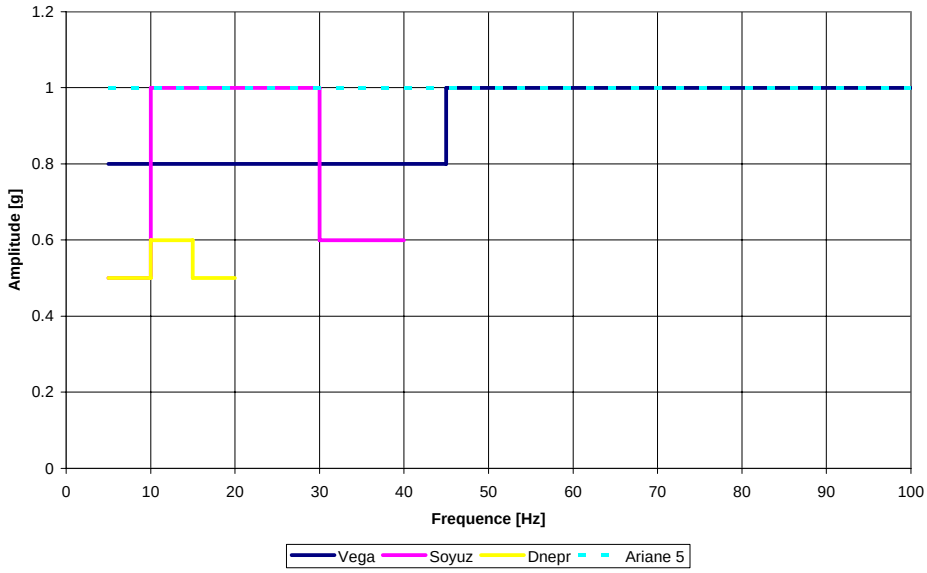


**Figure 81 Amplitude of the sine excitations for the longitudinal direction.**

[1] The POGO vibrational instability effect is due to a coupling between the principal structure of a launcher, the so-called secondary structure, and the thrust. Thrust fluctuations generate longitudinal vibrations which in turn bring about pressure vibrations, leading again to thrust variations.

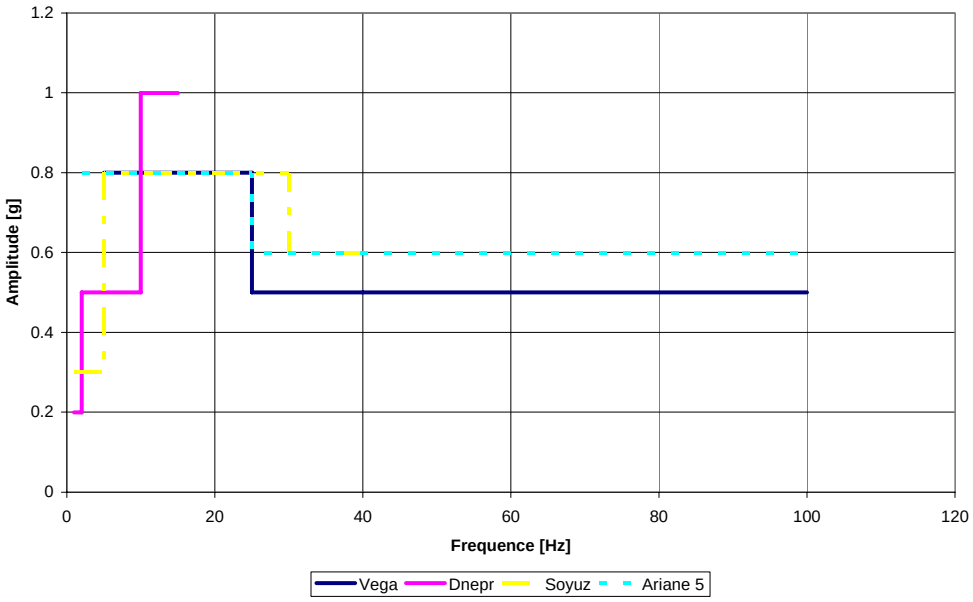


**Figure 82 Amplitude of the sine excitations for the lateral direction.**

## B.6 Random vibration

Random vibrations are generated by propulsion system operation and by the adjacent structure's vibro-acoustic response. Maximum excitation levels are obtained during the first-stage flight. Power spectral density (PSD) and root mean square vibration levels ($G_{RMS}$) along each of three axes are given in Table 19 and Table 20 for Soyuz and Dnepr LVs respectively.

For Soyuz, the random vibrations must be taken into account for equipment dimensioning in the 40 – 100 Hz frequency range, considering that at higher frequency it is covered by acoustic loads.

**Table 19 The maximum flight levels of random vibrations at Spacecraft Base for Soyuz LV.**

| Event | Frequency Band (Hz) | | | | | | $G_{RMS}$ (g) | Duration of application (s) |
|---|---|---|---|---|---|---|---|---|
| | 20 – 50 | 50-100 | 100-200 | 200-500 | 500-1000 | 1000-2000 | | |
| | PSD, Power Spectral Density(1) ($g^2$/Hz) | | | | | | | |
| 1st stage flight | 0.0050 | 0.0050<br>0.0100 | 0.0100<br>0.0250 | 0.0250 | 0.0250<br>0.0100 | 0.0100<br>0.0050 | 4.94 | 120 |
| 2nd stage and 3rd stage flight | 0.0025 | 0.0025<br>0.0050 | 0.0050<br>0.0100 | 0.0100 | 0.0100<br>0.0050 | 0.0050<br>0.0025 | 3.31 | 480 |
| FREGAT flight | 0,0020 | 0,0020 | 0,0020 | 0,0020 | 0,0020<br>0,0010 | 0,0010 | 1,63 | 875 |

**Table 20 Spectral Density of Vibro-accelerations at SC/LV Interface for Dnepr LV.**

| Frequency sub-band, Hz | Load Source | |
|---|---|---|
| | Liftoff, LV flight segment where M=1, $q_{max}$ | 1st stage burn (except for LV flight segment where M=1, $q_{max}$), 2nd stage burn, 3rd stage burn |
| | Spectral Density, $g^2$/Hz | |
| 20-40 | 0.007 | 0.007 |
| 40-80 | 0.007 | 0.007 |
| 80-160 | 0.007-0.022 | 0.007 |
| 160-320 | 0.022-0.035 | 0.007-0.009 |
| 320-640 | 0.035 | 0.009 |
| 640-1280 | 0.035-0.017 | 0.009-0.0045 |
| 1280-2000 | 0.017-0.005 | 0.0045 |
| Root Mean Square Value, σ, g | 6.5 | 3.6 |
| Duration, sec. | 35 | 831 |

For VEGA : payload above 300 kg, the broadband vibrations are covered by the acoustics.

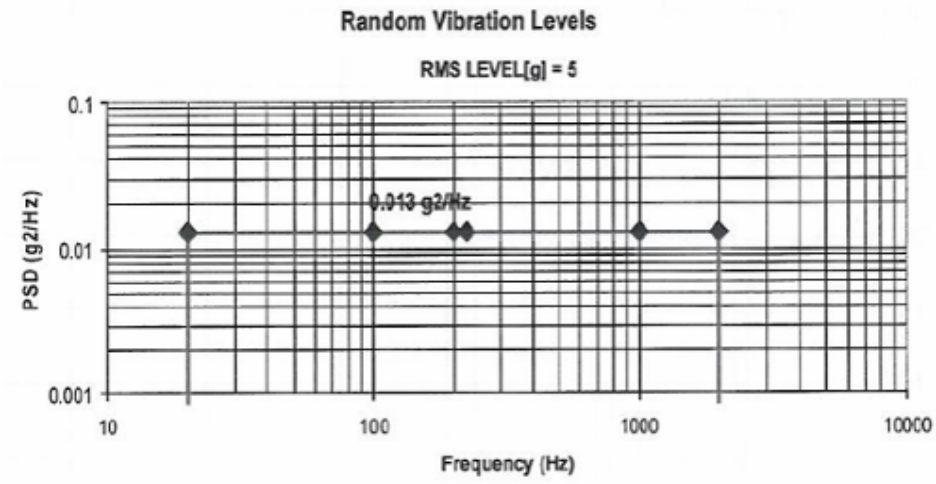


**Figure 83 Maximu random vibrations flight levels at SC Base for VEGA.**

For Ariane 5: under 100 Hz, the random environment is covered by the sine environment. The acoustic spectrum covers excitations produced by random vibration at the spacecraft base for frequency band above 100 Hz.

## B.7 Acoustic vibration

On ground, the noise level generated by the venting system does not exceed 94 dB. This value is for the case of the Ariane 5, Vega or Soyuz LV at the GSC.

In flight, acoustic pressure fluctuations under the fairing are generated by engine operation (plume impingement on the pad during lift-off) and by unsteady aerodynamic phenomena during atmospheric flight (i.e., shock waves and turbulence inside the boundary layer), which are transmitted through the upper composite structures. Apart from lift-off and transonic/Q max flight, acoustic levels are substantially lower than the values indicated hereafter.

The envelope spectrum of the noise induced inside the fairing during flight is shown in Table 11 and Figure 84.

**Table 1 Acoustic noise spectrum under the fairing.**

| | Vega | Soyuz | Dnepr | Ariane 5 |
|---|---|---|---|---|
| Octave Center Frequency [Hz] | Flight limit level [dB] | | | |
| 31.5 | 124 | 125 | 125 | 128 |
| 63 | 129 | 132 | 132 | 131 |
| 125 | 135 | 134 | 135 | 136 |
| 250 | 132 | 136 | 134 | 135 |
| 500 | 131 | 134 | 132 | 132 |
| 1000 | 120 | 125 | 129 | 126 |
| 2000 | 100 | 121 | 126 | 120 |
| 4000 | | | 121 | |
| 8000 | | | 115 | |
| OASPL | 138.5 | 141 | 140 | 140.5 |

Remark: reference 0 dB = $2 \cdot 10^{-5}$ Pa

OASPL: overall acoustic sound pressure level

These maximum environments are applied during a period of approximately 60 seconds in the case of Soyuz, 30 seconds for Vega and 35 seconds in the case of Dnepr. For Ariane 5 LV, any value is given.

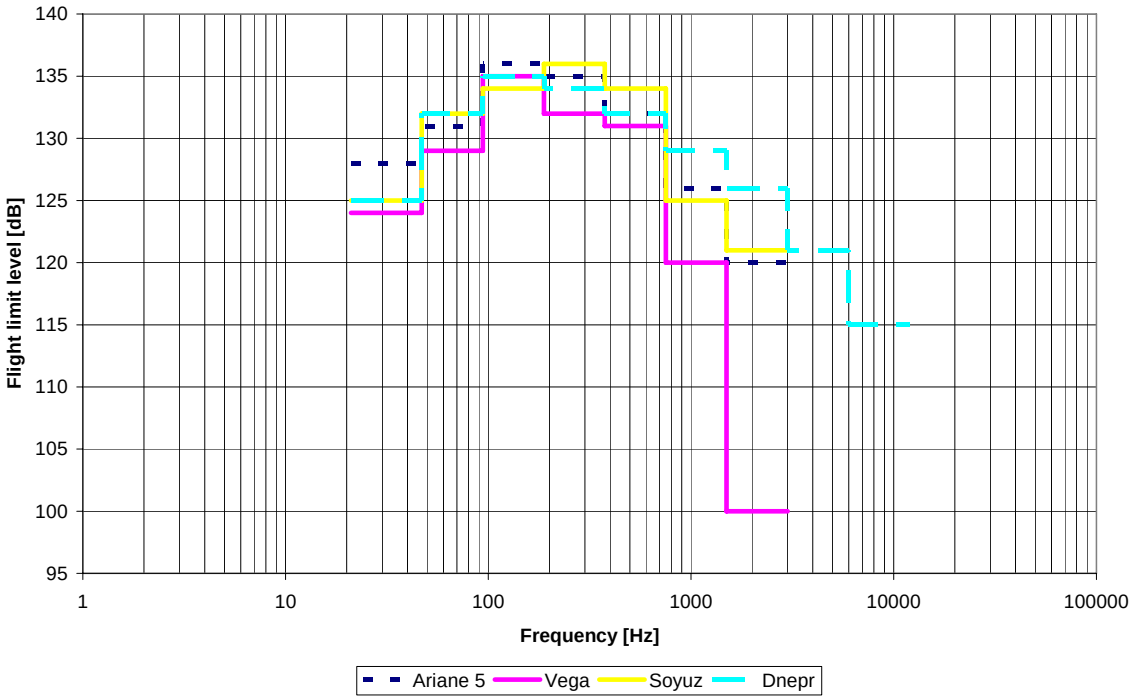


**Figure 84 Acoustic noise spectrum for the various LV.**

## B.8 Shocks

The spacecraft is subject to shock primarily during stage separations, fairing jettisoning, and actual spacecraft separation.

The envelope acceleration shock response spectrum (SRS) at the spacecraft base (computed with a Q-factor of 10) is showed on Figure 85 These levels are applied simultaneously in axial and radial directions.

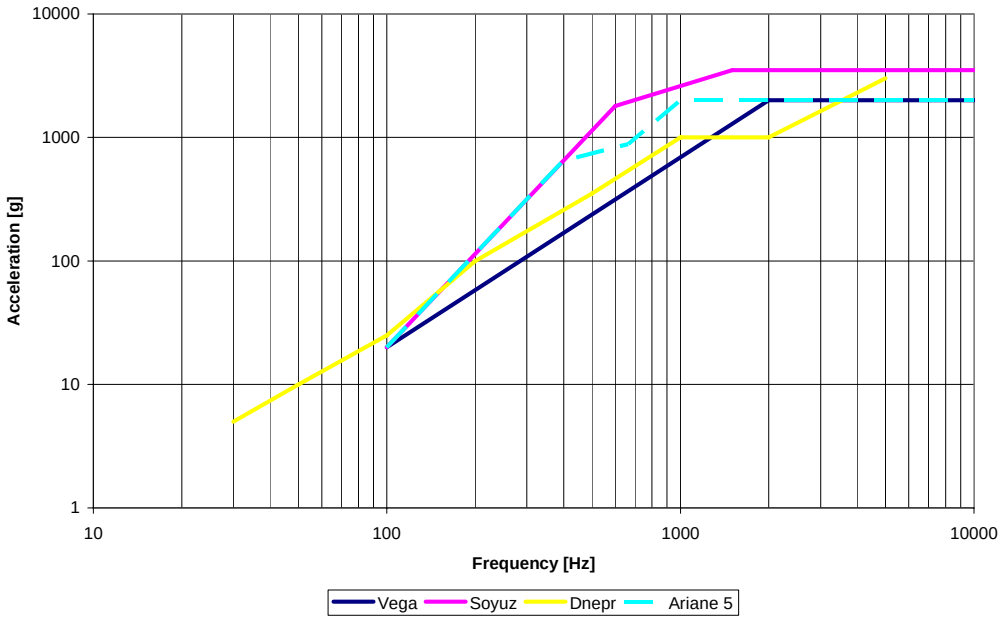


**Figure 85 Envelope acceleration shock response spectrum (SRS).**

## B.9 Static pressure under the fairing

On ground after encapsulation, the air velocity around the spacecraft due to the ventilation system is lower than 2 m/sec (value experienced in front of the air inlet) for Ariane 5 and Vega, 5 m/sec for Soyuz. The velocity may locally exceed this value.

In flight, the payload compartment is vented during the ascent phase through vent holes insuring a low depressurization rate of the fairing compartment. For Vega, the depressurization rate under the fairing does not exceed 5,0 kPa/s (50 mbar/s).

For Soyuz, the depressurization rate does not exceed 2,0 kPa/s (20 mbar/s) for a sustained length of time. Locally at the time of maximum dynamic pressure, at ~ 50s, there is a short period of about 2 seconds when the depressurization rate can reach 3,5 kPa/s (35 mbar/s). The difference between the pressure under fairing and free-stream external static pressures, at the moment of the fairing jettisoning, is lower than 0,2 kPa (2 mbar).

For Dnepr, the maximum rate of in-flight pressure change inside the fairing envelope does not exceed 3,4 kPa/s (34 mbar/s), except for transonic phase of flight where a short term (2-3 seconds) increase up to 3,4 kPa/s (34 mbar/s) is possible.

And finally for Ariane 5, the depressurization rate does not exceed 2,0 kPa/s (20 mbar/s) for most time. Locally at the time of maximum dynamic pressure, at ~ 50s, there is a short period of less than 2 seconds when the depressurization rate can reach 4,5 kPa/s (45 mbar/s) in dual launch and 5,0 kPa/s (50 mbar/s) in single launch.

## B.10 Thermal Environment

The thermal environment provided during spacecraft preparation and launch has to be considered during the following phases:

- Ground operations
  - The spacecraft preparation within the CSG facilities;
  - The upper composite and launch vehicle operations with spacecraft encapsulated inside the fairing
- Flight
  - Before fairing jettisoning;
  - After fairing jettisoning

### B.10.1 Ground operations

The environment that the spacecraft experiences both during its preparation and once it is encapsulated under the fairing is controlled in terms of temperature, relative humidity, cleanliness, and contamination.

For the Vega, Soyuz and Ariane 5 LVs, the typical thermal environment within the air-conditioned GSC facilities is kept around 23°C ± 2°C for temperature and 55% ± 5% for relative humidity.

After encapsulation under the fairing, the environment around the spacecraft is ensured by the insulation capability of the fairing and by an air-conditioning system.

The fairing cavity is vented since encapsulation, including transfer of the upper composite, and the standby phase on the launch pad, up to the lift-off, except during short maintaining operation with the LV on the launch pad. Air-conditioning characteristics are described in Table 21.

**Table 21 Thermal environment on ground (for Vega).**

| S/C location | Transfer between EPCU buildings | S/C in EPCU | | Transfer from EPCU to SLV | S/C on L/V |
|---|---|---|---|---|---|
| | In CCU container | Not encapsulated | Encapsulated | Encapsulated | On launch pad |
| **Hygrometry level** | 55% ± 5% | 55% ± 5% | 55% ± 5% | ≤ 20% | ≤ 20% |
| **Temperature** | ≤25°C | ≤25°C | Air input temperature of injected air is adjustable between 11°C and 25°C (Accuracy: ± 1°C) Outlet temperature of air ≤25°C for payload radiating less than 200 W | 15°C min | ≥ 11°C |

For information, in the EPCU buildings 998 mbar ≤ $P_{atm}$ ≤ 1023 mbar

### B.10.2 Flight environment

Before fairing jettisoning, the thermal flux density radiated by the fairing does not exceed at any point 1000 W/m$^2$ for Vega and Ariane 5, and 800 W/m$^2$ for Soyuz. For the complete estimation of the thermal environment under the fairing the spacecraft dissipated power shall be taken into account.

After fairing jettisoning, the nominal time for jettisoning the fairing is determined in order not to exceed the aerothermal flux of 1135 W/ m$^2$ for Vega, Soyuz and Ariane 5. Typically the aerothermal flux varies from 1135 W/ m$^2$ to less than 200 W/ m$^2$ within 20 seconds after the fairing jettisoning, as presented in Figure 86.

Solar-radiation flux, albedo and terrestrial infrared radiation and conductive exchange with LV must be added to this aerothermal flux. While calculating the incident flux on spacecraft, account must be taken of the altitude of the launch vehicle, its orientation, the position of the sun with respect to the launch vehicle, and the orientation of the considered spacecraft surfaces.

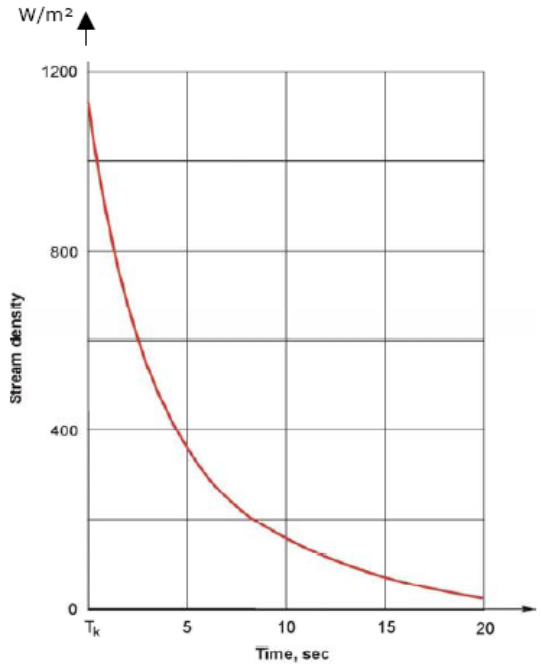


**Figure 86 Typical Aerothermal Flux Decay after fairing jettisoning for Vega, Soyuz and Ariane 5.**

## B.11 Cleanliness and contamination

### B.11.1 Cleanliness

At the GSC (for Vega, Soyuz and Ariane 5), the following standard practices ensure that spacecraft cleanliness conditions are met:

- A clean environment is provided during production, test, and delivery of all upper-composite components (upper stage, interstage section, fairing, and adapter) to prevent contamination and accumulation of dust. The LV materials are selected not to generate significant organic deposit during all ground phases of the launch preparation.
- All spacecraft operations are carried out in payload preparation complex buildings in controlled Class 100'000 clean rooms. During transfer between buildings the spacecraft is transported in payload containers with the cleanliness Class 100'000. All handling equipment is clean room compatible, and it is cleaned and inspected before its entry in the facilities.
- Prior to the encapsulation of the spacecraft, the cleanliness of the upper stages and fairing are verified based on the Visibly Clean Level 2 criteria, and cleaned if necessary.
- Once encapsulated and during transfer and standby on the launch pad, the upper composite will be hermetically sealed and a Class 10'000 air-conditioning of the fairing will be provided.
- On the launch pad access can be provided to the payload. The gantry not being air-conditioned cleanliness level is ensured by the fairing overpressure.

### B.11.2 Contamination

The following values are coming from the User's Manual of Vega, Soyuz and Ariane 5.

During all spacecraft ground activities from spacecraft delivery to launch site and up to lift-off, the maximum organic non-volatile deposit on the spacecraft surface will not exceed 2 mg/ $m^2$/week. The organic contamination in facilities and under the fairing is controlled.

The non-volatile organic deposit on the spacecraft surface generated by the materials outgassing does not exceed 2 mg/$m^2$ (4 mg/$m^2$ in the case of Ariane 5 LV).

The LV systems are designed to preclude in-flight contamination of the spacecraft. The LVs pyrotechnic devices used by the LV for fairing jettison and spacecraft separation are leak proof and do not leads to any satellite contamination.

The non-volatile organic deposit generated by the attitude control thrusters plume on the adjacent spacecraft surfaces is does not exceed 2 mg/$m^2$.

The non-volatile organic contamination generated during ground operations and flight is cumulative.

### B.11.3 Selection of spacecraft materials

Arianespace gives the following outgassing criteria that the spacecraft materials must satisfy:

- Total Mass Loss (TML) ≤ 1 %
- Collected Volatile Condensable Material (CVCM) ≤ 0.1 %

measured in accordance with the procedure "ECSS-Q-70-02A".

# Appendix C Material Properties

## C.1 Certal

These data come from the website http://www.aluplus.dk/pdf/CERTALeng.pdf

Technical Datasheet

**CERTAL®**

**EN AW-7022 / AlZn5Mg3Cu**

Edition September 2001

**ALCAN ROLLED PRODUCTS**

Alcan Aluminium Valais Ltd t +41 27 457 51 11
CH-3960 Sierre, Switzerland f +41 27 457 65 15

### BRIEF DESCRIPTION

Certal® thick plates have been optimised to provide excellent **machinability, shape stability** and **high strength**. Certal® is therefore ideal for industrial tools. Applications include injection and blow-moulds for plastic bottles, plastic containers and shoes as well as heating plates, mechanical guides, tooling supports, jigs and fixtures.

### PROCESSING METHODS

**Weldability**

| | |
|---|---|
| • TIG/MIG filler alloy | possible<br>AA 5183<br>AA 5356 |
| • by resistance | good |

**Surface Treatments**

**Anodizing**

| | |
|---|---|
| • technical | good |
| • decorative | not adequate |
| Polishing | excellent |
| Hard Chroming | good |
| Chemical Nickel-Plating | good |
| Chemical texturing | well adapted |
| **Machinability** | excellent |

### AVAILABILITY

Certal® plates are delivered in temper T651 (quenched – stretched – artificially aged) in the following dimensions :

| Thickness | Max. width |
|---|---|
| 8.0 - 70 mm | 2020 mm |
| 71 - 90 mm | 1820 mm |
| 91- 120 mm | 1520 mm |
| 121- 140 mm | 1020 mm |

For thicknesses above 140 mm, the alloy Certal® SPC is recommended.

### CHEMICAL COMPOSITION (weight %)

| Si | Fe | Cu | Mn | Mg | Cr | Zn | Ti +Zr |
|---|---|---|---|---|---|---|---|
| max. | max. | 0.5 | 0.1 | 2.6 | 0.1 | 4.3 | max. |
| 0.5 | 0.5 | 1.0 | 0.40 | 3.7 | 0.3 | 5.2 | 0.2 |

### PHYSICAL PROPERTIES (nominal values)

| | |
|---|---|
| Density | 2.76 g/cm$^3$ |
| Elastic Modulus | 72000 MPa |
| Lin. thermal expansion coefficient (20°-100°C) | 23.6 $10^{-6}$ K$^{-1}$ |
| Thermal conductivity (Temper T651) | 120 - 150 W/mK |
| Electrical conductivity (Temper T651, 20°C) | 18 - 22 MS/m |

### MECHANICAL STRENGTH

**Min. tensile properties (Temper T651)**[1)]

| Thickness (over ... to ) | Rm [MPa] | Rp0.2 [MPa] | A50 [%] |
|---|---|---|---|
| 12.5 - 25 mm | 540 | 460 | 8 |
| 25 - 50 mm | 530 | 460 | 7 |
| 50 - 100 mm | 500 | 420 | 6 |
| 100 - 140 mm | 490 | 400 | 6 |

1) These guaranteed values are much higher than EN AW-7022 T651 values

**Typical strength for various thicknesses**

| Thickness (over ... to ) | Rm [MPa] | Rp0.2 [MPa] | A50 [%] | HB |
|---|---|---|---|---|
| 8.0 - 25 mm | 555 | 495 | 9 | 170 |
| 25 - 100 mm | 550 | 495 | 8 | 165 |
| 100 - 140 mm | 545 | 490 | 7 | 165 |

# C.2 Titanium Grade 5

## TITAN Grade 5 (6Al-4V) W-Nr. 3.7165

Die Legierung Ti-6Al-4V ist die am meisten verwendete der Alpha-Beta Gruppe und ist die bekannteste aller Titanlegierungen. Bearbeitetes Material wird in der Luftfahrtindustrie, Medizin und anderen Anwendungen eingesetzt, bei denen eine gute Festigkeit im Verhältnis zum Gewicht, sowie gute korrosionsbeständige Eigenschaften gefordert werden. Weiter ist sie giesbar und findet vermehrt Anwendungen auch bei Sportgeräten.

Ti-6Al-4V alloy is the most widely used titanium alloy of the alpha-plus-beta class, and is also the most common of all titanium alloys. The alloy is castable and is utilized "as cast" in sporting goods. The wrought material is used in aerospace, medical, and other applications where moderate strength, good strength to weight, and favorable corrosion properties are required.

| | | |
|---|---|---|
| Produktformen<br>Product Forms | Blech, Band, Stab, Draht, Gussteile, Schmiedestücke, Ringe und Knüppel | Sheet, Plate, Strip, Bar, Rod, Wire, Castings, Forgings, Rings and Billet |
| Normen und Bezeichnungen<br>Major Specifications | UNS R56400<br>W-Nr.: 3.7165<br>ASTM B 265 / AMS 4911 (Blech, Band),<br>ASTM B 348 / AMS 4928 (Stab)<br>MIL-T-9046 | UNS R56400<br>W-Nr.: 3.7165<br>ASTM B 265 / AMS 4911 (plate, sheet, strip),<br>ASTM B 348 / AMS 4928 (bar)<br>MIL-T-9046 |
| Chem. Zusammensetzung<br>Chemical Composition,% | **Grenzwerte**<br>Ti ..... Rest O ..... 0.20 V ..... 3.5/4.5<br>Fe ..... 0.40 AL ... 5.50 - 6.75 H ... max. 0.015<br>N ..... 0.05 C ..... 0.08 | **Limiting**<br>Ti .... Remainder O ..... 0.20 V ..... 3.5/4.5<br>Fe ..... 0.40 AL ... 5.50 - 6.75 H ... max. 0.015<br>N ..... 0.05 C ..... 0.08 |
| Physikalische und thermische Eigenschaften<br><br>Physical Constants and Thermal Properties | Dichte, lb/in³ ..... 0.160<br>g/cm³ ..... 4.43<br>Schmelzbereich, etwa. °F ..... 3000<br>°C ..... 1648<br>Beta Transus °F +/- 25 ..... 1784<br>°C +/- 4 ..... 980<br><br>Ausdehnungsbeiwert,<br>$10^{-6}$ in/in • F 32 - 212°F ..... 5.0 32 - 1200°F ..... 5.9<br>32 - 600°F ..... 5.3 32 - 1500°F ..... 6.1<br>32 - 1000°F ..... 5.6<br>um/m • °C 0 - 100°C ..... 9.1 0 - 649°C ..... 10.7<br>0 - 316°C ..... 9.6 0 - 816°C ..... 11.0<br>0 - 538°C ..... 10.1<br><br>Wärmeleitfähigkeit, Btu • in/ft²•h•°F ..... 3.9<br>W/m•°C ..... 0.56<br>Elastizitätsmodul, $10^6$ psi ..... 16.5<br>Torsionsmodul, $10^6$ psi ..... 6.1<br>Spezifische Wärme, Btu/lb•°F ..... 0.135<br>J/kg•°C ..... 565.2<br><br>Glühtemperatur<br>ganz °F .. 1300-1525°/15 min., -2 Std., AC<br>°C ..... 704-838°/15 min., -2 Std., AC<br>spannungsarm °F ..... 900-1200°/1-4 Std., AC<br>°C ..... 495-659°/1-4 Std., AC<br><br>Schmiedetemperatur<br>Vorschmieden °F ..... 1750 - 1800°<br>°C ..... 962 - 989°<br>Fertigschmieden °F ..... 1650 - 1750°<br>°C ..... 812 - 962° | Density, lb/in³ ..... 0.160<br>g/cm³ ..... 4.43<br>Melting Range, approx. °F ..... 3000<br>°C ..... 1648<br>Beta Transus °F +/- 25 ..... 1784<br>°C +/- 4 ..... 980<br><br>Coefficient of Expansion<br>$10^{-6}$ in/in • F 32 - 212°F ..... 5.0 32 - 1200°F ..... 5.9<br>32 - 600°F ..... 5.3 32 - 1500°F ..... 6.1<br>32 - 1000°F ..... 5.6<br>um/m • °C 0 - 100°C ..... 9.1 0 - 649°C ..... 10.7<br>0 - 316°C ..... 9.6 0 - 816°C ..... 11.0<br>0 - 538°C ..... 10.1<br><br>Thermal Conductivity, Btu • in/ft²•h•°F ..... 3.9<br>W/m•°C ..... 0.56<br>Elasticity-Tension Modulus, $10^6$ psi ..... 16.5<br>Elasticity-Torsion Modulus, $10^6$ psi ..... 6.1<br>Specific Heat, Btu/lb •°F ..... 0.135<br>J/kg • °C ..... (565.2)<br><br>Annealing Temp<br>full °F ..... 1300-1525°/15 min., -2 hrrs, AC<br>°C ..... 704-838°/15 min., -2 hrs, AC<br>stress relief °F ..... 900-1200°/1-4 hrs, AC<br>°C ..... 495-659°/1-4 hrs, AC<br><br>Forging Temp<br>Blocking °F ..... 1750 - 1800°<br>°C ..... 962 - 989°<br>Finishing °F ..... 1650- 1750°<br>°C ..... 812 - 962° |
| Typische mechanische Eigenschaften<br><br>Typical Mechanical Properties | **(Geglüht)** **ksi** **MPA**<br>Zugfestigkeit, RT ..... min. 130 min. 895<br>Streckgrenze, RT ..... min. 120 min. 826<br>Dehnung, % RT ..... min. 10<br>(Bruch) Einschnürung, %<br>Bar ..... 25 | **(Annealed)** **ksi** **MPA**<br>Tensile Strength, RT ..... min. 130 min. 895<br>Yield Strength, RT ..... min. 120 min. 826<br>Elongation, % RT ..... min. 10<br>Reduction of Area, %<br>Bar ..... 25 |

## C.3 FR4 laminate

This data comes from the website: http://www.jjorly.com

FR4 laminate grades are produced by inserting continuous glass woven fabric impregnated with an epoxy resin binder while forming the sheet under high pressure. This material is used extensively in the electronics industry because its water absorption is extremely minimal. The FR4 is most commonly used in PCB (Printed Circuit Boards) applications. FR4 has excellent dielectric loss properties, and great electrical strength. It is also a fire retardant grade of G10. FR4 is also known as Garolite.

**Table 22 Various properties of the FR4 laminate.**

| | units | values |
|---|---|---|
| *Mechanical properties* | | |
| Bond Strength | LBS | 2,500 |
| Compressive Strength | PSI | 60,000 |
| Flexural Strength | PSI | 55,000 |
| Shear Strength | PSI | 19,000 |
| Tensile Strength | PSI | 40,000 |
| Impact Strength, IZOD (Notched) | FT-LBS PER INCH OF NOTCH | 7 |
| Specific Gravity | | 1.82 |
| Flexural Modulus of Elasticity | PSI | 2,700,000 |
| Rockwell Hardness | M SCALE | M110 |
| | | |
| *Electrical properties* | | |
| Dielectric Constant | 1 MEGACYCLE | 5.2 |
| Dielectric Strength | VOLTS PER MIL | 400 |
| Dissipation Factor | 1 MEGACYCLE | 0.025 |
| Arc Resistance | SECONDS | 80 |
| | | |
| *Thermal properties* | | |
| Max Constant Operating Temperature | ° F | 285 |
| Insulation Resistance | Condition: 96 hrs., 90% relative humidity, 95°F megohms | 200,000 |
| Water Absorption | % 24 HRS | 0.11 |
| Thermal Conductivity | Calories/Sec./cm2/°C/cm | 7 X 10-4 |
| Coefficient of Thermal Expansion | Cm/Cm°C | 0.9 |

# Appendix D Composite Panels

## D.1 Carbon fiber TORAY M55J

Torayca http://www.torayca.com/properties/en/images/report_eng01_2.html

Carbon Fiber

| Designation | Fiber Type | Number of Filament | Tensile Strength (MPa) | Tensile Strength (kgf/m?) | Tensile Modulus (Gpa) | Tensile Modulus (kgf/m?) | Elongation (%) | Mas per Unit Length tex(g/1000m) | Density ($g/cm^3$) |
|---|---|---|---|---|---|---|---|---|---|
| **T300** | | | | | | | | | |
| T300-1000 | T300 | 1000 | 3530 | 360 | 230 | 23500 | 1.5 | 66 | 1.76 |
| T300-3000 | T300 | 3000 | 3530 | 360 | 230 | 23500 | 1.5 | 198 | 1.76 |
| T300-6000 | T300 | 6000 | 3530 | 360 | 230 | 23500 | 1.5 | 396 | 1.76 |
| T300-12000 | T300 | 12000 | 3530 | 360 | 230 | 23500 | 1.5 | 800 | 1.76 |
| T300- | T300 | 1000 | 3530 | 360 | 230 | 23500 | 1.5 | 70 | 1.76 |
| **T300B** | | | | | | | | | |
| T300B-1000 | T300B | 1000 | 3530 | 360 | 230 | 23500 | 1.5 | 66 | 1.76 |
| T300B-3000 | T300B | 3000 | 3530 | 360 | 230 | 23500 | 1.5 | 198 | 1.76 |
| T300B-3000 | T300B | 3000 | 3530 | 360 | 230 | 23500 | 1.5 | 198 | 1.76 |
| T300B-6000 | T300B | 6000 | 3530 | 360 | 230 | 23500 | 1.5 | 396 | 1.76 |
| T300B-12000 | T300B | 12000 | 3530 | 360 | 230 | 23500 | 1.5 | 800 | 1.76 |
| **T400HB** | | | | | | | | | |
| T400HB-3000 | T400HB | 3000 | 4410 | 450 | 250 | 25500 | 1.8 | 198 | 1.8 |
| T400HB-6000 | T400HB | 6000 | 4410 | 450 | 250 | 25500 | 1.8 | 396 | 1.8 |
| **T700SC** | | | | | | | | | |
| T700SC-12000 | T700SC | 12000 | 4900 | 500 | 230 | 23500 | 2.1 | 800 | 1.8 |
| T700SC-24000 | T700SC | 24000 | 4900 | 500 | 230 | 23500 | 2.1 | 1650 | 1.8 |
| **T800HB** | | | | | | | | | |
| T800HB-6000 | T800HB | 6000 | 5490 | 560 | 294 | 30000 | 1.9 | 223 | 1.81 |
| T800HB-12000 | T800HB | 12000 | 5490 | 560 | 294 | 30000 | 1.9 | 445 | 1.81 |
| **T1000GB** | | | | | | | | | |
| T1000GB-12000 | T1000GB | 12000 | 6370 | 650 | 294 | 30000 | 2.2 | 485 | 1.8 |
| **M35JB** | | | | | | | | | |
| M35JB-6000 | M35JB | 6000 | 4510 | 460 | 343 | 35000 | 1.3 | 225 | 1.75 |
| M35JB-12000 | M35JB | 12000 | 4700 | 480 | 343 | 35000 | 1.4 | 450 | 1.75 |
| **M40JB** | | | | | | | | | |
| M40JB-6000 | M40JB | 6000 | 4400 | 450 | 377 | 38500 | 1.2 | 225 | 1.75 |
| M40JB-12000 | M40JB | 12000 | 4400 | 450 | 377 | 38500 | 1.2 | 450 | 1.75 |
| **M46JB** | | | | | | | | | |
| M46JB-6000 | M46JB | 6000 | 4200 | 430 | 436 | 44500 | 1 | 223 | 1.84 |
| M46JB-12000 | M46JB | 12000 | 4020 | 410 | 436 | 44500 | 0.9 | 445 | 1.84 |
| **M50JB** | | | | | | | | | |
| M50JB-6000 | M50JB | 6000 | 4120 | 420 | 475 | 48500 | 0.9 | 216 | 1.88 |
| **M55J** | | | | | | | | | |
| M55J-6000 | M55J | 6000 | 4020 | 410 | 540 | 55000 | 0.8 | 218 | 1.91 |
| **M55JB** | | | | | | | | | |
| M55JB-6000 | M55JB | 6000 | 4020 | 410 | 540 | 55000 | 0.8 | 218 | 1.91 |
| **M60JB** | | | | | | | | | |
| M60JB-3000 | M60JB | 3000 | 3820 | 390 | 588 | 60000 | 0.7 | 103 | 1.93 |
| M60JB-6000 | M60JB | 6000 | 3820 | 390 | 588 | 60000 | 0.7 | 206 | 1.93 |
| **M30SC** | | | | | | | | | |
| M30SC-18000 | M30SC | 18000 | 5490 | 560 | 294 | 30000 | 1.9 | 760 | 1.73 |

# D.2 HexPly M18 epoxy matrix

**HexPly® M18**
**180°C curing epoxy matrix**

*Product Data*

## Description

HexPly M18 has been developed to fulfil the requirements of the aerospace industry for primary structures using standard manufacturing processes. The matrix has improved properties which allow easy lay-up, good tack life and a good component surface finish. A low moisture uptake allows good hot/wet performance up to 150°C and a general service temperature up to 180°C.

## Benefits and Features

- Low density matrix offering potential weight saving
- Excellent toughness and damage tolerance
- Outstanding low moisture uptake
- Simple straight up cure cycle (no post cure needed)
- High strain to failure
- Good hot/wet properties up to 150°C
- Processes to a good surface finish on components
- Suitable for low pressure moulding

## Resin Matrix Properties

Rheology

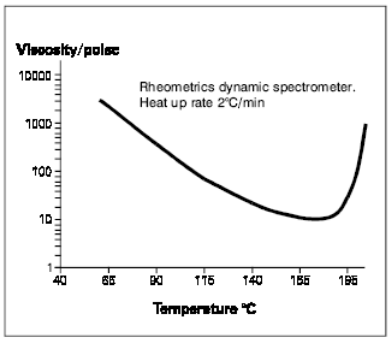


Gel Time

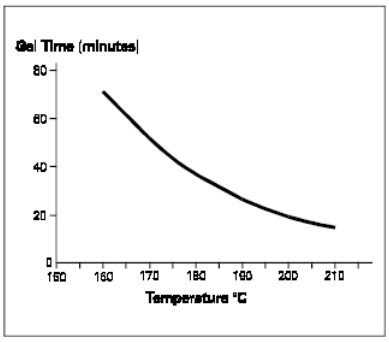


## Prepreg Curing Conditions

2 hours at 180°C and 700kN/m² (7 bar) pressure.

Heat up rate 2°C to 8°C.

Components up to 30 mm thick can be cured without a dwell in the schedule provided that the heat-up rate is not more than 3°C/minute. There is no deterioration in performance after 3 times the recommended cure schedule (verified by interlaminar shear strength tests).

HEXCEL Composites

# HexPly® M18 *Product Data*

## Cured Matrix Properties (cured at 180°C)

| | | Method |
|---|---|---|
| Tensile strength | 81.1 MPa | ISO R527 type 1 |
| Tensile modulus | 3.50 GPa | ISO R527 type 1 |
| Tensile strain | 3.7% | ISO R527 type 1 |
| Poisson's ratio | 0.38 | ISO R527 type 1 |
| Flexural strength | 140 MPa | ISO 178 |
| Flexural modulus | 2.86 GPa | ISO 178 |
| Compression strength | 373 MPa | ISO 604 |
| Toughness $K_{1C}$ | 0.89 MPa √m | Tested in accordance with |
| Toughness $G_{1C}$ | 193 J/m² | EGF Task Group on Polymers and Composites protocol. |
| Glass transition temperature (Tg) | 198°C | DMTA |
| Cured density | 1.16 g/cm³ | |
| Vol. shrinkage | 1.12% | |

## Prepreg Storage Life

- Tack Life @ 23°C 30 days (processing out life @ 23°C, 40 days)
- Guaranteed Shelf Life @ -18°C 12 months

- Storage conditions.

HexPly M18 prepregs should be stored as received in a cool dry place or in a refrigerator. After removal from refrigerator storage, prepreg should be allowed to reach room temperature before opening the polythene bag, thus preventing condensation. (A full reel in its packaging can take up to 48 hours).

## Precautions for Use

The usual precautions when handling uncured synthetic resins and fine fibrous materials should be observed, and a Safety Data Sheet is available for this product. The use of clean disposable inert gloves provides protection for the operator and avoids contamination of material and components.

## Important

All information is believed to be accurate but is given without acceptance of liability. Users should make their own assessment of the suitability of any product for the purposes required. All sales are made subject to our standard terms of sale which include limitations on liability and other important terms.



For further information, please contact your nearest sales office, or visit our website at **www.hexcelcomposites.com**

**Australia**
Suite 2, 86 Grimshaw Street
Greensborough, Victoria 3088
Tel: **61** 3 9432 7100
Fax: **61** 3 9432 7200

**China**
Room B707, Yin Hai Bldg.
250 Cao Xi Rd
Shanghai 200233
Tel: **86** 21 6483 6741/2
Fax: **86** 21 6483 6744

**Japan** - *Joint Venture*
DIC - Hexcel Limited
Room 603, Santsu-Mori Bldg.
2-22-1 Nishi - Shimbashi
Minato-Ku, Tokyo 105
Tel: **81** 3 5401 0271
Fax: **81** 3 5401 0270

**USA**
101 East Ridge Drive, Suite 102
Danbury, CT 06810
Tel: **1** 203 798 8311
Fax: **1** 203 798 8161

**Austria**
Industriestrasse 1
A-4061, Pasching
Tel: **43** (0)7229 7720
Fax: **43** (0)7229 772299

**France**
ZI La Plaine, B.P.27 Dagneux
01121 Montluel CEDEX
Tel: **33** (0)4 72 25 26 27
Fax: **33** (0)4 72 25 27 30

**Spain**
Bruselas, 10 - 16
Polig. Ind. "Ciudad de Parla"
28980 Parla, Madrid
Tel: **34** 91 664 4900
Fax: **34** 91 698 4914

**USA**
42705 Grand River
Suite 201
Novi, MI 48375
Tel: **1** 248 344 8688
Fax: **1** 248 305 9760

**Belgium**
Rue Trois Bourdons, 54
B-4840 Welkenraedt
Tel: **32** 87 307 411
Fax: **32** 87 882 895

**Germany**
Postfach 1560
21655 Stade
Tel: **49** 4141 7879-00
Fax: **49** 4141 7879-01

**United Kingdom**
Duxford, Cambridge
CB2 4QD
Tel: **44** (0)1223 833141
Fax: **44** (0)1223 838808

**USA**
2350 Airport Freeway, Suite 550
Bedford, TX 76022-6027
Tel: **1** 817 315 3939
Fax: **1** 817 571 8629

**Brazil**
Av. J. Guilhermino, 474/72
S.J.Campos, SP 12210-130
Tel: **55** 12 3941 2242
Fax: **55** 12 3923 1186

**Italy**
Via San Cristoforo, 44
21047 Saronno (VA)
Tel: **39** 02 96709082
Fax: **39** 02 9600809

**USA**
11711 Dublin Blvd.
Dublin, CA 94568-2832
Tel: **1** 925 551 4900
Fax: **1** 925 828 9202

**USA**
16310 NE 80th Street, Suite 102
Redmond, WA 98052
Tel: **1** 425 558 4400
Fax: **1** 425 861 5847

# D.3 Manufacturing data

In the following pages the numerical and graphical temperature record during the manufacturing of the composite plate are stated. Keep in mind that the temperature measured with the external sensor (Tf) is not representative for the temperature inside the plate. We have used this sensor only for monitoring the system. And we have no record of the actual plate temperature. But we know that the temperature control of the system is very good, i.e. the actual temperature should follow the desired temperature (Tsoll) quite accurately.

*CFRP-Plate_Prot_070118.xls*

**Herstellung HM-CFK-Platte für Swiss Cube** | **070118**

Material: Prepregs Hexcel **NCTHM M18/32%/116/M55J**
Werkzg: Ebene Aluplatten oben und unten ( B x L : 320mm x 470mm ) Datum: 18.01.2007
Ort: Laborheizpresse PEQ Protokoll: W. Fuchs
Tsoll = Solltemperatur manuell eingestellt an der Heizpresse.
Tf = Kontrolltmperatur mit Fühler am äusseren Rand der Platten (ist immer tiefer als Plattel).
F = Presskraft ( F-1 und F-2 sind zwei getrennte Druckanzeigen ).
F-1 zeigt kN an, F-2 zeigt Tonnen an. F-2* ist aus F-2 umgerechnet in kN.
Ab ca. 170 kN ist die Anzeige F-1 im Anschlag.

| dt | t | Tsoll | | dt | t | Tf | F-1 | F-2 | F-2* | Bemerkungen |
|---|---|---|---|---|---|---|---|---|---|---|
| [m] | [h:m] | [°F] | [°C] | [m] | [h:m] | [°C] | [kN] | [tons] | [kN] | |
| 0 | **12:00** | 32 | 0 | --- | **12:00** | 22.5 | 0.0 | | | |
| 60 | **13:00** | 32 | 0 | 60 | **13:00** | 22.5 | 0.0 | | | |
| 0 | **13:00** | 80 | 27 | 0 | **13:00** | 22.5 | 50.0 | | | 13:00 Presskraft: 50 kN |
| 5 | **13:05** | 80 | 27 | 5 | **13:05** | 26.8 | 50.0 | | | |
| 0 | **13:05** | 105 | 41 | 5 | **13:10** | 38.4 | 50.0 | | | 13:10 Presskraft 85 kN |
| 5 | **13:10** | 105 | 41 | 0 | **13:10** | 38.4 | 85.0 | | | |
| 0 | **13:10** | 130 | 54 | 5 | **13:15** | 51.8 | 85.0 | | | |
| 5 | **13:15** | 130 | 54 | 5 | **13:20** | 66.9 | 86.0 | | | |
| 0 | **13:15** | 155 | 68 | 5 | **13:25** | 79.5 | 86.0 | | | |
| 5 | **13:20** | 155 | 68 | 5 | **13:30** | 92.0 | 88.0 | | | |
| 0 | **13:20** | 180 | 82 | 5 | **13:35** | 101.0 | 89.0 | | | |
| 5 | **13:25** | 180 | 82 | 5 | **13:40** | 115.0 | 92.0 | | | |
| 0 | **13:25** | 205 | 96 | 5 | **13:45** | 132.0 | 95.0 | | | |
| 5 | **13:30** | 205 | 96 | 5 | **13:50** | 148.0 | 97.0 | | | |
| 0 | **13:30** | 230 | 110 | 5 | **13:55** | 161.0 | 100.0 | | | |
| 5 | **13:35** | 230 | 110 | 25 | **14:20** | 162.0 | 107.0 | | | |
| 0 | **13:35** | 255 | 124 | 15 | **14:35** | 163.0 | 113.0 | | | |
| 5 | **13:40** | 255 | 124 | 35 | **15:10** | 162.0 | 136.0 | | | |
| 0 | **13:40** | 280 | 138 | 30 | **15:40** | 164.0 | 161.0 | | | |
| 5 | **13:45** | 280 | 138 | 20 | **16:00** | 164.0 | | 19.8 | *194.2* | 16:02 Heizung aus |
| 0 | **13:45** | 305 | 152 | 6 | **16:06** | 160.8 | | 20.0 | *196.2* | 16:07 Wasserkühlung ein |
| 5 | **13:50** | 305 | 152 | 4 | **16:10** | 157.9 | | 20.1 | *197.2* | |
| 0 | **13:50** | 330 | 166 | 5 | **16:15** | 152.8 | | 20.4 | *200.1* | |
| 5 | **13:55** | 330 | 166 | 2 | **16:17** | 137.0 | | 20.1 | *197.2* | |
| 0 | **13:55** | 355 | 180 | 4 | **16:21** | 110.0 | | 19.8 | *194.2* | |
| 127 | **16:02** | 355 | 180 | 5 | **16:26** | 82.0 | | 19.5 | *191.3* | |
| 0 | **16:02** | 32 | 0 | 4 | **16:30** | 59.0 | | 19.1 | *187.4* | |
| 120 | **18:02** | 32 | 0 | 3 | **16:33** | 52.0 | | 19.0 | *186.4* | |
| | | | | 1 | **16:34** | 46.0 | 157.5 | 17.3 | *169.7* | |
| | | | | 1 | **16:35** | 43.0 | 134.0 | 15.0 | *147.2* | 16:35 Kraft langsam reduziert |
| | | | | 0 | **16:35** | 42.0 | 103.0 | 11.9 | *116.7* | |
| | | | | 1 | **16:36** | 40.0 | 71.0 | 8.1 | *79.5* | |
| | | | | 0 | **16:36** | 39.0 | 30.0 | 3.3 | *32.4* | |
| | | | | 1 | **16:37** | 38.0 | 10.0 | 1.0 | *9.8* | |

Beachte: Der Druckanstieg ab ca. 13:20 über 85 kN hinaus ergibt sich automatisch durch die Erwärmung der Presse, d.h. des Druckzylinders und des Hydrauliköls.
Der Pressdruck wird nicht automatisch nachgeregelt.

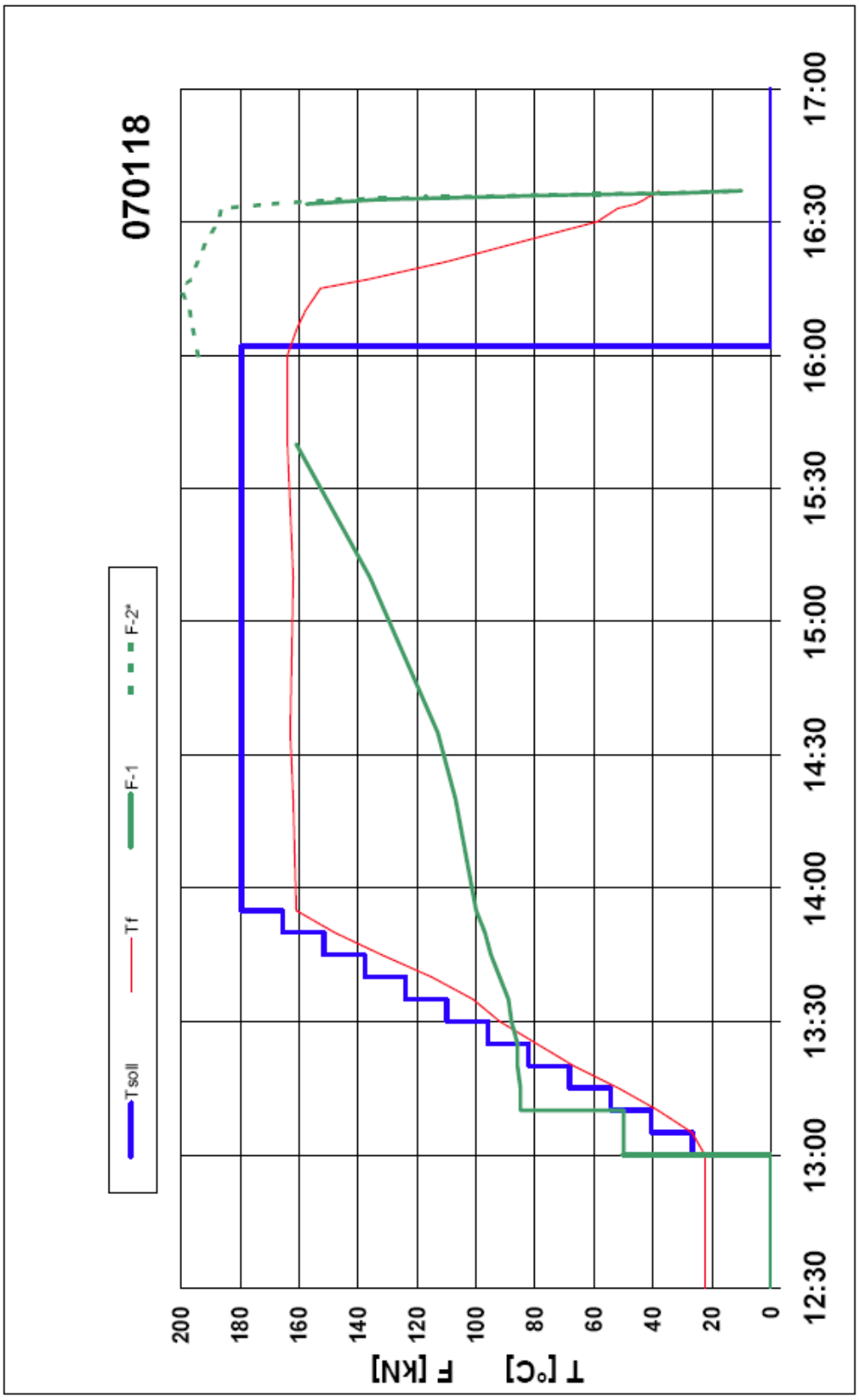
070118
T soll
Tf
F-1
F-2*
T [°C] F [kN]
200
180
160
140
120
100
80
60
40
20
0
12:30
13:00
13:30
14:00
14:30
15:00
15:30
16:00
16:30
17:00

# Appendix E Adhesive properties

| Adhesive | Product type | Chemical comp. | Shear strength [Mpa] | Temp. range [°C] | CTE [µm/K] |
|---|---|---|---|---|---|
| *Structural* | | | | | |
| Araldite AV138/HV998 | 2-part paste | Epoxy | 43 (tensile) | <120 | 67 |
| Scotchweld 2216 (B/A) | 2-part paste | Modified epoxy | 21,3 | 50(-) to 80 | 45 - 182 |
| Scotchweld 1614 (B/A) | 2-part paste | Epoxy | 21,1 | 55(-) to 80 | - |
| Epo-tek U300 | 2-part paste | Epoxy | 10,3 | <200 | 43 (T<130°C) |
| DC 93500 | 2-part paste | Silicone | 5,8 (tensile) | 65(-) to 200 | 300 |
| Redux 312 | Adhesive film | Modified epoxy | 43 | 55(-) to 120 | - |
| Redux 340 | Adhesive film | Modified epoxy | 43 | 55(-) to 200 | - |
| FM 73 | Adhesive film | Epoxy | 39,8 | 55(-) to 82 | - |
| *Thermal* | | | | | |
| Epo-tek 930 | 2-part thermal | Epoxy (Boron nitride) | - | - | 40 |
| Epo-tek H74 | 2-part paste | Epoxy | 17,2 | <150 | 38 |

| Adhesive | Thermal cond. [W/mK] | Resistivity [Ω m] | Cure Temp. [°C] | Outgassing (TML / RML / | Fabricant | ECSS |
|---|---|---|---|---|---|---|
| *Structural* | | | | | | |
| Araldite AV138/HV998 | 0,35 | | | | www.vantico.com | yes |
| Scotchweld 2216 (B/A) | 0,39 | 1,90E+13 | 65 | 0,84 / 0,57 / 0,02 | www.3m.com | yes |
| Scotchweld 1614 (B/A) | - | 1,90E+10 | 70 | 1,42 / 0,75 / 0,01 | www.3m.com | no |
| Epo-tek U300 | - | - | 65 | - | www.epotek.com | no |
| DC 93500 | 0,15 | 1,00E+14 | 80-150 | (passed NASA specs) | www.dowcorning.com | yes |
| Redux 312 | - | 6,90E+13 | RT | 0,30 / 0,28 / 0,03 | www.hexcel.com | yes |
| Redux 340 | - | - | 120 | 1,10 / 0,40 / 0,05 | www.hexcel.com | no |
| FM 73 | - | - | 175 | - | www.cytec.com | no |
| *Thermal* | | - | 121 | 0,78 / - / 0,00 | | |
| Epo-tek 930 | 4,1 | - | - | - | www.epotek.com | yes |
| Epo-tek H74 | 1.1 | 2,5E+17 | 50-150 | 0,31 / - / 0,01 | www.epotek.com | yes |

[1] 24 hours at 125°C and $10^{-3}$Pa (ECSS)

## E.1 Effects of space environment on adhesive

The space environment can significantly decrease the properties of adhesives. The various effects, summarized in the ECSS report [8] are as follows:

- Exposure of adhesives to vacuum provokes outgassing. The major components which outgas are unreacted compounds, low-molecular-weight constituents and the bi-products from chemical reactions. As the exposed surface is small (only the bond line), outgassing rates can be quite low. Effects of vacuum alone on the bond integrity are normally not observed, but some of the evolved constituents can be condensable and can create a contamination danger in a spacecraft ("coating" of electrical or optical components). Many epoxies are acceptable from an outgassing point of view, but are rather sensitive to humidity conditions at the time of curing. "Modified" epoxies, particularly the flexible ones, can have outgassing rate. Nearly all RTV silicones are known to be contaminant, but some manufacturers have developed special compounds for space use. All coatings and varnishes outgas. This is particularly noticeable for types containing solvent. This phenomenon can sometimes be reduced by extended curing at high temperature and under vacuum, but such a method is not very practical and is not always successful. Atmospheric gases trapped within cracks and voids in the coating can leak out under vacuum and produce pressures in the "corona range". Cracks formed under vacuum can fill with outgassing products up to the same pressures. These two phenomena lead to troubles when high electric field strengths are present during spacecraft equipment operation.
- Particle radiation at the level encountered in space is not harmful for adhesives, which are in any case protected by the items (adherends) they are bonding. Only coatings on satellite surfaces experience exposure to radiation, often combined with UV; see comments for UV. Insulating varnishes used inside "black boxes" are well protected against particle fluxes.
- UV radiation can darken optical adhesives. In this regard silicones are superior to epoxies. UV and particle radiation can both increase the outgassing rate of adhesives. UV radiation and proton fluxes are the main factors and can cause darkening and hardening of coatings and increase the outgassing rate. Insulating varnishes used in "black boxes" are not subjected to UV.
- High temperature degrades adhesives. For long-term exposure polyimide can be used up to more than 300 °C; the best epoxies are normally limited to 170 °C. Phenolics and silicones lie between. High temperature accelerates outgassing. Silicone-type coatings and varnishes are recommended for high temperatures. For very high temperatures, "ladder-polymers", such as polyimide or polybenzimide, are the only possible candidates. When flammability is a property to be considered, silicone materials should be chosen in preference to polyurethane coatings.
- Low temperature stiffens adhesives and causes brittle bonds. Some polyurethane adhesives are still useful at very low temperatures (cryogenic). A similar effect is seen with coatings which tend to harden, shrink and crack.
- Thermal cycling leads to failure of the adhesive bond when the expansion coefficients of the adherents and adhesives are not matched and when the adhesive is not flexible enough to cope with the strain. Thick layers of rigid adhesives are prone to high stresses. Coatings and

varnishes experience thermal- cycling due to shadow-sunlight passage or to variable internal heat sources caused by switching equipment on and off. Mismatch of expansion coefficients between coating and coated items gives rise to high stresses and eventually to cracks. Thermal insulation by the coating can lead to overheating of high-power components, particularly in vacuum.

- Atomic oxygen (in LEO) is only applicable to adhesives exposed to ATOX (such as those on solar-cell and panel assemblies) which can be attacked. Exposed coatings are susceptible: silicones are resistant.

## E.2 Epoxy EPO-TEK H74

EPOXY TECHNOLOGY

**DATA SHEET**

EPO-TEK
**H74**

Thermally Conductive Epoxy

Rev. I
1/98

# TYPICAL PROPERTIES

(To be used as a guideline only)

NUMBER OF COMPONENTS ..... 1

MIXING RATIO — PARTS BY WEIGHT
- Part "A" ..... 10
- Part "B" (hardener) ..... 0.3

A convenient way to mix EPO-TEK H74 in small quantities is as follows:
- Part "A" ..... 2 grams
- Part "B" ..... 2 drops

CURE SCHEDULE (minimum bond line temperature - use one of the following)
- 100°C ..... 20 minutes
- 50°C ..... 12 hours

PHYSICAL PROPERTIES
- Color ..... Tan
- Consistency ..... smooth flowable paste
- Specific Gravity (mixed) ..... 2.11
- Viscosity (@ 23°C/5 rpm) ..... 40,000 - 80,000 cPs
- Glass Transition Temp. (Tg)
  - cured @ 150°C/1 hour ..... > 100°C
- Coefficient of Thermal Expansion
  - Below Tg ..... 38 x $10^{-6}$ in/in/°C
  - Above Tg ..... 127 x $10^{-6}$ in/in/°C
- Lap Shear Strength (Al to Al) ..... 2,500 psi
- Die Shear Strength ..... > 10kg/3,400 psi
- Degradation Temperature ..... 410°C
- Operating Temperature
  - Continuous ..... 150°C

ELECTRICAL - THERMAL PROPERTIES
- Volume Resistivity ..... 2.5 x $10^{15}$ ohm-cm
- Dielectric Strength ..... 470 V/mil
- Dielectric Constant (1 megacycle) ..... 5.5
- Thermal Conductivity ..... 1.1 W/m°K

POT LIFE ..... 4 hours

SHELF LIFE
One year when stored at room temperature.

REFRIGERATION NOT REQUIRED

EPO-TEK H74 is a two component, thermally conductive epoxy designed especially for bonding of large substrates in IC packages.

EPO-TEK H74 is a soft, smooth flowable paste with good handling characteristics. The 100% solids system is characterized by outstanding high temperature properties and excellent solvent, chemical, and moisture resistance. Other important characteristics include a long pot life and fast curing at relatively low temperatures.

EPO-TEK H74 is designed to be used in the 300°C to 400°C range for wire bonding operations. Furthermore, because of its unique composition EPO-TEK H74 will not outgas. It contains no solvents or thinners.

EPO-TEK H74 can be applied by brush, spatula, silk screen, hypodermic needle or with commercial dispensing equipment.

A unique feature of EPO-TEK H74 is the built-in color indicator when the product is cured. This color change varies from a tan to dark red, depending upon the curing conditions. It is normal for EPO-TEK H74 to turn a very deep red when subjected to wire bonding temperatures.

EPO-TEK H74 has been approved as an adhesive for hybrid modules in space applications.

**EPOXY TECHNOLOGY, INC.** 14 Fortune Drive Billerica, MA 01821-3972 USA

**PHONE:** 978.667.3805 1.800.227.2201 **FAX:** 978.663.9782

# Appendix F Push Button Switch Grayhill 39-2

Grayhill — Butt Contact Pushbutton Switches

## SERIES 39
**SPST, 150 mA to 1/2 Amp**

### FEATURES
- Requires an Absolute Minimum of Space
- Molded-In Terminals in SPST–N.O.
- Solder Lug Terminals

### DIMENSIONS In Inches (and millimeters)

**Normally Open–SPST Economy and Standard Version**

39-1
39-3
39-601*

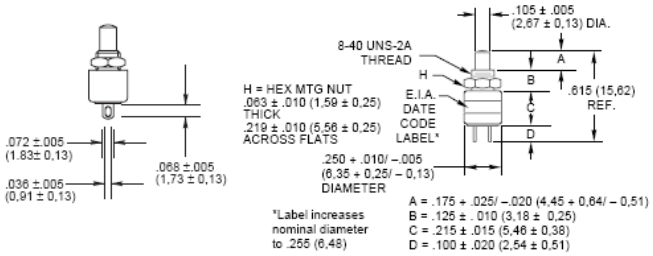


**Economy Version**

| Electrical Ratings | | Operations at Rated Load | *Complete Part Number | Button Color |
|---|---|---|---|---|
| At 5 Vdc 150 mA | At 20 Vdc 20 mA | 1,000,000 | 39-601 RED 39-601 BLK | Red Black |

| Action | Total Travel | Actuating Force (oz.) | Mtg. Hole |
|---|---|---|---|
| Momentary | .035 ± .015 (0,89 ± 0,38) | 4 + 4 - 2 | 11/64" (4,37) DIA. |

**Standard**

| Electrical Ratings | | Operations at Rated Load | Complete Part Number | Button Color |
|---|---|---|---|---|
| At 115 Vac ½ Amp Res. | At 220 Vac ¼ Amp Res | 1,000,000 | 39-1 39-3 | Red Black |

| Action | Total Travel | Actuating Force (oz.) | Mtg. Hole |
|---|---|---|---|
| Momentary | .035 ± .015 (0,89 ± 0,38) | 4 + 4 – 2 | 11/64" (4,37) DIA. |

**Normally Open–SPST with Sealed Bushing and Button**

39-351*

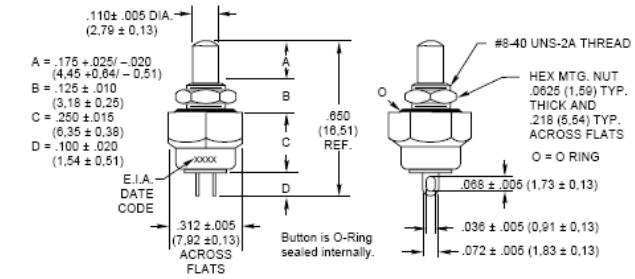


| Rating at 115 Vac Resistive | Rating at 220 Vac Resistive | Operations at Rated Load | *Complete Part Number | Button Color |
|---|---|---|---|---|
| ½ Amp | ¼ Amp | 250,000 | 39-351 RED 39-351 BLK | Red Black |

| Action | Total Travel | Actuating Force (oz.) |
|---|---|---|
| Momentary | .035 ± .015 (0,89 ± 0,38) | 16 ± 8 |

**Normally Open–SPST with Overtravel**

39-12
39-24

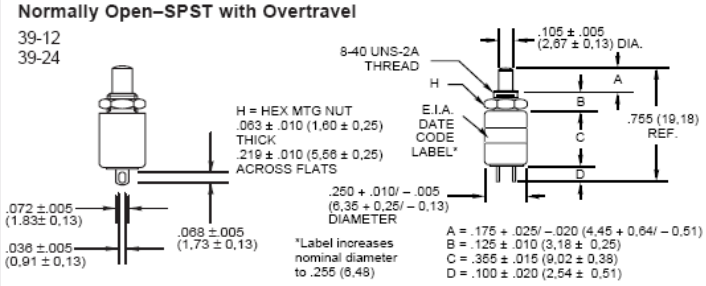


| Rating at 115 Vac Resistive | Rating at 220 Vac Resistive | Operations at Rated Load | Complete Part Number | Button Color |
|---|---|---|---|---|
| ½ Amp | ¼ Amp | 100,000 | 39-12 39-24 | Red Black |

| Action | Total Travel | Over Travel | Actuating Force (oz.) | Mtg. Hole |
|---|---|---|---|---|
| Momentary | .130 ± .025 (3,30 ± 0,64) | .015 (0,38) Min. | 5 ± 3 | 11/64" (4,37) DIA. |

## DIMENSIONS In Inches (and millimeters)

### Normally Closed–SPST

39-2

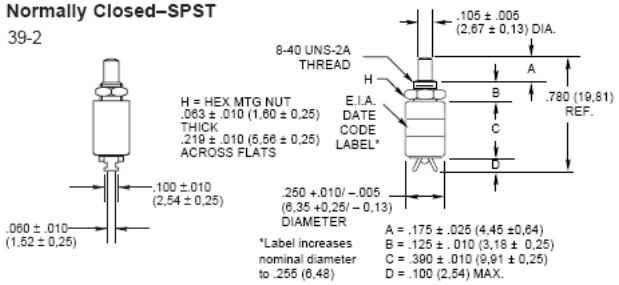


| Rating at 115 Vac Resistive | Rating at 220 Vac Resistive | Operations at Rated Load | Part Number | Cap Color |
|---|---|---|---|---|
| 1/4 Amp | 1/8 Amp | 250,000 | 39-2 | Black |

| Action | Total Travel | Actuating Force (oz.) | Mtg. Hole |
|---|---|---|---|
| Momentary | .042 ± .010 (1,07 ± 0,25) | 4 +4 −2 | .172 (4,37) DIA. |

### Normally Closed–SPST with Sealed Bushing and Button

39-352*

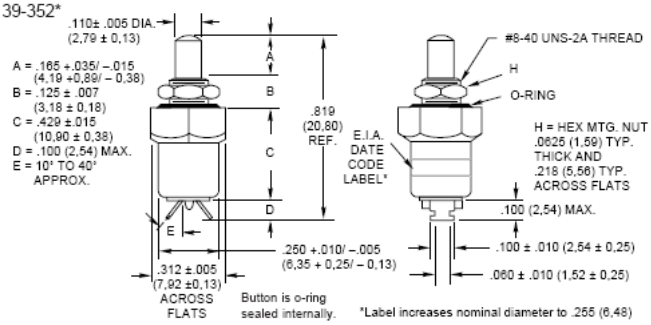


| Rating at 115 Vac Resistive | Rating at 220 Vac Resistive | Operations at Rated Load | *Complete Part Number | Button Color |
|---|---|---|---|---|
| 1/4 Amp | 1/8 Amp | 100,000 | 39-352 RED<br>39-352 BLK | Red<br>Black |

| Action | Total Travel | Actuating Force (oz.) |
|---|---|---|
| Momentary | .042 ± .010 (0,17 ± 0,25) | 8 ± 4 |

## CIRCUITRY

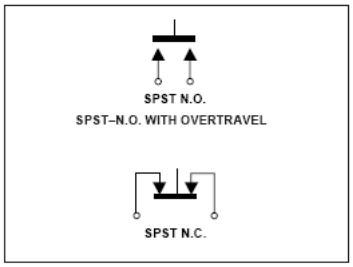


## SPECIFICATIONS

**Rating Criteria**

**Contact Resistance:** 25 milliohms maximum on a new switch
**Voltage Breakdown:** 1,000 Vac between mutually insulated parts
**Insulation Resistance:** 1,000 megohms minimum
**Operating Temperature:** -40°C to +85°C
**Mounting Torque:** 2 inch-pounds

**Materials and Finishes**

**Mounting Nut:** Brass, cadmium-plated
**Housing:** Aluminum, clear anodized for 39-351 and 39-352; Brass, cadmium-plated for others
**Button:** Thermoset plastic
**Base:** Thermoset plastic
**Shorting Bar:** Fine silver for 39-2 and 39-352; brass, gold-plated over nickel plate for 39-601; fine silver, gold-plated for others
**Terminals:** Fine silver for 39-2 and 39-352; commercial bronze with gold-plated fine silver contact surface for others
**Spring:** Tinned music wire
**O-Rings:** (39-351 and 39-352) Internal ring is silicone; external ring is buna 'N'

## ACCESSORY

**Button Cap**
Part No. 30B1012
For use with part numbers 39-351 and 39-352.
(Fasten to button with Cyanoacrylate Adhesive)
See page E-36 for dimensions.

## STANDARD OPTIONS

Epoxy sealed and wire leads, see page E-34.

## ORDERING INFORMATION

| Part Number | Description |
|---|---|
| 39-1 | N.O., Red Button |
| 39-2 | N.C., Black Button |
| 39-3 | N.O., Black Button |
| 39-12 | N.O., Overtravel Red Button |
| 39-24 | N.O., Overtravel Black Button |
| 39-351 RED | N.O., Sealed, Red Button |
| 39-351 BLK | N.O., Sealed, Black Button |
| 39-352 RED | N.C., Sealed, Red Button |
| 39-352 BLK | N.C., Sealed, Black Button |
| 39-601 RED | N.O., Economy, Red Button |
| 39-601 BLK | N.O., Economy, Black Button |

Accessory cap may be used with all switches shown except 39-2.

| Accessory Part Number | Description |
|---|---|
| 30B1012-5 | Red Button Cap |
| 30B1012-9 | Black Button Cap |
| 30B1012-8 | White Button Cap |

**Available from your local Grayhill Distributor.**
For prices and discounts, contact a local Sales Office, an authorized local Distributor or Grayhill.

# Appendix G Spring Plunger McMASTER 84985A76

This is the suggested springs in the CubeSat Specificatrion Document

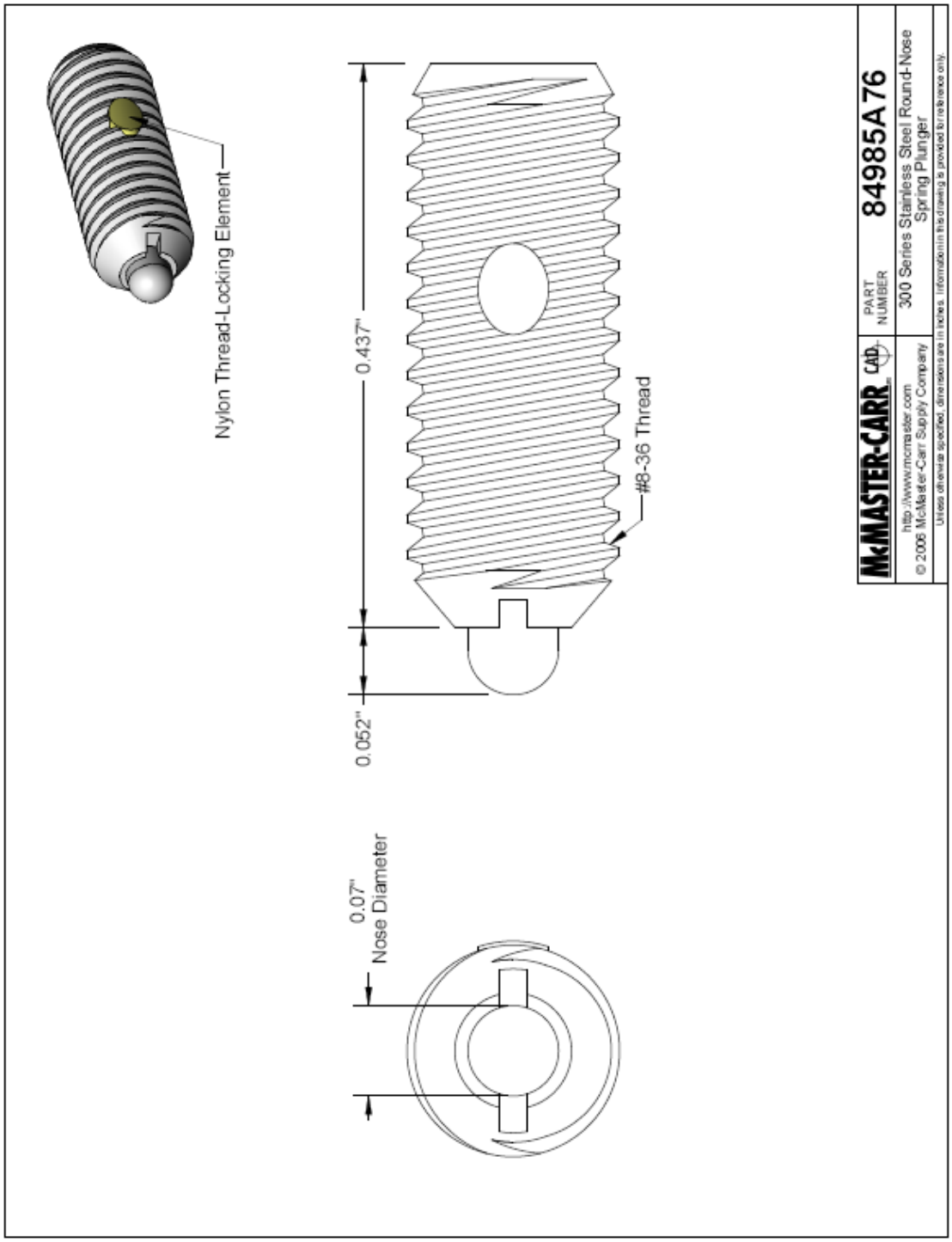

# Spring Plungers

*For an index of fixturing components, see page 2450. For information about spring plungers, see page 2452.*

## Round-Nose Spring Plungers

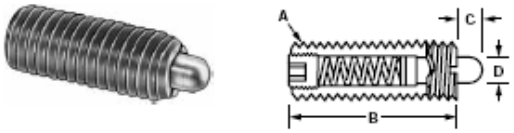



**To Order:** Please specify *with or without nylon thread-locking element*, except where noted. When threading into aluminum and other soft materials, select a plunger without the nylon thread-locking element. For information about nylon thread-locking elements, see page 2452.

These plungers have a round, cylindrical nose that offers long travel and has a large bearing surface so it rides smoothly inside the plunger body. A single plunger can serve as an indexing stop on a rotary switch or as a latch on a cabinet door; a number of plungers can hold a door onto a cabinet. They also are used for proper positioning in fixtures and to eject parts from a punch press or forging die. A slot in the body allows installation with a plunger wrench (sold separately on page 2455); the short length plungers have a slot in the rear so they can also be installed with a screwdriver.

Choose from standard and short length plungers. Also known as stubby, *short length* plungers combine the short body of a ball-nose spring plunger with the longer nose of a round-nose spring plunger. They can be used in thinner materials and tight spaces while still providing ample plunger travel and high end forces.

*Body Materials*—Choose from steel and stainless steel. *Standard length steel plungers* have a black-oxide finish. *Short length steel plungers* are zinc-plated with a clear chromate finish, unless noted. Color is silver. *Stainless steel plungers* are made of corrosion-resistant 300 series stainless steel, so they're a good choice for food processing applications.

*Nose Materials*—Choose from heat-treated steel, 300 series stainless steel, Delrin, and phenolic. *Delrin* and *phenolic* won't mar softer materials such as aluminum and brass. Phenolic has higher tensile, dielectric, and impact strength than Delrin. It is also a good insulator and resists heat, chemicals, acids, and solvents. Maximum temperature of steel and stainless steel nose plungers is 250° F. Maximum temperature for Delrin is 195° F. Maximum temperature for phenolic is 284° F.

**Inch Sizes**—Class 2A threads

| Thread Size (A) | Body Lg. (B) | Nose Lg. (C) | Nose Dia. (D) | End Force, lbs. Initial | End Force, lbs. Final | STEEL BODY Steel Nose | Each ♦ | STEEL BODY Delrin Nose | Each ♦ | STEEL BODY Phenolic Nose | Each | STAINLESS STEEL BODY Stainless Steel Nose | Each ♦ | STAINLESS STEEL BODY Delrin Nose | Each |
|---|---|---|---|---|---|---|---|---|---|---|---|---|---|---|---|
| *Standard Length* | | | | | | | | | | | | | | | |
| 6-32 | 0.375" | 0.063" | 0.045" | 1 | 1.6 | 3126A2 | $4.15 | | | | | 84975A37 | $5.66 | | |
| 6-32 | 0.375" | 0.063" | 0.046" | 0.5 | 3.5 | 3126A75■ | 4.12 | 8499A48 | $3.63 | | | | | | |
| 6-32 | 0.531" | 0.063" | 0.045" | 1.5 | 4.5 | 3126A3 | 3.86 | 8499A47▲ | 4.10 | | | 84975A39 | 5.66 | | |
| 6-32 | 0.531" | 0.063" | 0.045" | 0.5 | 1.5 | 3126A1 | 4.15 | 8499A46▲ | 4.10 | | | 84975A36 | 5.66 | | |
| 8-32 | 0.625" | 0.094" | 0.07" | 0.7 | 2.3 | 3126A4 | 3.08 | 8499A11 | 3.67 | 8490A19 | $5.08 | 84975A42 | 5.09 | 84765A71 | $5.58 |
| 8-32 | 0.625" | 0.094" | 0.07" | 2.7 | 7.3 | 3126A5 | 3.08 | 8499A12 | 3.67 | 8490A11 | 5.02 | 84975A44 | 5.09 | 84765A61 | 5.58 |
| 10-32 | 0.75" | 0.125" | 0.092" | 1.3 | 2.7 | 3126A6 | 3.12 | 8499A13 | 3.49 | 8490A21 | 5.08 | 84975A46 | 4.95 | 84765A72 | 5.58 |
| 10-32 | 0.75" | 0.125" | 0.092" | 2.9 | 11.1 | 3126A7 | 2.89 | 8499A14 | 3.49 | 8490A12 | 5.02 | 84975A48 | 4.95 | 84765A62 | 5.58 |
| 1/4"-20 | 0.75" | 0.125" | 0.119" | 0.25 | 2 | 3126A68• | 3.07 | | | | | | | | |
| 1/4"-20 | 0.75" | 0.125" | 0.118" | 2 | 9 | 3126A25 | 2.92 | | | | | 84975A53 | 4.93 | 84765A65 | 5.09 |
| 1/4"-20 | 1" | 0.188" | 0.118" | 1 | 4 | 3126A9 | 2.95 | 8499A15 | 3.63 | 8490A22 | 4.80 | 84975A51 | 4.93 | 84765A73 | 5.40 |
| 1/4"-20 | 1" | 0.188" | 0.118" | 3 | 13 | 3126A26 | 2.92 | 8499A16 | 3.63 | 8490A13 | 4.80 | 84975A55 | 4.93 | 84765A63 | 5.40 |
| 1/4"-28 | 1" | 0.188" | 0.118" | 1 | 4 | 3126A27■♥ | 4.47 | 8499A17 | 3.63 | 8490A23 | 4.80 | 84975A57 | 4.93 | 84765A74 | 5.40 |
| 1/4"-28 | 1" | 0.188" | 0.118" | 3 | 13 | 3126A28 | 2.99 | 8499A18 | 3.63 | 8490A14 | 4.80 | 84975A59 | 4.93 | 84765A64 | 5.40 |
| 5/16"-18 | 1" | 0.188" | 0.135" | 1.5 | 4.5 | 3126A29 | 3.22 | 8499A19 | 3.63 | 8490A24 | 4.80 | 84975A62 | 5.07 | 84765A75 | 5.40 |
| 5/16"-18 | 1" | 0.188" | 0.135" | 3 | 15 | 3126A43 | 2.98 | 8499A21 | 3.63 | 8490A15 | 4.80 | 84975A64 | 5.07 | 84765A66 | 5.40 |
| 3/8"-16 | 1.125" | 0.188" | 0.187" | 2.8 | 7.2 | 3126A44 | 3.04 | 8499A22 | 3.40 | 8490A25 | 4.80 | 84975A66 | 5.57 | 84765A76 | 6.07 |
| 3/8"-16 | 1.125" | 0.188" | 0.187" | 5.5 | 14.5 | 3126A45 | 3.11 | 8499A23 | 3.40 | 8490A16 | 4.80 | 84975A68 | 5.57 | 84765A67 | 6.07 |
| 1/2"-13 | 1.25" | 0.25" | 0.248" | 2.7 | 9.3 | 3126A46 | 3.50 | 8499A24 | 3.60 | 8490A26 | 4.80 | 84975A71 | 7.64 | 84765A77 | 7.57 |
| 1/2"-13 | 1.25" | 0.25" | 0.248" | 6.6 | 17.4 | 3126A47 | 3.50 | 8499A25 | 3.60 | 8490A17 | 4.80 | 84975A73 | 7.64 | 84765A68 | 7.57 |
| 5/8"-11 | 1.5" | 0.313" | 0.31" | 3.5 | 10.5 | 3126A48 | 5.51 | 8499A26 | 4.16 | 8490A27 | 6.31 | 84975A75 | 12.50 | 84765A78 | 14.04 |
| 5/8"-11 | 1.5" | 0.313" | 0.31" | 10.5 | 25.5 | 3126A49 | 5.51 | 8499A27 | 4.16 | 8490A18 | 6.31 | 84975A86 | 12.50 | 84765A69 | 14.04 |
| 3/4"-10 | 1.75" | 0.312" | 0.374" | 4 | 16 | 3126A39• | 7.01 | | | | | | | | |
| 3/4"-10 | 1.75" | 0.313" | 0.374" | 6.7 | 37.3 | 3126A61 | 7.95 | | | | | 84975A77 | 19.93 | | |
| 1"-8 | 2.406" | 0.5" | 0.498" | 4 | 31 | 3126A72 | 11.21 | | | | | 84975A79 | 38.20 | | |
| 1"-8 | 2.406" | 0.5" | 0.498" | 16 | 68 | 3126A73 | 12.39 | | | | | 84975A83 | 38.20 | | |
| *Short Length* | | | | | | | | | | | | | | | |
| 6-32 | 0.375" | 0.036" | 0.046" | 0.5 | 1.5 | 3126A69•★ | 3.50 | 8499A52•★ | 3.78 | | | | | | |
| 8-32 | 0.437" | 0.052" | 0.07" | 0.5 | 1.5 | 3126A76 | 3.39 | 8499A28 | 3.28 | | | 84985A41 | 5.60 | 84765A11 | 5.23 |
| 8-32 | 0.437" | 0.052" | 0.07" | 1.5 | 4.75 | 3126A77 | 3.39 | 8499A29 | 3.28 | | | 84985A43 | 5.60 | 84765A14 | 5.23 |
| 8-32 | 0.5" | 0.094" | 0.07" | 0.5 | 2 | 3126A78■★ | 4.12 | 8499A49★ | 3.63 | | | | | | |
| 8-32 | 0.5" | 0.094" | 0.07" | 0.5 | 4 | 3126A79■★ | 4.12 | 8499A51★ | 3.63 | | | | | | |
| 8-36 | 0.437" | 0.052" | 0.07" | 0.5 | 1.5 | 3126A81 | 3.39 | 8499A31 | 3.28 | | | 84985A45 | 5.60 | 84765A17 | 5.23 |
| 8-36 | 0.437" | 0.052" | 0.07" | 1.5 | 4.75 | 3126A82 | 3.39 | 8499A32 | 3.28 | | | 84985A47 | 5.60 | 84765A81 | 5.23 |
| 10-32 | 0.468" | 0.065" | 0.093" | 0.75 | 2.5 | 3126A83 | 2.79 | 8499A33 | 2.91 | | | 84985A49 | 4.37 | 84765A84 | 4.91 |
| 10-32 | 0.468" | 0.065" | 0.093" | 1.75 | 6.25 | 3126A84 | 2.77 | 8499A34 | 2.91 | | | 84985A52 | 4.37 | 84765A87 | 4.91 |
| 1/4"-20 | 0.531" | 0.078" | 0.119" | 1 | 3.5 | 3126A85 | 2.58 | 8499A35 | 2.91 | | | 84985A54 | 4.37 | 84765A91 | 4.80 |
| 1/4"-20 | 0.531" | 0.078" | 0.119" | 3 | 10.5 | 3126A86 | 2.79 | 8499A36 | 2.91 | | | 84985A56 | 4.37 | 84765A94 | 4.80 |
| 5/16"-18 | 0.562" | 0.084" | 0.135" | 1.25 | 4 | 3126A87 | 2.99 | 8499A37 | 3.05 | | | 84985A58 | 4.43 | 84765A97 | 4.80 |
| 5/16"-18 | 0.562" | 0.084" | 0.135" | 3.75 | 15.5 | 3126A89 | 2.83 | 8499A38 | 3.05 | | | 84985A61 | 4.43 | 84765A101 | 4.80 |
| 5/16"-18 | 0.563" | 0.084" | 0.134" | 1.5 | 4 | 3126A65•★ | 3.74 | 8499A53•★ | 2.98 | | | | | | |
| 3/8"-16 | 0.625" | 0.11" | 0.186" | 1.5 | 5 | 3126A91 | 2.75 | 8499A39 | 3.05 | | | 84985A63 | 5.53 | 84765A104 | 5.66 |
| 3/8"-16 | 0.625" | 0.11" | 0.186" | 4.5 | 18.5 | 3126A92 | 2.81 | 8499A41 | 3.05 | | | 84985A65 | 5.53 | 84765A107 | 5.66 |
| 1/2"-13 | 0.75" | 0.151" | 0.248" | 1.75 | 5.5 | 3126A93 | 3.21 | 8499A42 | 3.79 | | | 84985A83 | 7.27 | 84765A111 | 5.88 |
| 1/2"-13 | 0.75" | 0.151" | 0.248" | 5 | 28 | 3126A94 | 3.21 | 8499A43 | 3.79 | | | 84985A85 | 7.27 | 84765A114 | 5.88 |
| 5/8"-11 | 1.062" | 0.215" | 0.31" | 2 | 8.5 | 3126A95 | 4.46 | 8499A44 | 4.84 | | | 84985A87 | 8.30 | 84765A117 | 6.98 |
| 5/8"-11 | 1.062" | 0.215" | 0.31" | 7 | 50 | 3126A96 | 4.46 | 8499A45 | 4.84 | | | 84985A89 | 8.30 | 84765A121 | 6.98 |

♦ Prices are 10% to 15% lower for quantities of 12 or more of a given size. ■ Nose is not heat treated. ▲ Nose is 0.046" dia.
• Available only *with* a nylon thread-locking element. ♥ Nose is 0.119" dia. ★ Black-oxide finish.

*(Continued on following page)*

# Spring Plungers

*For an index of fixturing components, see page 2450. For information about spring plungers, see page 2452.*

## Round-Nose Spring Plungers *(Continued from previous page)*

**To Order:** Please specify *with or without nylon thread-locking element.* Select a plunger without the nylon thread-locking element when threading into aluminum and other soft materials. For information about nylon thread-locking elements, see page 2452.

**Metric Sizes**—Class 6G threads

| Thread Size (A) | Body Lg. (B) | Nose Lg. (C) | Nose Dia. (D) | End Force, lbs. Initial | End Force, lbs. Final | STEEL BODY Steel Nose | Each | STAINLESS STEEL BODY Stainless Steel Nose | Each |
|---|---|---|---|---|---|---|---|---|---|
| *Standard Length* | | | | | | | | | |
| M6 ×1 | 20 mm | 2.5 mm | 2.7 mm | 1.57 | 4.5 | 84995A41 | $4.90 | 8502A21 | $7.11 |
| M6 ×1 | 20 mm | 2.5 mm | 2.7 mm | 4.05 | 11.24 | 84995A43 | 4.76 | 8502A23 | 7.11 |
| M6 ×1 | 25 mm | 5 mm | 3 mm | 1.1 | 3.96 | 84995A19♣ | 5.69 | | |
| M8 ×1.25 | 22 mm | 3 mm | 3.5 mm | 2.02 | 7.87 | 84995A45 | 4.96 | 8502A25 | 7.26 |
| M8 ×1.25 | 22 mm | 3 mm | 3.5 mm | 5.62 | 15.74 | 84995A47 | 4.96 | 8502A27 | 7.26 |
| M10×1.5 | 22 mm | 3 mm | 3.5 mm | 2.02 | 7.87 | 84995A49 | 5.31 | 8502A29 | 7.39 |
| M10×1.5 | 22 mm | 3 mm | 4 mm | 5.62 | 15.74 | 84995A52 | 5.30 | 8502A32 | 7.39 |
| M12×1.75 | 28 mm | 4 mm | 6 mm | 2.25 | 12.36 | 84995A54 | 5.43 | 8502A34 | 7.54 |
| M12×1.75 | 28 mm | 4 mm | 6 mm | 10.12 | 24.73 | 84995A56 | 5.43 | 8502A36 | 7.54 |

♣ Steel body with zinc-plated finish.

## Brass and Type 316 Stainless Steel Round-Nose Spring Plungers

Similar to our other round-nose spring plungers, except these are made of brass or Type 316 stainless steel for more corrosive applications. A slot in the body allows installation with a screwdriver or plunger wrench (sold separately below). All have Class 2A threads and are nonmagnetic.

Choose from standard and short length plungers. *Short length* plungers combine the short body of a ball-nose spring plunger with the longer nose of a round-nose spring plunger. Good for use in thinner materials and tight spaces. Maximum temperature for brass and stainless steel plungers is 250° F.

*Body and Nose Materials—Brass* has a decorative finish and is great for use in marine environments. *Type 316 stainless steel* has superior corrosion resistance.


**To Order:** Please specify *with or without nylon thread-locking element.* When threading into aluminum and other soft materials, select a plunger without the nylon thread-locking element. For information about nylon thread-locking elements, see page 2452.

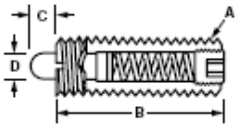


| Thread Size (A) | Body Lg. (B) | Nose Lg. (C) | Nose Dia. (D) | End Force, lbs. Initial | End Force, lbs. Final | BRASS BODY Brass Ball | Each | STAINLESS STEEL BODY Stainless Steel Ball | Each |
|---|---|---|---|---|---|---|---|---|---|
| *Standard Length* | | | | | | | | | |
| 6-32 | 0.375" | 0.063" | 0.045" | 1.00 | 1.60 | 8689A11 | $12.40 | 8688A11 | $17.70 |
| 8-32 | 0.625" | 0.094" | 0.070" | 0.70 | 2.30 | 8689A12 | 11.13 | 8688A12 | 15.90 |
| 8-32 | 0.625" | 0.094" | 0.070" | 2.70 | 7.30 | 8689A13 | 11.13 | 8688A13 | 15.90 |
| 10-32 | 0.750" | 0.125" | 0.092" | 1.30 | 2.70 | 8689A14 | 10.83 | 8688A14 | 15.48 |
| 1/4"-20 | 1.000" | 0.188" | 0.118" | 3.00 | 13.00 | 8689A15 | 10.78 | 8688A15 | 15.40 |
| 1/4"-28 | 1.000" | 0.188" | 0.118" | 1.00 | 4.00 | 8689A16 | 10.78 | 8688A16 | 15.40 |
| 1/4"-28 | 1.000" | 0.188" | 0.118" | 3.00 | 13.00 | 8689A17 | 10.78 | 8688A17 | 15.40 |
| 5/16"-18 | 1.000" | 0.188" | 0.135" | 3.00 | 15.00 | 8689A18 | 11.10 | 8688A18 | 15.85 |
| 3/8"-16 | 1.125" | 0.188" | 0.187" | 5.50 | 14.50 | 8689A19 | 12.18 | 8688A19 | 17.40 |
| 1/2"-13 | 1.250" | 0.250" | 0.248" | 6.60 | 17.40 | 8689A21 | 16.73 | 8688A21 | 23.88 |
| 5/8"-11 | 1.500" | 0.313" | 0.310" | 10.60 | 25.50 | 8689A22 | 19.89 | 8688A22 | 28.42 |
| 3/4"-10 | 1.750" | 0.313" | 0.374" | 6.70 | 37.30 | 8689A23 | 29.08 | 8688A23 | 38.35 |
| 1"-8 | 2.406" | 0.500" | 0.498" | 16.00 | 68.00 | 8689A24 | 55.72 | 8688A24 | 68.21 |
| *Short Length* | | | | | | | | | |
| 8-32 | 0.438" | 0.052" | 0.070" | 1.50 | 4.75 | 8689A31 | 12.25 | 8688A31 | 17.50 |
| 8-32 | 0.500" | 0.094" | 0.070" | 0.50 | 2.00 | 8689A32 | 12.25 | 8688A32 | 17.50 |
| 10-32 | 0.530" | 0.065" | 0.090" | 1.75 | 6.25 | 8689A33 | 9.55 | 8688A33 | 13.65 |
| 1/4"-20 | 0.531" | 0.078" | 0.119" | 3.00 | 10.50 | 8689A34 | 9.55 | 8688A34 | 13.65 |
| 5/16"-18 | 0.583" | 0.084" | 0.135" | 1.50 | 4.00 | 8689A35 | 9.70 | 8688A35 | 13.85 |
| 3/8"-16 | 0.625" | 0.110" | 0.186" | 4.50 | 18.50 | 8689A36 | 12.10 | 8688A36 | 17.28 |
| 1/2"-13 | 0.750" | 0.151" | 0.248" | 5.00 | 28.00 | 8689A37 | 15.90 | 8688A37 | 22.73 |
| 5/8"-11 | 1.063" | 0.215" | 0.310" | 2.00 | 8.50 | 8689A38 | 18.18 | 8688A38 | 25.95 |
| 5/8"-11 | 1.063" | 0.215" | 0.310" | 7.00 | 50.00 | 8689A39 | 18.18 | 8688A39 | 25.95 |

## Ball-Nose and Round-Nose Spring Plunger Wrenches

Specifically designed to install and remove ball-nose and round-nose spring plungers, these wrenches work better than screwdrivers because their center hole lets the ball- or round-nose pass through to avoid damaging or overloading the spring.

| For Thread Size | | Each |
|---|---|---|
| 6-32 | 3382A11 | $4.89 |
| 8-32 and M4 | 3382A12 | 5.05 |
| 10-32 and M5 | 3382A13 | 5.19 |
| 1/4"-20, 1/4"-28, and M6 | 3382A14 | 5.32 |
| 5/16"-18 and M8 | 3382A15 | 5.47 |
| 3/8"-16 and M10 | 3382A16 | $5.81 |
| 1/2"-13 and M12 | 3382A17 | 6.14 |
| 5/8"-11 | 3382A18 | 7.65 |
| 3/4"-10 | 3382A19 | 8.81 |
| 1"-8 | 3382A21 | 9.58 |

## Mounting Base for Spring Plungers

Also known as tooling flanges, these mounting bases let you mount ball-nose and round-nose spring plungers without having to drill and tap a hole. Bases have two holes for mounting to fixture surfaces (fasteners not included) and a threaded hole to insert the spring plunger. Ideal for fixtures that require a horizontal application. *Triangular* mounting base is made of zinc-plated steel; *rectangular* is nickel-plated steel.

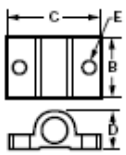


*Rectangular Base*

| For Thread Size | O'all Lg. (B) | O'all Wd. (C) | O'all Ht. (D) | Mounting Holes Hole Dia. (E) | Mounting Holes Ctr.-to-Ctr. | | Each |
|---|---|---|---|---|---|---|---|
| *Triangular Base* | | | | | | | |
| 1/4"-20 | 0.69" | 0.88" | 0.41" | 0.136" | 0.66" | 8685A11 | $5.16 |
| *Rectangular Base* | | | | | | | |
| 1/2"-13 | 1.00" | 1.50" | 0.63" | 0.203" | 1.13" | 8685A12 | 11.96 |

# Appendix H UHV Ribbon Cable CABURN

Section 6.7

## Connectors & Cables
### In-Vacuum Wiring - Kapton® Insulated

### Features

- High strength Kapton® type-F film
- Silver plated copper conductors
- Single, multi-strand and coaxial
- Cryogenic instrumentation wire
- Type-K thermocouple wire
- UHV compatible construction
- High temperature rated to 260°C

### Specifications

| | |
|---|---|
| Voltage[1] | See each table |
| Current | See each table |
| Materials | |
| Conductor | Silver plated copper |
| Insulation | Kapton® Type F film |
| Kapton® Properties | |
| Dielectric Constant | 2.9 |
| Dielectric Strength | 80KV/mm |
| Dissipation Factor | 0.001 |
| Initial Tear | 13.4kg/mm |
| Tensile Strength | 10MPa |
| Elongation | 75% |
| Moisture Absorption | 0.4% @ 50% RH |
| Radiation Resistance | $10^8$ Rads |
| Vacuum Range UHV | 1x10''mbar |
| Temperature Range[2] | |
| Conventional | 260°C |
| Cryogenic | -269°C |

[1] Electrical ratings are maximum test values
[2] Overall ratings must be adjusted to that of the lowest rated component

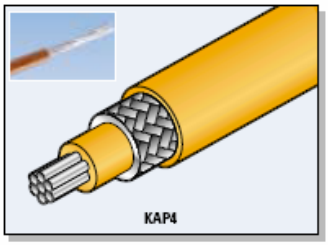
KAP4

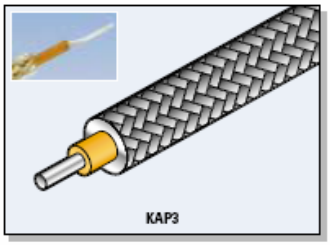
KAP3

### Description

Caburn's Kapton® insulated in-vacuum wiring is designed for high and ultrahigh vacuum environments up to 260°C. All conductors and braided shields (coaxial cable shields) are silver plated copper wire. Insulation is Kapton® Type-F film that is applied and heat treated to effectively minimize trapped volumes of gas and maintain mechanical strength.

Included in this section are Caburn exclusive in-vacuum ribbon cables. These ribbon cables are available in either high or ultrahigh vacuum grades. UHV ribbon cables consist of multiple strands of Kapton® insulated wires that are bundled together with a PEEK® (Polyether-Etherketone) monofilament weaving. Caburn ribbon cables are designed to complement its line of subminiature-C and D feedthroughs as detailed on pages 20 to 23. High vacuum PTFE ribbon cable is available as an economical solution for less demanding vacuum applications.

For sensitive UHV instrumentation applications such as AFM (atomic force microscopy) or STM (scanning tunnelling microscopy) requiring minimal loads and maximum flexibility, Caburn offers standard and cryogenic fine instrumentation wires. The cryogenic instrumentation wire is suitable for temperatures down to -269°C (4°K-Liquid Helium). Securing and fastening these fine instrumentation wires is made simple with the use of conductive in-vacuum adhesives as detailed on page 211.

Wire strippers and glass-ceramic colour identification beads are some of the accessories offered to facilitate working with the extensive selection of in-vacuum wire and cable products.

### UHV 0.61mm DIAMETER COAXIAL CABLE

| CABLE TYPE | CABLE LENGTH | JACKET DIA | WIRE DIA | REFERENCE | PART NUMBER | PRICE £ | PRICE € | PRICE SFr |
|---|---|---|---|---|---|---|---|---|
| COAXIAL | 10m | 1.47 | 7 X 0.2 | KAP4 | 1512005 | 86 | 135 | 192 |

Resistance of 87.2Ω/km, a capacitance 300pf/m, a voltage rating of 600VAC, 2kVDC and a current of 4.5A max Impendance = 18Ω

### UHV 0.25mm DIAMETER COAXIAL CABLE

| CABLE TYPE | CABLE LENGTH | JACKET DIA | WIRE DIA | REFERENCE | PART NUMBER | PRICE £ | PRICE € | PRICE SFr |
|---|---|---|---|---|---|---|---|---|
| COAXIAL | 10m | 0.89 | 0.25 | KAP3 | 1512004 | 62 | 98 | 140 |

Resistance of 375.8Ω/km, a capacitance 180pf/m, a voltage rating of 600VAC, 2kVDC and a current of 1.5A max Impendance = 32Ω

All dimensions are nominal in millimeters unless specified - Weights given are approximate

Contact your sales office for more details...

# Connectors & Cables
## In-Vacuum Wiring - Kapton® & PTFE Insulated

Section 6.7

## UHV 50 OHM COAXIAL CABLE

### KAP50-5

| CABLE TYPE | CABLE LENGTH | JACKET DIA | WIRE DIA | REFERENCE | PART NUMBER | PRICE £ | PRICE € | PRICE SFr |
|---|---|---|---|---|---|---|---|---|
| COAXIAL | 5000 | 2.3 | 7 x 0.15 | KAP50-5 | 1512006 | 101 | 159 | 227 |

Resistance of 159Ω/km, a capacitance 110pf/m, a voltage rating of 600VAC, 12kVDC and a current of 1A max
Kapton® insulated with a silver plated wire screen and Kapton® sheath

## UHV CIRCULAR CABLE - COLOUR CODED

### UHV Circular Cable

| NO WIRES | CABLE LENGTH | JACKET DIA | BRAID DIA | INSULATOR DIA | WIRE DIA | REFERENCE | PART NUMBER | PRICE £ | PRICE € | PRICE SFr |
|---|---|---|---|---|---|---|---|---|---|---|
| 9 | 500 | 1.47 | 1.22 | 0.89 | 7 x 0.1 | CCAB9-500 | 1512761 | 26 | 43 | 65 |
| 9 | 1000 | 1.47 | 1.22 | 0.89 | 7 x 0.1 | CCAB9-1000 | 1512762 | 42 | 70 | 105 |
| 9 | 2500 | 1.47 | 1.22 | 0.89 | 7 x 0.1 | CCAB9-2500 | 1512763 | 94 | 156 | 234 |

9 way cable with a PEEK® woven outer sleeving
Resistance of 222Ω/km, a voltage rating of 600VAC, 840VDC and a current of 1.5A

## KAPTON® INSULATED & HIGH VACUUM PTFE RIBBON CABLE

### UHV Ribbon

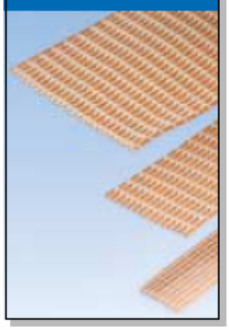

### HV Ribbon

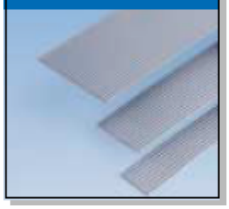

| NO WIRES | CABLE LENGTH | CABLE WIDTH | CABLE THICKNESS | WIRE DIA | REFERENCE | PART NUMBER | PRICE £ | PRICE € | PRICE SFr |
|---|---|---|---|---|---|---|---|---|---|
| **UHV KAPTON® INSULATED** | | | | | | | | | |
| 9 | 500 | 11 | 1 | 7 x 0.127 | KAP-R9-500 | 1512100 | 37 | 59 | 83 |
| 9 | 1000 | 11 | 1 | 7 x 0.127 | KAP-R9-1000 | 1512103 | 51 | 81 | 115 |
| 9 | 2500 | 11 | 1 | 7 x 0.127 | KAP-R9-2500 | 1512150 | 93 | 146 | 208 |
| 15 | 500 | 19 | 1 | 7 x 0.127 | KAP-R15-500 | 1512101 | 47 | 74 | 105 |
| 15 | 1000 | 19 | 1 | 7 x 0.127 | KAP-R15-1000 | 1512104 | 71 | 112 | 159 |
| 15 | 2500 | 19 | 1 | 7 x 0.127 | KAP-R15-2500 | 1512151 | 142 | 225 | 320 |
| 25 | 500 | 30 | 1 | 7 x 0.127 | KAP-R25-500 | 1512102 | 48 | 76 | 107 |
| 25 | 1000 | 30 | 1 | 7 x 0.127 | KAP-R25-1000 | 1512105 | 80 | 126 | 162 |
| 25 | 2500 | 30 | 1 | 7 x 0.127 | KAP-R25-2500 | 1512152 | 161 | 255 | 326 |
| **HV PTFE INSULATED** | | | | | | | | | |
| 9 | 500 | 10 | 1 | 7 x 0.2 | HVR9-500 | 1512770 | 12 | 19 | 29 |
| 9 | 1000 | 10 | 1 | 7 x 0.2 | HVR9-1000 | 1512771 | 18 | 30 | 45 |
| 9 | 2500 | 10 | 1 | 7 x 0.2 | HVR9-2500 | 1512772 | 35 | 59 | 87 |
| 15 | 500 | 19 | 1 | 7 x 0.2 | HVR15-500 | 1512773 | 14 | 23 | 36 |
| 15 | 1000 | 19 | 1 | 7 x 0.2 | HVR15-1000 | 1512774 | 23 | 37 | 56 |
| 15 | 2500 | 19 | 1 | 7 x 0.2 | HVR15-2500 | 1512775 | 48 | 79 | 119 |
| 25 | 500 | 30 | 1 | 7 x 0.2 | HVR25-500 | 1512776 | 19 | 32 | 47 |
| 25 | 1000 | 30 | 1 | 7 x 0.2 | HVR25-1000 | 1512777 | 31 | 50 | 77 |
| 25 | 2500 | 30 | 1 | 7 x 0.2 | HVR25-2500 | 1512778 | 68 | 113 | 168 |

Voltage rating of 1kVAC, 4kVDC and a current 1A maximum
Use two lengths of 25-wire cable for 50 pin applications
All UHV cable assemblies are bakeable to 250°C
All HV cable assemblies are bakeable to 105°C
PTFE cable without plugs bakeable to 200°C

All dimensions are nominal in millimeters unless specified - Weights given are approximate

Contact your sales office for more details...

CABURN

# Kapton® Wires & Ribbon Cables

PRODUCT DATA SHEET

## General Specifications for Kapton® Insulation

### Chemical (insulation only)

- Excellent Chemical Resistance (except for strong bases)
- Moisture Absorption @ 50% RH=1.3%
- Radiation Resistance = $10^7$ rads *

* Cables wrapped with F film will withstand this dosage in non-flexing applications

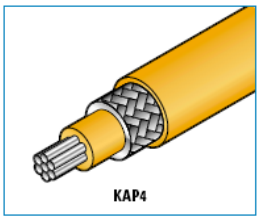

KAP4

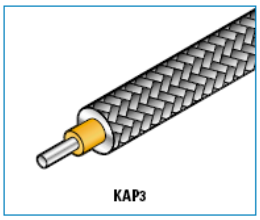

KAP3

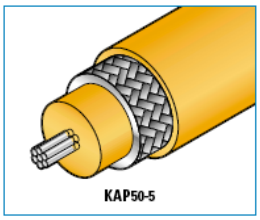

KAP50-5

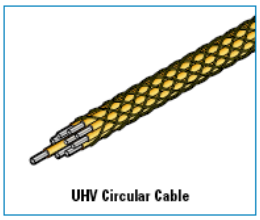

UHV Circular Cable

### Vacuum Range

Atmosphere – 5x10-11mbar

### Mechanical

| | |
|---|---|
| Density | 1.53 g/cm3 |
| Initial Tear | 13.4 N |
| Propagating Tear | 0.08 N |
| Tensile Strength | 10MPa |
| Tensile Modulus | 2.5GPa |
| Elongation | 75% |

### Electrical

| | |
|---|---|
| Dielectric Constant | 3.1 |
| Dielectric Strength | 80KV/mm |
| Dissipation Factor | 0.0015 |

### Thermal

| | |
|---|---|
| Maximum Operating Temperature | 200°C |
| Maximum Bakeout Temperature | 260°C |
| Minimum Operating Temperature | -269°C |
| Zero Strength Temperature | 1088K |
| Flammability | Will not propagate flame, No after flame |
| Limiting Oxygen Index | 37 |
| Shrinkage | 0.1 – 0.25% (after 30mins @ 150°C) |

### Description

Caburn's Kapton® insulated in-vacuum wire is designed for high and ultrahigh vacuum environments up to 260°C. All conductors and braided shields (coaxial shields) are silver plated copper wire (apart from KAP4K-04 which has a stainless steel conductor). Insulation is Kapton® Type F film that is applied and heat treated to effectively minimize trapped volumes of gas and maintain mechanical strength.

Kapton® ribbon cables consist of multiple strands of Kapton® insulated wires that are bundled together with a PEEK® (Polyether-Etherketone) monofilament weaving.

All of Caburn's Kapton® wires can be used at low temperatures down to -269°C, however KAP4K-014 is the only cable rated for cryogenic use as it employs a stainless steel conductor which reduces heat transfer into the cryogenic system along the cable itself.

® Kapton is a registered trademark of Dupont
® Peek is a registered trade mark of ICI

**This product is supplied on the understanding that the specific conditions of use are outside the control of Caburn. Caburn assumes no liability for the accuracy or completeness of the information contained herein.**

# CABURN Kapton® Wires & Ribbon Cables

PRODUCT DATA SHEET

| Part Reference | KAP1 | KAP2 | KAP3 | KAP4 | KAP4K-014 | KAP50-5 | KAP08 | KAP10 | KAP012 | KAP-TCK2 | UHV Circular Cable | UHV Ribbon 9 Way | UHV Ribbon 15 Way | UHV Ribbon 25 Way |
|---|---|---|---|---|---|---|---|---|---|---|---|---|---|---|
| Part Number | 1512002 | 1512003 | 1512004 | 1512005 | 1512081 | 1512006 | 1512001 | 1512009 | 1512000 | 1512070 | 1512761<br>1512762<br>1512763 | 1512100<br>1512103<br>1512150 | 1512101<br>1512104<br>1512151 | 1512102<br>1512105<br>1512152 |
| Conductor Material | Silver Plated Copper | Silver Plated Copper | Silver Plated Copper | Silver Plated Copper | 304 Stainless Steel | Silver Plated Copper | Silver Plated Copper | Silver Plated Copper | Silver Plated Copper | Chromel® Alumel® | Silver Plated Copper | Silver Plated Copper | Silver Plated Copper | Silver Plated Copper |
| Conductor Diameter (mm) | 0.25 | 0.6 | 0.25 | 7 x 0.2 | 0.12 | 7 x 0.15 | 7 x 0.08 | 1 | 7 x 0.12 | 0.16 | 7 x 0.127 | 7 x 0.127 | 7 x 0.127 | 7 x 0.127 |
| Conductor C.S.A. mm² | 0.049 | 0.283 | 0.049 | 0.22 | 0.011 | 0.124 | 0.035 | 0.785 | 0.079 | 0.02 | 0.088 | 0.088 | 0.088 | 0.088 |
| Maximum O.D. mm | 0.055 | 0.9 | 1.04 | 1.47 | 0.39 | 2.39 | 0.054 | 1.52 | 0.16 | 0.39 | 3.2 (Bundle) | 0.74 | 0.74 | 0.74 |
| Cable length (m) | 10 | 10 | 10 | 10 | 10 | 5 | 10 | 10 | 10 | 2 | 0.5<br>1.0<br>2.5 | 0.5<br>1.0<br>2.5 | 0.5<br>1.0<br>2.5 | 0.5<br>1.0<br>2.5 |
| Kapton® Outer Coating | Kapton® | Kapton® | Stainless Steel Braid | Kapton® | Kapton® | Kapton® | Kapton® | Kapton® | Kapton® | Kapton® | Kapton® | Kapton® | Kapton® | Kapton® |
| Voltage Rating AC (RMS) | 600V | 600V | 600V | 600V | 600V | 600V | 600V | 3.6kV | 600V | Signal | 600V | Signal | Signal | Signal |
| Voltage Rating DC | 2kV | 2kV | 2kV | 2kV | 2kV | 12kV | 2kV | 5kV | 2kV | Signal | 2kV | Signal | Signal | Signal |
| Current Rating (at 20°C above ambient) | 1.5A | 5.5A | 1.5A | 4.5A | 50mA | 1A | 1.5A | 10A | 0.5A | Signal | 2A | Signal | Signal | Signal |
| Resistance Ω/Km @ 20°C | 376 | 64 | 376 | 87 | n/a | 159 | 558 | 23 | 230 | n/a | 222 | 222 | 222 | 222 |
| Maximum Operating Temp °C | 200 | 200 | 200 | 200 | 200 | 200 | 200 | 200 | 240 | 240 | 200 | 200 | 200 | 200 |
| Maximum Bakeout Temp °C | 260 | 260 | 260 | 260 | 260 | 260 | 260 | 260 | 250 | 250 | 250 | 250 | 250 | 250 |
| Minimum Operating Temp °C | -269 | -269 | -269 | -269 | -269 | -269 | -269 | -269 | -269 | -269 | -269 | -269 | -269 | -269 |
| Vacuum range to: | 1 x $10^{-11}$ | 1 x $10^{-11}$ | 1 x $10^{-11}$ | 1 x $10^{-11}$ | 1 x $10^{-11}$ | 1 x $10^{-11}$ | 1 x $10^{-11}$ | 1 x $10^{-11}$ | 1 x $10^{-11}$ | 1 x $10^{-11}$ | 1 x $10^{-11}$ | 1 x $10^{-11}$ | 1 x $10^{-11}$ | 1 x $10^{-11}$ |
| Outgassing Characteristics | See Below | See Below | See Below | See Below | See Below | See Below | See Below | See Below | See Below | See Below | See Below | See Below | See Below | See Below |

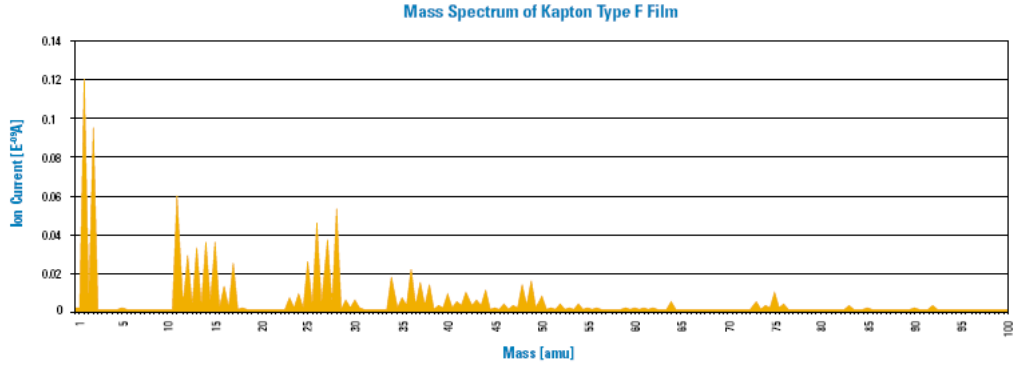


GD1263 Issue 01
**Sheet 2 of 2**

**Warranty** All Products sold by Caburn are warranted to be free from defects in materials and workmanship for a period of twelve months from the date of shipment by Caburn to the buyer. Liability under this warranty is expressly limited to repair or replacement of defective components at the option of Caburn. Products suspected of being defective should not be returned until an official return authorisation number has been issued by our service department. Products being returned must be sent carriage paid by customer to our head office in Glynde, UK.
Note: due to continued product development Caburn reserves the right to change specifications without prior notice.

# Appendix I OMNETICS Bi-Lobe Nano Connector

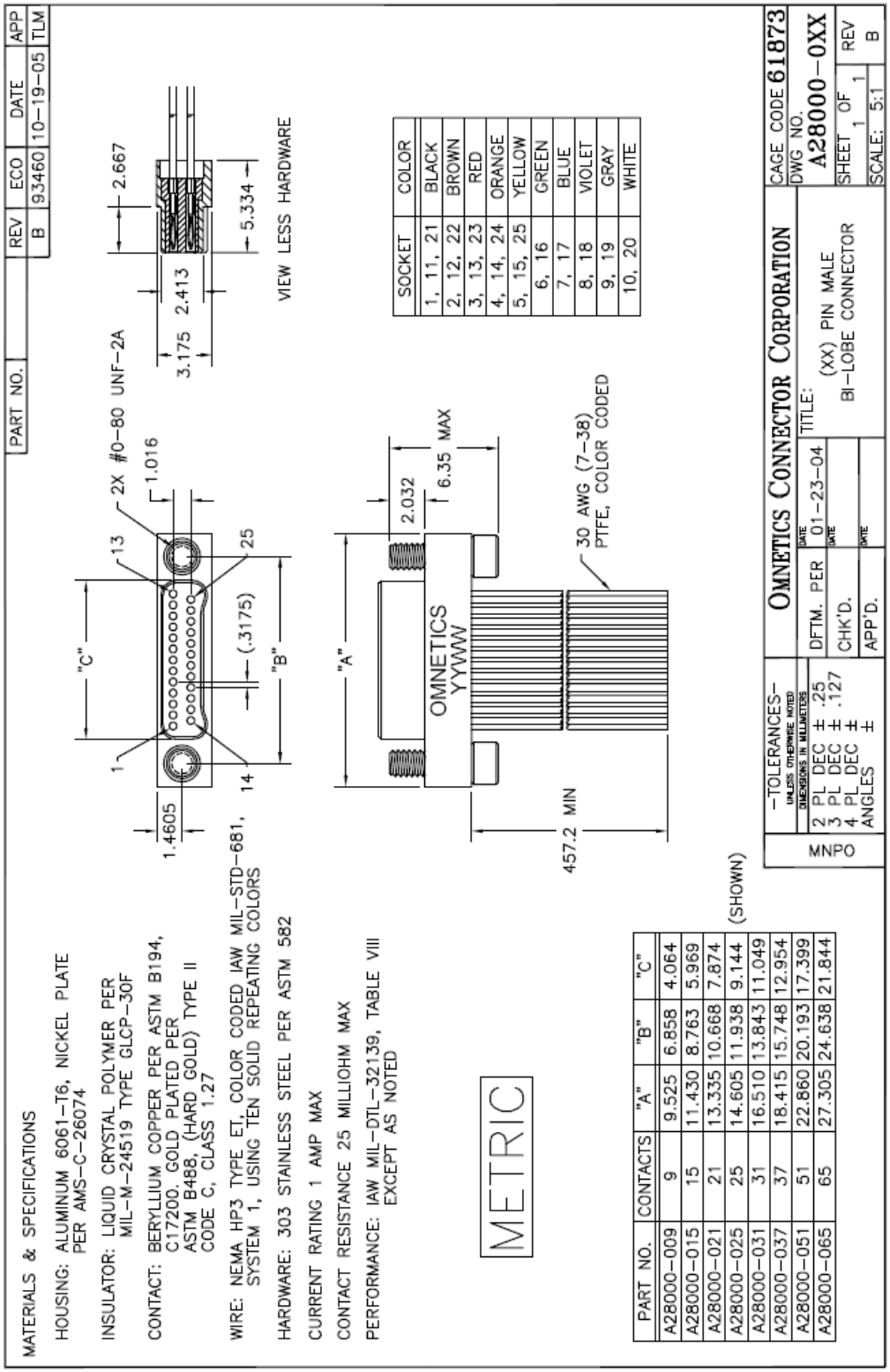

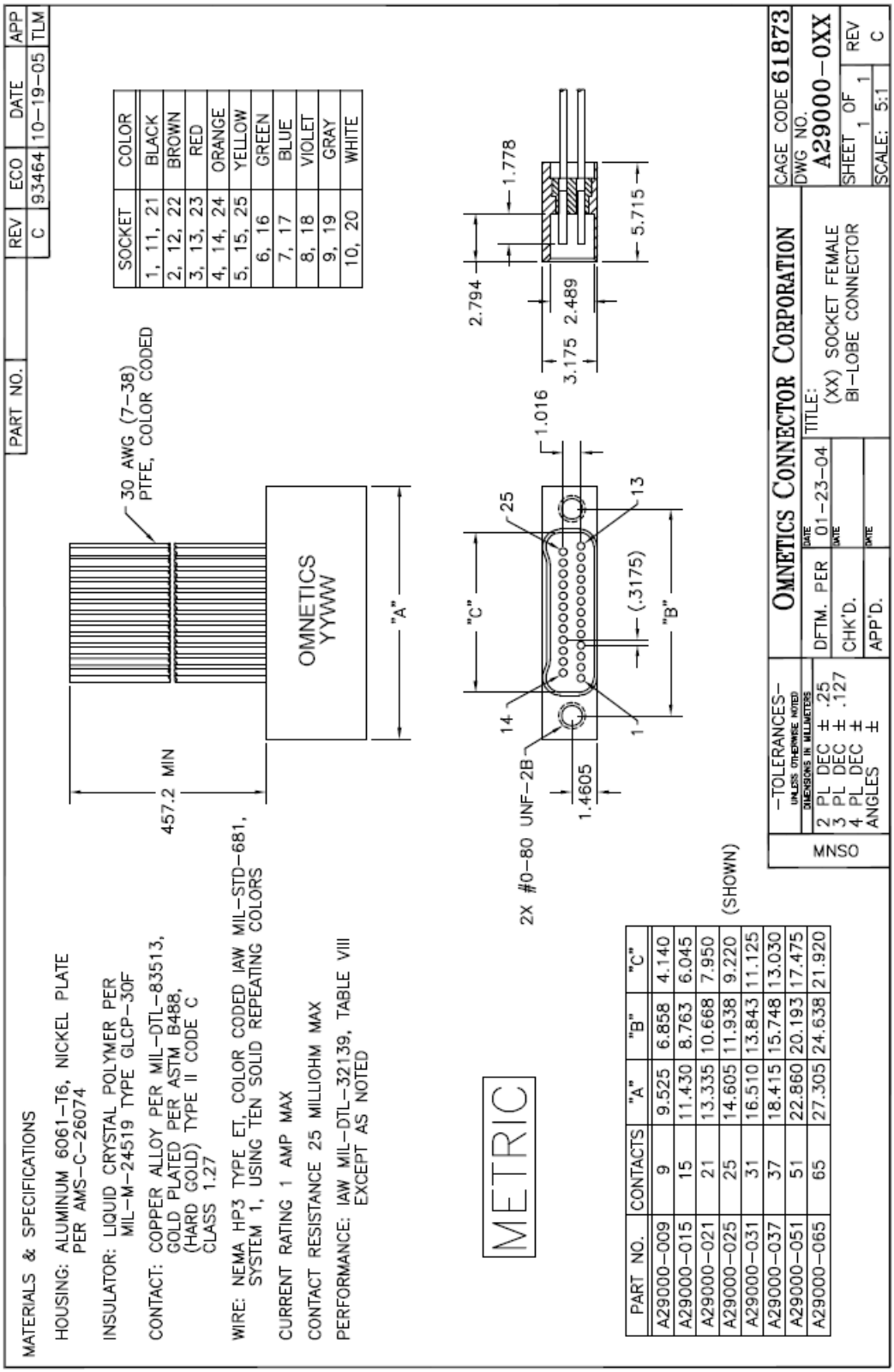
PART NO.
REV C
ECO 93464
DATE 10-19-05
APP TLM
MATERIALS & SPECIFICATIONS
HOUSING: ALUMINUM 6061-T6, NICKEL PLATE PER AMS-C-26074
INSULATOR: LIQUID CRYSTAL POLYMER PER MIL-M-24519 TYPE GLCP-30F
CONTACT: COPPER ALLOY PER MIL-DTL-83513, GOLD PLATED PER ASTM B488, (HARD GOLD) TYPE II CODE C CLASS 1.27
WIRE: NEMA HP3 TYPE ET, COLOR CODED IAW MIL-STD-681, SYSTEM 1, USING TEN SOLID REPEATING COLORS
CURRENT RATING 1 AMP MAX
CONTACT RESISTANCE 25 MILLIOHM MAX
PERFORMANCE: IAW MIL-DTL-32139, TABLE VIII EXCEPT AS NOTED
30 AWG (7-38) PTFE, COLOR CODED
457.2 MIN
OMNETICS YYWW
"A"
SOCKET | COLOR
1, 11, 21 | BLACK
2, 12, 22 | BROWN
3, 13, 23 | RED
4, 14, 24 | ORANGE
5, 15, 25 | YELLOW
6, 16 | GREEN
7, 17 | BLUE
8, 18 | VIOLET
9, 19 | GRAY
10, 20 | WHITE
METRIC
PART NO. | CONTACTS | "A" | "B" | "C"
A29000-009 | 9 | 9.525 | 6.858 | 4.140
A29000-015 | 15 | 11.430 | 8.763 | 6.045
A29000-021 | 21 | 13.335 | 10.668 | 7.950
A29000-025 | 25 | 14.605 | 11.938 | 9.220
A29000-031 | 31 | 16.510 | 13.843 | 11.125
A29000-037 | 37 | 18.415 | 15.748 | 13.030
A29000-051 | 51 | 22.860 | 20.193 | 17.475
A29000-065 | 65 | 27.305 | 24.638 | 21.920
(SHOWN)
2X #0-80 UNF-2B
1.4605
14
1
25
13
"C"
"B"
(.3175)
1.016
2.794
1.778
3.175
2.489
5.715
MNSO
-TOLERANCES- UNLESS OTHERWISE NOTED DIMENSIONS IN MILLIMETERS
2 PL DEC ± .25
3 PL DEC ± .127
4 PL DEC ±
ANGLES ±
OMNETICS CONNECTOR CORPORATION
DFTM. PER DATE 01-23-04
CHK'D. DATE
APP'D. DATE
TITLE: (XX) SOCKET FEMALE BI-LOBE CONNECTOR
CAGE CODE 61873
DWG NO. A29000-0XX
SHEET 1 OF 1
REV C
SCALE: 5:1

# Appendix J Spring Washer FS 3x4.5

FS

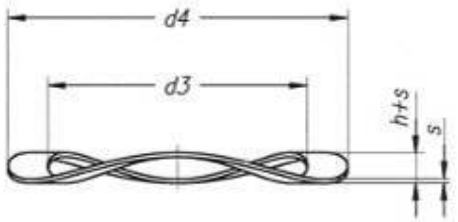


| Reference | h+s ±0.05 [mm] | s* ±0.01 [mm] | d3 [mm] | d4 [mm] | Suitable for bearings with bore Ø [mm] | bore Ø [inch] | outer Ø [mm] | outer Ø [inch] |
|---|---|---|---|---|---|---|---|---|
| FS 1.5 X 3 | 0.40 | 0.08 | 1.60 | 2.90 | - | - | 3 | - |
| FS 2 X 3.5 | 0.45 | 0.08 | 2.15 | 3.10 | 2 | - | - | .1250 |
| FS 2.5 X 4 | 0.50 | 0.08 | 2.70 | 3.80 | 2.5 | - | 4 | .1563 |
| FS 3 X 4.5 | 0.50 | 0.10 | 3.20 | 4.30 | 3 | .1250 | - | - |
| FS 3.5 X 5 | 0.55 | 0.10 | 3.70 | 4.80 | - | - | 5 | - |
| FS 4 X 6 | 0.65 | 0.12 | 4.20 | 5.75 | 4 | .1563 | 6 | - |
| FS 4.5 X 6.35 | 0.60 | 0.12 | 4.80 | 6.10 | - | .1875 | - | .2500 |
| FS 5 X 7 | 0.65 | 0.12 | 5.20 | 6.75 | 5 | - | 7 | - |
| FS 6 X 8 | 0.70 | 0.15 | 6.20 | 7.75 | 6 | - | 8 | .3125 |
| FS 7 X 9 | 0.90 | 0.15 | 7.20 | 8.70 | 7 | - | 9 | - |
| FS 8 X 10 | 0.85 | 0.18 | 8.20 | 9.70 | 8 | .3125 | 10 | - |
| FS 9 X 11 | 1.15 | 0.18 | 9.20 | 10.70 | 9 | - | 11 | - |
| FS 10 X 12 | 1.05 | 0.20 | 10.20 | 11.70 | 10 | - | 12 | - |
| FS 11 X 13 | 1.30 | 0.20 | 11.20 | 12.70 | - | - | 13 | - |
| FS 12 X 14 | 1.30 | 0.22 | 12.20 | 13.70 | - | - | 14 | - |
| FS 13 X 15 | 1.30 | 0.22 | 13.20 | 14.70 | - | - | 15 | - |
| FS 7 X 9 | 0.90 | 0.15 | 7.20 | 8.70 | 7 | - | 9 | - |
| FS 8 X 10 | 0.85 | 0.18 | 8.20 | 9.70 | 8 | .3125 | 10 | - |
| FS 9 X 11 | 1.15 | 0.18 | 9.20 | 10.70 | 9 | - | 11 | - |
| FS 10 X 12 | 1.05 | 0.20 | 10.20 | 11.70 | 10 | - | 12 | - |
| FS 11 X 13 | 1.30 | 0.20 | 11.20 | 12.70 | - | - | 13 | - |
| FS 12 X 14 | 1.30 | 0.22 | 12.20 | 13.70 | - | - | 14 | - |
| FS 13 X 15 | 1.30 | 0.22 | 13.20 | 14.70 | - | - | 15 | - |
| FS 14 X 16 | 1.55 | 0.25 | 14.20 | 15.65 | - | - | 16 | - |
| FS 15 X 17 | 1.55 | 0.25 | 15.20 | 16.65 | - | - | 17 | - |
| FS 16 X 19 | 2.15 | 0.30 | 16.20 | 18.55 | - | - | 19 | .7500 |

* For «s» > 0.25 mm, tolerance of «s» = ± 15 µm

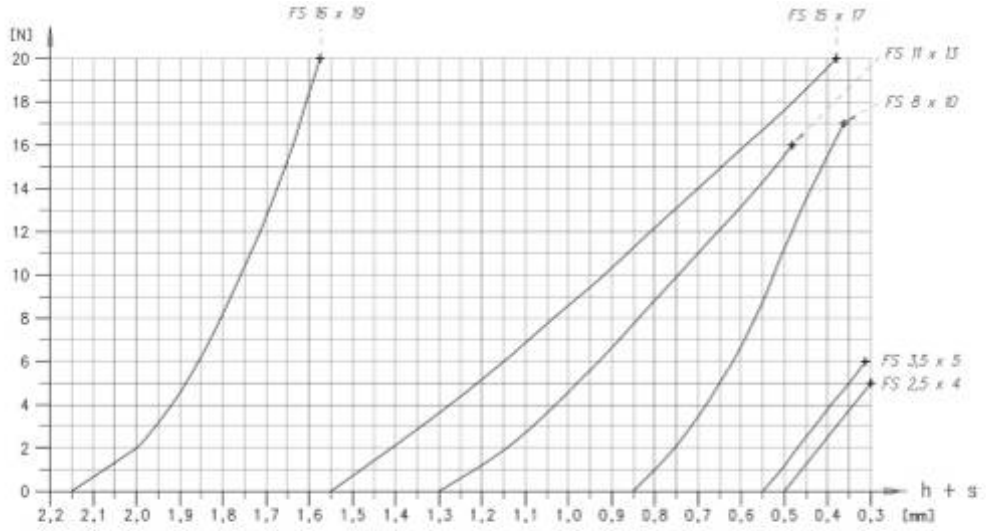
FS 16 x 19
FS 15 x 17
FS 11 x 13
FS 8 x 10
FS 3,5 x 5
FS 2,5 x 4
[N]
h + s
[mm]

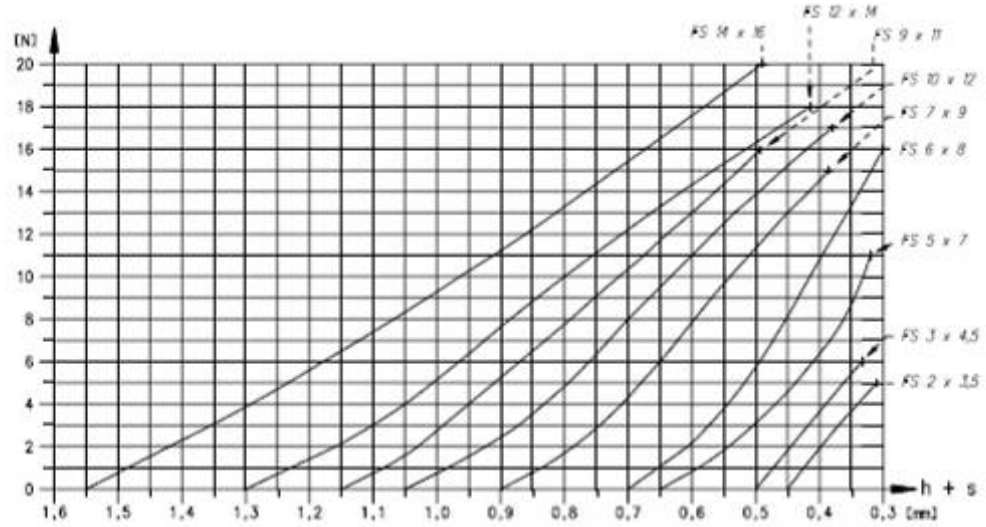
FS 14 x 16
FS 12 x 14
FS 9 x 11
FS 10 x 12
FS 7 x 9
FS 6 x 8
FS 5 x 7
FS 3 x 4,5
FS 2 x 3,5
[N]
h + s
[mm]

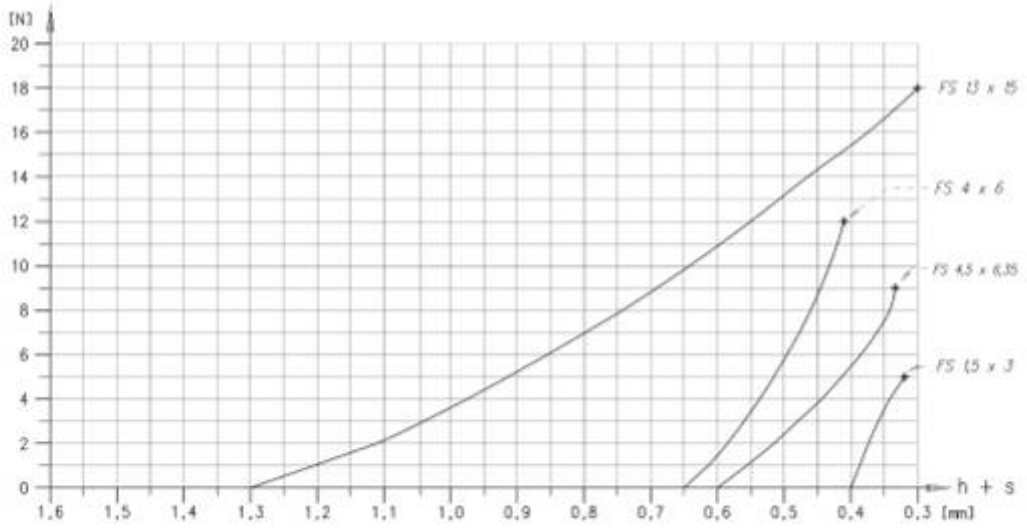
FS 13 x 15
FS 4 x 6
FS 4,5 x 6,35
FS 1,5 x 3
[N]
h + s
[mm]

# Appendix K Static analysis

## K.1 Maximum compressive stresses

### K.1.1 In rails

E = 72 GPa

L = 113.5 mm

S = 9 mm

P = (3kg @ 10 g)/4 = 73.6 N

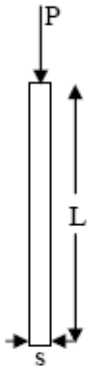


$$\sigma_{\max} = \frac{P}{s^2} = 0.91 MPa$$

### K.1.2 In main crossbar

E = 72 GPa

L = 82 mm

A = 3x4 = 12 $mm^2$

P = (1kg @ 10 g)/4 = 24.5 N

$$\sigma_{\max} = \frac{P}{A} = 2.04 MPa$$

## K.2 Buckling of the rails and crossbars

The differential equation for the buckling of a column is given by Euler formula [11]:

$$\frac{\partial^2 \delta}{\partial z^2} = -\frac{P_{cr}}{EI}\delta \qquad \textbf{Equation 4}$$

where δ is the lateral displacement and z is the coordinate along the length of the column. E is the columns young modulus and $P_{cr}$ the critical load and I the moment of inertia in the plane perpendicular to z. This permits the solution:

$$\delta = C_1 \cos\left(z\sqrt{\frac{P_{cr}}{EI}}\right) + C_2 \cos\left(z\sqrt{\frac{P_{cr}}{EI}}\right) \qquad \textbf{Equation 5}$$

with boundary conditions given by the restraints of the column. For the simply supported case that we are considering the boundary conditions are $\delta = 0$ at $z = 0$ and $z = L$. Thus $C_1 = 0$ and for a non trivial solution:

$$\frac{P_{cr}L^2}{EI} = k^2\pi^2 \qquad \textbf{Equation 6}$$

where k is a positive integer.

This can be re-arranged to give the critical buckling load of a column:

$$P_{cr} = \frac{k^2\pi^2 EI}{L^2} \qquad \textbf{Equation 7}$$

The only mode of buckling observed in practice is the first mode (n=1), occurring at the lowest loads. The critical buckling stress is given by the following expression:

$$\sigma_{cr} = \frac{P_{cr}}{A} = \frac{\pi^2 EI}{AL_e^{\,2}} \qquad \textbf{Equation 8}$$

$L_e$ is the effective length of the column. The effective length is the length of a simply supported column that would have the same critical load as that of a column of length L but with different boundary conditions. In this case we are going to use a factor of K=1 for the expression $L = K L_e$ which is also a worst case assumption.

Values used:

E = 72 GPa

| | | | | |
|---|---|---|---|---|
| Rail: | a = 9mm | d = 7,5mm | A= 47.8 $mm^2$ | $L_e$ = 90mm |
| Main crossbar: | b = 3mm, | h = 4mm, | A= 12$mm^2$ | $L_e$ = 82mm |
| Wheel attachment crossbars | b = 2mm, | h = 2mm, | A= 4$mm^2$ | $L_e$ = 55mm |

(the chamfers on the rails are neglected)

The inertia moment for the rails can be calculated by [11]:

$$I = \frac{a^4}{12} - \frac{\pi r^4}{4} = 391.5mm^4 \qquad \textbf{Equation 9}$$

where r is the radius of the hole and a is the side length

The inertia moment of a rectangular section (main crossbar) can be calculated by:

$$I = \frac{bh^3}{12} = 16mm^4 \qquad \textbf{Equation 10}$$

where b and h are the length and width of the section

The inertia moment of a square section (attachment wheel crossbar) can be calculated by :

$$I = \frac{bh^3}{12} = 1.\bar{3}mm^4 \qquad \textbf{Equation 11}$$

where b and h are the length and width of the section

Using the previous equation we obtain the following critical stresses:

Rail: $\sigma_{cr}$ = **718.5MPa**

Crossbar: $\sigma_{cr}$ = **140.9MPa**

Wheel attachment crossbar: **78.3MPa**

## K.3 Bending of flat plates

The main requirement about the stiffness of the composite panels is that the external plates should not enter in contact with internal components during launch. At the same time, the composite panels should be enough stiff to guarantee that the solar cells remain undamaged during launch.

The three points flexural tests have shown that the solar cells are passably flexible if the constraints are uniform (see §7.5). The driven requirement about the stiffness is the gap between the external composite panels and internal components. This gap is set to 1mm. It means that the composite panels can have a maximal deflection of 1mm

The following equation process was used to estimate the maximal deflection as well as maximum bending stress of the composite panels according to the environment described in Appendix B. The equations are coming from [12].

The study of bending is separated in two cases, depending of the type of supports of the flat plate. In our case, the support is between the both options described below.

### K.3.1 Case A

Shape and supports: Rectangular plate; two long edges simply supported, two short edges fixed

Loading: Uniform over entire plate

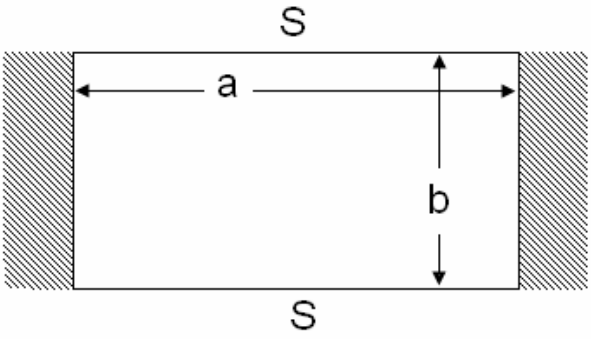


**Figure 87 Flat plate with straight boundaries, case A.**

**Table 23 Case A: factors α and β in accordance with a and b.**

| a/b | 1.0 | 1.2 |
|---|---|---|
| β | 0.4182 | 0.5208 |
| α | 0.021 | 0.0349 |

a = 100 mm — length

b = 82 mm — width

t = 0.8 mm — thickness

E = 103.6 GPa — Young's modulus of composite panel

G = 10 g = 98 m/s$^2$ — max acceleration (with FOS of 1.25 including)

ϱ = 1720 kg/m$^3$ — Density

$$q = G \cdot \frac{\rho abt}{ab} = G \cdot \rho \cdot t$$ — Uniform load

$$\sigma_{\max} = \frac{-\beta q b^2}{t^2} = \frac{-\beta \cdot \rho \cdot b^2}{t} = -7.53kPa$$ (at center of short edges)

$$y_{\max} = \frac{-\alpha q b^4}{Et^3} = 4\mu m$$ (at center)

## K.3.2 Case B

Shape and supports: Rectangular plate; all edges fixed

Loading: Uniform over entire plate

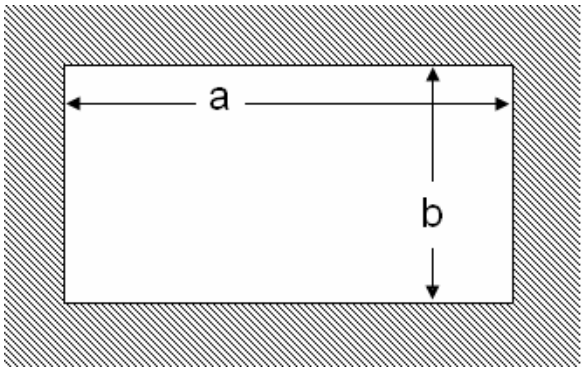


**Figure 88 Flat plate with straight boundaries, case B.**

**Table 24 Case B: factors α and β in accordance with a and b.**

| a/b | 1.0 | 1.2 |
|---|---|---|
| $\beta_1$ | 0.3078 | 0.3834 |
| $\beta_2$ | 0.1386 | 0.1794 |
| α | 0.0138 | 0.0188 |

a = 100 mm — length

b = 82 mm — width

t = 0.8 mm — thickness

E = 103.6 GPa — Young's modulus of composite panel

G = 10 g = 98 m/s$^2$ — max acceleration (with FOS of 1.25 including)

ϱ = 1720 kg/m$^3$ — Density

$$q = G \cdot \frac{\rho abt}{ab} = G \cdot \rho \cdot t$$ — uniform load

$$\sigma_{\max} = \frac{-\beta_1 q b^2}{t^2} = \frac{-\beta_1 \cdot \rho \cdot b^2}{t} = -5.54kPa$$ — maximal bending stress (at center of long edges)

$$\sigma = \frac{\beta_2 q b^2}{t^2} = \frac{\beta_2 \cdot \rho \cdot b^2}{t} = 2.59kPa$$ — bending stress (at center)

$$y_{\max} = \frac{-\alpha q b^4}{Et^3} = 2.1\mu m$$ — maximal deflection (at center)

### K.3.3 Results

As we can see, the deflections as well as the bending stresses are very small in the both cases, and will probably not be a problem for the solar cells.

A FEA of the interaction of composite panels with aluminum frame shall be performed during the next semester to validate these values.

# Appendix L Finite Elements Analysis

## L.1 Vertical static worst case

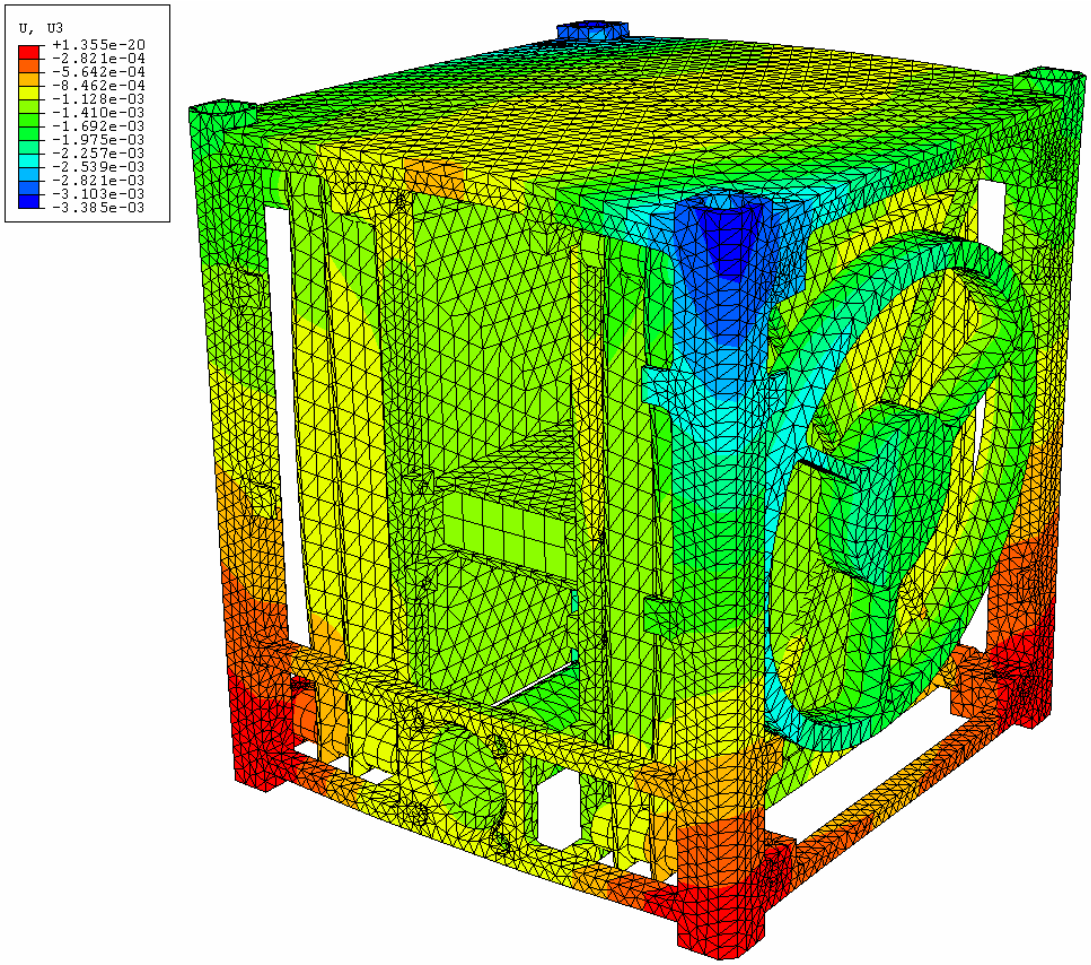


**Figure 89 Displacement in axis 3 in the vertical worst case.**

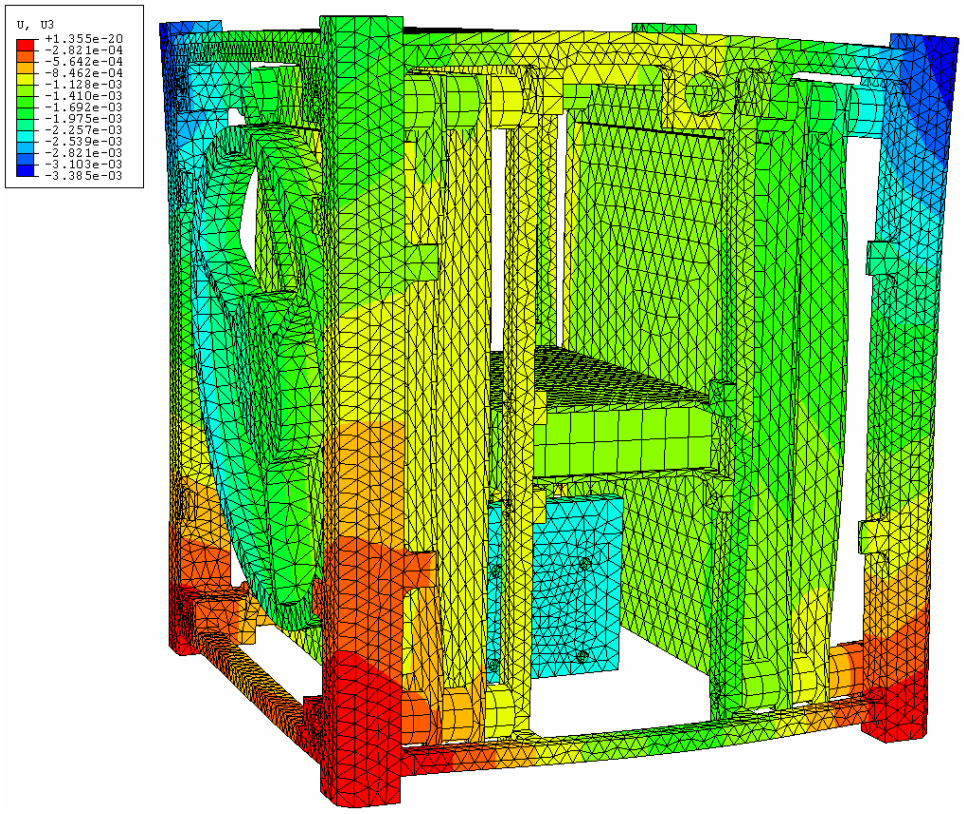


**Figure 90 Displacement in axis 3 in the vertical worst case.**

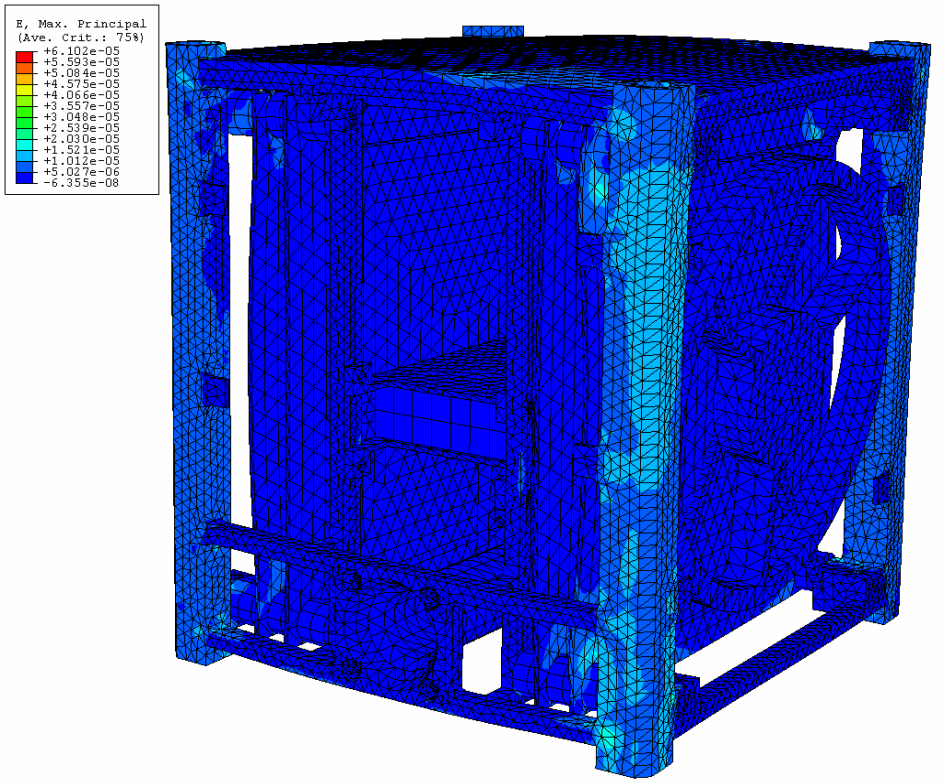


**Figure 91 Strain in the vertical worst case.**

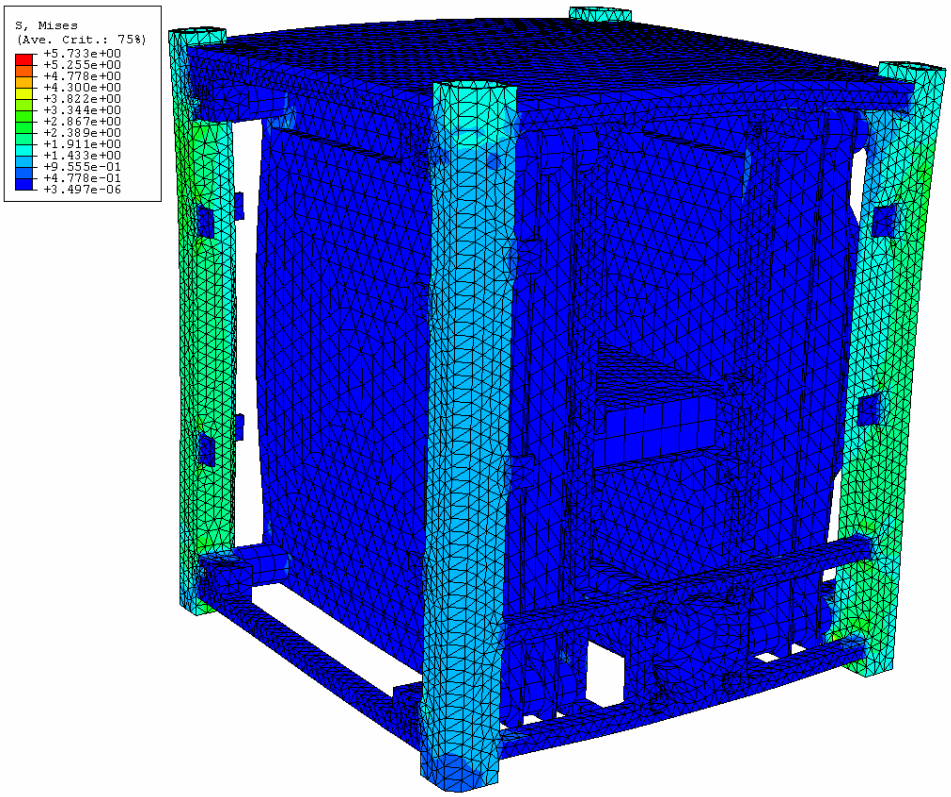


**Figure 92 Von Mises in the vertical worst case.**

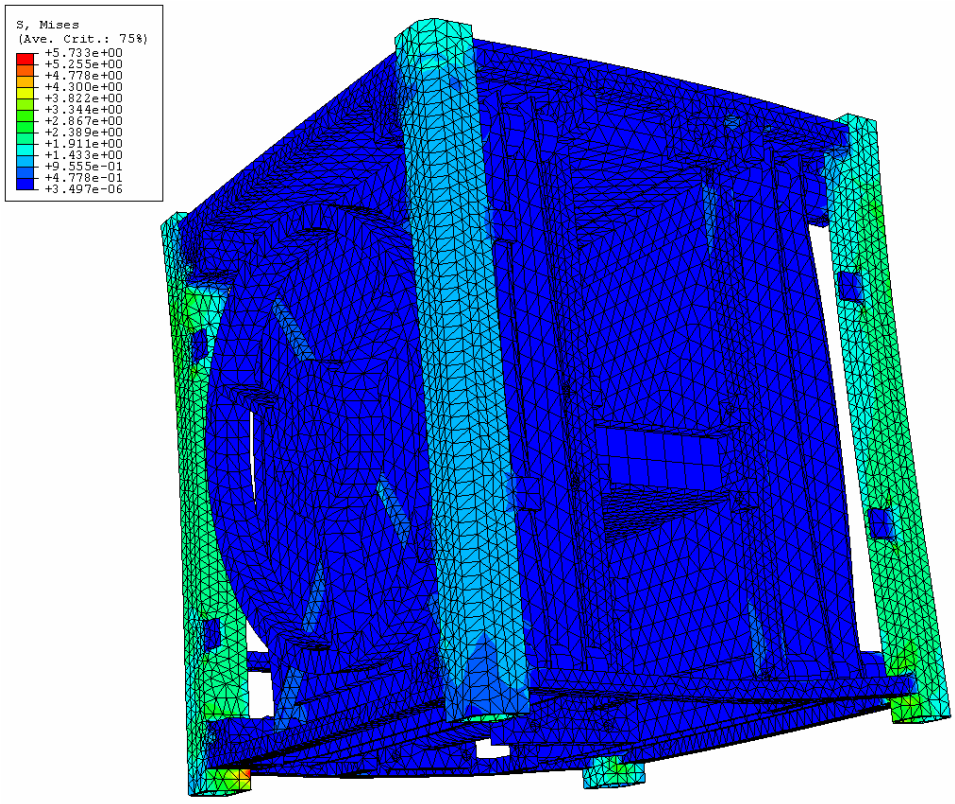


**Figure 93 Von Mises in the vertical worst case.**

## L.2 X-horizontal static worst case

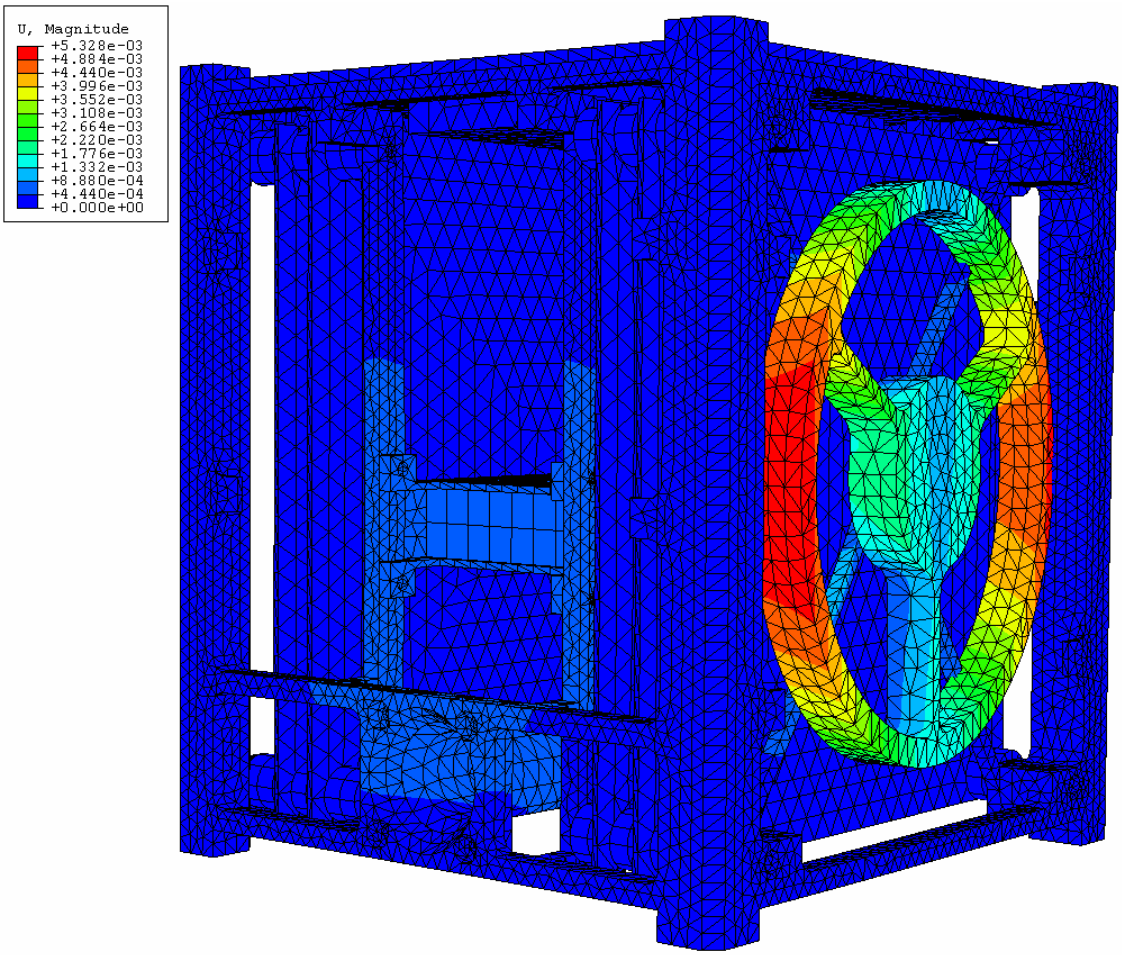


**Figure 94** Displacement in the X-horizontal worst case.

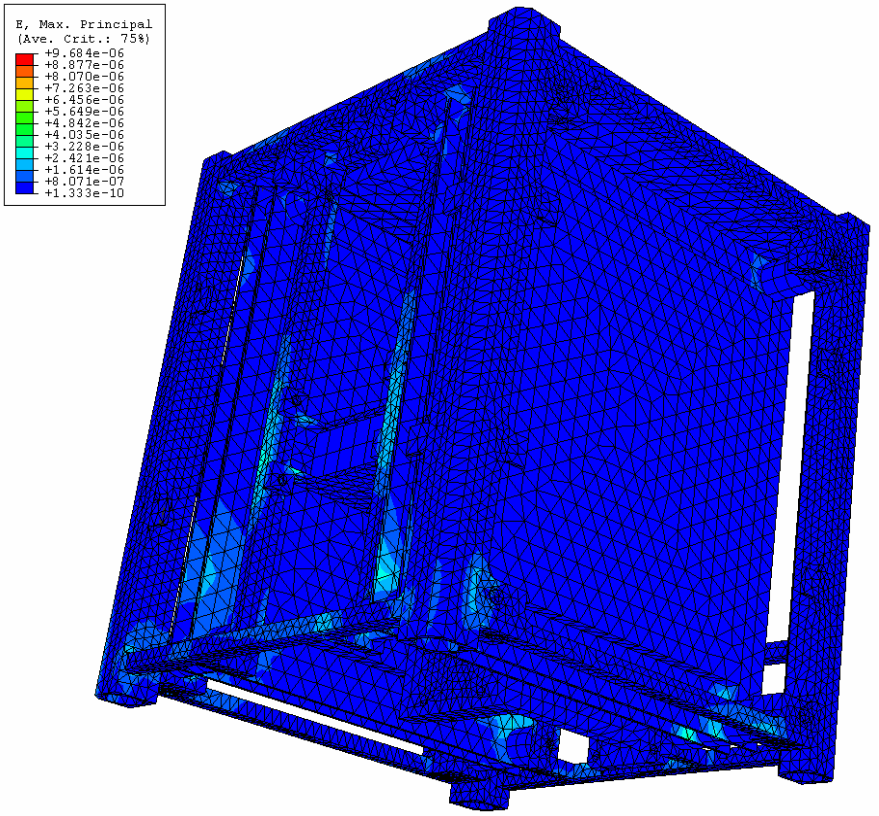


**Figure 95 Strain in the X-horizontal worst case.**

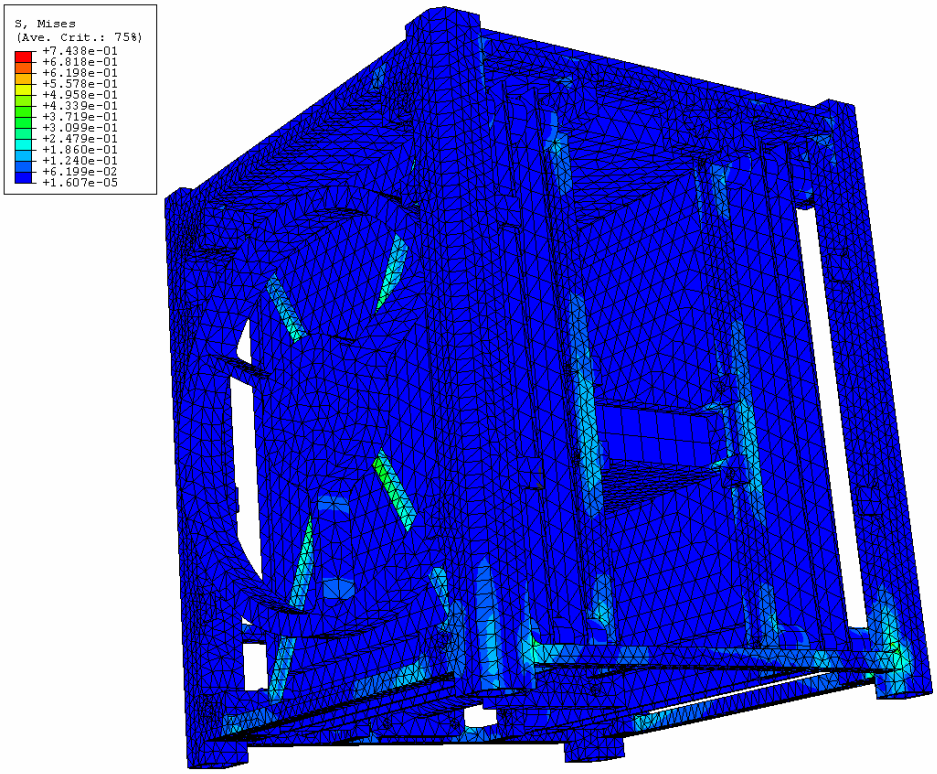


**Figure 96 Von Mises in the X-horizontal worst case.**

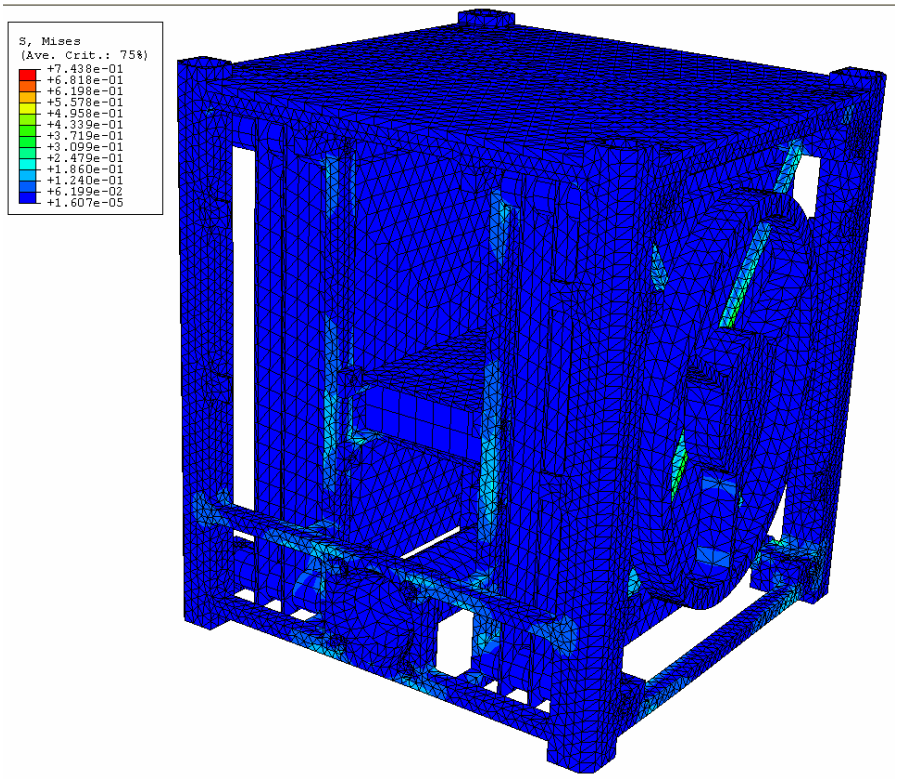


**Figure 97 Von Mises in the X-horizontal worst case.**

## L.3 Y-horizontal static worst case

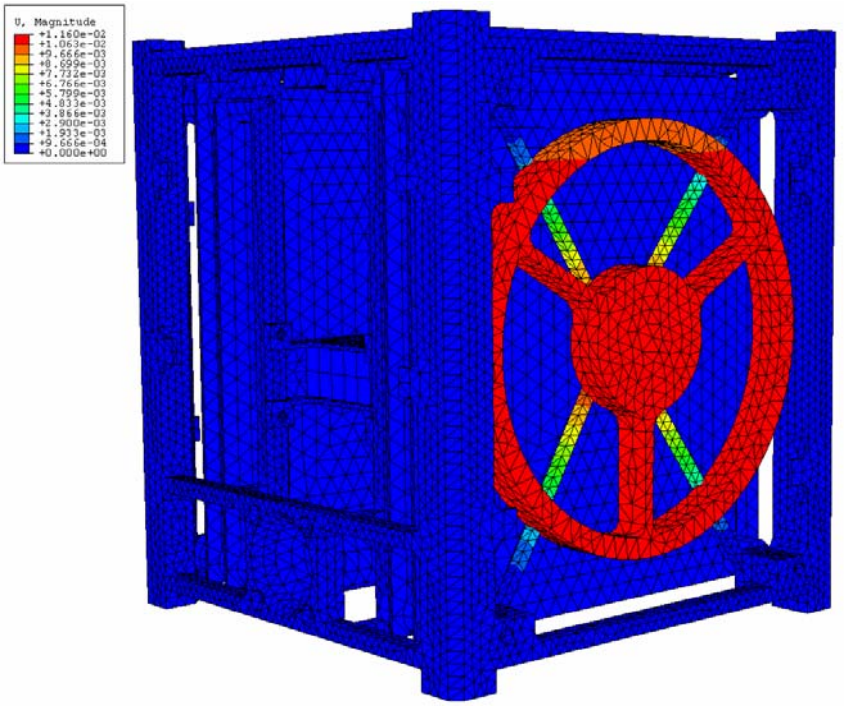


**Figure 98 Displacement in the Y-horizontal worst case.**

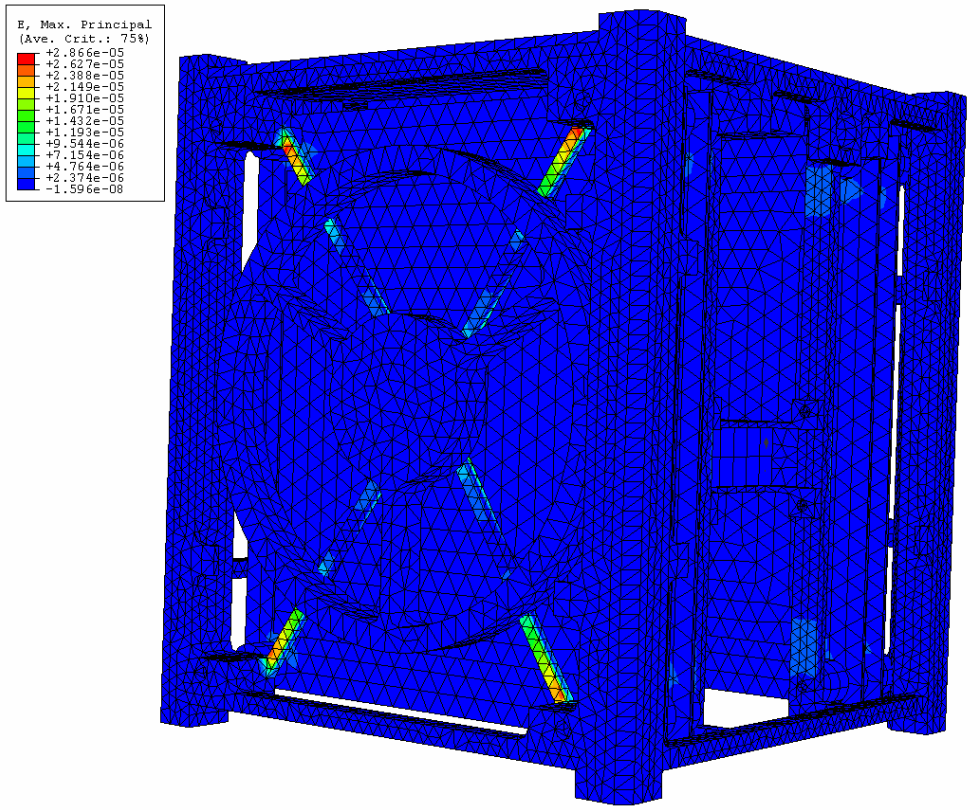


**Figure 99 Strain in the Y-horizontal worst case.**

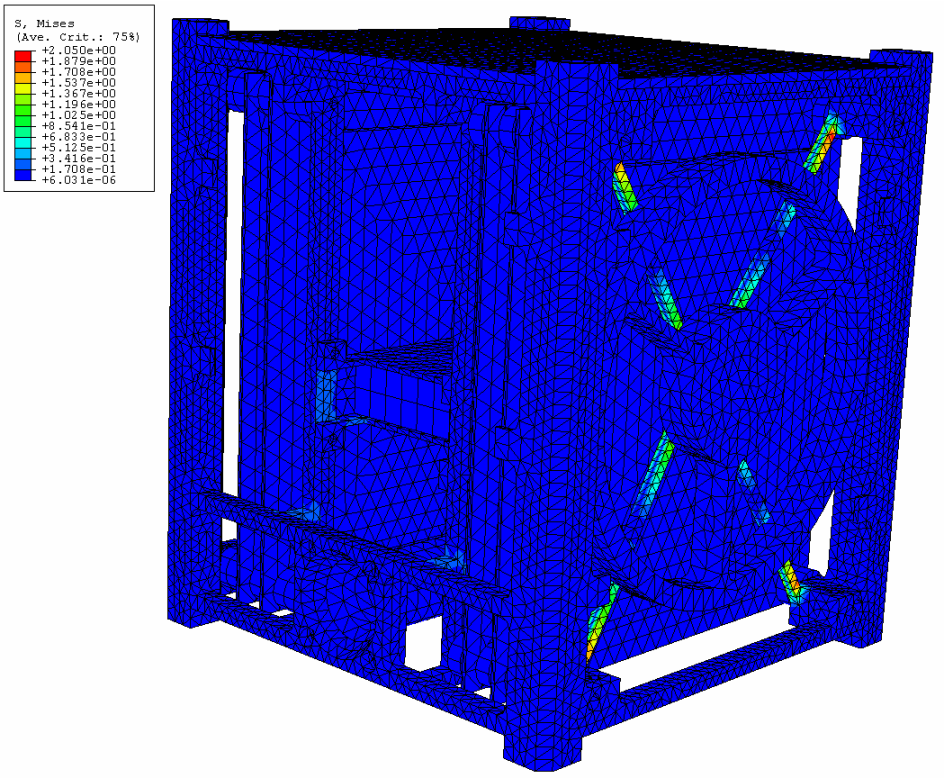


**Figure 100 N.4 Figure 73 Von Mises in the Y-horizontal worst case.**

## L.4 Natural frequencies

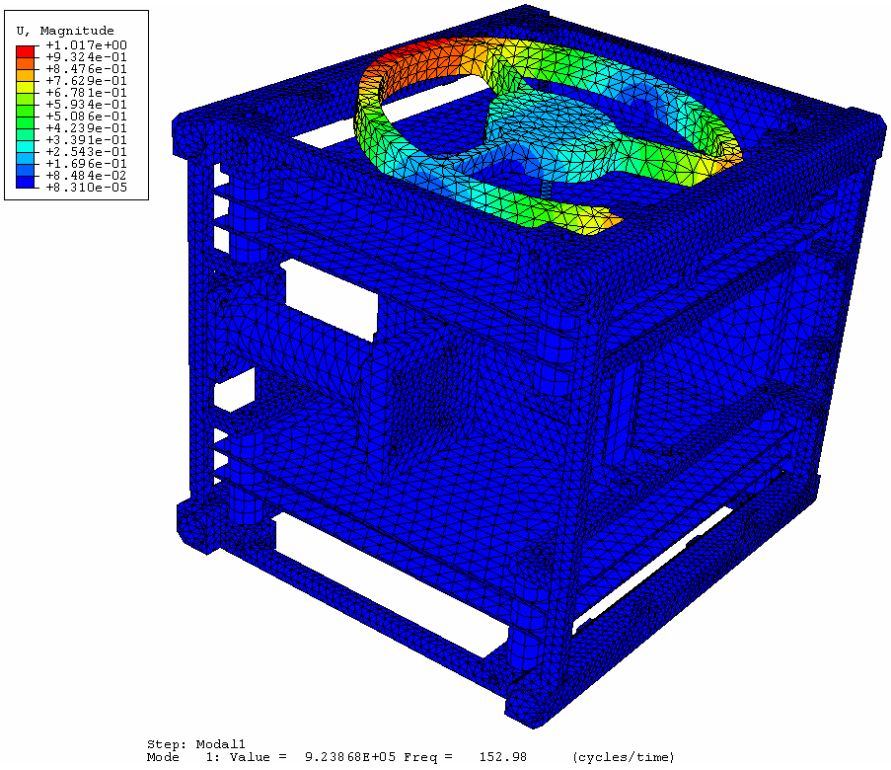


**Figure 101 1st mode of vibration of the model, 153 Hz.**

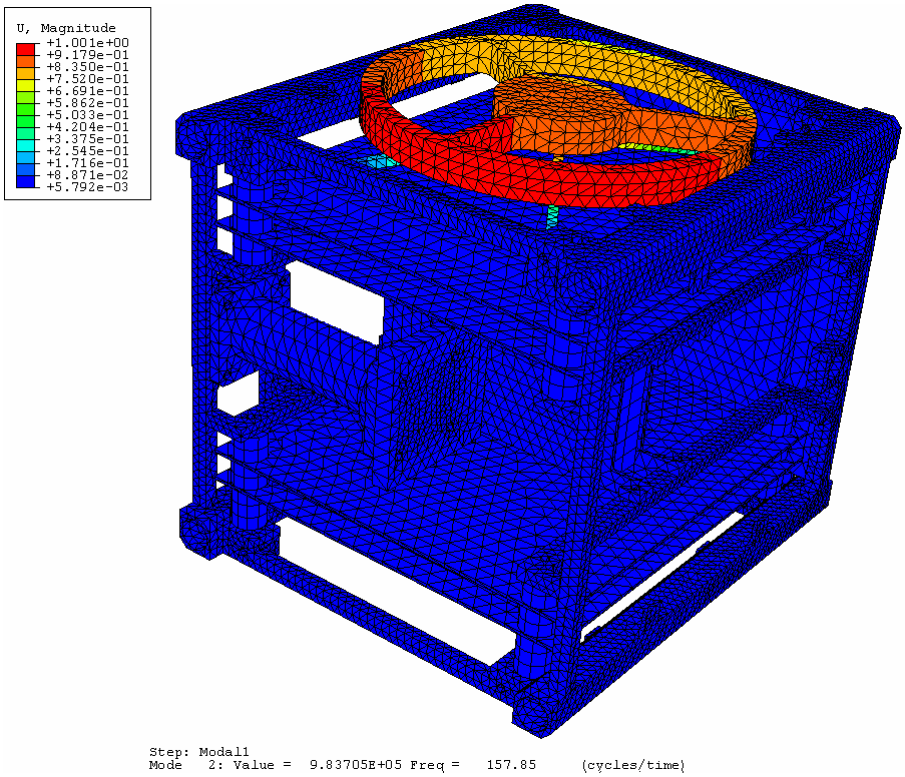


**Figure 102 2nd mode of vibration of the model, 158 Hz.**

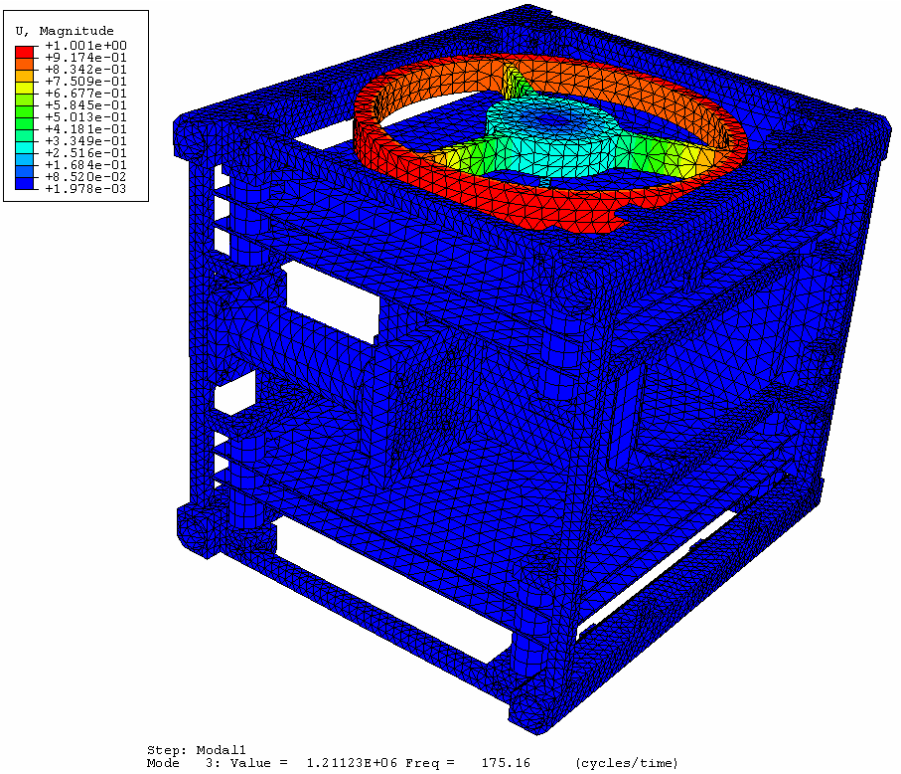


**Figure 103 3rd mode of vibration of the model, 175 Hz.**

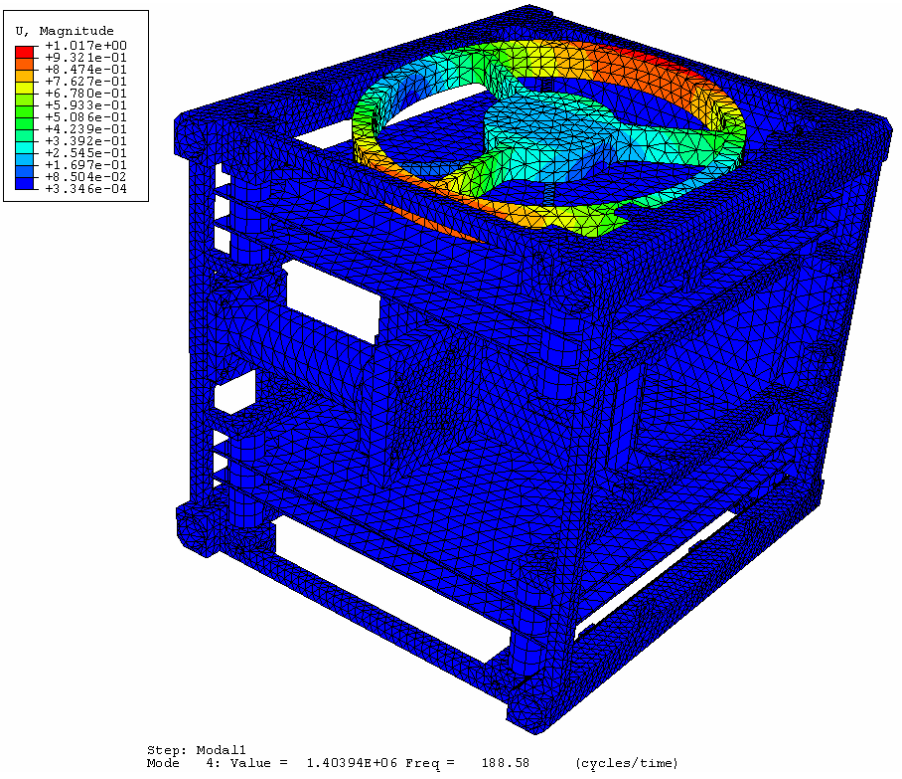


**Figure 104 4th mode of vibration of the model, 189 Hz.**

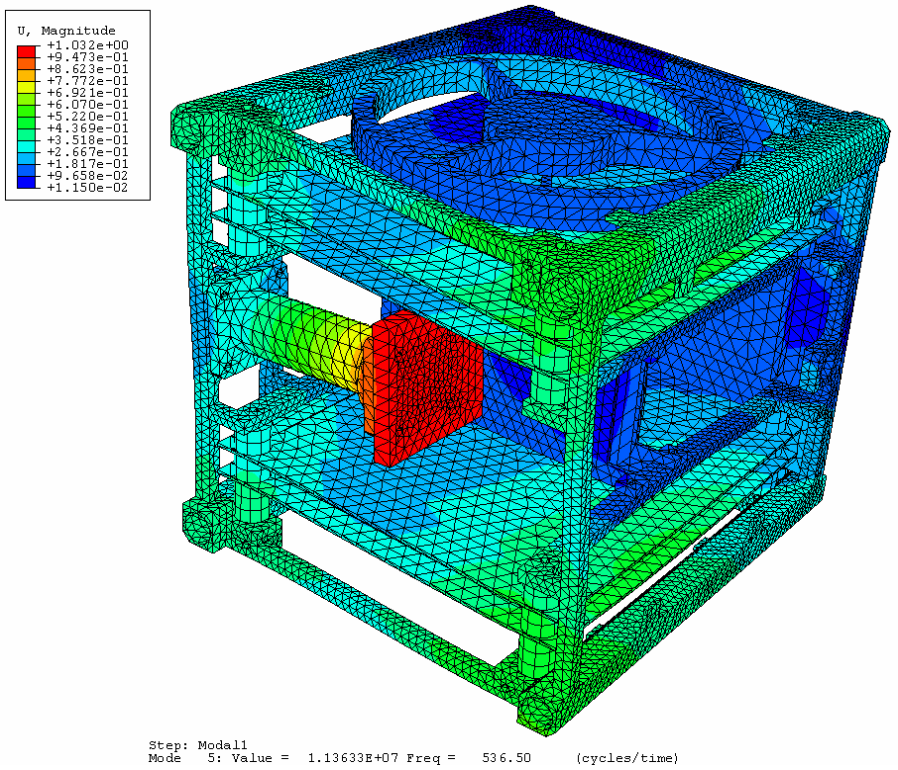


**Figure 105 5th mode of vibration of the model, 537 Hz.**

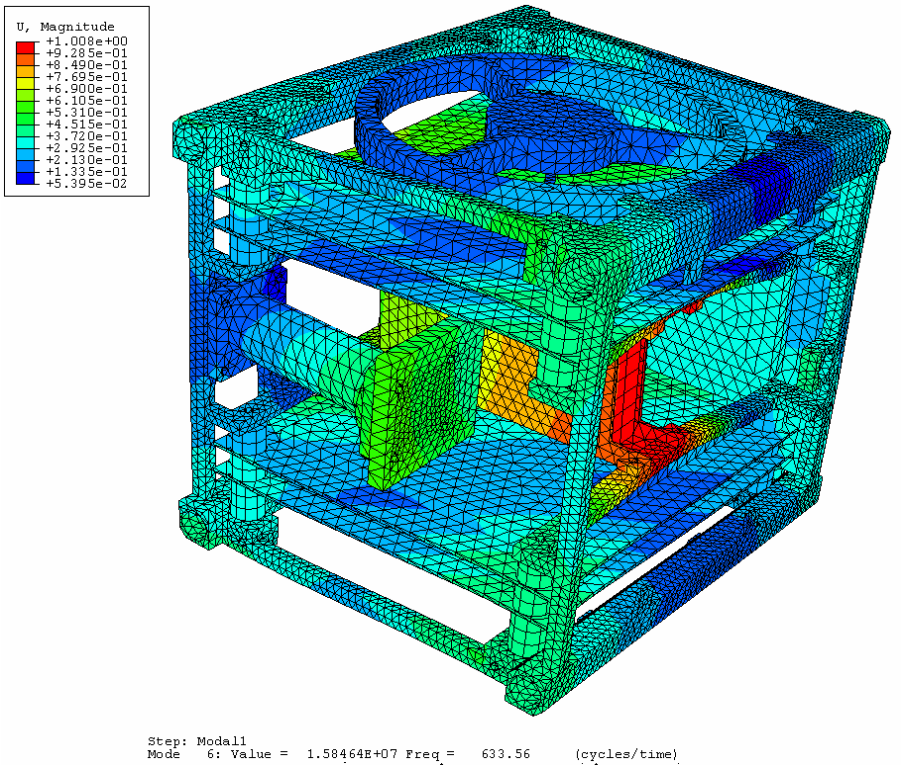


**Figure 106 6th mode of vibration of the model, 634 Hz.**

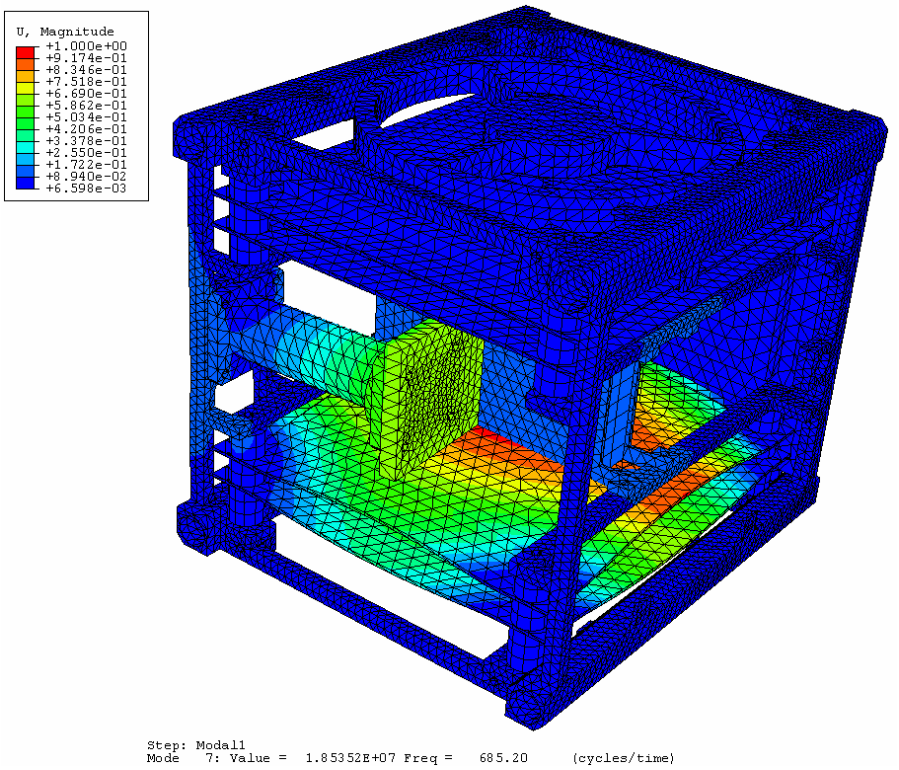


**Figure 107 7th mode of vibration of the model, 685 Hz.**

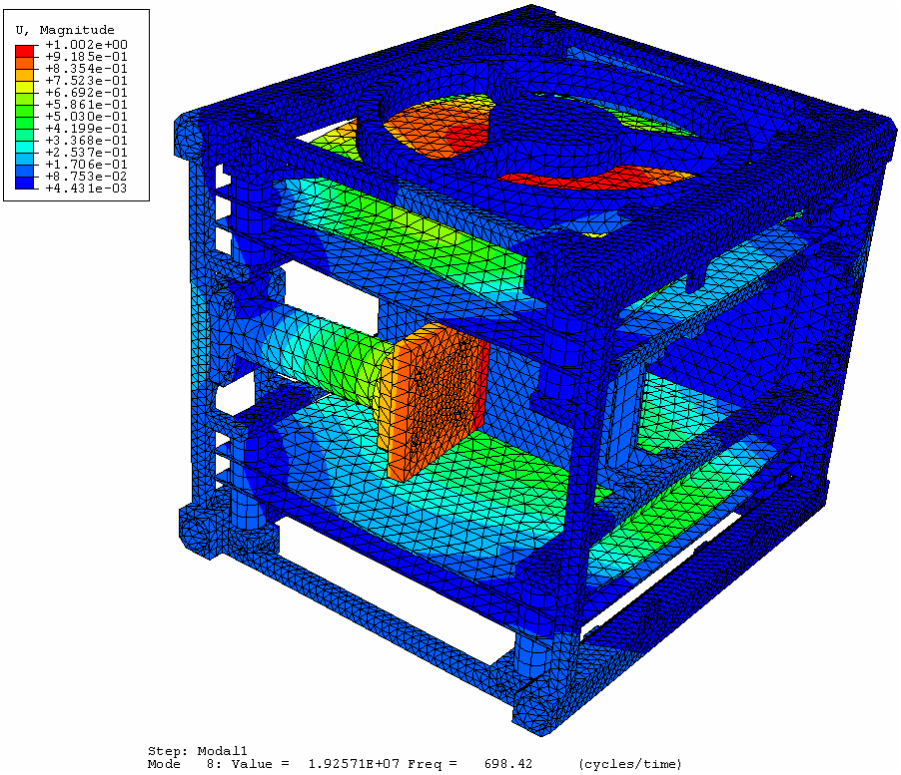


**Figure 108 8th mode of vibration of the model, 698 Hz.**

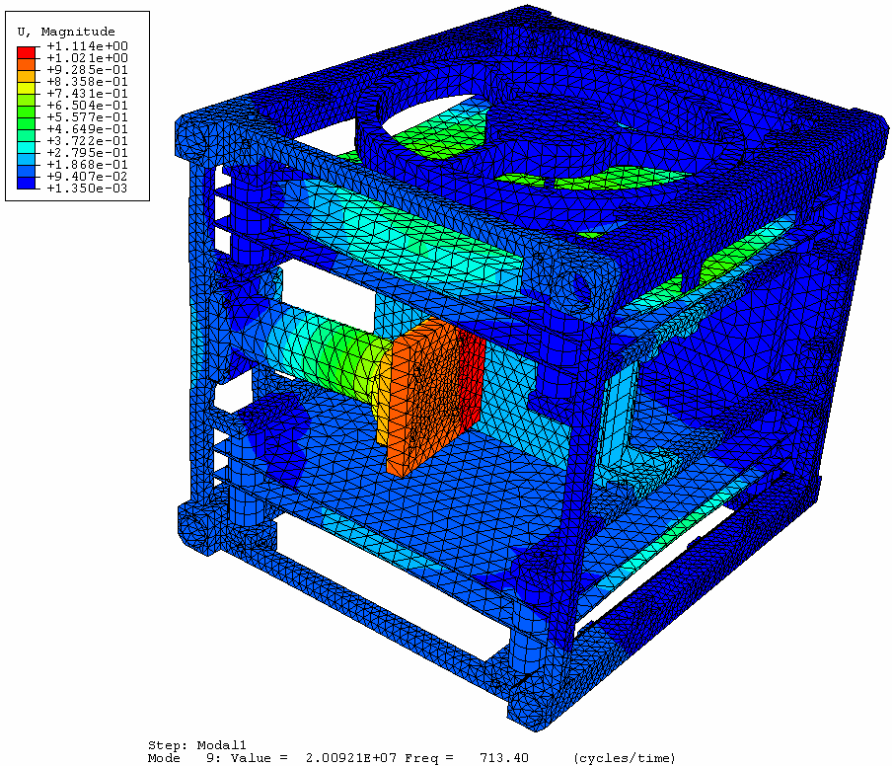


**Figure 109 9th mode of vibration of the model, 713 Hz.**

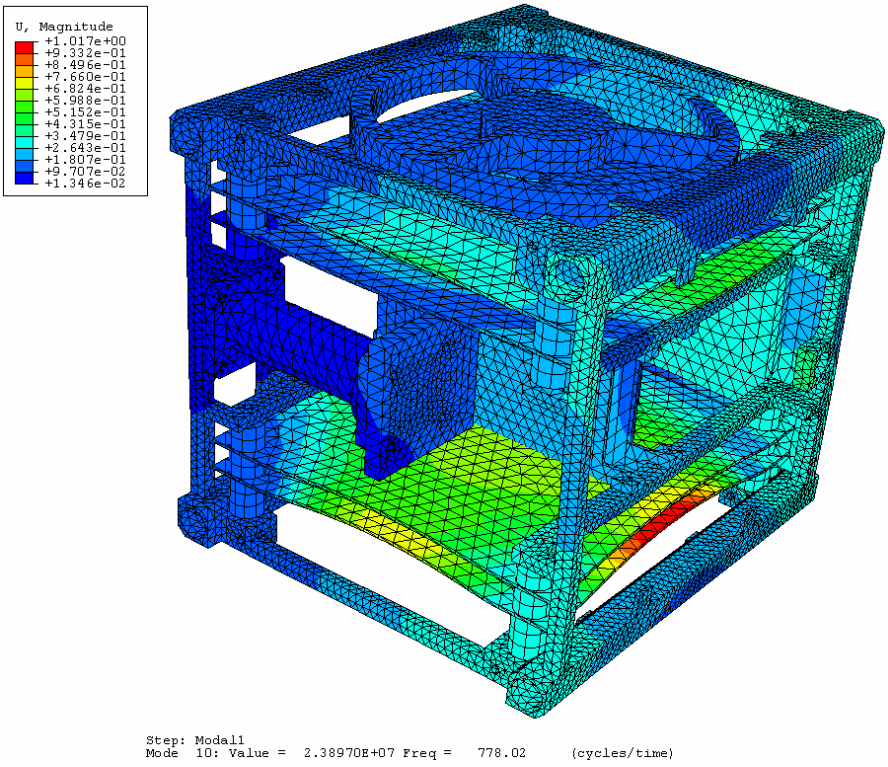


**Figure 110 10th mode of vibration of the model, 778 Hz.**

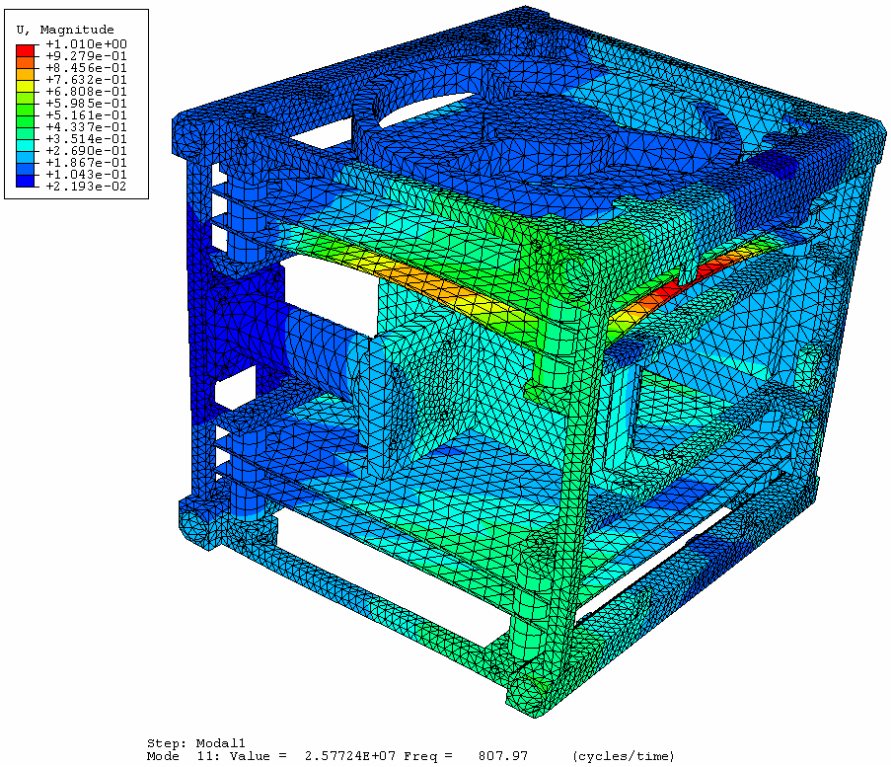


**Figure 111 11th mode of vibration of the model, 808 Hz.**

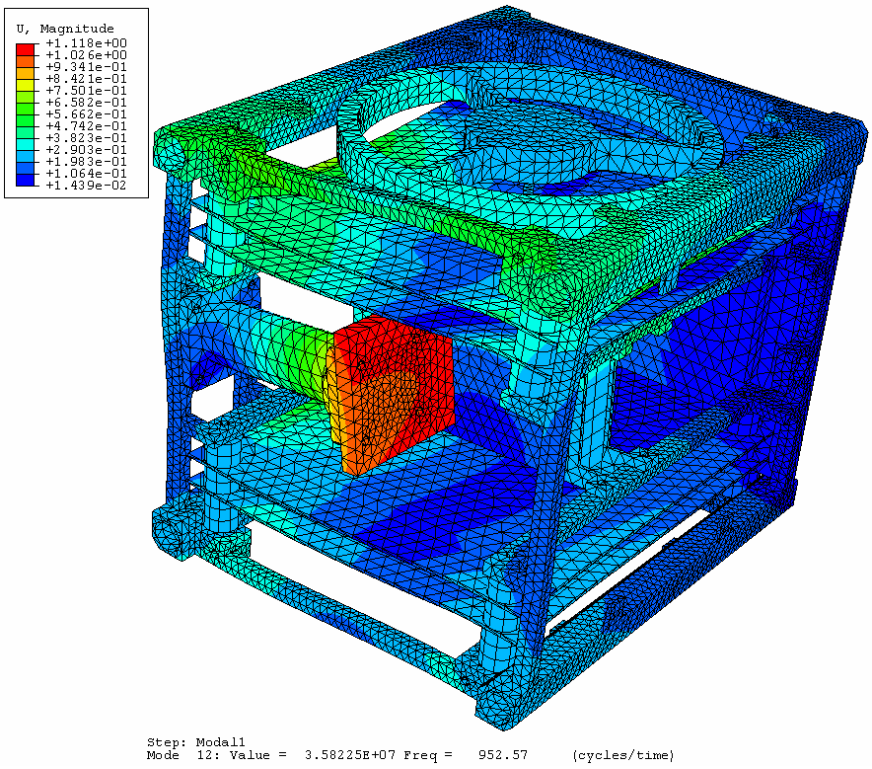


**Figure 112 12th mode of vibration of the model, 953 Hz.**

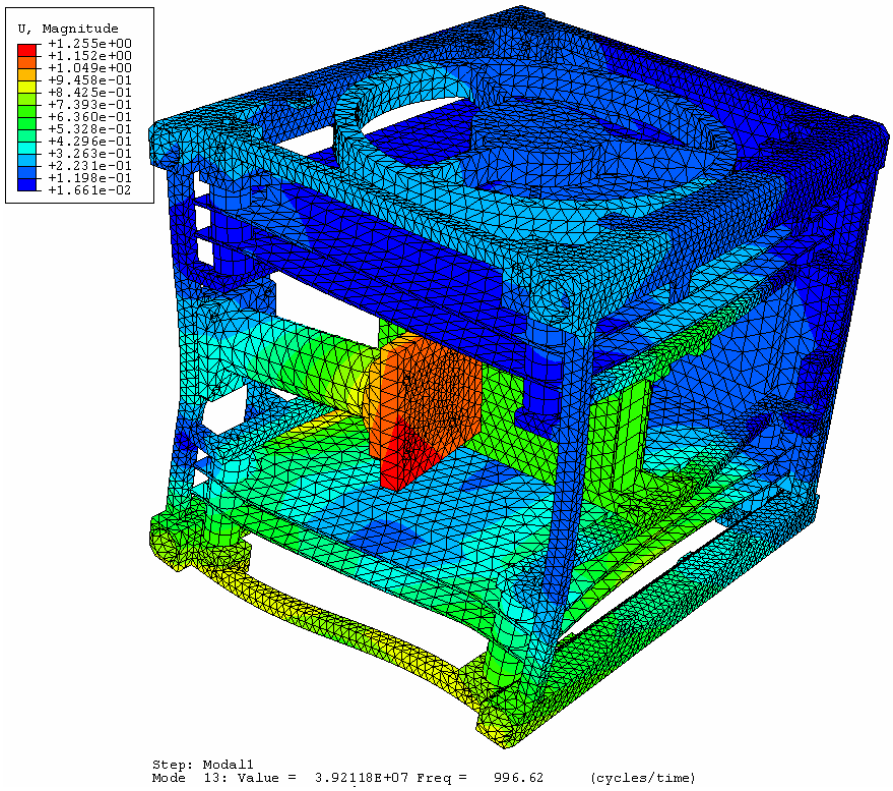


**Figure 113 13th mode of vibration of the model, 996 Hz.**

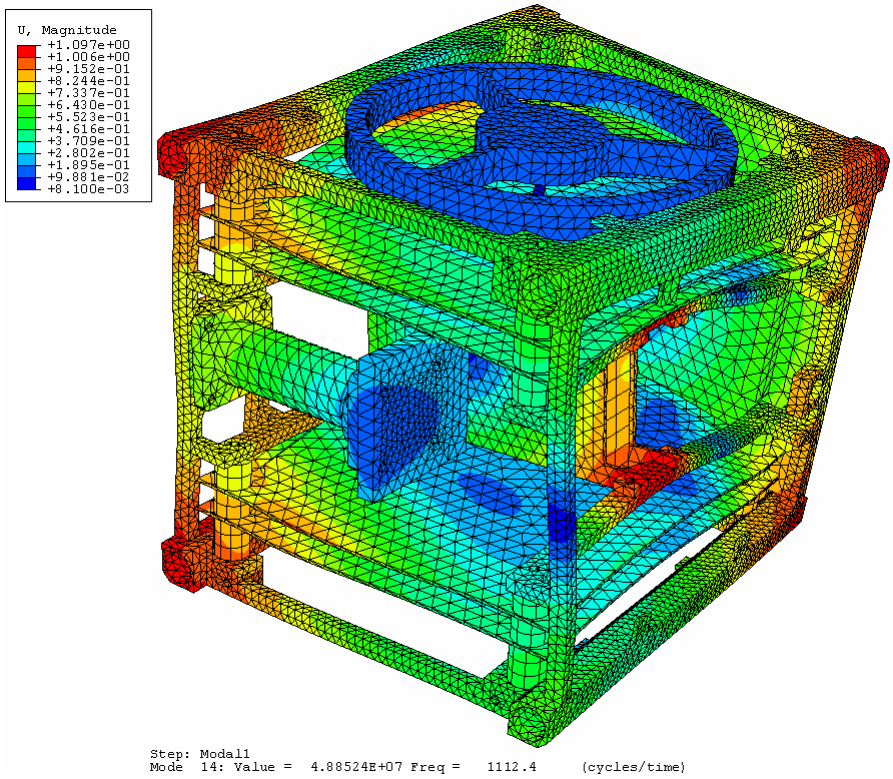


**Figure 114 14th mode of vibration of the model, 1112 Hz.**

# Appendix M Test procedure

## M.1 Physical properties

### M.1.1 Test objectives

The purpose of physical properties measurements is to confirm the satellite physical characteristics, like external dimensions.

The goal of the physical properties test is to verify the requirement 4_STRUCT_45_01.

### M.1.2 Identification and configuration of the test article

The test article is the structural model of the satellite, i.e. the monobloc frame, five composite panels glued onto the frame, a simplified payload frame with a dummy headboard at the end, the battery box with 2 dummy batteries inside, a dummy wheel subassembly, 24 spacers, 2 dummy magneto-torquers, 4 dummy PCBs and a dummy motherboard.

### M.1.3 Test set-up identification

The instrument used to control the physical properties is a slide caliper with an accuracy of 0.01 mm.

### M.1.4 Test conditions

The dimensions to verify are listed in Figure 115 in categories width, height and diagonal.

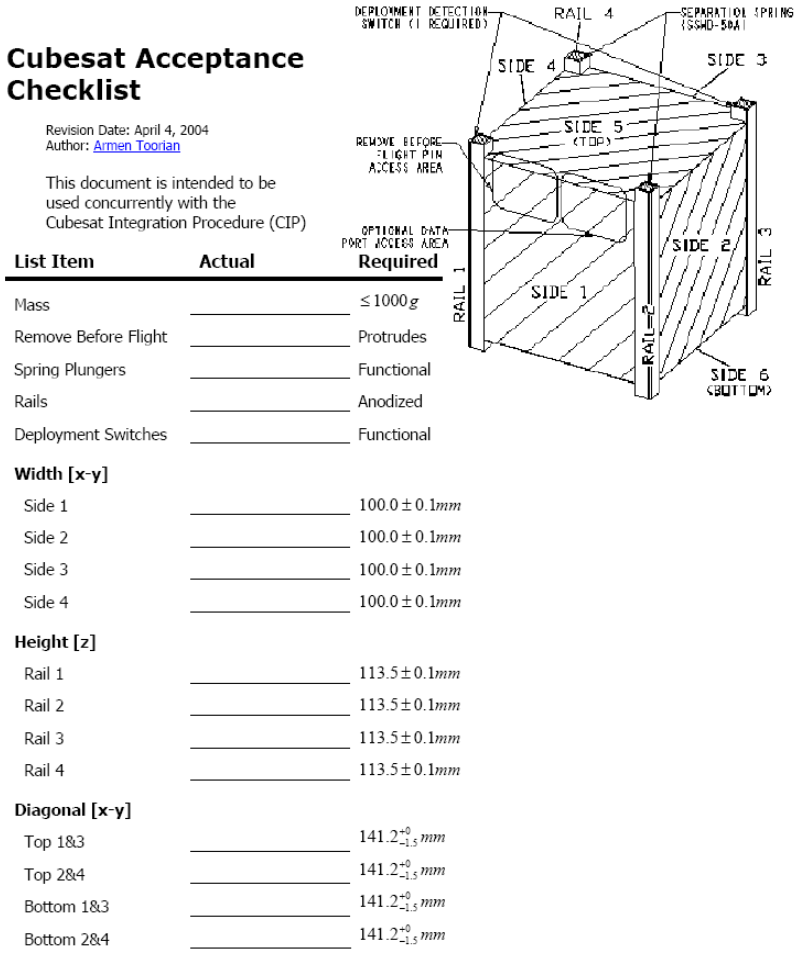

**Cubesat Acceptance Checklist**

Revision Date: April 4, 2004
Author: Armen Toorian

This document is intended to be used concurrently with the Cubesat Integration Procedure (CIP)

| List Item | Actual | Required |
|---|---|---|
| Mass | _____ | $\leq 1000 g$ |
| Remove Before Flight | _____ | Protrudes |
| Spring Plungers | _____ | Functional |
| Rails | _____ | Anodized |
| Deployment Switches | _____ | Functional |
| **Width [x-y]** | | |
| Side 1 | _____ | $100.0 \pm 0.1 mm$ |
| Side 2 | _____ | $100.0 \pm 0.1 mm$ |
| Side 3 | _____ | $100.0 \pm 0.1 mm$ |
| Side 4 | _____ | $100.0 \pm 0.1 mm$ |
| **Height [z]** | | |
| Rail 1 | _____ | $113.5 \pm 0.1 mm$ |
| Rail 2 | _____ | $113.5 \pm 0.1 mm$ |
| Rail 3 | _____ | $113.5 \pm 0.1 mm$ |
| Rail 4 | _____ | $113.5 \pm 0.1 mm$ |
| **Diagonal [x-y]** | | |
| Top 1&3 | _____ | $141.2^{+0}_{-1.5} mm$ |
| Top 2&4 | _____ | $141.2^{+0}_{-1.5} mm$ |
| Bottom 1&3 | _____ | $141.2^{+0}_{-1.5} mm$ |
| Bottom 2&4 | _____ | $141.2^{+0}_{-1.5} mm$ |



**Figure 115 CubeSat acceptance checklist from CalPoly.**

# M.2 Sinusoidal vibration test qualification

## M.2.1 Test objectives

The purpose of the sinusoidal vibration testing is to demonstrate the ability of the satellite to withstand excitations of the launcher increased by a qualification factor.

The requirement 4_STRUCT_52_03 shall be verified.

## M.2.2 Identification and configuration of the test article

The configuration of the test article is the same as in Appendix M.1.2.

## M.2.3 Test set-up identification

For this test, the facilities are:

a Test-POD
an adapter
a shaker
accelerometers
charge amplifiers
data acquisition card
2 PCs

The Test Pod [13] in Figure 116 is to be used by CubeSat developers as an environmental simulation of the P-Pod deployer; this will allow validation of the structural integrity of CubeSats under launch loads. The Test Pod interior is designed to simulate the environment inside the P-Pod deployer.

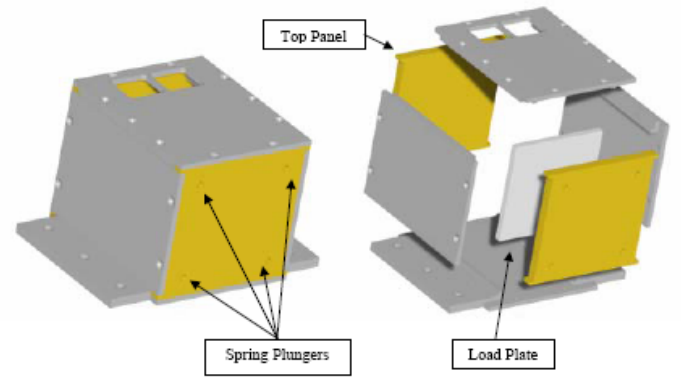


Figure 116 View of a Test POD.

The adapter consists of two brackets and two flat plates with attachment points for the Test-POD. These various parts are attached together with screws. Figure 117 shows the Test-POD attached to the adapter. There are three different configurations of the adapter, depending of the tested axis. For the X and Y axis, only the horizontal plate is used. To test the Z axis, both brackets and vertical plate are used in order to align the desired axis with the shaker displacement axis.

**Figure 117 Adapter with Test-POD.**

The shaker is a model of the mark RMS (see Figure 118). The type of shaker is a voice coil, i.e. a construction similar to common loudspeakers to convert electrical current flow into mechanical force over the widest frequency range with minimal spectral distortion of the input waveform. The maximum travel is 25mm, maximal force is 5.8kN, frequency range of 3 to 3 kHz

**Figure 118 Electrodynamic shakers.**

Accelerometers are used for two cases; on one hand to control the shaker (feedback loop), on the other hand to acquire data of acceleration on some components during test. The type of accelerometer is piezoelectric subminiature charge Accelerometer, Type 4374 from Brüel&Kjaer. Figure 119 shows an accelerometer, these physical properties are: diameter of 5mm, height of 6.7mm, and weight of 0.75 gram.

**Figure 119 Accelerometer Type 4374 from Brüel&Kjaer.**

One charge amplifier per accelerometer is used to converts an input charge (stored on a capacitor, or significantly capacitive transducer) to a voltage output. These amplifiers are connected to a data acquisition card. Two PCs are used, one for the control of the shaker, the other for the data acquisition.

## M.2.4 Test conditions

The structural subsystem shall be able to sustain the sinusoidal vibration qualification test for the frequency range specified in Figure 7. Vibrations shall be applied in three mutually orthogonal directions, one being parallel to the thrust axis.

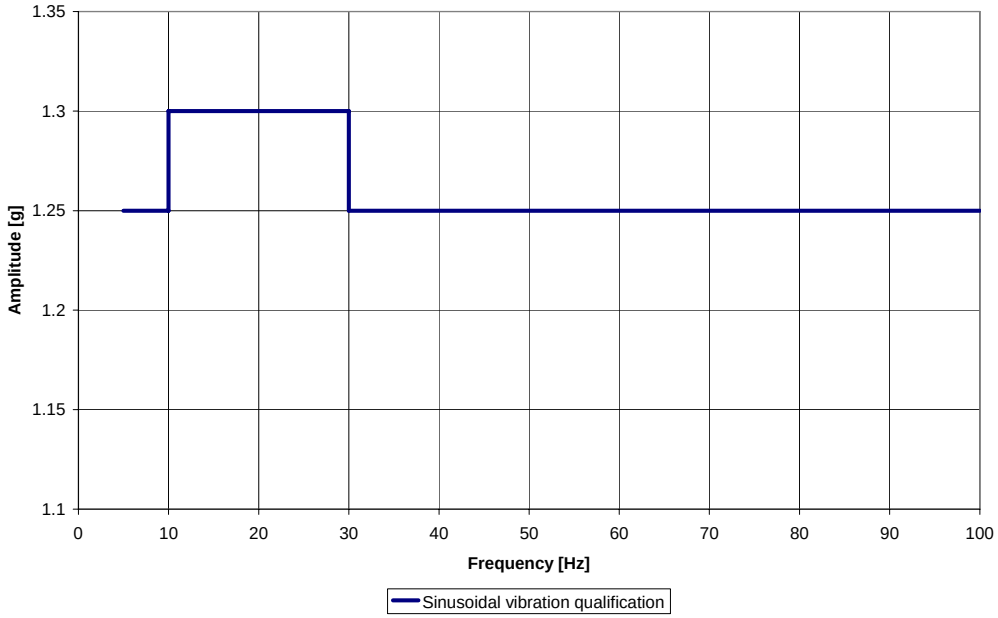


**Figure 120 Amplitude of the sinusoidal vibtation qualification test.**

Sinusoidal excitations shall be applied at the base of the mounting adapter, and shall be swept through at a sweep rate of 2 octaves/min.

The variation of transmissibility between test item mounting points shall not exceed a factor of 3 dB between 5 Hz and 100 Hz.

Due to limited capabilities of the shaker, the lower possible frequency for a 1.25 g of sinusoidal excitation is 6 Hz, and not 5 Hz as specified in the requirement.

### M.2.5 Step by step instruction for operation

The following is a suggested test sequence for each axis to be tested:

1. Mount accelerometers on surface perpendicular to the shaker displacement
2. Insert satellite into the Test-POD. Add the top panel from the test pod assembly
3. Setup Test Pod so that the X axis of the satellite is the test axis of the shake table.
4. Be sure to check all fasteners and data lines between tests to ensure a safe operating environment and accurate results
5. Input sine-sweep parameters for X-axis into controller and run
6. Alignment check and visual inspection (see below)
7. Repeat steps 1 through 6 with the satellite/Test-POD oriented to in a way to have vibration along the satellite Y-axis and Z-axis

The structural qualification tests detailed above shall be complemented with alignment checks and visual inspections between each axis test. Ensure that all parts of the satellite are intact and deployables are properly secured. Below is a list of things to look for:

- Make sure dimensions have not changed by measuring all lengths/widths/heights and diagonal distances.
- Check all solar panels to ensure that they are not protruding beyond the specified allowance described in the dimensional checklist.
- Examine all deployables. Ensure that they are firmly attached and in the dimensional tolerance described in the dimensional checklist.
- Check for sharp edges or protruding objects that could get caught.
- Check for any loose wires or dangling components.
- Check all fasteners and make sure they are still tight and staking compound is intact, if staking compound is applied.

## M.3 Random vibration test qualification

### M.3.1 Test objectives

The purpose of the random vibration testing is to demonstrate the ability of the satellite to withstand excitations of the launcher increased by a qualification factor.

The requirement 4_STRUCT_52_02 shall be verified.

### M.3.2 Identification and configuration of the test article

The configuration of the test article is the same as in Appendix M.1.2.

### M.3.3 Test set-up identification

The needed facilities are the same as the sinusoidal vibration test procedure, see Appendix M.2.3.

### M.3.4 Test conditions

The structural subsystem shall be able to sustain the random vibration qualification test for the frequency range specified in Figure 8. Random excitations shall be applied in three mutually orthogonal directions, one being parallel to the thrust axis. The test duration shall be two minutes per axis.

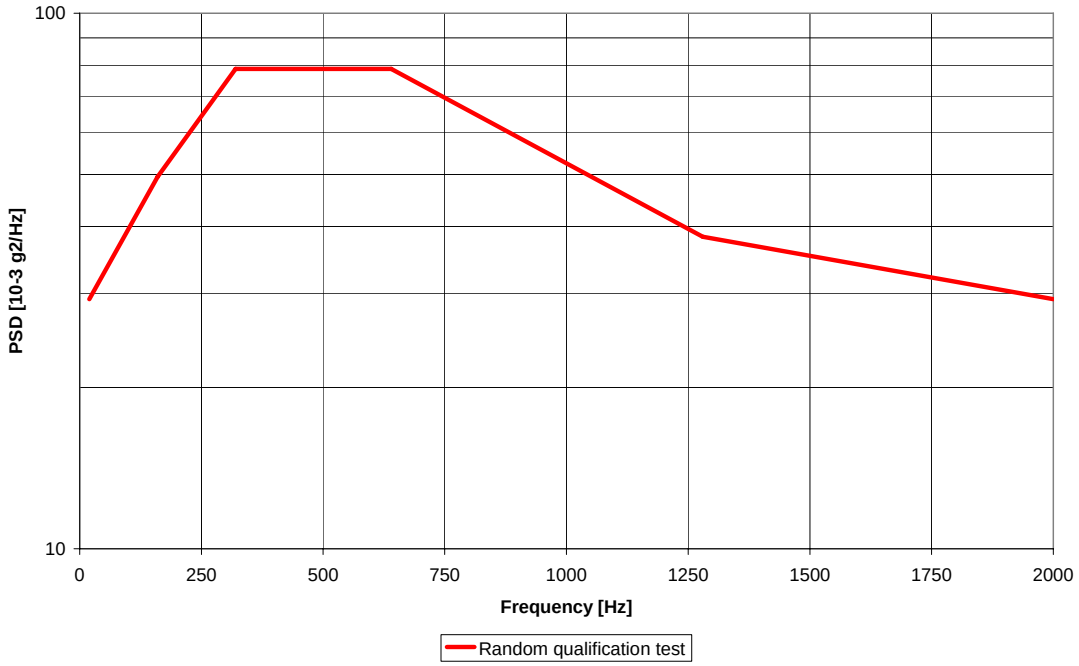


**Figure 121 PSD for qualification and acceptance.**

With Gaussian random excitation applied at the base of the adapter, the spectrum, as measured by the control accelerometer(s), shall be equalized such that the power spectral density, throughout the frequency range, lies within (-1/+3) dB of the levels specified in the qualification test specification.

### M.3.5 Step by step instruction for operation

The random vibration qualification test is as follow:

1. Mount accelerometers on surface perpendicular to the shaker displacement

2. Insert satellite into the Test-POD. Add the top panel from the test pod assembly
3. Setup Test Pod so that the Y axis is the test axis of the shake table.
4. Be sure to check all fasteners and data lines between tests to ensure a safe operating environment and accurate results
5. Input random parameters for Y-axis into controller and run
6. Alignment check and visual inspection (see below)
7. Repeat steps 1 through 6 with the satellite/Test-POD oriented to in a way to have vibration along the spacecraft X-axis and Z-axis

The structural qualification tests detailed above shall be complemented with alignment checks and visual inspections between each axis test. Ensure that all parts of the satellite are intact and deployables are properly secured. Below is a list of things to look for:

- Make sure dimensions have not changed by measuring all lengths/widths/heights and diagonal distances.
- Check all solar panels to ensure that they are not protruding beyond the specified allowance described in the dimensional checklist.
- Examine all deployables. Ensure that they are firmly attached and in the dimensional tolerance described in the dimensional checklist.
- Check for sharp edges or protruding objects that could get caught.
- Check for any loose wires or dangling components.
- Check all fasteners and make sure they are still tight and staking compound is intact, if staking compound is applied.

## M.4 Shock test qualification

### M.4.1 Test objectives

The purpose of shock testing is to demonstrate the ability of the satellite to withstand the shocks induced by the separation of the payload from the launcher, or the booster burn out.

The requirement 4_STRUCT_52_05 shall be verified.

### M.4.2 Identification and configuration of the test article

The configuration of the test article is the same as in Appendix M.1.2.

### M.4.3 Test set-up identification

TBD

## M.4.4 Test conditions

The structural subsystem shall be able to sustain the shock qualification test for the frequency range specified in Figure 10.

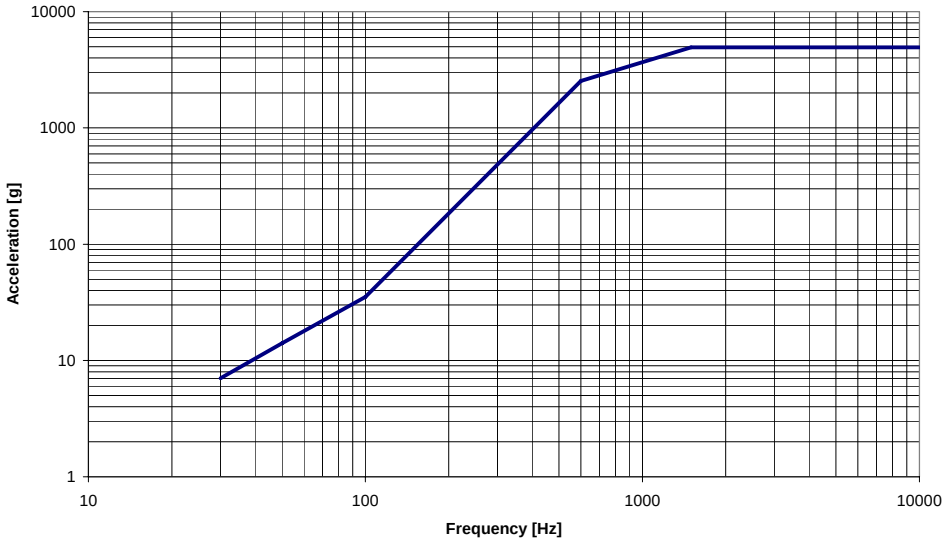


**Figure 122 Envelope acceleration shock response spectrum for the shock qualification test.**

At least three shocks shall be imposed to meet the amplitude criteria in both directions on each of the three orthogonal axes.

If a suitable test environment can be generated to satisfy the amplitude requirement in all six axial directions by a single application, that test environment shall be imposed three times.

If an imposed shock meets the amplitude requirements in only one direction of a single axis, the shock test shall be conducted a total of 18 times in order to get three valid test amplitudes in both directions of each axis.

## M.4.5 Step by step instruction for operation

TBD

The shock tests shall be complemented with alignment checks and visual inspections between each axis test. Ensure that all parts of the satellite are intact and deployables are properly secured. Below is a list of things to look for:

- Make sure dimensions have not changed by measuring all lengths/widths/heights and diagonal distances.
- Check all solar panels to ensure that they are not protruding beyond the specified allowance described in the dimensional checklist.

- Examine all deployables. Ensure that they are firmly attached and in the dimensional tolerance described in the dimensional checklist.
- Check for sharp edges or protruding objects that could get caught.
- Check for any loose wires or dangling components.
- Check all fasteners and make sure they are still tight and staking compound is intact, if staking compound is applied.

# M.5 Three points flexural test of solar cell

## M.5.1 Test objectives

Test of the mechanical resistance of the solar cells are performed in order to determine their bending resistance. This will permit to determine maximal allowable bending/vibration amplitude of the composite panels during launch that will not endanger the solar cells.

The three points bending flexural test provides values for the modulus of elasticity in bending $E_B$, flexural stress $\sigma_f$, flexural strain $\varepsilon_f$ and the flexural stress-strain response of the material.

## M.5.2 Identification and configuration of the test article

The test article consists of solar cells RWE3G-ID2/150-8040, see Figure 123.

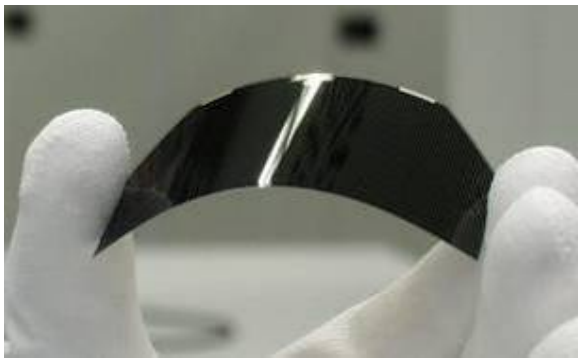

**Figure 123 RWE triple junction solar cells.**

The Young's modulus given by the manufacturer is 7.5 GPa. The thickness of the solar cell is 0.16mm.

## M.5.3 Test set-up identification

For this test, the facilities are: solar cells

Three points bending support

a CNC milling machine

The three points support is stated in Figure 124. It consists of two main parts, one with two cylindrical contacts, and the other with one cylindrical contact.

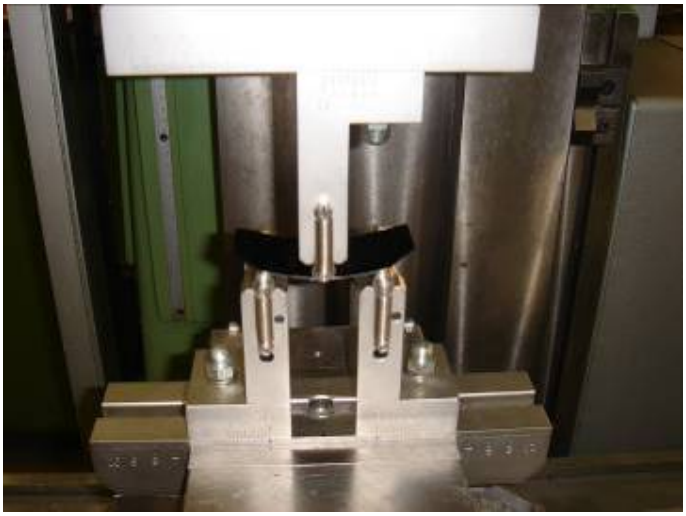

**Figure 124 Three points bending support.**

The CNC milling machine is used in order to know the depth at which the cell breaks. The upper part of the three points support is inserted into the head of the CNC machine, and the lower part of the three points support is attached onto the CNC machine's table.

## M.5.4 Step by step instruction for operation

The following is a recommended test sequence for the three points bending of solar cells:

1. Install the three points bending support on the CNC machine
2. Set the zero position of the three points bending support
3. Set the spacing of the lower part of the three points bending support at 50mm
4. Place the solar cell between upper and lower parts of the three points bending support, with the active face on the top
5. Start to go down the CNC machine head; this should be done very slowly and regularly
6. As soon as cracks are visible or audible, stop the action and record the depth of the CNC machine head
7. Restart the experiment with another cells and place it in the other direction

## M.5.5 Theory about 3 points flexural experience

The material is homogenous and isotropic. The shape is like a rectangular plate with a rectilinear axis and a constant cross-section. The loads are applied in a vertical plan.

The plate is placed on two supports forming a horizontal plan. The load operates at the middle of the length (see Figure 125).

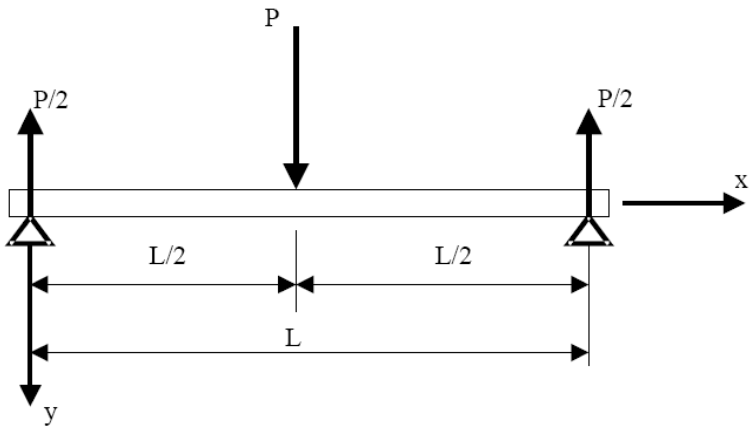


**Figure 125 Three points bending.**

The normal constraint σ for a point at the distance y of the surface is defined by the following relationship [12]:

$$\sigma = \frac{M_b \cdot y}{I}$$ **Equation 12**

with $M_b$ the bending moment and $I$ the inertial moment of the section in relation to the neutral axis.

The vertical deformation at any point of the plate is defined by the following relationship:

$$EI\frac{d^2v}{dx^2} = -M_b$$ **Equation 13**

In the case of the 3 points flexural test, the maximal bending moment at the center of the plate is:

$$M_{b\max} = \frac{P \cdot L}{4}$$ **Equation 14**

The maximal deformation at the center of the plate is:

$$v_{\max} = \frac{P \cdot L^3}{48EI}$$ **Equation 15**

with $I = \frac{b \cdot h^3}{12}$ b is the width of the plate and h its thickness.

If we combine the two previous equations, we can obtain the bending moment according to the deformation:

$$M_b = \frac{v \cdot 48E \cdot I}{L^2}$$

The maximal bending stress is given by:

$$\sigma_{\max} = \frac{M_b \cdot h/2}{I} = \frac{v \cdot 24E \cdot h}{L^2}$$

# Appendix N Existing CubeSats and their main structural properties

| Institution | Project | Status | Structural Configuration and Layout | Materials | % of total mass |
|---|---|---|---|---|---|
| CalPoly | CP1 | Launch with DNEPR-1, June 2006 | All components are fastened to the structural frame | Al | 43 |
| CalPoly | CP2 | Launch with DNEPR-1, June 2006 | 2 Part modular structure t allow easy access to internal components | Al | N/A |
| Cornell | ICE-Cube 1 | Launch with DNEPR-1, June 2006 | Frame structure with braces and bolts used to connect PCBs and payload | Al-7075 for load bearing members Al-6061 for non load bearing | 31 |
| Washington University | UW CubeSat | N/A | N/A | Al-7075 and Al-6061 | 21 |
| University of Toronto | CanX-1 | Launched June 2003, non-operational | Shelf (stack) style layout | Al-7075 and Al-6061-T6 | 37 |
| University of Tokyo | CubeSat XI-IV | Launched June 2003 | N/A | Al-7075 | N/A |
| Iowa State University | CySat | Design and fabrication | Piecewise machined aluminum construction | Aluminum | N/A |
| Stanford | NarcisSat | N/A | 6 part machined aluminum structure bolted together | Aluminum | N/A |
| University of Hawaii | Mea Huaka (Voyager) | Launch with DNEPR-1, June 2006 | CubeSat Kit | CubeSat Kit | 35 |
| Technical University of Denmark | DTUsat | Launched June 2003, no contact | Monolithic cube machined out of solid piece of aluminum. Circuit boards were placed along inside walls with the battery and payload in the center. | Al-7075 | N/A |
| Montana State University | MEROPE | Launch with DNEPR-1, June 2006 | Machined from aluminum with PCBs fastened to structural walls. | Al-7075 and Al-6060-T6 | 28 |
| Aalborg University | AAU CubeSat | Launched June 2003, non-operational | Same frame as DTUsat, PCBs placed along walls with camera payload in center | Aluminum | N/A |
| Dartmouth College | Dartsat | N/A | Does not use any screws, all components epoxied | N/A | N/A |
| Taylor University | TUSAT1 | N/A | Aluminum frame with PCB board shell. It is a double CubeSat | AL-6061-T6 | 20 |